THE INFLUENCE OF TURBULENCE ON THE TIME-MEAN RATE OF CHEMICAL REACTIONS

by

ARNOLD OMOKHEKHAI OKPO ODIDI

(B.Sc.(Eng.), M.Sc.(Eng.), D.I.C., A.C.G.I.)

Thesis submitted for the degree of

DOCTOR OF PHILOSOPHY

in the Faculty of Engineering

University of London

1974

ABSTRACT

At the Imperial College hypotheses linking the time-mean reaction rate to turbulence parameters have been incorporated into computational procedures for predicting turbulent reacting flows. Data of fluctuating quantities, which are scarce in the literature, are required: to facilitate the improvement of these hypotheses by enhancing understanding of the interaction of turbulence and reaction; and for validating the prediction procedures. The collection of data of the kind required was the objective of the study reported in this thesis. The measurements were performed in axisymmetric, turbulent flames burning in still air.

Specifically, the mean, rms, probability density and spectral density of temperature in a methane diffusion flame have been measured. Also, the mean, rms, probability density and spectral density of positive ion current as well as the probability of combustion and the combustion count data have been obtained in a town gas diffusion and town gas/air premixed flames.

The temperature fluctuations data were obtained using a bare thermocouple, its thermal inertia was compensated up to a frequency of 10 kHz with an active filter. A thermocouple coated with a non-catalytic ceramic was used for mean temperature measurement and a correction for radiation loss, determined from the in vacuo temperature versus radiant energy curve of the probe, was applied. The positive ion current was measured by employing a small streamlined probe consisting of a negatively-biased probe wire insulated from the flame gases except for a 2 mm length at its pointed tip. The probability of combustion and the combustion count data were derived from the ion current signal.

Physical pictures of the influence of turbulence on combustion in diffusion and premixed jet flames have emerged from the measurements. The combustion zone of the diffusion flame may be broadly divided into three regions: (1) the outer 'flame edge' region where large air 'lumps' are entrained with combustion occurring in the relatively few fuel/air interfaces, and where the temperature fluctuations are intermittent; (2) the intermediate region where the air 'lumps' experience a breakdown into smaller vortices which results in an increase in available fuel/air interfaces for combustion and in the rms of temperature fluctuations; and (3) the inner region in which the temperature fluctuations and scale of the air vortices are diminished and where the probability density functions of temperature reveals appreciable preheating of the predominantly fuel vortices.

The picture which emerges for flame propagation in <u>fully</u> turbulent premixed flames suggests that the combustion occurs in vortex tubes (diameter equal to the Kolmogorov micro-scale) which are randomly distributed in the flow. The combustion is more intense in these tubes than in a laminar flow because of augmented molecular transport processes. This picture is in conflict with the "wrinkled laminar flame" concept.

ACKNOWLEDGEMENTS

The author is deeply grateful to his supervisor, Dr. F.C. Lockwood for his supervision of the research programme and for his interest in the author's welfare. Dr. J.H. Whitelaw kindly permitted the author to use a Laser Doppler Anemometer, designed and constructed by his team, for obtaining the velocity data.

The valuable help and professional advice given by the technical staff of the Heat Transfer Section contributed greatly to the expeditious execution of the research programme. In this regard, special thanks are due to: Mr. A. Robinson for his assistance in the construction of the ionisation probe; Mr. L. Varty who made numerous sales enquiries in order to procure the required items of equipment; Mr. J. Pilmer who did the photographic work; and Mr. J. Laker who assisted in the construction of the electronic circuits.

Mr. N. Wagner taught the author the art of designing and constructing electronic circuits: without the knowledge he imparted the measurements could not have been made.

The author is also grateful to his colleagues for the enlightening discussions he had with them on various aspects of the investigation. In this connection special mention must be made of: Mr. A. Melling who proof-read the thesis and made many useful criticisms; Mr. D. Durão for the useful discussions on the velocity field in isothermal jets and flames; Mr. J. Asalor who helped in the measurement of mean velocity using the Laser Doppler Anemometer; and Mr. M. Ribeiro for assisting in the measurement of probability density functions using the PDP8 unit.

The final stage of the preparation of this thesis took a short time because Mrs. E. Barker did the typing and Mrs. S. Kingsbury traced the diagrams quickly.

The research grant awarded by the Shell-BP Petroleum Development Company of Nigeria Limited is gratefully acknowledged: without the assistance, the author would not have embarked on this investigation.

Finally, the author is indebted to the Mid-Western State Government of Nigeria for offering a loan when the Shell-BP grant lapsed.

CONTENTS

	Page
ABSTRACT	2
ACKNOWLEDGEMENTS	4
CONTENTS	6
NOMENCLATURE	11
1. INTRODUCTION	15
1.1 The Problem	15
1.1.1 Preliminary remarks	15
1.1.2 Previous pertinent work	18
1.1.2 State of present knowledge	25
1.1.4 Summary of suitable experimental techniques	27
1.2 Research Objectives	29
1.3 Experimental Programme	29
1.3.1 Burners and measurement techniques	29
1.3.2 The measurements	30
1.4 Thesis Outline	31
2. TEMPERATURE MEASUREMENT TECHNIQUE	33
2.1 Introduction	33
2.1.1 Preliminary remarks	33
2.1.2 Previous work	33
2.1.3 Comments on techniques	36
2.1.4 Scope of remainder of chapter	36

		Page
2.2	Thermocouple Probe	37
	2.2.1 Preliminary remarks	37
	2.2.2 Theory	39
	2.2.3 Requirements of the thermocouple	41
	2.2.4 Probe construction	46
2.3	Mean Temperature	49
	2.3.1 Preliminary remarks	49
	2.3.2 Conduction error	50
	2.3.3 Thermal inertia error	50
	2.3.4 Radiation error	52
2.4	Fluctuating Temperature	54
	2.4.1 Preliminary remarks	54
	2.4.2 Catalytic and radiation error	54
	2.4.3 Conduction error	54
	2.4.4 Thermal inertia considerations	55
	2.4.5 Compensating and probe heating circuits	56
	2.4.6 Magnitude of sound harmonic error	59
2.5	Concluding Remarks	59
3.	ION CONCENTRATION AND CHEMI-LUMINESCENCE MEASUREMENT TECHNIQUES	61
3.1	Introduction	61
	3.1.1 Preliminary remarks	61
	3.1.2 Previous work	61
	3.1.3 Comments on previous work	63
	3.1.4 Scope of remainder of chapter	64

		Page
3.2	Ionisation Probe	64
	3.2.1 Principle of operation	64
	3.2.2 Requirements of probe	66
	3.2.3 Fabrication	68
3.3	Instrumentation	70
	3.3.1 Electronic circuit	70
	3.3.2 Need to square the probe signal	71
	3.3.3 Effect of comparator discrimination level	72
3.4	Suggestions for Future Work	74
	3.4.1 Improvements in the present method	74
	3.4.2 Other methods	74
3.5	Concluding Remarks	75
4.	EXPERIMENTAL PROGRAMME	77
4.1	Introduction	77
4.2	Experimental Rig	78
	4.2.1 Choice of burners and Reynolds numbers	78
	4.2.2 Description of burners	79
	4.2.3 Flow rate measurement and Reynolds number calculations	80
	4.2.4 Flame traverse, flame axis location, and flame screening	81
4.3	Temperature Measurement	82
	4.3.1 Mean temperature apparatus	82
	4.3.2 Fluctuating temperature apparatus	83
	4.3.3 Evaluation of the spectral density and the probability density of temperature	84

		Page
4.4	Ionisation Measurement	85
	4.4.1 Ionisation measurement apparatus	85
	4.4.2 Evaluation of the combustion count and the probability of combustion	86
4.5	Concluding Remarks	87
5.	RESULTS AND DISCUSSION	88
5.1	Introduction	88
5.2	Methane Diffusion Flame	89
	5.2.1 Results	89
	5.2.2 Discussion	90
5.3	Turbulent Town Gas Diffusion Flame	95
	5.3.1 Results	95
	5.3.2 Discussion	96
5.4	Turbulent Town Gas-Air Premixed Flames	99
	5.4.1 Results	99
	5.4.2 Discussion	100
5.5	Implications for Combustion Prediction Procedures	103
	5.5.1 Free turbulent diffusion flames	103
	5.5.2 Free turbulent premixed flames	107
	5.5.3 Validation of prediction procedures	107
5.6	Conclusions	109

		Page
6.	SUMMARY AND CONCLUSIONS	112
	6.1 Summary	112
	6.2 Conclusions	113
APPENDIX A.	The Design of Electronic Circuits Associated with the Measurement Programme	116
APPENDIX B.	Time-mean Velocity Measurements in Turbulent Methane Diffusion Flame	133
BIBLIOGRAPHY		138
FIGURES		
	Figure for Chapter 1	147
	Figures for Chapter 2	149
	Figures for Chapter 3	158
	Figures for Chapter 4	168
	Figures, fuel compositions and properties for Chapter 5	179
	Figures for Appendix A	233
	Figures for Appendix B	243

NOMENCLATURE

Symbol	Meaning	Chapters and Appendices where used
A,B	Reactants	1
A,B	Probes	3
a	Inverse of time constant, τ	2
a*, b*	Distances to support wires from thermocouple junction	2
C	Capacitance	Appendix A
C	Specific heat of wire	2
C*	Comparator output voltage	4
D	Burner diameter	5
D*	Wire diameter	2
D^*_b	Thermocouple bead diameter	5
E	Thermocouple emf	2
E	Electric voltage	Appendix A
e	The electron charge	2
e_a	The all-pass output of wave analyser	4
e_f	The band-pass (center frequency, f_c) output of wave analyser	4
F	Spectral density	4
F(k*)	Spectral density in wave-number space	1,5
F(n*)	Spectral density in Fourier space	1,5
f	The combustion count	1,3,4,5
f^*	Doppler signal frequency	Appendix B
f_c	Center frequency of band pass of wave analyser	4
Δf_c	Width of band pass of wave analyser	4
I	Electric current	Appendix A
i_d	Ionisation probe current	3

Symbol	Meaning	Chapters and Appendices where used
K	Thermal diffusivity	2
K_R	Reaction rate constant	1
K_i	Reaction rate constant for the formation of reactant i	1
k	Boltzman constant	3
k^*	Wave-number axis	1,5
L	Length of thermocouple between supports	2
M_i	Instantaneous concentration of reactant i	1
n	Non-dimensional frequency	2
n^*	Frequency axis	1,5
p	The probability of combustion	1,3,4,5
$p(z)$	The probability density function of variable z	1,5
p^*	Perimeter of thermocouple wire	2
Q	Total transport of temperature	5
q	Catalytic term for bare wire	2
R	Resistance	Appendix A
r	Electrical resistivity	2
S	Operator notation	Appendix A
T	Temperature	2,5
T_e	Electron temperature	3
t	Time	1,2
U	Velocity	Appendix B
u_1	Component of velocity fluctuation due to large eddy motion	5
V	Given by $\overline{u_1\theta}/\overline{\theta}$	5
V_d	Voltage between probes A and B	3
x	Distance co-ordinate	2,5

Symbol	Meaning	Chapters and Appendices where used
Y_{mn}	Admittance of network $\Psi(m,n)$	Appendix A
Greek Symbols		
α	Parameter in an admittance equation	Appendix A
β	Function of gas temperature and wire properties, defined by equation 2.2.9	2
Γ_R	Characteristic time of chemical reaction given by $\frac{1}{K_A \overline{M}_B + K_B \overline{M}_A}$.	1
Γ_T	Characteristic time for diffusion on a molecular scale in a turbulent flow given by $\lambda_T^2/2\mathcal{D}$. $\mathcal{D}$ is the molecular diffusion coefficient.	1
δ	Intermittency factor for turbulent flow	5
ε	Emissivity	2
ε_t	Thermal inertia error in mean temperature data	2
$\varepsilon(2\omega)$,	Second harmonic error in temperature fluctuations data	2
η	Wire property defined in subsection 2.3.2	2
θ	Temperature difference between point of observation and ambient fluid	5
ϑ	Wire property defined by equation 2.4.6	
λ	Wave-length of laser beam	Appendix B
λ_T	The dissipative length scale (for species concentration)	1
μ_T	Property of fully turbulent fluid	5
ρ	Density of wire	2
ρ	Parameter in admittance equation	Appendix A
σ	Stefan-Boltzmann constant	2
τ	Time constant	2, Appendix A

Greek Symbol	Meaning	Chapters and Appendices where used
ϕ	Phase angle	2
$\Psi_{(m,n)}$	Network	Appendix A
Ψ_m	Conduction error parameter	2
ω	Frequency	2, Appendix A
ω^*	Wire cross-sectional area	2

CHAPTER 1

INTRODUCTION

1.1 The Problem

1.1.1 Preliminary Remarks

Turbulent reacting flows are encountered in such diverse and important phenomena and devices as: photochemical smog formation in the atmosphere; the spread of forest fires by winds; process reactors in the chemical industry; the furnaces of central electricity generating boilers; and the combustion chambers of rocket engines. Many investigations into the fundamental nature of these flows (see for example Corrsin (1958); Eschenroeder (1965); Lee (1966); O'Brien (1966, 1969, 1971); Vassilatos and Toor (1965); Chung (1972); Donaldson and Hilst (1972)) as well as into their practical aspects (see for example Shchetinkov (1959); Karlovitz (1953); Spalding (1967, 1971); Chomiak (1970); Rhodes and Harsha (1972)) have been motivated by their widespread significance in engineering and in the environment.

The fundamental investigations were primarily concerned with providing qualitative generalizations. Accordingly, they were restricted to first and second order reactions in idealized turbulence (e.g. isotropic turbulence) to render tractable the mathematical analysis of the flow. The studies by Eschenroeder (1965), and Vassilatos and Toor (1965) illustrate some of the generalizations which have elucidated the interaction of turbulence and chemical reaction.

Eschenroeder performed a mathematical analysis of a locally isotropic turbulent fluid in which the rate of heat release is a function of the gas density, such as occurs for example, in exothermic combustion. He concluded that the exothermal source strongly influences the energy

containing eddies of the flow leading to enhanced turbulent diffusivity and an enlarged effective Reynolds number.

For a simple, isothermal second order reaction, Vassilatos and Toor have shown that, for given local time-mean concentrations, the influence of turbulence on the time-averaged reaction rate is, relative to a laminar flow, an augmentation for premixed reactants, and a diminution for reactants not premixed. These assertions are readily justified by inspection of the expression for the time-mean reaction rate for reactants A and B, $K_R(\overline{M}_A\overline{M}_B + \overline{M'_A M'_B})$, ($K_R$ is the reaction rate constant; M_A is the concentration of reactant A; over-bars indicate time-averaging; and primes designate fluctuating components). If the reactants are premixed, the fluctuations M'_A and M'_B are always of the same sign when they are both finite, so that $\overline{M'_A M'_N} > 0$; if the reactants are not premixed, the reverse is true and hence $\overline{M'_A M'_N} < 0$.

The relative diminution or augmentation of the time-averaged reaction rate by turbulence is determined by the type of reaction. Three broad categories of reactions may be delineated: (1) slow reactions, $\Gamma^*_R/\Gamma_T << 1$; (2) fast reactions, $\Gamma_R/\Gamma_T \sim 1$; and (3) very fast reactions $\Gamma_R/\Gamma_T >> 1$. Chemical kinetics dominates the first category since the reactants become mixed on a molecular scale before they experience appreciable conversion. The reaction ($N_2 + 3H_2 \rightleftharpoons 2NH_3$) that would occur in hot turbulent mixing streams of nitrogen and hydrogen belongs to the first category. Kinematically-influenced turbulent reacting flows fall into the second category of reactants. A turbulent premixed town gas-air flame is an example of this kind of flow. The reacting flows of the third category which are often termed diffusion controlled, are dominated by the turbulent mixing. A flow in the third category is a turbulent methane diffusion flame.

---

* Γ_R and Γ_T defined in Nomenclature.

In contrast to the fundamental studies, those into the practical aspects of turbulent reacting flows have sought to provide quantitative information about velocity, species concentration and temperature in the domain of the reacting fluid. The ability to calculate such quantitative information is a pre-requisite of a satisfactory design method for practical combustion systems: it is necessary not only to calculate the aerodynamics but also to take into account the influence of the turbulence on the combustion.

General prediction procedures for calculating turbulent non-reacting flows in such equipment have been successfully developed and applied (see for example, Launder and Spalding (1972), Patankar and Spalding (1973)). In order to extend these techniques to the circumstances of reacting flows, mathematical models are required for the influence of the turbulence on the rate of chemical reaction at all points within the flow field. Turbulence reaction models have been proposed by Spalding (1969, 1971), Rhodes and Harsha (1972) and Chomiak (1970). Research is in progress in the Mechanical Engineering Department at Imperial College to test the models suggested by Spalding.

A systematic validation programme is being prosecuted, commencing with the simplest flows where the turbulence is reasonably well understood, and progressing to more complex combustion systems. However, there is a dearth of empirical information for simple and well defined turbulent reacting flows. Measurements of fluctuating quantities are particularly scarce; this is unfortunate considering that such measurements would facilitate the improvement of the reaction models, in addition to providing a sensitive test for them, by enhancing understanding of the influence of turbulence on the local reaction rate.

To provide the kind of data required, this thesis is addressed to the problem of obtaining measurements of the time-mean and fluctuating components of temperature and positive ion concentration in turbulent, round-jet diffusion and premixed flames burning in stagnant surroundings. These simple flames were of interest for two main reasons:

In the first place, such reacting flows belong to the 'boundary layer' class, that is, they possess one predominant flow direction. The prediction procedures developed for this class of flow have provided accurate predictions of non-reacting axisymmetric jet flows, Rodi (1972), and they are economic of computer time.

Secondly, the structure of the turbulence in an axisymmetric jet flow is reasonably well understood, Townsend (1956a), and although the flow is simple it exhibits many features, such as inhomogeneity and non-isotropy, found in many practical flows.

1.1.2 Previous pertinent work

The work of Mallard and Le Chatelier (1883) inaugurated the scientific attack on the problem of turbulent reacting flows. Stoichiometric mixtures of CS_2 and NO_2 contained in various glass tubes each closed at one end were ignited at the open end. The movement of the reaction zone in each tube was recorded photographically. Initially the reaction zone was well defined and a few mm thick, and its movement was uniform. Then it was transformed into a distorted zone having a thickness of up to 10 cm and its movement became "vibrational": and, its velocity of propagation though variable was always greater than during the uniform movement. During the "vibrational" movement the reaction was noisier and more intense.

Numerous research workers subsequently expended considerable effort on elucidating the complex processes involved in turbulent reacting flows. However, the present review is restricted to experiments performed on free axisymmetric jet flames burning in stagnant surroundings in which local quantitative data were obtained.

(a) Concentration (stable species, ionisation, emission) measurements

Axial mean concentration (and visible flame length) data of stable species (such as hydrogen, carbon dioxide) in various turbulent diffusion flames were obtained by Hawthorne et al (1949). The fuels burned were hydrogen, propane, city gas, hydrogen-propane mixture, and city gas - carbon dioxide mixture. The diameters were: for the rounded nozzles 1/8", 3/16", and 1/4"; and for the orifice nozzles .179", and .182" based on the vena contracta values. The flow Reynolds numbers ranged from 2,870 to 32,400. The axial distances to the location of 99% complete combustion calculated from the compositions of the axial gas samples (analytical flame length) were 10% to 20% shorter than the visible flame lengths. The consistent agreement between the visible and the analytical flame lengths implies that the measurements were of good accuracy.

Positive ion current measurements in a turbulent premixed natural gas-air flame Reynolds number 10^4 and burner tube diameter 3.16 cm were made by Karlovitz et al (1953). They analysed the probe signal to obtain the fluctuation frequency with which, and the percentage of time, the flame contacted the probe wire. The objective was to validate the "wrinkled laminar flame" concept of turbulent flames. They arrived at the conclusion that their measurements were in agreement with this concept. However, Summerfield et al (1955) who employed the same technique as Karlovitz et al in a two-dimensional (2" x $\frac{1}{2}$" nozzle) premixed methane-air

flame, flow velocity 120 f.p.s. were led to the conclusion that the "wrinkled laminar flame" concept was invalid.

Measurements of the concentration of carbon dioxide and of dynamic pressure were made by Ievlev (1957). The burner tube was 30 mm diameter and 200 mm long. The fuel was premixed Moscow city gas - air, with equivalence ratios ranging from 0.86 to 1.37 and the gas-air feed velocity was from 10 to 30 m/sec. He obtained contours of the percentage ratio of the local time-mean CO_2 concentration to the maximum concentration obtained from complete combustion of an air-gas mixture of the composition used. As no details of the sampling and analysis procedures were given in his paper, it is impossible to form an opinion of the accuracy of his results.

The total fluctuating emission from radicals in a turbulent diffusion flame of Karlsruhe city gas was measured by Guenther and Simon (1969) using an optical probe. The nozzle burner diameter was 10 mm and the Reynolds number was 4.35×10^4. They measured the spectral density, the macro-scale and micro-scale of emission fluctuations and the intensity of emission fluctuations. They obtained good agreement between their measured spectral density and the theoretical curve based on the theory of local isotropy. Guenther and Simon also reported the axial distributions of mean CO_2, CO, O_2, H_2O, H_2, CH_4 and C_mH_n concentrations and of mean temperature in the flame.

Recently, Kuhnert and Guenther (1973) briefly reported measurements of the macro-scale of OH-emission from a turbulent diffusion flame obtained with a crossed-beam optical probe. The flow Reynolds number was not stated in their paper. Their axial distribution of the macro-scale was qualitatively similar to that measured by Guenther and Simon (1969).

(b) Temperature measurements

The frequency spectra of temperature fluctuations were first measured in turbulent diffusion flames by Kunugi and Jinno (1959). They employed a 0.06 mm diameter Platinum versus Platinum/13% Rhodium thermocouple and compensated the probe signal for thermal inertia up to a frequency of about 1 kHz. They used tube burners of 4.8 mm and 6.4 mm diameter and the flow Reynolds numbers were 2,850 and 5,700. The frequency spectrum of temperature fluctuations was measured. They were led to the conclusion that the turbulent diffusion flame may be divided into three regions: the inner jet of unburnt gas, the burning zone, and the flame envelope, each region with a characteristic peak in the frequency spectrum. However, the accuracy of their data was limited by the fact that the harmonics of the probe signal in the region of 1 kHz were over-compensated.

The mean temperatures in various turbulent diffusion flames of fuel mixtures (such as Hydrogen/Argon/Air, Hydrogen/N_2O) used in flame spectroscopy were measured by Smith et al (1969) using 0.005 inch diameter Iridium versus 60% Iridium/Rhodium thermocouple. They employed Jarrel-Ash 82-341 HECTO and Zeiss burners. Fuel flow rates ranged from 9.3 l./min to 17.0 l./min, and aspirant flow rates ranged from 5.9 to 16.0 l./min. They measured isothermal contours. The main error in the temperature measurements which was due to radiation loss was corrected for by calibrating the thermocouple against the sodium-line reversal technique in uniform flame gases. The maximum uncertainty due to all the residual sources of error was estimated to be $\pm$ 50°K for a flame temperature of 2400°K and $\pm$ 40°K for a flame temperature of 2000°K.

The light scatter technique was first employed to measure fluctuating temperature in a turbulent premixed flame by Williams et al (1969). They used a nozzle burner 2.80 inches diameter and an approximately stoichiometric natural gas-air mixture. The flow velocities were 11.7, 13.8 and 18.7 fps. The probe signal was analysed to obtain information on the local fluctuations of the reacting zone. The data (which agreed qualitatively with those obtained by Karlovitz et al (1953) discussed in (a) above) were consistent with the "wrinkled laminar flame" model. Furthermore, high speed photographs of the flame indicated a wrinkled structure as deduced from the local data. The measured wavelengths and amplitudes within the flame brush were independent of upstream conditions implying that, for their experimental conditions, upstream turbulence had a negligible influence on the flame structure. The wavelengths and amplitudes increased with vertical position in the flame.

Contours of mean temperature (and concentration of radicals such as OH) were measured in a turbulent stoichiometric premixed methane-oxygen flame by Fisan (1970) using absorption and emission spectrometry. The burner tube diameter was 8 mm and the mass flow was 2.3 g/s. He used a grating spectrograph with a range of 2500 - 8000 A^{o} and a photomultiplier detector. He obtained the local data from the spatial average across the flame by mathematical inversion. The emission and absorption temperatures so derived were accurate to $\pm$ 25^{o}K. However the method is not accurate for temperatures below 2600^{o}K, so that the data were only obtained in the flame regions with temperatures in excess of this value.

(c) Velocity measurements

The rms of fluctuating longitudinal velocity in a turbulent flame were first obtained by Ebrahimi (1967). He made his measurements in a

hydrogen diffusion flame and used a condenser microphone probe to record pressure fluctuations. The nozzle diameter was 4 mm and the flow velocity at exit from the nozzle was 220 m/s. The method required the calibration of the measuring probe by means of a hot-wire anemometer in a cold flow. The axial distributions of local mean velocity and rms of longitudinal velocity fluctuations were derived. However, in the theory of his method, Ebrahimi ignored the fluctuations in gas density without providing any justification for so doing. Since the gas density fluctuations are not negligible the accuracy of his data is dubious.

Becker and Brown (1969) and Eickhoff (1968) independently derived the radial velocity fluctuations in turbulent diffusion flames from the measured static pressure defect. Becker and Brown measured in a propane flame. The nozzle diameter was 0.635 cm, the flow Reynolds number was 45,000. Because no flame stabilizer was used, the visible flame was lifted 18 cm above the nozzle. The data obtained in a cold air flow were in good agreement with published hot-wire anemometer data. Becker and Brown therefore argued that in a flame, according to the theoretical formulae of the method, the data are accurate if the transverse velocity and the density fluctuations are negligibly correlated. However, some evidence is required to support this supposition. Eickhoof measured in towns gas flames: Reynolds numbers of 7.14×10^4 and 5.05×10^4 for lifted flames, and of 5.05×10^4 and 3.2×10^4 for flames stabilized on the nozzle. His results were in qualitative agreement with those of Becker and Brown.

Durst et al (1972) were the first to employ the Laser Doppler Anemometer to obtain local fluctuating velocity data in a turbulent flame. The fuel was premixed town gas and air in the volumetric ratio of 1:5.5,

the flow Reynolds number was 2,100 and the nozzle diameter was 10 mm. In principle, the method provides accurate data. However, Durst et al employed silicone oil droplets to scatter light for the purpose of measurement and in later publications (Durst et al (1972a) and Durst and Kleine (1973)) it was reported that these droplets affect the flame markedly. Durst et al (1972) measured the mean, the rms, the skewness factor and the flatness factor of the fluctuating velocity. The measurements showed that the mean velocity increased through the flame front and then fell rapidly: the flow subsequently accelerated. A sharp increase in the rms fluctuating velocity was found across the flame front. The probability density functions of velocity indicated combustion induced oscillations in the flow.

Baker et al (1973) used the La ser Doppler Anemometer to measure the fluctuating velocity in a turbulent methane diffusion flame, Reynolds number 4,400 and burner tube diameter 2.54 mm. The main flame was stabilized by means of an annular town gas pilot flame. Silicone oil droplets were used to scatter light for the measurements. As mentioned previously, these droplets are known to affect the flame processes. They measured the mean velocity, as well as the rms, the skewness factor, the flatness factor and the probability density of the longitudinal velocity fluctuations. They compared their flame data with those taken in a cold methane jet. They concluded from their measurements that: the decay of the centre-line mean velocity in the flame was significantly less than in the cold jet which implied that the combustion markedly accelerated the flame gases; the skewness factor and the flatness factor indicated that the velocity fluctuations were very approximately Gaussianly distributed; and the profiles of turbulence intensity were nearly the same as in an isothermal jet.

Durst and Kleine (1973) made velocity measurements with the Laser Doppler Anemometer in a stoichiometric natural gas-air flame, Reynolds number 16,000, burner tube diameter 30 mm and stabilized the flame with a hydrogen pilot flame. They employed MgO particles which have a negligible effect on the flames processes, to scatter light for the purpose of measurement. They measured the mean velocity, the rms of the longitudinal and the transverse velocity fluctuations in the flame and in an isothermal air jet for comparison. They were led to the conclusion that the fluctuation velocities and the average velocities increase when the mixture enters the turbulent flame front and that behind the flame front the radial fluctuations decrease more rapidly than the axial fluctuations. These conclusions are similar to those arrived at by Durst et al (1972). Durst and Kleine also observed the following: a strong change in the direction of flow when it entered the flame front; that the flame contributed to the overall effective value of the rms of the transverse and longitudinal velocity fluctuations; and that the shear stress reversed its sign within the flame reaction zone.

1.1.3 State of present knowledge

The brief review presented in the preceding sub-section on previous measurements in axisymmetric turbulent flames burning in still air has revealed the following:

Firstly, there exists in the literature time-mean data of velocity, concentrations and temperature. However, for mean velocity, the level

of accuracy of only the data obtained by Durst and Kleine (1973) in a turbulent premixed flame is known. In particular, these premixed flame data were not only free of interpretation difficulties (such as the effects of temperature and concentration variations on pressure sensitive probes) but also of the influence of the light scatterers on the combustion processes (i.e. MgO particles used not silicone oil droplets). The mean concentration (of stable species) data of Hawthorne et al (1949) and also of Guenther and Simon (1969) obtained in diffusion flames are accurate; no similar data are available for premixed flames. The mean temperature data of Smith et al (1969) and Guenther and Simon (1969) in diffusion flames, and of Fisan (1970) in a premixed flame are accurate. However, it would be useful to provide more comprehensive time-mean data of velocity, concentrations and temperature in fully turbulent flames.

Secondly, data of the rms and the probability density of velocity fluctuations also exist in the literature. The comments made for time-mean velocity data in the preceding paragraph also apply to the velocity fluctuations measurements. Therefore, still urgently required are more data in fully turbulent flames obtained with the Laser Anemometer and using light scattering particles that do not interact with the flame.

Finally, no data of the rms and the probability density of the temperature and stable species concentrations exist in the literature.

The role of experiments in turbulent combustion research was defined clearly by Guenther (1970), namely: to facilitate the development of procedures for predicting turbulent flame performance under prescribed boundary conditions. These procedures solve numerically the governing

partial differential equations of the flow and require expressions with empirically determined terms for modelling the turbulent transport processes, i.e. for closing the Reynold's stress equations, and for linking the transport processes with the time-mean chemical reaction rate. To this end, it is necessary to provide not only the time-mean data of the species concentration, temperature and velocity but also data for the fluctuations of these quantities.

Furthermore, measurements of the rms and the probability density of the fluctuating temperature and species concentration, which provide information on the level of reaction rate fluctuations, will assist the forming of an accurate physical picture of the influence of turbulence on the local reaction rate. This enhanced physical understanding will, in turn, aid in the formulation of reliable models linking the turbulent transport processes with the time-mean reaction rate.

In this context, the absolute lack of data on the rms and the probability density of the fluctuating components of temperature and species concentrations is a serious handicap.

1.1.4 Summary of suitable experimental techniques

A classification of the experimental techniques that could be employed for measuring the local instantaneous velocity, temperature and species concentration is shown in Table 1.1. Only techniques that do not require extensive calibration procedures are considered.

Table 1.1

Measurement Techniques

Property	Experimental Technique	References	Comments
Velocity	Laser Doppler Anemometer	Durst (1972 a) Durst et al (1972)	Well-developed and accurate.
Temperature	Thermocouple	Shepard and Warshawsky (1952) Kunugi and Jinno (1959)	Easy to use. Cheap and moderately accurate. Thermal inertia compensation required.
	Resistance thermometer	Parker and Guillon (1971)	Same as for thermocouple.
	Light-scatter technique	Williams et al (1969)	Accurate method but requires particle seeding of the ambient entrained air.
	Raman spectroscopy	Widhopf and Lederman (1971)	Requires considerable development and has not yet been applied in turbulent flames.
Stable and unstable specie concentrations	Raman spectroscopy	Widhopf and Lederman (1971)	Requires considerable development and has not yet been applied in turbulent flames.
Total emission	Total emission probe	Guenther and Simon (1969)	Signal is in arbitrary units, but can be analysed to give spectral density, probability of combustion* and the combustion count**.
Positive ion current	Ionisation probe	Karlovitz et al (1953)	Same as for total emission.

* Probability of combustion ≡ time-mean fraction of time combustion occurs locally.

** Combustion count ≡ time-mean number of times per second combustion occurs locally.

1.2 Research Objectives

This thesis describes an experimental investigation of axisymmetric turbulent premixed and diffusion flames burning in stagnant surroundings. The objectives of the investigation were:

(1) To measure the mean, the rms, the probability density and the spectral density of the fluctuating temperature.*

(2) To measure the mean, the rms, the probability density and the spectral density of the fluctuating positive ion current.

(3) To measure the probability of combustion and the combustion count (defined in Table 1.1) from the ion current signal.

1.3 Experimental Programme

1.3.1 Burners and measurement techniques

The burner used for the turbulent diffusion methane and town gas flames was a tube 5 mm i.d. and 75 diameters long. The Reynolds number of the methane flame was 14,500 and of the town gas flame, 24,000. The burner used for the turbulent lean and rich premixed flames was 29 mm i.d. and 50 diameters long. The equivalence ratios of the flames were 0.91 and 1.16 and the Reynolds number was 62,000.

The mean temperature data were obtained with a 100 μm diameter thermocouple coated with a non-catalytic ceramic and were corrected for radiation loss error. The temperature fluctuations data were obtained using a bare 40 μm diameter thermocouple with compensation for the probe thermal inertia. The positive ion current was measured using a negatively biased wire sheathed from the flame gases except for an exposed tip 2 mm long.

---

* See Fig. 1.1 for meaning of these quantities.

1.3.2 The measurements

The types of data obtained in the various flames are summarized in Table 1.2.

Table 1.2

Summary of the measurements.

	Methane diffusion flame.	Town gas diffusion flame.	Premixed town gas and air flames.
Temperature Measurements.			
Mean Temperature	✓	✓	✓
RMS of temperature fluctuations	✓		
Probability density of fluctuating temperature	✓		
Spectral density of temperature fluctuations	✓		
Positive Ion Concentration Measurements.			
Mean of positive-ion concentration		✓	✓
RMS of positive-ion concentration		✓	✓
Probability of combustion		✓	✓
Combustion Count		✓	✓
Probability density of positive-ion concentration		✓	✓
Spectral density of positive-ion concentration		✓	✓

1.4 Thesis Outline

The remainder of the thesis consists of five chapters and two appendices:

Chapter 2 is concerned with the description of the temperature measurement technique: the construction of the thermocouples which were employed for the mean and the fluctuating temperature measurements; the electronic circuit used for thermal inertia compensation in the fluctuating temperature measurement; the method for correcting for the radiation error in the mean temperature measurement. Lastly the accuracy of the temperature-measurement technique is appraised.

Chapter 3 is devoted to describing the positive ion current measurement technique: the design and construction of the ionisation probe; the electronic circuit used for measuring the positive ion current, and for deriving from the current the probability of combustion, p, and the combustion count, f. A discussion follows of the effect of background electronic noise on the measurement of p and f.

Chapter 4 deals with the experimental programme: the burners are described and the measurement procedures for obtaining the temperature data and the positive ion current data are presented.

The experimental results are presented and discussed in detail in Chapter 5. The physical pictures which emerge from the data on the influence of turbulent mixing on diffusion and premixed flames are portrayed. The implications of the results on the physical modelling of turbulent diffusion and premixed free flames are indicated.

The principal results and conclusions contained in this thesis are summarized in Chapter 6.

In Appendix A, a simplified description of the methods used for designing the electronic circuits employed in the experiments is presented; while Appendix B contains the mean velocity profiles* in a turbulent methane diffusion flame. These measurements were required for converting the spectral density measurements from frequency to wave-number space.

---

*Obtained with the help of Mr. J. Asalor of the Mechanical Engineering Department, Imperial College, London.

CHAPTER 2

TEMPERATURE MEASUREMENT TECHNIQUE

2.1 Introduction

2.1.1 Preliminary Remarks

Temperature is, strictly, not an accurately defined concept in the reaction zones of flames because neither thermal nor chemical equilibrium exists in these zones (Gaydon and Wolfhard, 1970a). However, in strongly exothermic small-scale open flames at atmospheric pressure, energy transfer between the translational, vibrational and rotational degrees of freedom is rapid enough for departures from thermal equilibrium to be marginal (Gaydon and Wolfhard, 1970b). Consequently, any one of the translational, vibrational and rotational energies of the gas molecules in such flames may be used to indicate the local instantaneous temperature; and the temperature thus derived should be nearly the same as that which would prevail for conditions of complete equilibrium.

2.1.2 Previous Work

(a) Optical Methods

Local mean temperatures in a turbulent premixed methane-oxygen flame were derived by Fissan, 1970, from measurements using an absorption spectrometry technique. With this technique, a spatial average through the flame is obtained; however, if the mean temperature field is axi-symmetric the local mean temperatures can be obtained from the spatial average by mathematical treatment, the Abel inversion. The inversion

provides accurate local data if a narrow light beam is used. But the measurement procedure is suitable for high temperature flames e.g. H_2/O_2 flames.

The local instantaneous temperature in a turbulent premixed natural gas/air flame has been measured by utilizing the Mie scattering of a light beam by MgO particles, Williams et al., (1969). Since MgO particles are chemically inert to the reactions in the flame studied, lack of chemical equilibrium did not affect the measurements. With this technique, the instantaneous local temperature is derived from the instantaneous local gas density. The method is suitable for use in flames where density changes are caused by temperature fluctuations only, but not if changes in the number of gas molecules during chemical transformations also occur.

Thus, in methane (main constituent of natural gas used by Williams et al, 1969) - air flames, no change in the number of gas molecules occurs; but in hydrogen (or town gas) - air flames there is a contraction in the number of molecules. Also, the use of the method in a free flame requires that the entrained ambient fluid be seeded with scattering particles. Otherwise, measurements can be made only in the restricted region of the flow where the seeded burner fluid has not been significantly diluted by entrainment of ambient fluid. However, the technique affords good spatial resolution $\approx$ 1.5 $[mm]^3$; and the frequency response (DC to 10 KHz) is adequate for studying temperature fluctuations in turbulent flames.

The feasibility of using Raman scattering of a 100 MW Q-switched Ruby Laser Beam to measure the local instantaneous temperature of gas molecules has been demonstrated (Widhopf and Lederman, 1971). These

workers did not employ this optical technique in a flame. However, as the technique does not require scattering particles, it can be applied to flames. The method has fairly good spatial resolution $\approx 3[\text{mm}]^3$, and extremely good frequency response (DC to 10 MHz).

(b) Contact Probes

Local time-mean temperatures in turbulent hydrogen diffusion flames have been measured using Iridium versus Iridium 60%/Rhodium 40% thermocouples coated with zirconia ceramic (Smith et al, 1969), and using Platinum versus Platinum 87%/Rhodium 13% thermocouples coated with a mixture of Beryllium oxide and Yttrium oxide (Kent and Bilger, 1973). These authors coated their thermocouples in order to eliminate the catalytic action which would otherwise occur on the bare wires. Both groups of workers corrected for the radiation loss error by calibrating the thermocouple in a laminar flame against the Sodium-Line reversal technique.

Kunugi and Jinno, 1959, were the first to measure the spectrum of temperature fluctuations in a turbulent diffusion flame (of Kyoto City Gas). They employed a bare 60 μm diameter Platinum versus Platinum 87%/Rhodium 13% thermocouple. The accuracy of their data was, however, limited by the fact that compensation for thermal inertia was only effected up to 1 kHz; compensation up to at least 5 kHz is required for measuring the spectrum of fluctuations in turbulent flames as shown by the data of Guenther and Simon (1969).

Parker and Guillon, 1971, employed a bare 18 μm diameter Iridium resistance wire probe to measure spectral density of the local fluctuating temperature in the burnt gases of a turbulent premixed

flame. These workers made analogue records of their probe signal and a subsequent compensation for the probe thermal inertia - on account of the short time the probes survived in the hot gases. The compensating circuit employed was a passive filter. The probe time constant was determined from its response to a square wave signal. The compensator time constant required to reproduce the square wave was employed for compensating the probe-temperature signal in the same measurement location.

2.1.3 Comments on Techniques

The absorption spectrometer was not considered for use because relatively low temperature methane/air and town gas/air flames were investigated.

The Raman spectroscopy probe (Widhopf and Lederman) would be ideal for measurement of fluctuating temperature (and fluctuating species concentrations). Unfortunately, because it is very expensive its use in this experimental programme was not contemplated.

The light scatter technique of Williams et al. has the serious practical drawback of requiring uniform seeding of the nozzle and entrained ambient fluid before it can be applied in all regions of the flow. For this reason, it was not employed.

The thermocouple is simpler to use and it affords better spatial resolution than the resistance thermometer probe. The former probe was therefore chosen.

2.1.4 Scope of Remainder of Chapter

The thermocouple probes are considered in detail in Section 2.2. The criteria for selecting the materials and the diameters of the

thermocouples employed for the mean and fluctuating temperature measurements are outlined and discussed. The method for constructing the probes is described.

The errors involved in mean temperature measurement are discussed in Section 2.3. The probe radiation loss calibration in vacuo is described as well as the radiation loss correction in a flame.

Section 2.4 is concerned with the measurement of temperature fluctuations. The inherent errors in the measurement procedure are discussed, and the method of compensating the probe for the thermal inertia is described.

The main conclusions arrived at in this chapter are summarized in Section 2.5.

2.2 Thermocouple Probe

2.2.1 Preliminary Remarks

The instantaneous temperature recorded by a thermocouple in a turbulent flame is different from the instantaneous gas temperature for the following reasons:

(1) The probe has a finite thermal inertia which is a function of the wire properties, fluid properties and fluid velocity.

(2) Complex fluctuations of the probe thermal inertia are induced by the fluctuating fluid temperature and velocity.

(3) Radiative interchange occurs between the probe, the flame gases and the surrounding walls.

(4) In general, there is a temperature gradient along the thermocouple wire with a resultant conduction of heat to or from the probe

junction.

(5) Catalytic activity may occur on the probe surface causing erroneously high temperatures to be recorded.

All these effects are expressed in the heat balance equation given in Sub-section 2.2.2 below.

2.2.2 Theory

Equations

The governing partial differential equations and the relevant boundary conditions for the instantaneous energy balance of a composite wire in a fluctuating temperature field were derived by Carslaw and Jaeger (1959). Gilbert and Lobdell (1953) introduced the catalytic term, q, to account for extraneous heat generated on the wire surface by chemical reaction. Adopting this term, and with reference to Fig. 2.2.1, the equations and boundary conditions are:

$$\frac{\partial T_1}{\partial t} = K_1 \frac{\partial^2 T_1}{\partial x^2} - \frac{1}{\tau_1}(T_1 - T_g) - \left\{\frac{\sigma\varepsilon_1 (T_1^4 - \varepsilon_g T_g^4) p_1^*}{\rho_1 C_1 \omega_1^*}\right\} + q_1 \quad (a^* < x < 0) \qquad (2.2.1)$$

A B C D E

$$\frac{\partial T_2}{\partial t} = K_2 \frac{\partial^2 T_2}{\partial x^2} - \frac{1}{\tau_2}(T_2 - T_g) - \left\{\frac{\sigma\varepsilon_2 (T_2^4 - \varepsilon_g T_g^4) p_2^*}{\rho_2 C_2 \omega_2^*}\right\} + q_2 \quad (0 < x < b^*) \qquad (2.2.2)$$

Boundary conditions:

$$T_1 = T_2 \; ; \qquad \omega_1^* K_1'' \frac{\partial T_1}{\partial x} = \omega_2^* K_2'' \frac{\partial T_2}{\partial x} \quad \text{at } x = 0 \qquad (2.2.3)$$

where:

subscripts 1, 2 and g pertain to the two metal alloys of the thermocouple and to the gas respectively.

The terms in the equations

From equation 2.2.1, it is evident that the difference between the instantaneous probe and gas temperatures, term C, at x = 0, arises as a consequence of:

(1) The thermal inertia of the thermocouple, term A.

(2) Conduction along the thermocouple wire, term B.

(3) Radiant energy transmitted to, and emitted by the wire, term D.

(4) Chemical reaction on the wire surface promoted by heterogeneous catalysis, term E.

Simplification of general equation

When $[(T_g - T_1)/T_g] \ll 1$, we may introduce the linear approximation $T_g^4 - T^4 \approx 4T_g^3 (T_g - T)$ after Scadron and Warshawsky, 1952a. Equation 2.2.1 then takes the following form:

$$\tau_1' \frac{\partial T_1}{\partial t} = K_1' \frac{\partial^2 T_1}{\partial x^2} - (T_1 - T_{f_1}) + q_1' \qquad (2.2.4)$$

where:

$$T_{f_1} = T_g \left[1 + \frac{(1 - \varepsilon_g)\, \tau_1\, \varepsilon_1\, \beta_1}{1 + 4\varepsilon_1 \beta_1 \tau_1}\right] \qquad (2.2.5)$$

$$\tau_1' = \frac{\tau_1}{1 + 4\varepsilon_1 \beta_1 \tau_1} \qquad (2.2.6)$$

$$K_1' = K_1 \left(\frac{\tau_1}{1 + 4\varepsilon_1\beta_1\tau_1}\right) \qquad (2.2.7)$$

$$q_1' = q_1 \left(\frac{\tau_1}{1 + 4\varepsilon_1\beta_1\tau_1}\right) \qquad (2.2.8)$$

$$\beta_1 = \frac{T_g^3 \sigma p_1^*}{\rho_1 C_1 \omega_1^*} \qquad (2.2.9)$$

The subscripts 1 and 2 may be discarded and replaced by effective values: the effective thermal conductivity is the harmonic mean, and the effective thermal capacity and emissivity are the arithmetic means of the respective values for the alloys, Scadron and Warshawsky, 1952b.

2.2.3 Requirements of the Thermocouple

(a) Criteria

The criteria used for selecting the materials and diameters of the thermocouple are as follows:

(1) The maximum permissible working temperature should be higher than the maximum instantaneous temperature which the probe can attain in the flames investigated. The latter temperature is dependent at any instant on: the local gas temperature; the net radiant energy interchange between the wire and the surroundings; the heat transfer coefficient between the wire and the gas; and the thermal capacity of the wire.

(2) There should be negligible catalytic activity on the surface. This criterion is unimportant for the measurement of mean temperature because the probe employed can be coated with a suitable non-catalytic ceramic as described in Section 2.2.4 below. For fluctuating temperature measurement, the criterion is relevant since a similar ceramic coating on the wire would, obviously, considerably reduce the probe frequency response.

(3) The sensitivity of the thermocouple, $\tilde{S}$, that is, its thermo-electric output per degree temperature change, should be as high as possible in order to ensure a high signal to noise ratio in the measurements. This criterion is especially important for the measurement of fluctuating temperature. As shown in Section 2.4.1 below, the effect of probe thermal inertia is an attenuation of the higher Fourier harmonics of the indicated probe temperature relative to those of the gas temperature. A high value of $\tilde{S}$ is required so that these attenuated harmonics are still well above the background electronic noise of the circuits used to compensate for the probe thermal inertia.

(4) The thermocouple should possess adequate mechanical strength in order to provide the required data before failing. An indication of the mechanical strength of the probe wires is their ultimate tensile strength.

(5) For fluctuating temperature measurement, the wire diameter must be small enough to ensure sufficiently rapid response to the fluctuating gas temperatures. Some thermocouples, for example, Iridium versus Iridium/40% Rhodium, which would otherwise be satisfactory are available as relatively thick wires (250 μm).

(b) Wire materials

Table 2.2 was prepared to facilitate the choice of the thermocouples on the basis of the above criteria.

It is evident that thermocouple number 4 is preferable to numbers 1 to 3 since it permits use at higher temperatures and it possesses a higher ultimate tensile strength without being markedly inferior in the other tabulated properties. Therefore, thermocouples 1 to 3 were not considered for use in the experiments.

Thermocouples 6 to 8 were ineligible for use because the wires available commercially are too thick (see Table 2.2).

It is seen from Table 2.2, that thermocouple 4 is three times as sensitive as thermocouple 5. The former, however, has a lower maximum working temperature and a smaller ultimate tensile strength. Since it permits a higher working temperature, thermocouple 5 was chosen for mean temperature measurements: as will be explained in Sub-section 2.3.4, it is necessary to heat the thermocouple electrically, while immersed in the flame, in order to correct for radiation loss. As mentioned in the third criterion in this sub-section, sensitivity is very important for fluctuating temperature measurement and consequently thermocouple 4 was chosen for this purpose.

Thermocouple	Max. Working Temp. (^{o}K)	Sensitivity at 1400^{o}K. ($\mu V/^{o}K$)	Ultimate Tensile Strength Annealed. (Kg/mm^2)	Min. Wire Dia. Available Commercially. (μm)	Remarks on Usage in Flames at Atmospheric Pressure.	References.
1) Platinum–10% Rhodium versus Platinum	2033	12	31 14	25	Suitable in oxidising regions of flame. Sheathing of wires with refractory material required in reducing conditions.	Engelhard Data Sheet (1973).
2) Platinum–13% Rhodium versus Platinum	2032	14	35 14	25	Same as for (1) above.	Ditto.
3) Platinum–20% Rhodium versus Platinum–5% Rhodium	2063	9	41 24	25	Same as for (1) above.	Ditto.
4) Platinum–30% Rhodium versus Platinum–6% Rhodium	2093	10	47 25	25	Same as for (1) above.	Ditto.
5) Platinum–40% Rhodium versus Platinum–20% Rhodium	2123	3.3	49 41	25	Same as for (1) above.	Ditto.
6) Iridium–40% Rhodium versus Iridium	2263	5	113 112	250	Same as for (1) above. Also, catalytic effects in methane/air flames negligible.	Ditto. Smith et al, 1969.
7) Tungsten versus Iridium	2573	22	110 112	250	Not suitable for use in flames. Tungsten wire becomes very brittle after use at elevated temperatures.	Engelhard Data Sheet (1973).
8) Tungsten versus Tungsten–26% Rhenium	2873	20	110 157	500	Same as for (7) above.	Ditto.

TABLE 2.2

Relevant Properties of Thermocouple Wires

(c) Types of flame investigated and probe wire diameters

The effect of catalysis is more pronounced in a premixed flame than in a diffusion flame. The thermal inertia of the probe wire, which produces a phase lag in probe temperature relative to the gas temperature, coupled with surface catalysis can cause reaction on the wire when cold premixed fuel and air come in contact with it. But in diffusion flames at atmospheric pressure, negligible amounts of premixed fuel and air exist . Catalysis is a more severe problem in hydrogen/air flames (and hence in town gas/air flames where the fuel is mainly hydrogen) than in natural gas/air flames (the fuel is mainly methane), Smith et al. It was, therefore, decided to perform the fluctuating temperature measurements in a methane diffusion flame. It was decided to obtain mean temperature data in a town gas diffusion flame and in a town gas/air premixed flame using a probe coated with a non-catalytic ceramic.

The choice of the optimum diameter of the wire of thermocouple 4 of Table 2.2 employed for the temperature fluctuations measurement was determined from an endurance test in which 25 μm, 30 μm and 40 μm diameter wires were placed in a methane diffusion flame, Reynolds Number 14,500. A period of 2 hours was considered adequate for obtaining a profile of measurements of temperature fluctuations. Only the 40 μm diameter wire passed the test.

The spatial resolution afforded by a 100 μm diameter wire ($\approx$ 0.1 mm^3) was considered adequate for mean temperature measurement. In an endurance test performed with such a wire in a premixed town gas/air flame, Reynolds number 62,000, for a period of 12 hours the wire did not fail.

2.2.4 Probe Construction

Great care was exercised in the construction of the thermocouples. The wires were cleaned thoroughly prior to being welded in order to preclude contamination from extraneous matter and a consequent alteration of the thermo-electric calibration. After mounting the thermocouple on support wires annealing, by electrical heating, relieved stresses in the probe wire. Otherwise, if a stressed section of the wire is situated in a temperature gradient, the thermocouple might indicate erroneous readings, Zysk, 1962.

The sequence of steps in the fabrication of the thermocouples were:

(1) the cleaning of the wires

(2) formation of the thermocouple junction by flame welding

(3) annealing the thermocouple after mounting it on support wires

and (4) for the mean temperature measurements, coating the probe with a mixture of Alumina and MgO ceramic.

(a) Cleaning

The wires were first cleaned in acetone in order to remove the bulk of any organic material on their surface. The last traces of organic and inorganic impurities were eliminated by placing the wires in boiling dilute HCl for ten minutes, followed by a further cleaning of the wires in distilled water, and a subsequent immersion in boiling dilute HNO_3 for ten minutes. Finally, the wires were washed in distilled water before welding the thermocouple junction.

(b) Thermocouple Junction

Flame welding was used to form the thermocouple junction; this technique has been described in detail by Fristrom and Westenberg, 1965.

The bead sizes of the probes (especially the 40 μm diameter Platinum/30% Rhodium versus Platinum/6% Rhodium probe used for measuring fluctuating temperature) were monitored by observation of the junctions under a microscope. Moffat, 1962, has shown that for a thermocouple of junction bead diameter, D_b^*, the probe time constant, τ, (the parameter which characterizes the transient response) is increased by the factor $(\frac{D_b^*}{D^*})^{0.375}$ where D^* is the diameter of the uniformly cylindrical part of the probe. Thus, provided the junction bead diameter is less than 1.1 times the wire diameter, the increase in τ is less than 3.5%. Fig. 2.2.1 (b), a photomicrograph of a 40 μm diameter probe, shows the maximum bead size that was acceptable. It is seen that the junction beads of the probes used for fluctuating temperature measurement satisfied this requirement.

(c) Probe Mounting and Annealing

Satisfactory thermocouples were selected for mounting on support wires of the kind described by Fristrom and Westenberg, 1965. The support wires used for the 40 μm diameter Platinum/30% Rhodium versus Platinum/6% Rhodium thermocouples were of 250 μm diameter and of the same alloys. The corresponding support wires for the 100 μm diameter Platinum/40% Rhodium versus Platinum/20%

Rhodium were 500 μm in diameter. The support wires were carried in twin-bore alumina insulator tubes. Fig. 2.2.1a is a schematic of the assembled probe.

Annealing of the mounted thermocouple was accomplished by electrically heating the wire to a temperature of 1300°C for a period of three minutes as recommended by Zysk, 1962. (The electrical circuit employed for heating the probe wire and measuring its temperature simultaneously is described in Sub-section 2.4.5).

(d) Non-catalytic Ceramic Coating

Three of the various coatings which have been applied on thermocouples in order to preclude catalysis on, and chemical attack of, the probe wire are: Silica used by Fristrom and Westenberg,1965; Zirconia used by Smith et al, 1969; and a mixture of Beryllia and Yttrium oxide ceramic used by Kent, 1970. However, siliceous materials are known to form platinum silicide, when in contact with platinum alloy thermocouples, at temperatures above 1400°K (Bennet, 1961). The mixture ceramic developed by Kent was not considered for use because Beryllia is an extremely poisonous compound. In this work, an alumina-based ceramic was employed following the recommendation in the Engelhard Data Sheet for Pt/40% Rh versus Pt/20% Rh.

The latter ceramic consisted of 90% by weight alumina powdor and 10% by weight magnesium oxide. The dry mixture was ground with an agate pestle and mortar in order to produce a very fine powder; 0.5 g of the mixture was stirred into 100 cc of distilled water to form a thin cream.

The coating was applied by electrically heating the wire to 900°C and towelling it with cotton wool which had been immersed in the thin cream. Several thin coatings were applied in this manner. To ensure that the composite coating would not fail during measurements in a flame, the probe wire was electrically heated to a temperature of 1800°C, the estimated maximum probe temperature in a flame. Then the appearance and the thickness of the coating was observed with a travelling microscope.

When a smooth continuous covering was obtained, without "pin-holes", the thermocouple was tested for catalytic activity in a near stoichiometric turbulent pre-mixed town gas/air flame. The test consisted of passing the protected thermocouple from the outer edge of the flame into its cold cone. Lack of catalytic activity was indicated by the temperature of the probe falling quickly to the prevailing temperature on reaching the cold gas. The uncoated probe continued to glow red-hot when it was in the cold gas region because chemical reaction was sustained on its surface by catalysis.

2.3 Mean Temperature

2.3.1 Preliminary Remarks

The time-averaged version of equation (2.2.4), using effective property values and discarding the catalytic term, is

$$\overline{\left(aK'\frac{\partial^2 T}{\partial x^2}\right)} - \overline{\{a(T - T_f)\}} = 0 \qquad (2.3.1)$$

where $a = 1/\tau'$ and over-bars indicate time-averaging.

2.3.2 Conduction Error

According to Scadron and Warshawsky, 1952c, the time-averaged conduction error is given by $(\overline{T}_b - \overline{T}_f)\ \psi_m$ where: T_f is given by equation 2.3.1 above; T_b is the support temperature; and ψ_m = Sech $(\eta L/2)$ (for the case where the junction is at the mid-point in a sensing wire of length L) and $\eta^2 = 1/K\overline{\tau}$.

A quantitative estimate of the percentage conduction error of a ceramic coated 100 μm Platinum/40% Rhodium versus Platinum/20% Rhodium thermocouple was obtained with the probe at 30 mm from the axis in a plane 40 diameters from the burner in a turbulent diffusion flame of methane. $\overline{\tau}$ was measured as 80 ms (the method of measuring $\overline{\tau}$ is described in Sub-section 2.4.5 below); L for the probe was 2 ins; K for the probe was 1.6×10^{-2} in^2/sec. Accordingly, ψ_m = Sech $(\eta L/2) < 10^{-3}$. Thus the percentage conduction error $\left(\frac{T_b - T_f}{T_g}\right) \psi_m < .1\%$, for the case $T_b = 0$, since $T_f \approx T_g$.

2.3.3 Thermal Inertia Error

The existence of a finite probe thermal inertia does not cause an error in the mean temperature measurement. However, the variation of the thermal inertia with gas temperature and velocity, and wire properties, causes a relative displacement between the mean probe temperature and the mean gas temperature.

Chomiak and Niedzialek, 1967, obtained solutions for the relative displacement of the mean probe temperature and mean gas temperature for an infinitely long probe. The solutions depend strongly on the phase angle between the fluctuating gas temperature and the

fluctuating probe thermal inertia. In a randomly varying temperature field (such as in a turbulent flame) this phase angle is not known a priori; therefore, the solutions are not quantitatively useful in such circumstances.

A quantitatively useful expression is obtained from equation (2.3.1) without the conduction term:

$$0 = \overline{a}\,(\overline{T} - \overline{T}_f) + \overline{a'T'} - \overline{a'T_f'} \qquad (2.3.2)$$

The mean temperature thermal inertia error, ε_t, is from equation (2.3.2)

$$\varepsilon_t = \frac{1}{\overline{a}}\,(\overline{a'T'} - \overline{a'T_f'}) \qquad (2.3.2a)$$

Assuming a correlation coefficient of unity (the worst case):

$$\varepsilon_t = \frac{\sqrt{\overline{a'^2}}}{\overline{a}}\,\left(\sqrt{\overline{T'^2}} - \sqrt{\overline{T_f'^2}}\right)$$

Since $\dfrac{\sqrt{\overline{T'^2}}}{\overline{T}_g} \ll 1$ for a coated wire,

$$\frac{\varepsilon_t}{T_g} \approx -\frac{\sqrt{\overline{a'^2}}}{\overline{a}}\,\frac{\sqrt{\overline{T_f'^2}}}{\overline{T}_g} \qquad (2.3.2b)$$

Measurements of fluctuating temperature (presented in Chapter 5) indicate that $\dfrac{\sqrt{\overline{T_f'^2}}}{\overline{T}_g} \approx 10\%$, when the temperatures are in [°K].

Also, $\frac{\sqrt{\overline{a'^2}}}{\overline{a}} \approx 10\%$ since τ is principally dependent on T.

Hence $\frac{\varepsilon_t}{T_g} \approx 1\%$.

2.3.4 Radiation Error

The technique used to correct the radiation error is similar to that employed by Berkenbush, 1899, and Schmidt, 1909.

Firstly, the radiation loss calibration curve, which represents the power radiated by the probe at any temperature, was obtained. This was accomplished by electrical heating of the thermocouple and simultaneous measurement of the heating current and of the probe temperature in a high vacuum ($\sim 10^{-6}$ torr). The resulting plot of probe temperature versus electrical power per unit probe length* is shown in Fig. 2.2.2 Also plotted is $\{T_w^4 - T_{amb}^4\}$ $(^\circ K)^4$ versus electrical power per unit length of probe*: the linearity of the plot shows that radiation according to a fourth power law dissipated the supplied energy;, the emissivity of the ceramic coating (90% Al_2O_3 and 10% MgO) was calculated as 0.38.

Secondly, the thermocouple, while in the measuring position in the flame, was electrically heated and the heating current and the probe temperature were measured simultaneously. The plots of probe temperature versus electrical heating power per unit length which were obtained at various positions along the axis of a methane diffusion flame, Reynolds Number 14,500, are shown in Fig. 2.2.2.

Finally, the temperature at the point of intersection of the curve obtained in the flame and of the radiation loss calibration

*For given wire cross-sectional area.

curve is the required probe temperature corrected for the radiation loss. The energy being radiated at that temperature from the probe immersed in the flame is being supplied electrically.

However, two implicit assumptions were made in the above discussion, namely: that radiant heat interchange between the probe and flame gases is negligible; and that the effective time-mean radiating temperature of the probe in the flame is equal to the time-averaged probe temperature.

The first assumption is readily justified. The radiant energy transmitted (or absorbed) by hot gases in gas-fired, small scale laboratory flames at atmospheric pressure ("clear" flames) is small because $\varepsilon_g \ll 1$, Gaydon and Wolfhard, 1970 c.

Now, the effective time-mean radiating temperature is:

$$\overline{(\overline{T} + T')^4}$$

$$= \overline{T}^4 \left\{1 + 6 \frac{\overline{T'^2}}{\overline{T}^2} + \text{smaller order terms}\right\}$$

Since $\frac{T'}{\overline{T}} < .04$ for a ceramic coated probe in the regions of the flame where radiation loss is important, it is seen that the percentage error involved in the second assumption,

$$\frac{\overline{(\overline{T} + T')^4} - \overline{T}^4}{\overline{T}^4} < 1\% .$$

The high vacuum apparatus employed for obtaining the radiation loss calibration curve is shown in Fig. 2.2.3.

2.4 Fluctuating Temperature

2.4.1 Preliminary Remarks

The measurement of fluctuating temperature using the 40 μm diameter Platinum/30% Rhodium versus Platinum/6% Rhodium thermocouple is considered in this section. The thermocouple heat-balance equation is first simplified by showing that for the methane diffusion flame investigated, Reynolds Number 14,500, the errors associated with some of the terms of the equation are relatively small.

The simplified equation suggests the method for obtaining the gas temperature fluctuations. The instrumentation employed for this purpose is described. It is shown that the most significant source of error is the fluctuation in τ.

2.4.2 Catalytic and Radiation Error

The combined catalytic and radiation error in the fluctuating temperature measurements was estimated from data of mean temperature obtained along the axis of the flame investigated. First, a bare probe was employed, and then a ceramic coated probe with radiation loss correction. The data are plotted in Fig. 5.2. d . It is seen that the combined catalytic and radiation error is less than 5% at the maximum mean temperature.

2.4.3 Conduction Error

It was shown in Section 2.3.2 that the error caused by heat conduction to the probe support wires from a 100 μm diameter thermocouple is less than .1%. Obviously, a lower conduction error will

apply for a 40 μm diameter probe.

2.4.4 Thermal Inertia Considerations

Neglecting the conduction, radiation and catalytic terms (on the basis of the discussion in Sections 2.4.2 and 2.4.3) the probe heat-balance equation reduces to

$$\tau \frac{dT}{dt} + T = T_g , \tag{2.4.1}$$

A solution of equation 2.4.1 has been obtained by Chomiak and Niedzialek (1967) under the following circumstances:

$$T_g(t) = \overline{T}_g + \Delta T_g \sin(\omega t + \phi) \tag{2.4.2a}$$

$$a(t) = \overline{a} + \Delta a \sin(\omega t) \tag{2.4.2b}$$

$$\text{where } a(t) = 1/\tau(t). \tag{2.4.2c}$$

Over-bars indicate time-averages and ϕ is the phase difference between the gas temperature and the probe time constant.

The solution of equation 2.4.1 (Chomiak and Niedzialek) is:

$$T(t) = \overline{T}_g - \tfrac{1}{2} \Delta T_g \cdot \frac{\Delta a}{\overline{a}} \cdot \frac{n}{\sqrt{(1 + n^2)}} \sin(\phi - \arctan n)$$

A B

$$+ \Delta T_g \frac{1}{\sqrt{(1 + n^2)}} \sin(\omega t + \phi - \arctan n)$$

C

$$+ \Delta T_g \frac{\Delta a}{\bar{a}} \underbrace{\frac{n\sqrt{(n^4 + 5/4n^2 + 1/4)}}{(1 + n^2)(1 + 4n^2)} \sin\left(2\omega t + \phi + \arctan\frac{3n}{2n^2-1}\right)}_{D} \qquad (2.4.3)$$

where $n = \omega/\bar{a}$.

It is seen from equation (2.4.3), that under the conditions stipulated by equations (2.4.2 a,b,c) the probe temperature fluctuation consists of <u>two</u> components:

(1) The first harmonic term; term C. It is independent of Δa. The variation with n of its amplitude relative to the amplitude of the gas temperature fluctuation is depicted in Fig. 2.4.2. The correction for the amplitude attenuation with increasing frequency is discussed in Sub-section 2.4.5.

(2) The second harmonic which is extraneous, term D. This term arises because of the non-linearity of equation 2.4.1 when τ is a function of time. The variation with n of its amplitude relative to the amplitude of the gas temperature is shown in Fig. 2.4.2. The error caused by this term in the compensated probe signal is estimated in Sub-section 2.4.6.

Term B is the relative displacement of the probe mean temperature with respect to the mean gas temperature, (term A). This error term has been discussed under "mean temperature ", section 2.3.

2.4.5 <u>Compensating and Probe Heating Circuits</u>

As discussed in the preceding Sub-section, of the two components of the probe response to a sinusoidally varying gas temperature, the first harmonic component has the same frequency as that of the gas.

Therefore, it is the only required component: its attenuation at high frequencies depicted in Fig. 2.4.2 can be corrected. Since this component is independent of time constant fluctuations the relevant form of equation 2.4.1 is

$$\bar{\tau} \frac{dT(t)}{dt} + T = T_g \qquad (2.4.4)$$

The principles of probe thermal inertia compensation have been described in detail by Shepard and Warshawsky, 1952. In brief, compensation is achieved by use of a circuit which performs upon the thermocouple e.m.f., E, the operation:

$(\bar{\tau} \frac{dE}{dt} + E)$ to obtain E_g the e.m.f. of the thermocouple at the gas temperature.

The method for determining the probe time constant was similar to that employed by Kunugi and Jinno, 1959. The thermocouple, when in the measurement location, was heated by an alternating current at 50 kHz and the mean thermocouple temperature was measured simultaneously. Heating was by alternating current in order that the time-averaged Thomson and Peltier effects would be zero. (Heat is generated in a wire by the Thomson effect at a rate proportional to the current and to the temperature gradient. When a current flows across the junction of two dissimilar metals, depending on the direction of current flow, heat is liberated or absorbed at the junction by the Peltier effect). The heating circuit is shown in Fig. 2.4.3.

Including the electrical heating term, ϑI^2, in equation (2.4.4) and time-averaging, $\bar{\tau}$, $\bar{T}$, $\bar{T}_g$ and $\overline{I^2}$ are related by:

$$(\overline{T}_g - \overline{T})/\overline{\tau} + \vartheta \overline{I^2} = 0 \qquad (2.4.5)$$

where $$\vartheta = r/\rho C \omega^{*2} \qquad (2.4.6)$$

where r, ρ, C and ω^* are the electrical resistivity, density, specific heat and cross-sectional area of the wire respectively. The values of the specific heat and resistivity of the wire at $\overline{T}$ were obtained from the International Critical Tables and the Engelhard Data Sheet for the thermocouple. By applying two values of heating current, $\overline{\tau}$ was determined by eliminating $\overline{T}_g$.

Compensation for thermal inertia was achieved by means of a differentiating active filter. The compensating circuit is shown in Fig. 2.4.4, and its design is described in Appendix A. There is provision for matching the compensator time constant with the local probe time-averaged time-constant. The frequency response curves of the compensator and the compensated thermocouple are shown in Fig. A.7 It is seen that the performance was satisfactory up to 10 kHz.

Figs. (2.4.5 a to e) illustrate qualitatively the effect of compensation on the probe signal. It is seen that there is a phase difference between the compensated and the uncompensated signals.

2.4.6 Magnitude of Second Harmonic Error

An expression for the second harmonic error $\varepsilon(2\omega)$ at first harmonic frequency ω is obtained by substituting T(t) from equation (2.4.3) in equation (2.4.4) and subtracting $T_g(t)$ in equation (2.4.2a):

$$\varepsilon(2\omega) = \Delta T_g \cdot \frac{\Delta a}{a} \cdot n \frac{\sqrt{(n^4 + 5/4n^2 + 1/4)}}{(1 + n^2)(1 + 4n^2)} \sin\left(2\omega t + \phi + \arctan \frac{3n}{2n^2 - 1}\right)$$

$$+ 2\Delta T_g \cdot \frac{\Delta a}{a} \; n^2 \frac{\sqrt{(n^4 + 5/4n^2 + 1/4)}}{(1 + n^2)(1 + 4n^2)} \cos\left(2\omega t + \phi + \arctan \frac{3n}{2n^2 - 1}\right) \qquad (2.4.7)$$

A plot of $\varepsilon(2\omega)$ as a function of ω is shown in Fig. 2.4.6 for $\bar{\tau}$ = 10 ms, and $\Delta a/a$ = 0.7% (The worst case from observed temperature fluctuations).

An estimate of the magnitude of the second harmonic error was calculated to be ±15% using Fig. 2.4.6 and a measured spectral density of the kind shown in Fig. 5.2g.

2.5 Concluding Remarks

The principal points contained in this chapter are:

(1) A bare 40 μm diameter Platinum/30% Rhodium versus Platinum/6% Rhodium thermocouple was chosen for fluctuating temperature measurements. These measurements were made in a methane diffusion flame rather than in a premixed flame or in a town gas flame because catalytic effects are, comparatively, least in the first-mentioned.

(2) The thermal inertia of the fluctuating temperature probe was compensated up to a frequency of 10 kHz using an active filter. The maximum error associated with the thermal inertia fluctuations was estimated as $\pm$ 15%. The combined catalytic and radiation loss error was estimated to be less than + 0, - 5%.

(3) A 100 μm diameter Platinum/40% Rhodium versus Platinum/20% Rhodium thermocouple coated with a non-catalytic ceramic mixture (90% Al_2O_3 and 10% MgO) was used for the mean temperature measurements in town gas diffusion and town gas/air premixed flames.

(4) The significant error in the mean temperature measurements, the radiation loss error, was corrected for by using an in vacuo calibration method.

CHAPTER 3

ION CONCENTRATION AND CHEMI-LUMINESCENCE MEASUREMENT TECHNIQUES

3.1 Introduction

3.1.1 Preliminary Remarks

Copious amounts (typically $\sim 10^6/[\text{mm}]^3$ at atmospheric pressure) of free electrons and positive ions, such as H_3O^+ and CHO^+ exist in hydrocarbon/air reaction zones by virtue of the lack of chemical equilibrium. This phenomenon is frequently referred to as chemi-ionisation or ionisation. Radicals, such as CH*, C_2^*, OH*, also occur in the reaction zone. These have high electronic excitation levels and emit, in characteristic bands, radiation known as chemi-luminescence which is considerably stronger than thermal radiation.

Detailed knowledge of the fundamental processes involved in these phenomena is still lacking. However, it is known that the life times of the electronically excited states of CH*, C_2^*, OH* are 10^{-8} to 10^{-6} sec. (Bulewicz, 1967), and that the recombination time of ions is about one order of magnitude longer (Chomiak, 1972). Therefore diagnostic techniques based on ionisation or on chemi-luminescence possess adequate frequency response when used to study fluctuations, time-scale $\sim 10^{-4}$ sec, in turbulent flames (c.f. spectral measurements by Guenther and Simon, 1969).

3.1.2 Previous Work

(a) Ionisation Technique

Karlovitz et al (1953) introduced the use of the electrostatic probe for measuring positive ion concentrations in turbulent flames.

They analysed the signal from the probe in a free turbulent premixed natural gas/air flame to obtain the frequency with which the "flame surface" passes, and the probability of finding it in the measurement location. They tested many probes. Their probes consisted of negatively-biased bare wires (0.05 cm to 0.08 cm. dia.), carried in insulating ceramic tubes, with parts of the wires (from a few mm to 3 cm) exposed to the flame. However, their measurements were of limited accuracy because the probe, not being streamlined, disturbed the flame markedly (Denniston et al (1957)). This factor caused their data, at any given radial position, to be dependent on whether or not the probe had traversed the flame axis.

Other investigators (see for example, Summerfield et al (1955); Richmond et al (1956); Vlasov (1959); and Kliene (1971)) have employed the ionisation probe, similar to that of Karlovitz et al, for investigating the structure of turbulent flames. In particular, the probes used by these workers were also not streamlined.

b. Chemi-luminescence Technique

Guenther and Simon (1969) measured the total emission (caused by chemi-luminescence) using an optical probe in a free turbulent diffusion flame of city-gas. They measured the spectral functions and macro-scales of the emission fluctuations. Their probe was designed to minimize flow disturbance. The radiation penetrated through a hollow water-cooled cone (included angle 12^{o}), at right angles to the flow direction, to a system of lens and diaphragm and to a photomultiplier. The photomultiplier converted the radiation

signal into an electrical signal.

Chomiak (1972) used an optical probe to measure chemi-luminescence in a turbulent pre-mixed propane/air flame. The aim was to resolve the validity of the "wrinkled laminar flame" concept. He measured the intensity of chemi-luminescence in the turbulent flame and in laminar flames and concluded that no laminar flame existed in the turbulent reacting flow he studied. The probe he employed was essentially a microscope which was focussed in the measurement location to collect the radiation from this region. The probe had a 40 mm viewing distance and a depth of focus of about 4 mm.

Recently, Kuhnert and Guenther (1973) employed a cross-correlation technique to measure the spectral density and the macro-scale of fluctuating OH* chemi-luminescence. In this technique, the signals along two different light paths are the two inputs to a correlator: only the radiation signal emanating from a small region ($\sim$ 0.5 cm dia.) are in phase; the correlator eliminates other signals leaving the signal from this small region for subsequent processing.

3.1.3 Comments on Previous Work

At the inception of this research programme, the chemi-luminescence techniques of Chomiak, and Kuhnert and Guenther had not been introduced.

The ionisation probe was chosen in preference to the probe of Guenther and Simon because of its better spatial resolution (wire diameters of .2mm in comparison to viewing ranges of 5mm). It was decided to improve the ionisation probe design by streamlining it, and by cooling the insulation of the negatively-biased wire.

3.1.4 Scope of Remainder of Chapter

A simplified description of the principle of operation of the ionisation probe is presented in Sub-section 3.2.1. The requirements of the probe are outlined in Sub-section 3.2.2. The fabrication of the probe is described in Sub-section 3.2.3. The electronic circuit, designed and constructed for measuring the probe signal, is described in Sub-section 3.3.1. The need to square the probe signal is explained in Sub-section 3.3.2. In Sub-section 3.3.3 the effect of varying the comparator discrimination level is shown to imply a need to arbitrarily define the occurrence of combustion in the present measurements. Ways of improving the present technique, and an alternative technique based on chemi-luminescence are briefly discussed in Sub-sections 3.4.1 and 3.4.2 respectively. The principal conclusions in this chapter are summarized in Section 3.5.

3.2 Ionisation Probe

3.2.1 Principle of Operation

The principle of operation of the ionisation probe has been treated in great detail in the literature (see for example: Johnson and Malter, 1950; Travers and Williams, 1965; Clements and Smy, 1969). Therefore, only a brief exposition is presented here.

Consider the system shown schematically in Fig. 3.2a. It consists of probes A and B, immersed in an ionised gas, between which a variable voltage, V_d, is applied. Three conditions may be distinguished.

(1) V_d equals zero. Each probe is at the same floating potential. Current i_d equals zero since no potential drop exists in the circuit. This condition corresponds to point 0 in Fig. 3.2. b.

(2) $0 < V_d \leq 2\ kT_e/e$ where k is the Boltzman constant, T_e the electron temperature and e the electron charge. $2kT_e/e$ is a measure of the potential barrier which even the most energetic electrons cannot cross. Probe B approaches, while probe A departs from the ionised gas potential. Probe B collects more electrons, and probe A collects fewer electrons but more positive ions. The total electron current to the probes equals the total positive ion current. This corresponds to point j in Fig. 3.2. b.

(3) $V_d \gg kT_e/e$. Probe B approaches more closely the space potential and probe A is now so negative that it repels even the most energetic electrons. The total electron current is, again, equal to the total positive-ion current. The positive ion current to probe A is determined by the number of positive ions in the sheath surrounding it. When $V_d \gg kT_e/e$, small changes in V_d do not appreciably affect the ion current to probe A which is then said to be in positive ion saturation. This situation corresponds to the portion k-l in Fig. 3.2.b.

The probe used in this investigation was operated in the positive ion saturation region, $V_d \gg kT_e/e$, in view of the following advantages:

(1) spurious electron current effects do not exist (Clements and Smy, 1969);

(2) currents are much higher, and so easier to measure than otherwise (Clements and Smy, 1969);

(3) detailed theoretical and empirical knowledge exists for the case of a moving ionised gas.

Empirical relations between probe current i_d, bias voltage V_d, ionised gas velocity U, electron density n_e have been obtained by Clements and Smy, 1969. They are as follows:

i_d proportional to $(U)^{0.6 \pm 0.1}$ for equal positive ion and electron temperature (3.2.1)

i_d proportional to $(V_d)^{0.65 \pm .05}$ (3.2.2)

i_d proportional to $(n_e)^{0.8 \pm 0.1}$ (3.2.3)

Equations (3.2.1) and (3.2.3) were used to compare the ionisations in turbulent flames and laminar flames in Chapter 5.

3.2.2 Requirements of Probe

Desirable attributes of the ionisation probe are: (1) Minimal aerodynamic, thermal and chemical disturbance of the flame; and (2) a good spatial resolution ($\sim$ 1 mm^3). The probe which was designed and fabricated to fulfil these requirements is best described by reference to Fig. 3.2c.

The probe components are:

(1) A 300 μm diameter 40% Rh/Pt sensing wire with a pointed tip for measurement; the negative terminal of the 22V bias battery is connected to the other end of the wire.

(2) A composite boron nitride and brass cone.

(3) A water cooling jacket soft-soldered to the brass end of the composite cone to achieve good thermal contact.

(4) A silicone rubber tube for insulating the portion of the probe wire which is carried in the central tube of the cooling jacket.

Boron nitride was used in the composite cone because of its physical and chemical properties. It is inert to the chemical reactions in the flame; it is easily machined; it remains a good electrical insulator at high temperatures; and it is a good thermal conductor (for a ceramic) so that it was easily cooled by the water jacket. Cooling the boron nitride insulator was essential: there was appreciable leakage current when an uncooled quartz supported probe with a boron nitride end cone was used in turbulent flames.

Minimal aerodynamic disturbance of the flame was ensured by making the wire tip sharply pointed, and by making the included angle of the composite cone small (25^{o}).

Elimination of chemical disturbance of the flame in the region of the wire tip was achieved by: the use of boron nitride which is inert to chemical reactions in the flame as the insulator; and the use of Platinum/40% Rhodium wire which is known to have negligible catalytic activity when biased negatively in hydrocarbon/air flames (Calcote (1963)). Lack of chemical disturbance was confirmed by the fact that when the probe was passed from the combustion products side of a turbulent premixed town gas/air flame to the cold core, the probe wire tip did not continue to glow and no signal was obtained.

Thermal disturbance of the flame was negligible because at high bias (condition (3) in Sub-section 3.2.1; $e V_d/kT_e \sim 10^2$ in the

present measurements; V_d = 22 V, $T_e \approx 2400^{\circ}K$) the electrical sampling of ions by the probe is very fast compared to the convection process. For example, ion drift velocities in the sheath are about 10^4 m/sec, (Clements and Smy, 1969), two orders of magnitude faster than the gas velocities in the measurements.

The spatial resolution was estimated to be .3 $[mm]^3$, from the fact that: (1) the sheath thickness of the probe wire was about 1.5 times the wire radius (Clements and Smy, 1969); and (2) the exposed wire was 2 mm long.

3.2.3 Fabrication

(a) Probe wire

A suitable length of 40% Rh/Pt wire was annealed by electrical heating. Burrs were removed with a file from the end to be shaped to a point. The wire was held in a pin chuck so that the cleaned end protruded by 3 mm. The pin chuck (with the wire) was mounted in a lathe and rotated at 1200 r.p.m. A No. 4 Arkansas stone lubricated with oil was used to sharpen to a point the protruding end of the wire by gently pressing from underneath. The wire tip was observed at intervals with a magnifying glass and when a satisfactory point was obtained, a very smooth Arkansas stone was used to polish the tip. A photomicrograph of a typical wire tip is shown in Fig. 3.2d.

(b) Composite boron nitride and brass cone

A number 6 BA thread and tap were made on the boron nitride and brass respectively, and the composite piece assembled. The brass end

was held in the lathe, and turned at 1200 rpm. After centre drilling the boron nitride end, a No. 80 drill was held in a hand-chuck and fed, by hand, slowly into the boron nitride. The drill was removed frequently for cleaning. After drilling the hole, the 25^{o} included angle cone was cut on the composite piece. Fig . 3.2 e shows a sketch of the composite cone.

(c) Silicone rubber insulator and central tube

The insulating silicone rubber, see Fig. 3.2c, was .055" o.d. Silicone rubber was chosen because of its ability to withstand the temperature of soft solder (during probe assembly).

The central tube consisted of a half meter length of stainless steel tube, 2.4 mm o.d., 1.8 mm i.d., bent 8 cm from one end. The tube was cleaned and tinned with soft solder.

(d) Water cooling jacket

The water cooling jacket consisted of 5 stainless steel hypodermic tubes 1 mm o.d. soft-soldered on the central tube (c above). Each tube was bent and folded back on itself at its midpoint (while red hot), Fig. 3.2f. The five bent tubes were thoroughly cleaned with a needle file to facilitate the soft soldering of them on to the central tube. The diameter of the water cooling jacket, Fig. 3.2g was 5 mm. The ends of the stainless steel tubes were connected to inlet and outlet manifolds for the cooling water.

(e) Probe assembly and testing

The probe was assembled as shown in Fig. 3.2c. The assembled probe was dried in an oven, set at 120°C and containing silica gel, for 48 hours in order to expel any liquid absorbed by the boron nitride during the probe fabrication. Moisture adversely affects the electrical insulating properties of boron nitride. The electrical resistance between the probe wire and the water cooling jacket was tested with a Solartron LM 1240 multimeter: a resistance exceeding 20 MΩ - the highest range of the multimeter - indicated that the probe insulation was satisfactory.

3.3 Instrumentation

3.3.1 Electronic Circuit

The diagram of the electronic circuit designed and constructed for measuring the probe signal is shown in Fig. 3.3a. The circuit consists of two parts:

One part pertains to the measurement of the mean, rms, spectral density and probability density of the probe signal. (The instrumentation used for signal processing is described in Chapter 4). The essential components in this part are: a 1 kΩ resistor for converting the probe current into a voltage; a pre-amplifier (Model AD 41K) connected in the differential mode with an amplification of 100; and an amplifier (Model AD45K) connected in the inverting mode with an amplification of 100. The frequency response of the pre-amplifier and amplifier was flat from DC to 30 kHz.

The other part pertains to the evaluation of the probability of combustion, p, and the combustion count, f (p is the fraction of time

combustion occurs at a point; f is the time-averaged number of times combustion occurs per second) and the instrumentation used for signal processing is described in Chapter 4 . The essential components of this part are: a high accuracy multiplier (Model AD427) for squaring the probe signal (the reason for squaring the signal is explained in the Sub-section 3.3.2); and a comparator (model AD 351J) for producing pulses of fixed amplitude when the squared probe signal exceeds a pre-determined level. The effect of the pre-determined level which is set for the comparator on the measured frequency and probability of combustion is discussed in Sub-section 3.3.3. There were impedance matching buffers before the multiplier and the comparator, and after the comparator.

3.3.2 Need to Square the Probe Signal

The probe signal was squared in order to simulate, approximately, the reaction rate of H_3O^+ ions which are the predominant positive ions in Hydrocarbon/air flames, (Calcote (1962)). This simulation is seen from the following consideration :

The probable recombination process is (Calcote (1962)):

$$H_3O^+ + OH^- \longrightarrow \text{products} \qquad (3.3.1)$$

or

$$H_3O^+ + e^- \longrightarrow \text{products} \qquad (3.3.2)$$

The concentration of the positive charges $\approx [H_3O^+]$ must equal the total concentration of negative charges $[n^-]$. Now, the total concentration of negative charges consists primarily of the concen-

tration of electrons, $[e^-] = (1 - \alpha)[n^-]$, say, and the concentration of hydroxyl ions, $[OH^-] = \alpha[n^-]$. From the stoichiometry represented by equations (3.3.1) and (3.3.2), it is seen that substituting the expressions for $[OH^-]$ and $[e^-]$ in the equations and adding them, results in:

$$[H_3O^+] + [n^-] \longrightarrow \text{products} \qquad (3.3.3)$$

Since

$[H_3O^+] = [n^-]$, it is evident that the recombination rate of H_3O^+ is $[H_3O^+]^2$. Thus, it does not matter that the reactions (equations (3.3.1) and (3.3.2)) occur concurrently.

Recalling that the probe current is proportional to ion concentration to the power (0.8 ± 0.1), equation (3.2.3), it is seen that squaring the probe signal approximately simulates the recombination rate of the H_3O^+ ions.

A comparison of the probe signal before and after squaring is shown in Fig. 3.3b. It is seen that, as expected, the effect of squaring is to increase the magnitude of a large probe signal relatively more than a small signal.

3.3.3 Effect of Comparator Discrimination Level

The function of the comparator was to convert the peaks in the squared probe signal into pulses: thus, when the recombination rate of H_3O^+ ions exceeded a pre-set value, a pulse of fixed amplitude was obtained. Traces of the squared signal and the comparator output are shown in Fig. 3.3c.

Ideally, the comparator should trigger a pulse when the squared probe signal exceeds zero. However, because of electronic background noise, and especially because of low frequency drift of the outputs of the circuit components, a finite discrimination level was necessary. Fig. 3.3d shows the effect of varying the discrimination level on the measured probability of combustion and the combustion count at a point in a turbulent town gas diffusion flame.

It is evident that the discrimination level has an effect on the probability of combustion, p and the combustion count, f —(p and f were defined in Sub-section 3.3.1). Therefore, the existence of combustion has to be defined in an arbitrary way. In this investigation combustion was considered to occur when the square of the probe current exceeded 4.5 mV; this discrimination level was the smallest that could be set without spurious comparator triggering caused by electronic noise. Typically, the maximum squared signal obtained was .2V.

The dotted curves in Fig. 3.3d are extrapolations of the curves through the measurements not influenced by spurious noise triggering. It is seen that the differences between the values of the probability of combustion and the combustion count at a discrimination level of 0 mV (the ideal case) and 4.5 mV (the value used in the measurements) was of the order of 10%. Therefore, the measured probability of combustion and the combustion count though based on an arbitrary definition of combustion are useful for defining the limits of the reaction zones in turbulent flames.

3.4 Suggestions for Future Work

3.4.1 Improvements in the Present Method

An obvious way to improve the present method is to employ electronic components with improved noise characteristics when they become commercially available. In this way, the discrimination level for the comparator could be set closer to zero. This would result in the discrepancy between the measured values of the probability of combustion and of the combustion count, and the values of these quantities for the ideal case of zero discrimination level, to be less than the present 10%.

Furthermore, graphs such as Fig. 3.3c should be obtained at all measurement positions in the reaction zone and the curves through the measurements that are free of noise effects extrapolated to zero as in the figure. This would improve the accuracy of the measurements.

3.4.2 Other Methods

The use of the optical chemi-luminescence probe, Chomiak (1972), is advocated because it has the following advantages in comparison with the ionisation technique:

(1) No object is introduced into the flame. Thus the processes occurring in the reaction zone are not disturbed in any manner.

(2) Individual radical concentrations may be measured by use of appropriate optical filters. Measurements of this kind are useful for validating combustion prediction procedures when they are developed for predicting the formation of pollutants (NO, C)

in turbulent flames. It is necessary for such procedures to consider the detailed chemical kinetics of the formation of radicals.

(3) A direct proportionality exists between the probe signal and the radical concentration independent of gas flow velocity. This permits a more accurate interpretation of the probe signal.

(4) The chemi-luminescence process is at least an order of magnitude faster than the ion recombination process, Chomiak (1972). Thus this probe has a better temporal resolution than the ionisation probe.

However, a disadvantage is that it has a poorer spatial resolution than the ionisation probe used in the present measurements ($\sim$ 1 mm^3 compared to 0.3 mm^3).

3.5 Concluding Remarks

An ionisation probe suitable for local measurements of ion concentration has been reported. The description of the electronic circuit for processing the probe signal in order to obtain the mean, rms, spectral density and probability density of the ion concentration fluctuations has been presented. The need to square the probe signal in order to obtain the probability of combustion and the combustion count is explained. It has been shown that the occurrence of combustion required arbitrary definition because of electronic noise. Methods of improving the present technique are described. The chemi-luminescence

optical method is considered a good alternative technique for obtaining data on radical fluctuations in turbulent flames.

CHAPTER 4

EXPERIMENTAL PROGRAMME

4.1 Introduction

This chapter is devoted to the experimental programme. The following are presented: the description of the experimental rig; the block diagrams of the instrumentation required (including those described in detail in Chapters 2 and 3), and the procedures used for obtaining data from the signals of the thermocouples and the ionisation probe. The chapter contains four additional sections:

Section 4.2 is concerned with the experimental rig. The diffusion flame and the premixed flame burners are described. The motives for choosing the burners and the flow Reynolds numbers are explained. Also, the measures taken to minimise aerodynamic disturbance of the flames are described.

Section 4.3 is pertinent to the measurement of fluctuating temperature. The items of equipment employed for obtaining the mean, the rms, the spectral density and the probability density of the fluctuating temperature, as well as the procedures for evaluating the last two quantities, are described.

Section 4.4 is connected with the measurement of fluctuating positive ion current. Mention is made of the items of equipment used for obtaining the mean, the rms, the spectral density and the probability density of the fluctuating ion current, and also of the procedures for evaluating the last two quantities. The items of equipment and the procedures are

identical to those employed in Section 4.3 for the fluctuating temperature. In addition, the instrumentation and the procedures employed for deriving the combustion count and the frequency of combustion from the square of the positive ion current signal are described.

The principal parts of this chapter are summarized in Section 4.5.

4.2 Experimental Rig

4.2.1 Choice of burners and Reynolds numbers

Parabolic procedures which are used for predicting jet flames require the specification of the initial profiles of the mean and the fluctuating components of velocity, temperature and species concentrations. A parabolic procedure which is applicable to two-dimensional flows, is easy to apply and is very economic of computer time was developed by Patankar and Spalding (1970). It was decided to perform measurements in a simple flow geometry which could be calculated with this procedure.

Accordingly, long, circular, vertical-tube burners were chosen in order to obtain simple axisymmetric free flames with well defined initial profiles in stagnant surroundings. The initial temperature and species concentration profiles are, of course, uniform for diffusion flames on large diameter burners (except for a thin region near the rim of the burner). This condition also applies to premixed flames if adequate mixing of fuel and oxidant occurs in the delivery pipe. Furthermore, the initial profiles of the mean and the fluctuating components of velocity are available in the literature for fully-developed pipe flow. Laufer (1953) and Coantic (1967) made detailed measurements (at the Reynolds

numbers of 5×10^4 and 5×10^5; and 5×10^4, 1.8×10^5, 3.2×10^5 and 4.5×10^5) of the mean and the rms of fluctuating velocity in fully developed pipe flows. The minimum developing region recommended for turbulent pipe flow is 40 diameters Hinze (1959a). In order to ensure fully-developed velocity profiles, the burner tubes were greater than 40 diameters in length in this investigation.

Ideally, fully turbulent jet flows free from Reynolds number effects are obtained for Reynolds numbers greater than 10^5, Hinze (1959b). However, for practical purposes jet flows may be considered fully turbulent for Reynolds numbers of about 17,000 and greater, Hinze (1959c). The diffusion flame of methane had a Reynolds number of 14,500; thus it was a borderline fully turbulent flow. Nevertheless, this flame was employed because it was the highest Reynolds number methane flame that could be stabilized with a reasonably small hydrogen pilot flame (less than 1% of main flow). The town gas diffusion flame, Reynolds number 24,000, and the town gas-air premixed flames, Reynolds number 62,000 (and equivalence ratios 0.91 and 1.16) were fully turbulent for practical purposes.

4.2.2 Description of burners

(a) Diffusion flame burner

Fig. 4.2a shows the details of the burner used for the methane and town gas turbulent diffusion flames. The burner tube was seventy five diameters in length, and 5 mm i.d. Measurements made with a

travelling microscope revealed that the cross-section was symmetrical.

(b) Premixed flame burner

Fig. 4.2b illustrates the premixed flame burner. The burner tube was fifty diameters in length and 29 mm i.d. Its cross-section was symmetrical.

For safety reasons, a grade E sintered bronze disc was used at the upstream end of the burner tube. Experiments by Egerton et al (1953) have shown that grade E sintered bronze discs are satisfactory for arresting hydrogen/air explosions. Therefore, such a flame trap was certainly safe for use in town gas/air flames since the town gas contained methane in addition to hydrogen.

The length of pipe provided for mixing of fuel and oxidant was greater than 400 diameters thus ensuring a uniform mixture at the burner pipe exit.

4.2.3 Flow rate measurement and Reynolds number calculations

All the gas flows were metered by flow meters of the Rotameter type calibrated by the manufacturers. The calibrations were checked against a large (65 mm diameter) wet bubble flow meter: the agreement was better than $\pm$ 0.5%.

The fuel-gas compositions* as well as the property values used to compute the flow Reynolds numbers of the town gas flames were obtained

---

* Included in the section "Figures, and fuel compositions and properties for Chapter 5."

(each day) from the town gas manufacturers, the North Thames Gas Board. The maximum and minimum concentrations* of the constituents of the industrial grade methane (methane, 97.7% min.) employed in the experiments were provided by the fuel suppliers, the Greater London Council.

4.2.4 Flame traverse, flame axis location, and flame screening

(a) Flame traverse

During measurement, each burner was moved relative to the probe on a three-dimensional traverse mechanism. Traverses of 0.01 mm increments could be made along two perpendicular axes in the horizontal plane, and 1 mm increment along the vertical axis.

(b) Location of flame axis

In Fig. 4.2c is a photograph of the device used to facilitate the positioning of the probe on the flame axis. The device was made on a lathe, and it comprised a cylindrical portion and a conical portion with a pointed tip: the cylindrical and conical portions had a common axis.

The cylindrical section of the device was inserted in the exit of the burner. Then the tip of its conical section and the probe were viewed along two lines at right angles with cathetometers. The movements required to position the probe above the cone tip were made by traversing the burner in the horizontal plane.

Measurements of profiles, at 20 and 80 diameters, of the mean

---

*Included in the section "Figures, fuel compositions and properties for Chapter 5".

and the rms of fluctuating positive ion current indicated that the diffusion flames were symmetrical and vertical. The visible flame lengths of the methane and town gas flames were 200 and 120 diameters respectively. The rich premixed town gas-air flame, equivalence ratio 1.16, visible flame length 13 diameters, was similarly found to be vertical and symmetrical from the measured profiles at 2 and 8 diameters.

(c) Flame screening

Considerable care was taken to prevent the disturbance of the flames by draughts. An open-top cloth tent (4m wide x 8m long x 4m high) was erected in the laboratory. Furthermore, the burners were placed inside a fine steel wire mesh screen (1.5 m wide x 3m long x 4m high) situated inside the tent.

4.3 Temperature Measurement

4.3.1 Mean temperature apparatus

The arrangement of the apparatus is shown schematically in Fig. 4.3a and it consisted of: (1) a ceramic coated Rhodium 20%/Platinum versus Rhodium 40%/Platinum thermocouple 100 μm diameter; (2) a power amplifier, type Sinclair Z50, operated at 50 kHz; (3) a signal generator, type Advance H-I, which provided, the 50 kHz signal for the power amplifier; (4) an ammeter, Solatron LM 1240 for measuring the current for heating the probe; (5) a low-drift amplifying unit with a low-pass filter characteristic for amplifying the

thermocouple emf (details in Appendix A.3.3); and (6) a DISA true integrator whose output was displayed on a Solartron DVM Type 1420.2.

4.3.2 Fluctuating temperature apparatus

(a) Time constant determination

The electronic apparatus used to determine the time constant of the fluctuating temperature probe (Rhodium 6%/Platinum versus Rhodium 30%/Platinum thermocouple, 40 μm diameter) is identical to that shown schematically in Fig. 4.3a and described in sub-section 4.3.1 above.

(b) Fluctuating temperature data

The apparatus used is shown schematically in Fig. 4.3b and it consisted of: (1) the 40 μm diameter Rhodium 6%/Platinum versus Rhodium 30%/Platinum thermocouple; (2) the amplifying unit, a high turns ratio, 330:1, Gardners Electronic transformer; (3) the thermal inertia compensator, an active filter; and (4) the signal processing instruments.

Fig. 4.3c shows a photograph of the compensating active filter (left of photograph), the Gardners Electronic Transformer and a probe (bottom right hand corner of photograph).

The signal processing equipment consisted of: (1) a Solartron Time Domain Analyser for obtaining the rms of the probe signal; (2) a General Radio Sound and Vibration Analyser Type 1564-A and a DISA rms meter for measuring the Spectral Density; and (3) a PDP8 unit for digital sampling of the compensated probe signal in connection with the evaluation of the probability density.

4.3.3 Evaluation of the Spectral Density and the Probability Density of temperature

The procedures for evaluating the spectral density and the probability density of the temperature fluctuations are described in this sub-section. (These procedures were also used for the fluctuating ion current mentioned in sub-section 4.4.2 below).

The steps in the spectral density evaluation were as follows:

(1) The General Radio Analyser was switched to the all pass mode. In this mode its frequency pass band is 2.5 Hz to 25 kHz; i.e. it passes through most of the probe signal. The rms, $\sqrt{\overline{e}_a}$, of the Analyser output was measured with a DISA rms meter.

(2) The Analyser was then switched to the $\frac{1}{10}^{th}$ octave mode. In this mode the Analyser could be tuned to any frequency, f_c, such that it passes only signals in a narrow pass band Δf_c given by $\Delta f_c = (2^{\frac{1}{20}} - 2^{-\frac{1}{20}}) f_c$. The rms, $\sqrt{\overline{e}_f}$, of the signal passed was measured.

(3) The spectral density, F, at frequency f_c was obtained from

$$F = \overline{e}_f / \Delta f_c \ \overline{e}_a$$

The probability density of the temperature fluctuations was obtained as follows:*

(1) The amplitude of the signal was divided into 128 equal segments.

(2) Samples of the probe signal were taken in these segments at the

---

*This measurement system with the PDP8 (and the associated computer programmes) was developed by Mr. M. Ribeiro of the Mechanical Engineering Department, Imperial College, London. He has compared the rms of a signal derived from its probability density obtained using this system with the rms of the signal measured with a Solartron Time Domain Analyser and the agreement was excellent (better than ± 1%), Ribeiro (1973).

rate of 20,000 per second over a period of 2 minutes.

(3) The PDP8 provided a data print out (on paper tape) of the number of samples taken in each segment.

(4) The data was used as input into a computer programme for evaluating the probability density, the mean, and the rms of the temperature fluctuations.

4.4 Ionisation Measurement

4.4.1 Ionisation measurement apparatus

The apparatus used for obtaining the fluctuating positive ion current data is shown schematically in Fig. 4.4a - and it consisted of: (1) the ionisation probe; (2) the signal pre-amplifying, amplifying squaring circuit, and comparator circuit; (3) the probe signal processing equipment; and (4) the comparator output signal processing equipment.

Fig. 4.4b is a photograph of the probe signal pre-amplifying, amplifying and squaring circuit and an ionisation probe (foreground of the photograph).

The probe signal processing equipment was the same as that used for the fluctuating temperature, sub-section 4.3.2b, namely: (1) a Solartron Time Domain Analyser for measuring the mean and the rms of the probe signal; (2) a General Radio Sound and Vibration Analyser type 1564-A and DISA rms meter for spectral density measurements; and (3) a PDP8 unit for digital sampling of the probe signal in connection with the probability density measurement.

The comparator output signal processing equipment consisted of:

(1) a Verner Counter Type 15A6636/2 for obtaining the Combustion Count, f, (which is the time-mean number of times combustion occurs per second); and (2) a Solartron Time Domain Analyser for measuring the probability of combustion, p, (which is the time-averaged fraction of time combustion occurs).

4.4.2 Evaluation of the spectral density and the probability density of ion current

The procedures for evaluating the spectral density and the probability density of the fluctuating ion current are identical to those employed for the temperature fluctuations: these procedures were described in sub-section 4.3.3.

4.4.3 Evaluation of the combustion count and the probability of combustion

(a) Combustion count

The combustion count, f, was obtained simply by recording the number of pulses from the comparator with the Verner Counter over a known time period. A period of three minutes gave repeatable results (± 1%) within the flame reaction zone: but counting for at least five minutes was required at the "edge" of the flame reaction zone.

(b) Probability of combustion

The probability of combustion, p, was obtained from the time-average of the comparator output signal, $\overline{C}^*$ according to the relation:

$$p = \frac{\overline{C}^* - C_L^*}{C_H^* - C_L^*} \qquad (4.1)$$

where: C_L^* is the low signal output of the comparator (0.02V) and corresponds to values of the squared probe signal (input to comparator) less than the comparator discrimination level (see Fig. 4.4c);

C_H^* is the high signal output of the comparator (10.00V) and corresponds to values of the squared probe signal greater than the comparator discrimination level (see Fig. 4.4c).

That equation (4.1) gives the probability of combustion is readily seen from the fact that p is zero when $\overline{C}^* = C_L^*$, and p equals unity when $\overline{C}^* = C_H^*$.

4.5 Concluding Remarks

The principal points contained in this chapter are:

Round, vertical, tube burners with fully developed turbulent pipe flow initial velocity profiles were employed for the experiments. The flames were carefully screened to prevent disturbance by draughts.

The descriptions of the equipment and the measurement procedures used to obtain the following have been presented:

(1) The mean, the rms, the probability density and the spectral density of the fluctuating temperature.

(2) The mean, the rms, the probability density and the spectral density of the fluctuating positive ion current.

(3) The combustion count and the probability of combustion.

CHAPTER 5

RESULTS AND DISCUSSION

5.1 Introduction

In this chapter, the results obtained, using the experimental apparatus described in the preceding chapter and the thermocouple and ionisation probes described in Chapters 2 and 3 respectively, are presented and discussed. The chapter contains five further sections:

In section 5.2, the measurements obtained with a bare thermocouple in a methane diffusion flame are presented. These are: the mean and the rms of fluctuating temperature; and the probability density and the spectral density of temperature fluctuations. The physical picture of the influence of the structure of the turbulent flow on the fluctuating reaction field which emerges from the measured profiles of rms and probability density of temperature fluctuations is discussed.

In section 5.3, the measurements obtained in a town gas diffusion flame are presented. These are: mean temperatures with radiation loss correction using a non-catalytic ceramic coated thermocouple; the mean and rms of the fluctuating positive ion current; the probability of combustion and the combustion count; and the probability density and the spectral density of fluctuating positive ion current. The measurements confirm the physical picture of the influence of the structure of the turbulent flow on the reaction field discussed in section 5.2.

In Section 5.4, the measurements obtained in turbulent premixed town gas/air flames are presented. These measurements are: mean temperatures with radiation loss correction using a non-catalytic ceramic coated thermocouple; the mean and rms of the fluctuating

positive ion current; the probability of combustion and the combustion count; and the probability density and the spectral density of the fluctuating positive ion current. In the discussion of these measurements it is shown that they do not support the "wrinkled laminar flame" concept for the high Reynolds number (62,000) flames. An alternative mechanism for flame propagation in the turbulent flow which explains the measurements satisfactorily is discussed.

The implications of the physical pictures, which have emerged for the influence of turbulence on the reaction in the diffusion and premixed flames, for combustion prediction procedures are discussed in Section 5.5. Also, the errors in the measurements are discussed in this section.

The principal conclusions arrived at in this chapter are summarized in Section 5.6.

5.2 Methane Diffusion Flame

5.2.1 Results

The measurements obtained, using a bare thermocouple, of the fluctuating temperature field of a methane diffusion flame are summarized in Table 5.2.1.

TABLE 5.2.1

Measurements in Methane Diffusion Flame

Data	Probe Location
(1) Rms T', mean T, Probe time constant τ.	x/D = 40, 80, 120 and axially - Figs. 5.2 a to d.
(2) Probability density of T' : 3-Dimensional plot.	Radial variation at x/D = 40 and axial variation - Figs. 5.2 e and f.
(3) Spectral Density: Fourier space.	Flame axis at x/D = 20, 40, 60, 80, 100, 110. Fig. 5.2 g.
(4) Spectral Density: Wave-number space.	As in (3). Fig. 5.2h. Comparison with other spectral density curves Fig. 5.2 i.

5.2.2 Discussion

a. $\overline{T}$, $\sqrt{\overline{T'^2}}$ and τ

Consider the set of curves at 40 diameters, Fig. 5.2a, as an example. It is seen that, with increasing radius, the rms of temperature fluctuations first increases because of the existence of an increasing number of air vortices, and then decreases because of the growing size of these vortices. Confirmation of this statement is afforded by the observed variation of probability density, discussed below, and by high-speed photographs of a turbulent diffusion flame, Milson and Chigier (1973).

Relative to the peak in the rms of temperature fluctuations the maximum mean temperature is closer to the flame axis. This is because the maximum rms of temperature fluctuations occurs in the region where the fuel and air vortices are numerous, but of large enough size to possess large temperature drops from the reacting interface to the

interior of these vortices. But the maximum mean temperature occurs in the region where the concentration of reacted fluid is a maximum and the size of the air vortices has been reduced by chemical conversion resulting in diminished temperature fluctuations.

The monotonic increase of probe time constant with radius is primarily ascribable to the diminishing mean velocity.

Similar remarks apply to the results shown in Figs. 5.2 b to d: the radial profiles at 80 and 120 burner diameters downstream of the burner, and the distribution along the flame axis.

Mean temperatures were measured using a non-catalytic ceramic coated probe and correcting for the radiation loss in order to evaluate the combined catalytic and radiation error as discussed in Chapter 2.

b.) Probability Density Variations

The spatial variations of the probability density of temperature fluctuations along the flame axis and radially at 40 burner diameters downstream of the burner exit are depicted in Figs. 5.2 e and f.

The probability density is approximately Gaussian near the flame axis (at r = 0, 10 mm, 15 mm for x/D = 40) and, along the flame axis, near the burner exit (at x/D = 40, 60).

Then a transition to a combination of the Dirac delta function* and a continuous function that is approximately Gaussian occurs.

---

* If a variable, z, degenerates to a constant, $\tilde{C}$, the probability density of z is the Dirac delta function at $z = \tilde{C}$ (Hildebrand, 1962): in the mathematical limit, the probability density is infinite at $z = \tilde{C}$ and zero everywhere else.

In practice, when a time-dependent variable, z, assumes a constant value, $\tilde{C}$, for some of the time but varies at random otherwise, the delta function is manifest as a "spike" at $z = \tilde{C}$ in the measured density. The prominence of the spike provides some measure of the proportion of the time $z = \tilde{C}$.

The occurrence of the delta function signifies that quiescent periods began to appear in the fluctuating temperature signal. This implies that the air vortices are of such magnitude that allowing even for heat conduction, sigificant regions of these vortices were cold. This implication is confirmed by the following observation: the Dirac delta functions become prominent at 180 diameters along the flame axis (Fig. 5.2f) and at a radius of 25 mm (Fig. 5.2e), that is, precisely at the locations where the rms profiles, Fig. 5.2d and Fig. 5.2a respectively, begin to decline.

Conversely, the absence of the delta function in the probability density of temperature fluctuations inside the reaction zone implies appreciable preheating of the fuel and air vortices. The degree of preheating may be estimated to a rough approximation from the mean, rms and probability density of fluctuating temperature. For example, at x/D = 100 the probability density plot, Fig. 5.2f, shows a variation of 8 rms values or 600°C in the temperature fluctuations (in fact there were fluctuations up to 10 rms values but the values of probability density outside 8 rms were too small to be plotted in the figure): that is, fluctuations of 1720°C to 1120°C, about a mean temperature of 1420°C. Thus the minimum temperatures in the fuel and air vortices was about 1100°C.

This preheating of fuel vortices causes pyrolysis with consequent soot formation which is characteristic of diffusion flames of hydrocarbons in air (see for example, Gaydon and Wolfhard (1970d); Edelman et al (1973)).

On the basis of the variations of the probability density of temperature fluctuations, the picture envisaged of the reaction zone is that it may, broadly, be divided into three regions as follows:

(1) Outer region of the reaction zone. (Flame "edge"). The temperature fluctuations are characterized by long quiescent periods because large "lumps" of air are being entrained, with combustion occurring at the interface between the air vortices and the fuel. In this region the turbulent transport is by large-scale bulk convection and of an intermittent nature, Townsend (1956b).

(2) Intermediate region of the reaction zone. (Transition region of probability density plot). More and smaller air vortices are formed from the entrained large air vortices due to turbulent mixing. Consequently more interfaces for chemical reaction exist. The length of quiescent periods in the fluctuating temperature signal decreases since some of the air undergoes chemical transformation and since thermal conduction preheats the remaining portion of the air vortices. The rms of temperature fluctuations attains its maximum value in this region. Turbulent transport by bulk convection and by gradient type diffusion which characterises the inner region of the reaction zone overlap.

(3) Inner flame zone. (Approximately Gaussian probability density) An effect of the combined processes of turbulent transport, molecular transport and chemical reaction is a reduction of the sizes of the fuel and entrained air vortices. Furthermore, the hot combustion products preheat the fuel and air vortices to such an extent

that very few cold cores exist inside these vortices. Consequently, the amplitude of the temperature fluctuations decreases; also, significant pyrolysis of the methane with attendant soot formation occurs. The turbulent transport here is predominantly by small-scale gradient type diffusion, Townsend (1956b).

A sketch of the envisaged picture of a turbulent diffusion flame is shown in Fig. 5.5a.

The implications of this physical picture for the prediction of free turbulent diffusion flames are discussed in Sub-section 5.5.1.

(c) Spectral Density

A spectral distortion similar to that depicted in Figs. 5.2 g and h has been reported in the literature, Kuhnert and Guenther (1973), for the fluctuating OH emission signal. Also, such a distortion was predicted by Eschenroeder (1965) for a locally isotropic turbulent fluid with a density-sensitive heating mechanism as in combustion. According to Eschenroeder, this spectral distortion implied that the heat energy released in the combustion was converted into turbulence energy in the band of "eddies" that contained the bulk of the turbulence energy. This results in an enhanced turbulent diffusivity and an augmented effective Reynolds number.

Fig. 5.2i shows a comparison of the present spectral density of temperature fluctuations with the measurements of temperature fluctuations by Kunugi and Jinno (1959), total emission fluctuations by Guenther and Simon (1969), and OH emission fluctuations by Kuhnert and Guenther (1973). It is seen that the agreement is fairly good. The discrepancy

between the present result and that of Kunugi and Jinno is probably attributable to Reynolds number effects and to the fact that the compensation for thermal inertia in the latter measurements was effected up to about 1 KHz. The discrepancies between the present result and the other two results are probably ascribable to Reynolds number effects and to the fact that different fluctuating quantities were investigated.

5.3 Turbulent Town Gas Diffusion Flame

5.3.1 Results

The measurements obtained in the town gas diffusion flame, Reynolds number 24,000 with the pertinent figures are indicated in Table 5.3.1

Data	Profile or measurement location
Mean temperature with radiation error correction (Ceramic coated thermocouple)	x/D = 10, 40, 90, 120 and 150, and axially - Figs. 5.3 a to g.
Probability of combustion and Combustion count	x/D = 10, 20, 35, 79.06, 90, 100 and 113 - Figs. 5.3 h to n.
Mean and rms of ionisation current	x/D = 10, 20 and 35. - Fig. 5.3 h, j and ℓ respectively.
Probability density of ionisation current	Radial variation at x/D = 75 and axially Figs. 5.3o and p respectively.
Spectral density of ionisation current	On flame axis at x/D = 75 and 90 compared with Guenther and Simon's data, 1969, Fig. 5.3q.

TABLE 5.3.1

Town Gas Diffusion Flame Data

5.3.2 Discussion

(a) Mean Temperature Profiles

The maximum axial mean temperature (at x/D = 90) was 200°C less than the adiabatic flame temperature of 1960°C; the corresponding value for the turbulent methane diffusion flame (at x/D = 140) was 360°C less than the adiabatic flame temperature of 1880°C. The smaller amplitude of temperature fluctuations in the town gas flame is ascribable to the fact that it is much smaller (1 mole of methane requires about four times as much air as 1 mole of town gas; consequently the methane flame needs to entrain more air) and is mainly confined to the inner part of the jet. The turbulence structure in the inner part of a jet is predominantly small-scale, Townsend (1956b); Hinze (1959e). Temperature differences are rapidly erased by turbulent transport of heat which in this region is gradient-type heat conduction.

(b) Mean and rms of Ionisation Current, Probability of Combustion and Combustion Count

The mean and rms of fluctuating ion concentration, the probability of combustion, p, and the combustion count, f, (p is the fraction of time combustion occurs at a point and f is the time-averaged number of times per second combustion occurs at a point) are all derived from the ionisation signal. Significant ionisation currents indicate the existence of combustion. Therefore, any of the four profiles may, in principle, be used to define the limits of the flame. However, the probability of combustion and the combustion count are considerably more sensitive indications of the occurrence of combustion than the

mean and rms of the ionisation current: for example, it is seen from Figs. 5.3 h to k that the profiles of the former quantities vary by 5 orders of magnitude whereas the profiles of the latter quantities vary by 1 order of magnitude.

Quantitative information on the phenomenon of "unmixedness" is provided by the data of combustion count and the probability of combustion. For instance, it is seen from Fig. 5.3 h, at x/D = 10 and r = 6.5 mm, that on a time-average basis fuel and air mix to react 2,000 times per second; and the fraction of time combustion occurs is 0.5.

All the profiles of mean and rms of ionization current, Figs. 5.3 h, j, and ℓ - first increasing with radius and then decreasing - reflect, as previously discussed in Section 5.2, the initial increase in fuel/air interfaces caused by an increasing number of air vortices and then the increasing size of these vortices. The similar shape of the combustion count and the probability of combustion profiles in Figs. 5.3 h, j, and ℓ to the corresponding mean and rms profiles confirms this picture.

(c) Probability Density

The plots of probability density Figs. 5.3 o and p are characterized by the Dirac delta function (c.f. sec. 5.2.2) at zero values of ionisation current. This implies that there are always periods when combustion is not detected at the measurement location. In Fig. 5.3 p , moving along the axis, the prominence of these delta functions first decreases and then increases as expected from the discussion in the preceding paragraph and the picture of the reaction zone described in sub-section 5.2.2 (b) above: i.e. the length of the quiescent periods in the positive ion signal first decreases and then increases.

The positive ion recombination rate fluctuations relative to the mean recombination rate may be estimated from the plots of probability density. For example, at x/D = 25 (Fig. 5.3 p) the range of fluctuation of $I^2 \approx 16\ \bar{I}^2$; since it was previously shown (Sec. 3.4.5) that the recombination rate of positive ions $\alpha\ I^2$, the maximum instantaneous recombination rate of positive ions is about 16 times the mean value.

(d) Spectral Density

In Fig. 5.3.q the present spectral density curves of positive ion current fluctuations at x/D = 75 and 90 on the flame axis are compared with the spectral density curve of total emission fluctuations (Guenther and Simon (1969)) at x/D = 60 on the flame axis. It is seen that the agreement in Fourier space is good.

Velocities were not measured at x/D = 75 and 90 in the present flame so that a comparison could not be made in wave number space. The curves in wave number space would be displaced, somewhat, relative to one another because the velocities in the three measurement positions (in the ionisation measurement at x/D = 75, 90; D = 5 mm; Reynolds number = 24000: in the emission measurement at x/D = 60; D = 10 mm; Reynolds number = 43,500) will be different. But it may reasonably be anticipated that the differences in the velocities will not be large since measurements of velocities in a methane diffusion flame, Reynolds number 14,500, Fig. B.5 show that the velocities at x/D = 75 and 90 are not significantly different (less than 10% difference). Furthermore, the higher Reynolds number in the emission

measurement than in the ionisation measurement (nearly twice) is compensated for by the burner diameter in the former measurement being twice that in the latter. Thus the magnitude of the relative displacement of the curves in Fig. 5.3 q when they are plotted in wave number space may be expected to be small.

5.4 Turbulent Town Gas-Air Premixed Flames

5.4.1 Results

The measurements obtained in the premixed flames, Reynolds number 62,000, and the corresponding Figures are shown in Table 5.4.1.

Data	Equiv. Ratio 0.91	Equiv. Ratio 1.16
Mean temperature with radiation error correction (ceramic coated thermocouple)	x/D = 0.517, 3.03, 4.41, 6.48 and axially - Figs. 5.4 a to e respectively	x/D = 0.517, 3.03, 4.41, 6.48, 8.48 and axially - Figs. 5.4. f to k respectively.
Probability of combustion, combustion count, normalized mean and rms of ionization current, and mean temperature	x/D = 3.03, 4.41 and axially - Figs. 5.4. ℓ to n respectively.	x/D = 3.03 and axially - Figs. 5.4. o and p respectively
Probability density of ionization current	Axial variation - Fig. 5.4. q	Axial and radial variation at x/D = 4.82 - Figs. 5.4. r and s respectively
Spectral density of ionization current	x/D = 4.38 on Flame axis - Fig. 5.4. t	x/D = 4.38 on flame axis - Fig. 5.4. t

TABLE 5.4.1

Town gas/air premixed flames data

5.4.2 Discussion

a) Mean Temperature

The maximum mean temperatures, ~1900°C (corrected for the radiation error) Figs. 5.4a to k are quite close to the adiabatic flame temperature 1960°C. This implies that in the region of maximum flame temperature, the temperature fluctuations are small, and that most of the fluid is combustion products. The latter implication is also evident from Figs. 5.4 ℓ to p: moving away from the inner cold cone of combustibles, each normalized mean temperature profile attains its maximum value after the corresponding normalized mean and rms of ionization current profiles have reached their maximum values.

b) Mean and rms of Ionisation Current, Probability of Combustion and Combustion Count

These profiles have some bearing on the validity of the "Wrinkled Laminar Flame" concept in a highly turbulent flame (Re = 62,000) on account of the following details:

(1) It is seen from the axial profiles, Figs. 5.4 n and p, that combustion occurs at a distance of 2 burner diameters from the burner exit. The gas velocity is considerably greater than the laminar burning velocity since measurements in a cold flow, Durão and Whitelaw (1973) show that the velocity at 2 burner diameters is equal to the maximum velocity in the tube: moreover, measurements of velocity in a turbulent premixed flame, Dürst et al, 1972, indicate that the combustion process does not appreciably affect the aerodynamics at this location.

(2) The probability of combustion, that is, the fraction of time combustion occurs, is greater than 0.5 in a significant region of the flame; for example, 4 cm along the axis, Fig. 5.4 p. Obviously, a fluctuating wrinkled laminar flame can not spend more than 50% of the time in such a wide zone. However, the possibility of fragmentation of the flame into laminar flamelets by the turbulent flow is considered in the next paragraph.

(3) The maximum amplitude of the ion current obtained was estimated from the measured rms profiles and the probability density plots. In the cold cone of combustibles, the maximum ionisation current was approximately 3 times the maximum laminar ion current after correcting for the velocity influence using equation (3.2.1). Chomiak, 1972, also observed that the chemi-luminescence signal obtained from a high Reynolds Number turbulent premixed flame was considerably greater than that obtained from a laminar flame. It may therefore be concluded that the combustion does not occur in laminar flamelets.

However, the hypothesis of turbulent flame propagation advanced by Chomiak, 1970 provides a plausible explanation of these details. According to Chomiak's hypothesis, the turbulent flame propagation consists in essence in the transfer of reacting fluid to regions of unreacting fluid, and unreacting fluid to the combustion zone by strong vortex tubes.* The experimentally observed details, previously mentioned, are explained by this hypothesis as follows.

---

*Formed by eddies of Taylor micro-scale rubbing against one another (Tennekes (1968)).

Firstly, the hypothesis predicts that ionisation or chemiluminescence signals in highly turbulent flames are greater than the corresponding signals in laminar flames: the stretching action of strong vortex tubes or sheets produces higher diffusivities of heat and matter with attendant higher reaction rates than in laminar flows.

Secondly, the occurrence of combustion at 2 burner diameters from the burner exit would be anticipated on the basis of Chomiak's hypothesis and the incipient increase of the rms of velocity in a cold flow at x/D = 2, Durão and Whitelaw (1973). The increase in the rms velocity indicates that turbulent transport by vortex tubes between the 'pipe fluid core' (this corresponds to the 'potential core' of a nozzle jet) and fluid in the mixing layer occurs at x/D = 2, leading to combustion at this location.

Finally, the local probability of combustion can exceed 0.5 in the reaction zone if a sufficiently large number of reacting strong vortex tubes passes through the measurement location intermittently.

A sketch of the envisaged picture of the structure of a turbulent premixed flame is shown in Fig. 5.5 b.

The implications of this physical picture for the prediction of free turbulent premixed flames are discussed in Sub-section 5.5.2.

(c) Probability Density

The plots of probability density of ionization current, Figs. 5.4 q to s, show the Dirac delta functions, see Sub-section 5.2.2, associated with zero ionisation. Moving away from the cold core of combustibles the prominence of the delta function first diminishes and then increases as the probability of combustion (fraction of time

ionisation is greater than zero) first increases and then decreases.

The axial plots of probability density exhibit an interesting feature at x/D = 4.8. The trough in the probability density curve at this location implies a combination of a sinusoidal variation and a random variation in the ionisation current Durst (1972b). A similar trough was observed in the probability density of velocity fluctuations in a premixed flame by Durst et al (1972). These investigators suggested that the effect was caused by combustion induced periodic oscillations in the flow. The present measurements seem to confirm the supposition that the premixed flames possess an inherent periodic nature.

(d) Spectral Density

The measured spectral density curves, Fig. 5.4 t, show a flat portion and then a very steep fall off. The latter feature is most probably due to the fact that the range of the wave analyser extended to 25 kHz and was therefore inadequate for these measurements in a turbulent premixed flame. The analyser was adequate for turbulent diffusion flames where the highest frequencies of interest were $\sim$ 10 kHz, see Fig. 5.3 q. The flat portion of the curve, up to 5 kHz, indicates that the fluctuations in the ionization signal were caused by small burning gas volumes.

5.5 Implications for Combustion Prediction Procedures

5.5.1 Free turbulent diffusion flames

(a) A General Implication

As discussed in Sub-section 5.2.2 the existence of the Dirac delta function in the probability density of temperature fluctuations,

in the outer region of the diffusion flame, is caused by large scale turbulent motion in this region. Now, the probability density of temperature completely describes the time-averaged fluctuating temperature field (for example, the mean and $(\text{rms})^2$ of the fluctuating temperature are the first and second order moments respectively of the probability density of the fluctuating temperature). It follows, therefore, that this large scale turbulent motion must be considered when predicting the fluctuating temperature in the outer region of the reaction zone.

A method for accounting for large scale motion in the turbulent transport of scalar quantities, such as temperature and specie concentration, in free flows was given by Townsend (1956b). According to Townsend, the net turbulent transport in free flows consists of two parts:

(1) Gradient-type diffusion caused by small scale turbulent motion with the effect of transporting the diffusing quantity down the mean intensity gradient.

(2) Bulk convection by eddies whose scale is of the same order as the width of the distribution of the diffusing quantity. The rate of transport is dependent more on the general distribution of the quantity than on its local intensity gradient.

For moderate temperature differences, such that the temperature fluctuations do not affect the turbulent motion, Townsend derived an expression for, Q, the total transport of temperature:

$$Q = \overline{\theta}\overline{V} + \overline{\delta}\mu_T \operatorname{grad} \frac{\overline{\theta}}{\overline{\delta}} \qquad (5.5.1)$$

where $V = \overline{u_1\theta}/\overline{\theta} < \overline{\delta u_1}/\overline{\delta}$ but approximates it when $\overline{\delta}$ is small,

δ is equal to unity within the turbulent fluid and is zero outside,

u_1 is the component of the turbulent velocity fluctuation due to large eddy motion,

θ is the instantaneous temperature difference between the point of observation and the ambient fluid,

and

μ_T is a property of the fully turbulent fluid.

In the outer entrainment region of the flow, $\overline{\delta}$ is small so that the second term in the right of equation (5.5.1) is small. Therefore, the term $\overline{\theta}V$ is important and it is necessary to model it by taking into consideration the intermittency of turbulence there. A similar kind of modelling would be required in the outer region of the flame.

(b) An Implication for Hydrocarbon Flames

As mentioned previously in Sub-section 5.2.2, the probability density of temperature fluctuations in the inner, predominantly fuel, region of the flame reveals appreciable preheating of the vortices. This leads to pyrolysis and soot formation. The combustion products also diffuse into the fuel and air vortices. As the vitiated and preheated air and fuel vortices continue to intermingle and react, partial oxidation of the fuel will occur because the available air is insufficient for complete combustion.

Pyrolysis/soot formation and partial oxidation of the fuel lead to diminished maximum instantaneous temperatures. The temperatures

are also reduced by the mechanism of thermal radiation from the soot particles.

It is necessary to account for partial oxidation and reduced temperatures when calculating turbulent diffusion flames of hydrocarbons. Otherwise the following shortcomings in the predictions will ensue:

(1) The predicted flame will be longer and broader than the real flame because the former is required to entrain more air (for complete combustion) than occurs in practice.

(2) The predicted mean and rms of fluctuating temperature will be higher than the real values. This results in unrealistic property values being employed in calculating the flow field. Again, the effect of this would be for the hotter theoretical flame to spread faster than the real flame.

Confronted with similar effects in attempting to predict laminar methane diffusion flames, Edelman et al (1973) developed the hypothesis of "shifting equilibrium". In this hypothesis, the equilibrium approximation is retained for combustion (i.e. chemical kinetics not considered), but the combustion products may contain soot and partial oxidation products (such as CO). This hypothesis has some detailed aspects that do not permit a brief exposition.

However, it is possible, and necessary to incorporate the hypothesis of Edelman et al, or a similar one, in a calculation procedure for turbulent hydrocarbon diffusion flames.

5.5.2 Free Turbulent Premixed Flames

As discussed in Sub-section 5.4.2 the "wrinkled laminar flame" concept is untenable in fully turbulent premixed flames. Obviously, it should not form the basis for the calculation of such flames.

The concept based on flame propagation by concentrated vortex tubes or sheets, Chomiak (1970), provides a satisfactory explanation of the ionisation probe data. These vortex tubes or sheets, whose diameter or thickness is the Kolmogorov micro-scale, are responsible for the dissipation of turbulence energy.

Accordingly, mathematical models for flame propagation based on the parameters of turbulence energy dissipation hold good prospects of universality in fully turbulent premixed flames. Such a model has been employed by Mason and Spalding (1973) to predict the spread of a premixed flame in a duct with fairly good accuracy. A different mathematical model proposed by Chomiak (1970) has at the present time not been tested.

5.5.3 Validation of Prediction Procedures

(a) Errors

The measurements with the highest precision and accuracy are the mean temperature data obtained with the non-catalytic ceramic coated thermocouple and corrected for radiation loss. These measurements are: all the mean temperature measurements in the town gas/air premixed flames and the town gas diffusion flame; and the appropriate axial distribution of mean temperature, broken curve in Fig. 5.2 d, in the methane diffusion flame. As discussed in Sub-section 2.3.4, the

error in the radiation loss correction was $< \pm$ 1%; the conduction error was $\sim \pm$ .1%; and the max. error caused by thermal inertia fluctuations was about $\pm$ 1%: a total of about $\pm$ 2%.

The rms of temperature measurements obtained in the methane diffusion flame have an error of $\pm$ 15% caused by the extraneous second harmonic component of probe temperature fluctuations (see Sub-section 2.4.6). The combined catalytic and radiation error was about $\left(\begin{smallmatrix} +0 \\ -5\% \end{smallmatrix}\right)$. The total error is therefore about $\left(\begin{smallmatrix} +15\% \\ -20\% \end{smallmatrix}\right)$ ignoring the very small conduction error.

The total error in the mean temperature data obtained in the methane diffusion flame with a bare thermocouple was $\left(\begin{smallmatrix} +1\% \\ -6\% \end{smallmatrix}\right)$ consisting of $\left(\begin{smallmatrix} +0 \\ -5\% \end{smallmatrix}\right)$ for combined radiation loss and catalytic effects and $\pm$ 1% for thermal inertia fluctuations.

The error in the combustion count and the probability of combustion data is $\left(\begin{smallmatrix} +0 \\ -10\% \end{smallmatrix}\right)$ - see Sub-section 3.3.3.

These errors are summarized in Table 5.1.

Data	Flame and Probe Position	Error
Mean temp.	All town gas flames (diffusion and premixed with air); axial mean temp. in methane flame corrected for radiation loss	$\pm$ 2%
Mean temp.	Methane flame	+ 1% - 6%
Rms temp.	Methane flame	+ 15% - 20%
Combustion Count Probability of Combustion	All town gas flames diffusion and premixed with air	+ 0 - 10%

TABLE 5.1

Summary of Measurement Errors

(b) Flame Shape Definition

A good combustion prediction procedure should be capable of accurately defining the extent of the reaction zone in a flame. In this connection, the profiles of combustion count and the probability of combustion constitute a very sensitive test for such prediction procedures.

The accuracy with which these measurements of the combustion count and the probability of combustion define the limits of the reaction zone is seen from a comparison of these measurements with long time exposure colour photographs of these flames - Figs. 5.6a, b, c and d. For example, in the lean premixed town gas/air flame, at x/D = 4.41, the width of the reaction zone is as judged: from the photograph (Fig. 5.6c), 1.7D; from the combustion count and probability of combustion profiles (Fig. 5.4m), very nearly 2D (burner diameter 29 mm, flame limit 2 x 28 mm).

5.6 Conclusions

The principal findings which emerge from the measurement programme are:

(1) A picture of turbulent diffusion flames in which the combustion zone may be divided into three regions, viz: (a) the outer edge of the flame with a relatively low rms of temperature fluctuations, implying large air vortices which are entrained by large scale turbulence. (b) The intermediate region, with the maximum rms of temperature fluctuations, where the engulfed large air vortices experience preheating, chemical transformation and a breakdown to smaller

vortices. (c) The inner edge of the flame, with a diminished rms of temperature fluctuations, where the air vortices suffer further breakdown and chemical transormation while the preheating of the fuel by combustion products leads to soot formation in hydrocarbon flames.

(2) It is inferred from the measurements that the amplitude of temperature fluctuations in a town gas diffusion flame is smaller than in methane diffusion flames. This is attributable to the fact that the former flame is more confined to the inner region of the jet where relatively smaller scale turbulence is mainly operative in the mixing of fuel and air.

(3) The details of the ionisation probe measurements in the premixed town gas/air flames cannot be explained by the wrinkled laminar flame concept. However, the concept proposed by Chomiak, 1970, that the flame propagation mechanism consists in transport of combustible mixture into the reaction zone and of reacting fluid into the fresh mixture by strong vortex tubes or sheets provides a satisfactory explanation.

(4) The measured spectral densities in the premixed flames reveal that the ionisation fluctuations in these flames are of a small scale.

The implications of the measurements for validating prediction procedures are:

(1) Special modelling of the intermittency in the outer entrainment region of the flow in turbulent diffusion flames is required.

(2) A sophisticated model of the thermodynamics of turbulent hydrocarbon diffusion flames is required to take into account pyrolysis/soot formation and partial oxidation of the fuel.

(3) The mean temperature measurements with radiation error correction obtained with a non-catalytic ceramic coated probe are the most accurate.

(4) The measured combustion count and probability of combustion profiles are very sensitive indications of the extent of the reaction zone.

CHAPTER 6

SUMMARY AND CONCLUSIONS

6.1 Summary

The research programme described in this thesis has been devoted to an experimental investigation of two categories of turbulent reacting flows, namely: diffusion flames which are dominated by turbulent mixing, and premixed flames which are kinetically-influenced. The objective of the research was to supplement data of fluctuating quantities, in especially simple circumstances, which are meagre in the literature. Such data are required to enhance understanding of the influence of turbulence on combustion and to provide a basis for validating turbulent reacting flow prediction procedures. The measurements were performed in free jet flames burning in still air. The quantities measured were mean temperature, temperature fluctuations, fluctuating positive ion current, the probability of combustion and the combustion count.

Chapter 2 is concerned with the temperature measurement technique. The mean temperature probe was a thermocouple coated with a non-catalytic alumina-based ceramic, while the temperature fluctuations probe was a bare thermocouple. The significant errors incurred when a thermocouple is used for measurements in turbulent flames are delineated and examined. The significant error associated with the present mean temperature probe was the radiation error and the correction for it was determined from the in vacuo temperature versus radiant energy calibration curve of the thermocouple. The thermal inertia of the temperature fluctuations probe was compensated up to a frequency of 10 kHz with an active filter.

The subject of Chapter 3 is the positive ion current measurement technique. The principle of operation of the ionisation probe is briefly outlined. The negatively-biased sensing wire was insulated from the flame gases except for a 2 mm length at its end which was machined to a sharp point. The probe exerted negligible aerodynamic, thermal and chemical disturbance on the flow. The rationale for deriving the probability of combustion and the combustion count from the probe signal is explained.

Chapter 4 pertains to the burners and the measurement equipment. The 5 mm diameter diffusion flame burner, and the 29 mm diameter premixed flame burner are described. The need for fully developed, turbulent, flow is explained. The precautions taken to minimize flame disturbance by draughts are mentioned. The items of measurement equipment are listed: they include circuits designed and constructed in the laboratory for the present study.

The experimental data are presented and discussed in Chapter 5. The measurements made in the methane diffusion flame were of the mean temperature, and of the rms, the probability density and the spectral density of temperature fluctuations. Those performed in the town gas diffusion flame and the town gas/air premixed flames were of the mean temperature and of the mean, the rms, the probability density and the spectral density of positive ion current as well as the probability of combustion and the combustion count.

6.2 Conclusions

The principal findings which emerged from the present study are:

(1) The combustion zone of a free jet diffusion flame may be, broadly, divided into three regions:

(i) The outer 'flame edge' region where large 'lumps' of air are entrained by large scale turbulent motion. Combustion occurs in the relatively few fuel/air interfaces. The cold core of the air 'lumps' causes quiescent periods in the temperature fluctuations signal. These periods produce a prominent 'spike' in the probability density function of temperature. The rms of temperature fluctuations is relatively small.

(ii) The intermediate region where the 'lumps' of air experience a breakdown to smaller vortices. The available fuel/air interfaces for combustion consequently increase. Furthermore, the action of molecular conduction in the smaller air vortices results in a decrease of the length and frequency of quiescent periods in the temperature fluctuations signal. The prominence of the spike in the temperature probability density function is diminished. The rms of temperature fluctuations attains a maximum in this region.

(iii) The inner region where the air vortices are further reduced in size by the combined action of turbulent mixing and chemical conversion. Small scale turbulent motion is effective in erasing the temperature and concentration gradients. This results in diminished temperature fluctuations, appreciable pre-heating of the predominantly fuel vortices and vitiation of the fuel and air vortices by combustion products. (In the case of a hydrocarbon fuel such as methane, pyrolysis and soot formation are initiated in this region). The probability density of temperature fluctuations is approximately Gaussian.

(2) The experimental data suggest that combustion in fully-turbulent free jet premixed flames occurs in vortex tubes of the Kolmogorov micro-scale diameter. The random distribution of these tubes in the flow results locally in intermittent combustion. The mechanism of vortex

stretching augments the molecular transport processes. As a consequence the combustion is more intense in these tubes than in laminar flow. This picture is in conflict with the "wrinkled laminar flame" concept of turbulent flame propagation.

The implications of the envisaged structures of turbulent free diffusion and premixed flames for prediction procedures are:

(1) Special modelling of the entrainment process at the edge of the flow is required to account for its intermittent character in this region.

(2) For hydrocarbon fuel flames at least a sophisticated thermodynamic model is required which incorporates the formation of intermediates such as CO and solid carbon.

(3) Turbulence reaction models for premixed flames should take into account the random motion of vortex tubes as well as the augmentation of molecular transport processes by the stretching mechanism of these tubes.

APPENDIX A

THE DESIGN OF ELECTRONIC CIRCUITS ASSOCIATED WITH THE MEASUREMENT PROGRAMME

A1. Introduction

This appendix presents, briefly*, the methods used for designing the active filter circuits which were constructed in the laboratory and used in the measurement programme. The principal components of these active filters were R-C networks and operational amplifiers (op-amps). Active filters are preferable to passive filters (which contain only capacitors, resistors and inductors) for three reasons:

Firstly, active filters incorporating op-amps can be designed, by using well-known negative feed-back principles and relatively simple R-C networks, to realise practically any desired frequency response curve (or mathematical operation) economically, reliably and accurately.

Secondly, for frequencies below 100 kHz, the capacitors required for passive filters are rather large and subject to high leakage currents. This leads to loss of accuracy.

Thirdly, passive components, being intrinsically dissipative, cause a high attenuation of the input signal, often to the level of background electronic noise: i.e. a low signal to noise ratio.

The remainder of this appendix consists of two sections. Section A2 contains the derivation of the basic equations employed for synthesizing the active filters, and also the required R-C networks and their admittance equations. In section A3, the circuits which were designed and constructed for the experimental programme are described. The electronic circuits were:

---

* See Welling (1969) for a detailed treatment.

(1) A two stage amplifying unit, consisting of: a differential pre-amplifier and an inverting amplifier. This electronic unit was used for the positive ion current measurement. It was required to produce a signal, 10 V max., from the low level probe current signal, 10^{-9}A to 10^{-6}A, with a minimum of noise introduction.

(2) A thermal inertia simulator unit with a variable time constant. This electronic circuit was required to progressively attenuate a sinusoidal wave-form as the frequency increases in the same way as a thermocouple diminishes the high frequency harmonics of a fluctuating gas temperature. The circuit was used to verify the frequency response of a thermal inertia compensator.

(3) A thermal inertia compensator unit with a variable time constant. This unit was required to amplify the higher harmonics of the thermocouple signal in exactly inverse proportion to the attenuation of these harmonics by the probe thermal inertia. Compensation up to a frequency of 10 kHz was required. The provision of a variable time constant for the circuit permitted the matching of the compensator and thermocouple time constants at each measurement location.

(4) A noise filter used for suppressing the noise harmonics in the thermal inertia compensator output above 10 kHz. The recommended upper frequency limit for temperature fluctuations is 10 kHz, Hinze (1959d). The noise filter was designed to rapidly attenuate harmonics above 10 kHz.

(5) The last circuit to be described is a low pass filter and two stage amplifying unit consisting of an inverting pre-amplifier, an inverting amplifier, a dc to 1 kHz low-pass filter and a 50 Hz band reject filter. This unit was employed for the thermocouple time constant determination, and the mean temperature radiation error correction procedures. During these procedures, a 50 kHz 4V max. wire heating signal had to be eliminated in order to recover the probe signal of about 10 mV. Also, the heating circuit introduced an appreciable mains 50 Hz hum which had to be suppressed.

A2. Basic Equations and the Required R-C Networks

A.2.1 Basic equations

(a) Notation

The notation used is best described by reference to Fig. A.1. $\Psi(m,n)$ designates the network (which may, itself, be active or passive) connected between lines m and n in which the respective currents I_m and I_n are flowing. The admittance of the network is defined such that the voltage E_n contributes $y_{nn} E_n$ to current I_n and $y_{mn} E_n$ to current I_m. In general:

$$y_{mn} = I_m/E_n \Big|_{E_m=0} \qquad \text{(A.1.a)}$$

$$y_{mm} = I_m/E_m \Big|_{E_n=0} \qquad \text{(A.1.b)}$$

Thus the second suffix of y is the same as for the driving voltage; and the first suffix is the same as that of the current augmented by the driving voltage.

The y-values are obtained from the configuration of the network and from the magnitude of the resistances and capacitances comprising it.

(b) System of equations

From the definition of admittance given above, equations (A.1.a) and (A.1.b), the following set of equations is obtained for the currents, I_j (j = 1,2, ..., 6), in Fig. A.1.

$$I_1 = y_{11} E_1 + y_{12} E_2 \qquad (A.2)$$

$$I_2 = y_{21} E_1 + y_{22} E_2 \qquad (A.3)$$

$$I_3 = y_{33} E_3 + y_{34} E_4 \qquad (A.4)$$

$$I_4 = y_{43} E_3 + y_{44} E_4 \qquad (A.5)$$

$$I_5 = y_{55} E_5 + y_{56} E_6 \qquad (A.6)$$

$$I_6 = y_{65} E_5 + y_{66} E_6 \qquad (A.7)$$

(c) Simplification

The simplification of the above set of equations is effected by using op-amps which possess certain characteristics. Then, the output voltage E_6 can be expressed as a function of the input voltages E_1 and

E_3 and the admittances.

Thus, if an op-amp with a very low input admittance is employed, for example, a Field-Effect-Transistor (FET) amplifier (input admittance typically 10^{-10} mho),

$$I_4 \approx o: I_i \approx 0; \quad \text{or } I_2 \approx I_5 \ ,$$

equation (A.5) becomes:

$$E_4 = - \frac{y_{43}}{y_{44}} E_3 \qquad (A.8)$$

and equations (A.3) and (A.6) yield:

$$y_{21} E_1 + y_{22} E_2 = - y_{55} E_5 - y_{56} E_6 \qquad (A.9)$$

If, in addition, the open-loop gain of the operational amplifier is large (typically gains of 10^5), the required differential input signal, $(E_2 - E_4)$, is very small. Accordingly,

$E_2 = E_4 = E_5$, to a very good approximation.

Then from equation (A.8),

$$E_5 = E_2 = - \frac{y_{43} E_3}{y_{44}} \ . \qquad (A.10)$$

Finally, substitution from equations (A.10) in equation (A.9) gives:

$$E_6 = - E_1 \left(\frac{y_{21}}{y_{56}}\right) + E_3 \left(\frac{y_{43}}{y_{44}}\right) \left(\frac{y_{22} + y_{55}}{y_{56}}\right) \qquad (A.11)$$

A.2.3 Admittances of the required networks

Equations (A.1.a) and (A.1.b) show how to obtain the admittance y_{mn} of any network $\Psi(m,n)$. y_{mn} is the quotient of the current, I_m, and voltage, E_n, implied by the subscripts of the admittance (see definition given above in A.2.1a) with the output short circuited. The admittances of the simple networks which were incorporated in the examples described below are contained in Table A.1.

Table A1

Admittances of some net-works

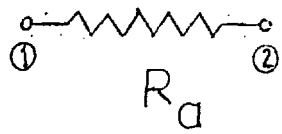
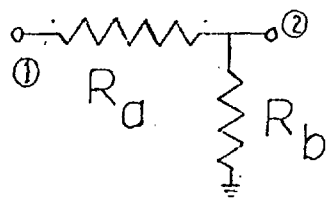
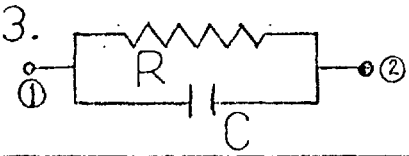
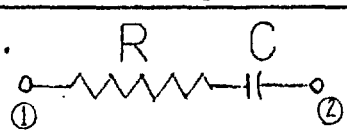
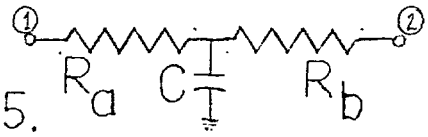
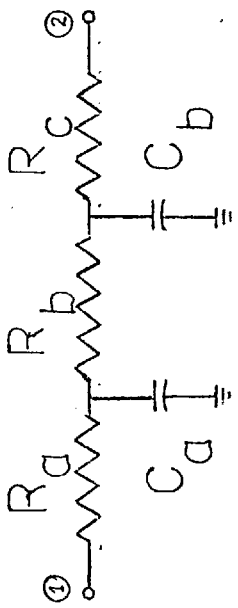
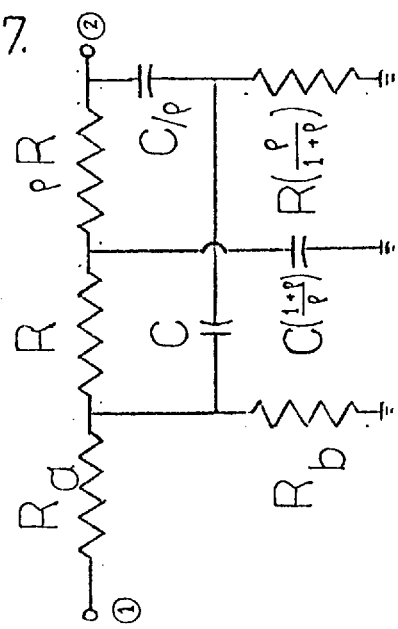
Network	Admittance and component relations	Reference
1. 	$y_{12} = y_{21} = -\frac{1}{R_a}$	By inspection using equations (A.1.a) and (A.1.b)
2. 	$y_{12} = y_{21} = -1/R_a$ $y_{11} = 1/R_a$ $y_{22} = 1/R_a + 1/R_b$	ditto.
3. 	$y_{12} = y_{21} = -\frac{1 + RCS}{R}$	ditto
4. 	$y_{12} = y_{21} = \frac{-SC}{1 + RCS}$	ditto
5. 	$y_{12} = y_{21} = \frac{-1}{R_a + R_b + R_a R_b CS}$	ditto

TABLE A1 (cont.)

Network	Admittance and component relations	Reference
6. 	$y_{12} = k_R \dfrac{1}{s^2 + \dfrac{\omega_p}{q_R} s + \omega_p^2}$ where $k_R = \dfrac{1}{R_a R_b R_c C_a C_b}$ $\omega_p^2 = (R_a+R_b+R_c)/R_a R_b R_c C_a C_b$ $q_R = \{R_a R_b R_c (R_a+R_b+R_c) C_a C_b\}^{\frac{1}{2}}$ $/(R_a(R_b+R_c)\, C_a + R_c(R_a+R_b) C_b$	Moschytz (1967)
7. 	$K_R \dfrac{s^2 + \omega_z^2}{s^2 + \dfrac{\omega_p}{q_R} s + \omega_p^2}$ where $K_R = 1/R_a$; $\omega_z = \dfrac{1}{RC}$ $\omega_p^2 = \dfrac{1}{R^2C^2}[1+(1+\rho)\alpha]$ $q_R = \dfrac{1}{1+\rho} \dfrac{1+(1+\rho)\alpha}{2+\alpha}$ $\alpha = R/\dfrac{R_a R_b}{R_a+R_b}$	Moschytz (1967)

A.3 Designed Circuits

In this section, the design of active filter circuits using op-amps and simple R-C networks is described. The circuits were required in connection with the positive ion current, temperature fluctuations and mean temperature measurements. All the circuits were tested and were satisfactory.

A.3.1 Amplification unit for ion current measurement

(a) Circuit requirements

The electronic unit was required to produce a voltage (max. 10 V) proportional to the ionisation probe current, (10^{-9}A to 10^{-6}A). The current to voltage conversion was performed by passing the probe current through a 1 K resistor. The resulting voltage (10^{-6}V to 10^{-3}V) would require an amplification of about 10^{4} which is too high for a single op-amp: therefore, a two stage amplifier was needed. In order to permit the water cooling jacket of the ionisation probe to float at the plasma potential, it was necessary to use a differential pre-amplifier.

(b) Pre-amplifier circuit diagram

The op-amp employed for the pre-amplifier was the Analog Devices Model AD41K. It was chosen because it possessed the following characteristics:

(1) Low input bias current, 2.5 x 10^{-13}A max., i.e. over three orders of magnitude smaller than the probe current.

(2) Low input noise current, 5×10^{-15} A max., i.e. over five orders of magnitude less than the probe current.

(3) Low offset voltage, $\pm$ 2 mV max., which could be trimmed to zero.

From a noise consideration, a great part of the gain, 10^2, was effected in the first stage.

It is seen from equation (A.11) that E_6 will be proportional to the difference between E_1 and E_3 if:

$$Y_{21} = Y_{43} \qquad \text{(A 12)}$$

and

$$Y_{44} = Y_{22} + Y_{55} \qquad \text{(A.13)}$$

The circuit diagram which satisfies equations (A.12) and (A.13) is shown in Fig. A.2. Ψ (1,2), Ψ (5,6) are the first "network" in Table A.1; Ψ (3,4) is the second network in the table. The gain of the circuit is $R_f/R_i = 10^2$. However, placed across the feedback resistor, R_f, was a small capacitor. Its effect was to provide an increasing amount of negative feedback and so reduce the gain of the circuit as the frequency is increased: that is, to filter extraneous high frequency noise harmonics from the signal.

The value of the capacitor was selected such that $1/R_fC_f = (2\pi)(50\text{ kHz})$ Thus the frequency response curve of this first stage of the amplification unit was 'flat' from DC to 50 kHz (-3db point). The slope of the amplitude versus frequency curve, (roll off rate), on a log-log plot, for frequencies greater than 50 kHz is 6 db/octave, Fig. A.4.

(c) Second stage amplifier circuit diagram

The second amplifying stage of the ion current amplification unit was an inverting amplifier with a gain of 10^2. The op-amp used was an Analog Devices Model AD 45K; no special characteristics were required of this op-amp.

If the positive input terminal of the amplifier, Fig. A.1, is connected to ground, $E_3 = 0$, and equation (A.11) becomes:

$$\frac{E_6}{E_1} = -\left(\frac{Y_{21}}{Y_{56}}\right) \qquad (A.14)$$

The circuit which has a gain of 10^2 and an upper frequency -3db point of 50 kHz is shown in Fig. A.3. As in example (a) above, $\Psi(1,2)$ and $\Psi(5,6)$ are the first 'network' in Table A1; also, $1/R_fC_f = (2\pi)(50\ \text{kHz})$. The frequency response curve of this circuit is shown in Fig. A.4.

A.3.2 Active filters associated with temperature fluctuations measurement

(a) Thermal inertia simulator

The differential equations for the thermocouple temperature, T, when in a gas at temperature, T_g, is:

$$\tau\frac{dT}{dt} + T = T_g \qquad (A.15a)$$

or in operator, S, notation:

$$\frac{T}{T_g} = \frac{1}{1 + S\tau} \qquad (A.15b)$$

If an inverting op-amp is employed, then from equations (A.15b) and (A.14) the simulator circuit should have the response:

$$\frac{E_o}{E_1} = -\left(\frac{y_{21}}{y_{56}}\right) = \frac{1}{1 + s\tau} \qquad (A.16)$$

No stringent characteristics are required of this op-amp. The Philbrick Nexus Model PN 1009 was used.

Fig. A.5 shows the circuit diagram of the simulator which satisfies equation (A.16). The frequency response curve, for τ = 10 ms, is shown in Fig. A.7.

(b) Thermal inertia compensator

The thermal inertia compensator should have the inverse of the characteristic given by equation (A.16). Therefore, from equation (A.16) the compensator should have the response:

$$\frac{E_o}{E_1} = 1 + \tau s = -\left(\frac{y_{21}}{y_{56}}\right) \qquad (A.17)$$

The main requirement to be fulfilled by the op-amp is that it should have a wide bandwidth so as to accommodate the gain which is increasing with frequency, see equation (A.17), and remain stable. An Analog Devices model AD 45K was found satisfactory if the d.c. gain, was made 1/10.

The circuit diagram of the compensator which satisfies equation (A.17) is shown in Fig. A.6. R_v and C_i in Fig. A.6 were both variable to permit the matching of the compensator and probe time constants at the measurement location. The frequency response curve, for τ = 10 ms,

is shown in Fig. A.7. It is seen from the combined response curve for the simulator and compensator circuits in Fig. A.7 that the latter circuit was satisfactory.

(c) Noise filter

The design criterion to be fulfilled by the noise filter was a steep roll off rate (24 db/octave) for frequencies greater than 10 kHz. Two op-amps were used to design the filter and its circuit diagram is shown in Fig. A.8. No stringent characteristics were required of the op-amps used which were Philbrick Nexus Model PN 1009. The circuit design is best explained by dividing the filter into two circuits as shown in Fig. A.8.

The main function of circuit A is to act as a buffer between the compensator circuit and this noise filter circuit. In this way the compensator is not connected directly to a frequency dependent impedance which could otherwise impair its performance. However, a standard capacitor, C_f, was placed across the feed-back resistor, R_f, such that $1/(R_f C_f) \approx (2\pi)(20\text{kHz})$. The gain at d.c., R_f/R_i was unity. The resistor and capacitor values are shown in Fig. A.8.

The greater part of the noise filtering occurred in circuit B. It is seen from Table A.1 that for net-work no. 6, if $R_a = R_b = R$ and $C_a = C_b = C$ (say), the admittance $y_{21} = \dfrac{1}{3R(1 + \frac{RCS}{3})(1 + RCS)}$.

Standard components were chosen such that $1/(RC) \approx (2\pi)(20\text{ kHz})$, the d.c. gain, $R_f/(R_a + R_b + R_c) = 1.0$, and $1/(R_f C_f) = (2\pi)(20\text{ kHz})$. The component values are shown in Fig. A.8.

The frequency response curve of the noise filter is shown in Fig. A.9. It is seen that a satisfactory roll off rate was obtained for frequencies above 10 kHz.

A.3.3 Low-pass filter for thermocouple time constant determination and radiation error correction

(a) Requirements of circuit

During the thermocouple radiation error correction and time constant determination, it was necessary to heat the probe with an alternating current at 50 kHz. Typically, heating currents were 2A max. The probe resistance was about 2Ω, so that an alternating voltage of 4V max. occurred simultaneously with the temperature signal (a few mV); the latter would be swamped by the periodically alternating voltage.

The main requirements of the low-pass filter were:

(1) To filter out the 4V max. signal at 50 kHz and recover the probe signal.

(2) To reject, 50 Hz, mains hum, introduced by the Advance Model H1 signal generator and Sinclair Z50 power amplifier which produced the heating current, without degrading the probe signal.

(3) Low-drift, low-voltage offset, and low-noise characteristics.

(4) A gain of 10^3.

(b) Circuit design

The filter design is best explained by reference to Fig. A.10 which shows the circuit in three sections. A two-stage amplifying unit was used, and from a noise consideration a gain of 10^2 was effected in the first stage, the pre-amplifier, and 10 in the second stage. The op-amp used for the pre-amplifier, circuit A Fig. A.10, was the Analog Devices Model AD 233L - an op-amp specially designed for thermocouple applications. The op-amp used in the second stage, circuit B Fig. A.10, was the Analog Devices Model 45K; no special characteristics were required of it. A third op-amp, Philbrick Nexus Model PN 1009 was used to design the unity gain active filter, circuit C Fig. A.10, for rejecting the 50 Hz mains hum; no stringent characteristics were required of this op-amp.

50 kHz suppression

The harmonics which contain practically all the energy of the uncompensated thermocouple signal are in the range d.c. to 1 kHz. Therefore, a steep roll off rate (24 db/octave) with the - 3db point at about 1 kHz was used to suppress the 50 kHz signal.

It is seen from Table A.1, that for network no. 5, if $R_a = R_b = R_1$, and $C = C_1$, the admittance is: $y_{21} = \dfrac{1}{2R_1(1 + \frac{R_1C_1S}{2})}$. Accordingly, standard component values (see Fig. A.10, circuit A) were chosen such that

$$2/(R_1C_1) \approx (2\pi)\ (1\ \text{kHz})$$

the d.c. gain, $\dfrac{R_2}{2R_1} = 10^2$; and, for the feed-back network,

$$1/R_2C_2) \approx (2\pi)\ (1\text{kHz})$$

In addition, the feed-back networks in circuits B and C Fig. A.10, were such that,

$$1/(R_2C_2) = 1/R_7C_6 \approx (2\pi)(1\ \text{kHz}).$$

The frequency response curve of the low-pass filter is shown in Fig. A.11. It is seen that a satisfactory roll off rate for frequencies above 1 kHz was obtained.

50 Hz, mains hum, rejection

Network No. 7 in Table A.1 was used by Welling (1969) for rejecting a 5 kHz signal. By appropriate scaling (of his R.C. values) the component values used in circuit C Fig. A.10 were obtained.

For network no. 7, Table A1 ;

$$y_{21} = K_R \frac{s^2 + \omega_z^2}{s^2 + \frac{p}{q_R} s + \omega_p^2} \qquad (A.14)$$

where

$$K_R = 1/R_1$$

$$\omega_z = 1/RC$$

$$\omega_p^2 = \frac{[1 + (1 + \rho)\alpha]}{R^2C^2}$$

$$q_R = \frac{1}{1 + \rho} \frac{1 + (1 + \rho)\alpha}{(2 + \alpha)}$$

$$\alpha = R/(R_1R_2/(R_1 + R_2)).$$

Calculations

$$\omega_z = \frac{1}{RC} = (2\pi)(50 \text{ Hz})$$

Set $R = 33\ k\Omega$, whence C 0.1 μF.

Set $R_1 = R_2 = 62\ k\Omega$ so that

$$\alpha = 1.06.$$

From stability considerations, Welling (1969), a value of ρ was found by trial and error which placed the poles of y_{21} (i.e. the roots of $S^2 + \frac{p}{q_r} S + \omega_p^2 = 0$), equation (A.14), on both sides of the notch (50 Hz). The value of ρ selected was 3.

$\therefore \omega_p = 2.29\ \omega_z = 2\pi\ (114.5 \text{ Hz})$,

$$q_r = 0.187$$

and the poles of y_{21} were obtained as,

$$S_1 = (2\pi)(590 \text{ Hz})$$
$$S_2 = (2\pi)(22.9 \text{ Hz})$$

Unity gain was obtained by selecting R_f, the op-amp feed-back resistor, such that,

$$y_{21}\Big|_{S=0} = \frac{\omega_z^2}{R_1 \omega_p^2} = \frac{1}{R_1(1+(1+\rho)\alpha)}$$

$$= y_{56}\Big|_{S=0} = \frac{1}{R_f} .$$

Substituting the values of R_1, ρ, and α, the value of R_f is 330 KΩ.

Circuit C, Fig. A.10 was constructed using these component values.

The satisfactory rejection of 50 Hz is seen in the frequency response curve, Fig. A.11.

Mean temperatures obtained in a laminar flame by measuring the thermocouple signal directly on a sensitive DVM, and by using the low-pass filter (without the probe heating current) were in agreement to within .2%.

APPENDIX B

TIME-MEAN VELOCITY MEASUREMENTS IN TURBULENT METHANE DIFFUSION FLAME

B.1 Introduction

The mean velocity measurements obtained in a turbulent methane diffusion flame, burner tube diameter 5 mm and Reynolds number 14,500, are presented in this appendix. Measurements of the time-mean velocity were required for two main reasons:

(1) To permit the conversion of the spectral density of temperature fluctuations obtained in the present investigation from frequency to wave number space.* This facilitated the comparison of the present temperature spectral density with the temperature data of Kunugi and Jinno (1959), the total emission data of Guenther and Simon (1969), and the OH emission data of Kuhnert and Guenther (1973).

(2) To provide accurate mean velocity data for validating prediction procedures.

A Laser Doppler Anemometer (L.D.A.), which is an optical probe, was employed for making the measurements. The probe relies on the availability of light scattering particles in the measurement location for its operation. By a suitable choice of the particles, i.e. size and chemical composition, negligible aerodynamic, thermal and chemical influence is exerted on the flow by their presence. The L.D.A. is, therefore,

---

* Spectral density data in frequency space are dependent on flow velocity, but in wave-number space they are not; the sets of data to be compared were taken in flows with different velocities.

preferable to pressure sensitive techniques which entail the insertion of a solid, flow-disturbing object in the flow; and there are no data reduction problems caused by the dependence of the instantaneous velocity on the instantaneous static pressure, temperature and species concentration. The hot-wire technique has not yet been successfully employed for measuring velocity in the reaction zone of a turbulent flame primarily because of probe failure.

This appendix consists of two further sections. In section B.2 the principle of the L.D.A. when used in the fringe mode is outlined, and the experimental apparatus is described. The mean velocity data are presented and discussed in section B.3.

B.2 Principle of Method and Apparatus

B.2.1 Principle of method

The theoretical principles and the practical aspects of the L.D.A. have been discussed thoroughly in the literature (see for example, Angus et al (1969), and Durst et al (1972)). The fringe mode of the L.D.A. was employed in this investigation because it is the best when the intensity of scattered light is low, and in the flame the concentration of light scattering particles was kept low to minimize thermal radiation from the particles in the high temperature regions of the flame.

The arrangement of the equipment in the fringe mode is best described by reference to Fig. B.1. It consists of: the Laser head which produces a monochromatic, coherent light beam; an "integrated optical unit" (incorporating a beam splitter, a mirror and a lens) for splitting the

Laser light beam into two beams of equal intensity and focussing them to intersect and produce a fringe pattern in the measurement volume; a lens which collects some of the light scattered by particles as they cross the measuring volume (the intensity of the scattered light fluctuates as particles cross the bright and dark fringes in the fringe pattern); and the photomultiplier which converts the light signal to a proportional electrical current.

The frequency of the signal is directly proportional to the velocity of the light scattering particle. This is easily shown by considering the geometry of the fringe pattern in Figs. B.2 and B.3. Fig. B.2 depicts the formation of the fringe pattern by the intersection of wave fronts, while Fig. B.3 shows two wavefronts from each light beam. The perpendicular distance between the wavefronts is λ, the wave-length of the beams; and 2θ is the angle between the beams 1 and 2. From Fig. B.3:

$$AC = \lambda/\sin\theta \qquad (B.1)$$

Hence

$$\Delta x = AC/2 = \lambda/2\sin\theta \qquad (B.2)$$

A complete cycle in the light intensity (and photomultiplier electrical signal) fluctuation occurs when a particle traverses the distance Δx. The signal frequency, f^*, is related to the particle velocity, U, and Δx by,

$$f^* = U/\Delta x \qquad (B.3)$$

Substituting for Δx from equation (B.2),

$$U = \lambda f^*/2\sin\theta \qquad (B.4)$$

Now, θ is determined by the geometry of the optical system and λ is a known property of the laser light source. Therefore an analysis of the electrical signal for its frequency yields the velocity of the particle directly.

B.2.2 Experimental apparatus

The experimental apparatus consisted of:

(1) The Laser source, a 5 mW Spectra-Physics Stabilite Model 120 Helium-Neon Laser;

(2) An "integrated optical unit" (designed by Durst and Whitelaw, Imperial College, London) which split the laser beam and focussed the two beams in the region of ther intersection, with an included angle of 16° when using a lens of focal length 150 mm;

(3) A photomultiplier, EMI Model 9558B, which converted the light signal to an electrical signal; and

(4) A Hewlett-Packard Model 8553A/8552B Spectrum Analyser used to obtain the probability density of the fluctuating velocity, from which the time-mean velocity was derived.

Titanium dioxide particles of mean diameter 2 μm were produced by passing the fuel stream through a fluidized bed. Titanium dioxide particles do not affect the combustion process (Zare (1972), Durst and Kleine (1973)). However, the mean diameter of these particles set an upper limit of 700 Hz on the frequency of fluid velocity fluctuations which they could follow to an accuracy of 99%; this upper limit was calculated using the equation for particle motion in a fluid quoted by Melling and Whitelaw (1973).

B.3 Results and Discussion

The mean velocity was obtained from the curve of the probability density function of velocity by using the relation given in Fig. 1.1 and the co-ordinates of the curve as data input to a computer program.

The mean velocity data so obtained on the flame axis and radially at 40 and 80 burner diameters are shown in Figs. B.4 and B.5. All the data are accurate to $\pm$ 1 m/s, which for the axial data is better than $\pm$ 2% near the burner exit and $\pm$ 10% for distances greater than 70 burner diameters from the burner exit.

BIBLIOGRAPHY

Angus, R.E., Morrow, D.L., Dunning, J.W. and French, M.J., 1969.
"Motion measurement by Laser-Doppler techniques."
Industrial and Engineering Chemistry, 61, p.9-20.

Baker, R.J., Bourke, P.J. and Whitelaw J.H., 1973.
"Measurements of instantaneous velocity in laminar and turbulent diffusion flames using an optical anemometer."
To be published by Journal of the Institute of Fuel. Available as a Department of Mechanical Engineering, Imperial College, Report ET/TN/A/11, (1971).

Becker, H.A. and Brown, A.P.G., 1969.
"Velocity Fluctuations in Turbulent Jets and Flames."
Twelfth Symposium (International) on Combustion, p. 1059-1068.

Bennett, H.E., 1961.
"The Contamination of Platinum Metal Thermocouples: Causes for failure in Hydrogen Atmospheres".
Platinum Metals Review, 5, p. 132-133.

Berkenbusch, von F., 1899.
"Zur Messung von Flammentemperaturen durch Thermoelemente, insbesondere über die Temperatur der Bunsenflamme."
Annalen der Physik und Chemie, Neue Folge, Band 67, p.649-667.

Bulewicz, E.M., 1967.
"Some observations on Chemiluminescence and Chemi-ionization in Flames."
Combustion and Flame, 11, p.297-308 (see p.304).

Calcote, H.F., 1962.
"Ion Production and Recombination in Flames".
Eight Symposium (International) on Combustion, p.184-199, (see pages, 195 & 196).

Calcote, H.F., 1963.
"Ion and Electron Profiles in Flames."
Ninth Symposium (International) on Combustion, p. 622-637 (see p.637).

Carslaw, H.S. and Jaeger, J.C., 1959.
Conduction of Heat in Solids, (Oxford University Press 1959). See p.149 and p.156.

Chomiak, J., 1970.
"A possible Propagation Mechanism of Turbulent Flames at High Reynolds Numbers."
Combustion and Flame, 15, p.319-321.

Chomiak, J., 1972.
"Application of Chemiluminescence Measurement to the Study of Turbulent Flame Structure."
Combustion and Flame, 18, p.429-433.

Chomiak, J. and Niedzialek, B., 1967.
"Measurement of Rapidly Varying Gas Temperatures in an Unsteady Flow."
International Journal Heat and Mass Transfer, 10, p.1571-1579.

Chung, P., 1972.
"Diffusion Flame in Homologous Turbulent Shear Flows."
The Physics of Fluids, 15, p.1735-1746.

Chung, P., 1972.
"Turbulent Diffusion Flame in Coutte Flow."
Paper presented at the 10th Aerospace Sciences Meeting, San Diego, California (Jan. 17-19, 1972).

Clements, R.M. and Smy, P.R., 1969.
"Electrostatic-Probe Studies in a Flame Plasma."
Journal of Applied Physics, 40, p.4553-4558.

Coantic, M., 1967.
"A Study of Turbulent Pipe Flow and the Structure of its Viscous Sublayer".
Paper presented at the Fourth Euromech Colloquium: "The Structure of Turbulence." Southampton, March 29-31, 1967.

Corrsin, S., 1958.
"Statistical Behaviour of a Reacting Mixture in Isotropic Turbulence".
The Physcis of Fluids, 1, p.42-47.

Denniston, D.W. Jnr., Oxendine, J.R. Knapschaeffer, D.H., Burgess, D.S. and Karlovitz, B., 1957.
"Applications of the Electronic Probe to the Study of Turbulent Flames".
Journal of Applied Physics, 28, p.70-75.

Donaldson, C. du P. and Hilst, G.R., 1972.
"Chemical Reactions in Inhomogeneous mixtures: The Effect of the Scale of Turbulent Mixing."
Paper presented to the 1972 Heat Transfer and Fluid Mechanics Institute.

Durão, D. and Whitelaw, J.H., 1973.
"Some Performance Characteristics of the Cambridge Consultants Frequency-Tracker Demodulator."
Available from Survey and General Instrument Co. (May 1973).

Durst, F., 1972a.
Thesis, Doctor of Philosophy, Faculty of Engineering, University of London, 1972.

Durst, F., 1972b.
Thesis, Doctor of Philosophy, Faculty of Engineering, University of London, 1972. See p.287.

Durst, F., Melling, A. and Whitelaw, J.H., 1972.
"The Application of Optical Anemometry to Measurements in Combustion Systems."
Combustion and Flame, 18, p.197-201.

Durst, F., Melling, A. and Whitelaw, J.H., 1972a.
"Optical Anemometer Measurements in Recirculating Flows and Flames".
Paper in: Fluid Dynamic Measurements in the Industrial and Medical Environments. Vol. 1, Conference Papers edited by D.J. Cockrell, Leicester University Press, 1972. p.81-87, see p.83.

Durst, F., Melling, A. and Whitelaw, J.H., 1972b.
"Laser Anemometry: A Report on EUROMECH 36."
Journal of Fluid Mechanics, 56, p.143-160.

Durst, F. and Kleine, R., 1973.
"Velocity Measurements in Turbulent Premixed Flames by Means of Laser Doppler Anemometers."
Sonderforschungsbereich 80 Ausbreitungs-und Transportvorgange in Stromungen, Universität, Karlsruhe. Report SFB/EM/3. (Translation of paper presented at the 6th German Flame Conference (Deutscher Flammentag) Essen, Germany, Sept. 1973).

Ebrahimi, I., 1967.
"A Method for the Measurement of the Local Distribution of Turbulence Intensity in Jet Flames."
Combustion and Flame, 11, p.255-259.

Edelman, R.B., Fortune, O.F., Weilerstein, G., Cochran, T.H. and Haggard, J.B. Jnr., 1973.
"An Analytical and Experimental Investigation of Gravity Effects upon Laminar Gas Jet-Diffusion Flames."
Fourteenth Symposium (International) on Combustion, p.399-412.

Egerton, A.C., Everett, A.J. and Moore, N.P.W., 1953.
"Sintered Metals as Flame Traps."
Fourth Symposium (International) on Combustion, p.689-695.

Eickhoff, H., 1968.
"Statischer Druck und Turbulenz in drehsymmetrischen Freistrahlen und Freistrahlflammen."
Thesis, Universität Karlsruhe (T.H.).

Engelhard, 1973.
Engelhard Industries Ltd., Data Sheet (for the pertinent thermocouple), May 1973.

Eschenroeder, A.Q., 1965.
"Turbulence Spectra in a Reacting Gas."
AIAA Journal, 3, p.1839-1846.

Fisan, H., 1970.
"Bestimmung der Temperatur-und Konzentrationsverteilung in einer offenen Methane-Sauerstoff-Flamme aus Strahldichtemessungen."
Doktor-Ingenieurs genehmigte Dissertation. Technischen Hochschule Aachen.

Fristrom, R.M. and Westenberg, A., 1965.
Flame Structure (McGraw-Hill Inc., 1965).

Gaydon, A.G. and Wolfhard, H.G., 1970a.
FLAMES: Their structure, radiation and temperature.
(Chapman and Hall Ltd., 1970).
See p.239.

Gaydon, A.G. and Wolfhard, H.G., 1970b.
FLAMES: Their structure, radiation and temperature.
(Chapman and Hall Ltd., 1970).
See p.217.

Gaydon, A.G. and Wolfhard, H.G., 1970c.
FLAMES: Their structure, radiation and temperature.
(Chapman and Hall Ltd., 1970).
See p.215.

Gaydon, A.G. and Wolfhard, H.G., 1970d.
FLAMES, Their structure, radiation and temperature.
(Chapman and Hall Ltd., 1970).
See p.199.

Gilbert, M. and Lobdell, J.H., 1953.
"Resistance-Thermometer Measurements in a Low-Pressure Flame."
Fourth Symposium (International) on Combustion, p.285-294.

Guenther, R., 1970.
"Measurement of Flame Turbulence: aims, methods and results."
Journal of the Institute of Fuel, 43, p.187-192.

Guenther, R. and Simon, H., 1969.
"Turbulence Intensity, Spectral Density Functions, and Eulerian Scales of Emission in Turbulent Diffusion Flames."
Twelfth Symposium (International) on Combustion, p.1069-1079.

Hawthorne, W.R., Weddell, D.S. and Hottel, H.C., 1949.
"Mixing and Combustion in Turbulent Gas Jets."
Third Symposium (International) on Combustion, p.266-288, (see p.276-280).

Hildebrand, F.B., 1962.
Advanced Calculus for Applications,
(Prentice-Hall, Inc., 1962). See p.64.

Hinze, J.O., 1959a.
Turbulence, (McGraw-Hill Inc., 1959).
See p.514.

Hinze, J.O., 1959b.
Turbulence, (McGraw-Hill Inc., 1959).
See p.423.

Hinze, J.O., 1959c.
Turbulence, (McGraw-Hill Inc., 1959).
See p.431 (data quoted in Sec. 6.10).

Hinze, J.O., 1959d.
Turbulence. (McGraw-Hill Inc., 1959).
See p.7.

Hinze, J.O., 1959e.
Turbulence (McGraw-Hill Inc. 1959).
See p.439.

Ielev, V.N., 1957.
"Combustion of a turbulent jet in burners with preliminary mixing."
Sixth Symposium (International) on Combustion. p.317-325.

Johnson, E.O. and Malter, L., 1950.
"A Floating Double Probe Method for Measurements in Gas Discharges."
Physical Review, 80, p.58-68.

Karlovitz, B., 1953.
"Open Turbulent Flames."
Fourth Symposium (International) on Combustion, p.60 - 67.

Karlovitz, B., Denniston, D.W. Jnr., Knapschaefer, D.H. and
Wells, F.E., 1953.
"Studies on Turbulent Flames.
A. Flame Propagation Across Velocity Gradients.
B. Turbulence Measurements in Flames."
Fourth Symposium (International) on Combustion, p.613-620.

Kent, J.H., 1970.
"A Non-Catalytic Coating for Platinum-Rhodium Thermocouples."
Combustion and Flame, 14, p.279-282.

Kent, J.H. and Bilger, R.W., 1973.
"Turbulent Diffusion Flames."
Fourteenth Symposium (International) on Combustion,
p.615-625.

Kleine, R., 1971.
"Passives und aktives Verhalten einer Flammen-front in
turbulenter Strömung."
Chemie Ingenieur Technik, 43. Jahrg. Heft 5, p.286-292.

Kuhnert, D. and Guenther, R., 1973.
"Turbulent Scale of OH-Radiation."
Combustion Institute European Symposium, paper 86, p.518-523.

Kunugi, M. and Jinno, H., 1959.
"Measurements of Fluctuating Flame Temperature."
Seventh Symposium (International) on Combustion p.942-948.

Laufer, J., 1953.
"The Structure of Turbulence in Fully Developed Pipe Flow."
NACA TN 2954.

Launder, B.E. and Spalding, D.B., 1972.
"Mathematical Models of Turbulence."
Academic Press, London.

Lee, J., 1966.
"Isotropic Turbulent Mixing under a Second-Order Reaction."
The Physics of Fluids, 9 p. 1753-1763.

Mallard et Le Chatelier, 1883.
"Combustion des Mélanges Gazeux Explosifs."
Annales des Mines, 4, p.274-568
(see p.331-335).

Mason,H.B., and Spalding, D.B., 1973.
"Prediction of Reaction-Rates in Turbulent Premixed Boundary-Layer Flows."
Combustion Institute European Symposium, paper 100, p.601-606.

Melling, A. and Whitelaw, J.H., 1973.
"Seeding of Gas Flows for Laser Anemometry."
DISA Information, No. 15, Oct. 1973, p.5-14.

Milson, A. and Chigier, N.A., 1973.
"Studies of Methane and Methane-Air Flames impinging on a Cold Plate."
Combustion and Flame, 21, p.295-305.

Moffat, R.J., 1962.
"Gas Temperature Measurement."
TEMPERATURE: Its Measurement and Control in Science and Industry, Vol. III, Part 2, Reinhold Publishing Company, 1962. Paper 52, p.553-571 (see p.556.)

Moschytz, G.S., 1967.
"Active RC filter Building Blocks Using Frequency Emphasizing Networks."
IEEE Journal of Solid-State Circuits, June 1967, Vol. SC-2, p.59-62.

O'Brien, E.E., 1966.
"Closure Approximations Applied to Stochastically Distributed Second-Order Reactants."
The Physics of Fluids, 9, p.1561-1565.

O'Brien, E.E., 1969.
"Postulate of Statistical Independence for Decaying Reactants in Homogeneous Turbulence."
The Physics of Fluids, 12, p.1999-2005.

O'Brien, E.E., 1971.
"Turbulent Mixing of Two Rapidly Reacting Chemical Species."
The Physics of Fluids, 14, p.1326-1331.

Parker, K.H. and Guillon, O., 1971.
"Local Measurements in a Turbulent Flame by Hot-Wire Anemometry."
Thirteenth Symposium (International) on Combustion, p.667-674.

Patankar, S.V. and Spalding, D.B., 1970.
Heat and Mass Transfer in Boundary Layers, (International Textbook Company, Ltd., 1970).

Patankar, S.V. and Spalding, D.B., 1973.
"A Computer Model for Three-Dimensional Flow in Furnaces."
Fourteenth Symposium (International) on Combustion,
p.605-614.

Rhodes, R.P. and Harsha, P.T., 1972.
"On putting the 'Turbulent' in Turbulent Reacting Flow."
Paper presented at the AIAA 10th Aerospace Sciences Meeting,
San Diego, California (Jan. 17-19, 1972).

Ribeiro, M., 1973.
Private Communication.

Richmond, J.K., Grumer, J. and Burgess, D.S., 1959.
"Turbulent Flame Propagation by Large Scale Wrinkling of
a Laminar Flame Front."
Seventh Symposium (International) on Combustion, p.615-620.

Rodi, W., 1972.
Thesis, Doctor of Philosophy, Faculty of Engineering,
University of London.

Scadron, M.D. and Warshawsky, I., 1952a.
"Experimental Determination of Time Constants and Nusselt Numbers
for Bare-wire Thermocouples in High-Velocity Air streams and Analytic
Approximations of Conduction and Radiation Errors."
NACA TN 2599. See p.7.

Scadron, M.D. and Warshawsky, I., 1952b.
NACA TN 2599.
See p. 51.

Scadron, M.D. and Warshawsky, I., 1952c.
NACA TN 2559.
See p.10.

Schmidt von H., 1909.
"Prüfung der Strahlungsgesetze der Bunsenflamme."
Annalen der Physik, 4^{E} Folge, Band XXIX, p.971-1028.

Shchetinkov, E.S., 1959.
"Calculations of Flame Propagation in a Turbulent Flow."
Paper 1: Proceedings of the Moscow Seminar on Combustion held
at the Energetics Institute of the U.S.S.R. Academy of Sciences.
(Pages 1-40 of "Combustion in Turbulent Flow": Translation for NASA
and the Nat. Sc. Found., U.S.A. by The Israel Program for Scientific
Translations.)

Shepard, C.E. and Warshawsky, I., 1952.
"Electrical Techniques for Compensation of Thermal Time Lag
of Thermocouples and Resistance Thermometer Elements."
NACA TN 2703.

Smith, R., Stafford, C.M. and Winefordner, J.D., 1969.
"Temperature Profiles of Turbulent Hydrogen Diffusion Flames Used in Atomic Fluorescence Spectrometry."
Analytical Chemistry, 41, p.946-952.

Spalding, D.B., 1967.
"The Spread of Turbulent Flames Confined in Ducts."
Eleventh Symposium (International) on Combustion.
p.807-815.

Spalding, D.B., 1969.
"Turbulence Effects on Combustion."
Mechanical Engineering Department, Imperial College, Report BL/TN/B/22.
(English Text of Lecture at VDI Tagung. "Verbrennung und Feuerungen" Karlsruhe, Oct. 1969).

Spalding, D.B., 1971 .
"Mixing and Chemical Reaction in Steady Confined Turbulent Flames."
Thirteenth Symposium (International) on Combustion, p.649-657.

Summerfield, M., Reiter, S.H., Kebely, V. and Mascolo, R.W., 1955.
"The Structure and Propagation Mechanism of Turbulent Flames in High Speed Flow."
Jet Propulsion (Journal of the American Rocket Society), 25, p.377-384.

Tennekes, H., 1968.
"Simple Model for the Small-Scale Structure of Turbulence."
The Physics of Fluids, 11, p.669-671.

Townsend, A.A., 1956a.
The Structure of Turbulent Shear Flow.
(Cambridge University Press, 1956).
See Chapters 5, 6, 7 and 8.

Townsend, A.A., 1956b.
The Structure of Turbulent Shear Flow.
(Cambridge University Press, 1956).
See Sub-section 5.14.

Travers, B.E.L. and Williams, H., 1965.
"The Use of Electrical Probes in Flames Plasmas."
Tenth Symposium (International) on Combustion, p.657-672.

Vassilatos, G. and Toor, H.L., 1965.
"Second Order Chemical Reactions in a Non-homogeneous Turbulent Fluid."
A.I.Ch.E. Journal, 11, p.666-673.

Vlasov, K.P., 1959.
"Experimental Investigation of the Combustion Zone in a Turbulent Flame."
Page 2: Proceedings of the Moscow Seminar on Combustion held at the Energetics Institute of the U.S.S.R. Academy of Sciences.
(Pages 41-47 of "Combustion in Turbulent Flow": Translation for NASA and the Nat. Sc. Found., U.S.A. by the Israel Program for Scientific Translations.)

Welling, B., 1969.
"Design Theory. Active Filters: Part 6. The Op. Amp. saves time and money."
Electronics, Feb. 3, 1969, p.82-90.

Widhopf, G.F. and Lederman, S., 1971.
"Specie Concentration Measurements Utilizing Raman Scattering of a Laser Beam."
AIAA Journal, 9 p.309-316.

Williams, G.C., Hottel, H.C., and Gurnitz, R.N., 1969.
"A Study of Premixed Turbulent Flames by Scattered Light."
Twelfth Symposium (International) on Combustion, p.1081-1092.

Zare, M.R., 1972.
Thesis, Master of Science, Faculty of Mechanical Engineering, University of London, 1972.

Zysk, E.D., 1962.
"Platinum Metal Thermocouples."
TEMPERATURE: Its Measurement and Control in Science and Industry, Vol. III, Part 2, Reinhold Publishing Company, 1962.
Paper 8, p.135-156 (see p.138).

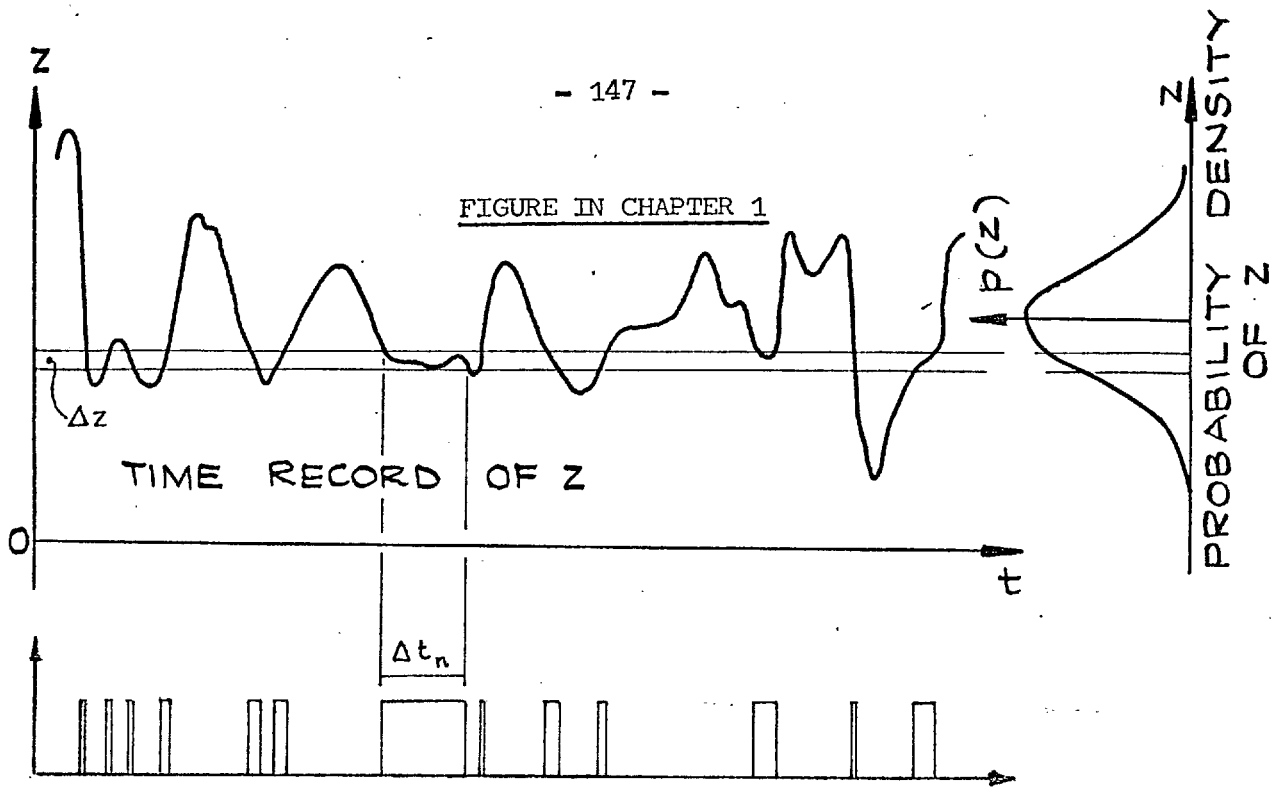


Fig. 1.1

Definitions of the mean, rms, higher order moments, probability density and spectral density of a stationary fluctuating variable, z.

Probability Density p(z).

$$p(z) \equiv \text{Lim}_{\substack{\Delta z \to 0 \\ \bar{T} \to \infty}} \frac{1}{\Delta z} \frac{\Sigma \Delta t}{\bar{T}} \qquad 1.1$$

$\bar{T}$ is the length of a time record of the variable.

Moments

Time-mean, $$\bar{z} = \int_{-\infty}^{\infty} z\, p(z)\, dz \ , \qquad 1.2$$

$$(z - \bar{z})^n = \int_{-\infty}^{\infty} (z - \bar{z})^n\, p\,(z)\, dz \ ,$$

$$n = 1, 2, \ldots \qquad 1.3$$

Rms of z $$\equiv \sqrt{(z - \bar{z})^2} \qquad 1.4$$

Spectral Density

The fluctuations of z, $(z - \overline{z})$, can be represented by a Fourier series:

$$(z - \overline{z}) = \sum_{\alpha=1}^{\infty} C_\alpha \sin (2\pi ft - \gamma_\alpha) \qquad 1.5$$

where $f = \alpha/T$, C_α and γ_α are the amplitude and phase angle associated with the αth harmonic of $(z - \overline{z})$.

The (one-dimensional) spectral density, $F(n^*)$, is defined by:

$$(z - \overline{z})^2 = \int_0^\infty F(n^*)\, dn^* \qquad 1.6$$

In wave number space, the spectral density, $F(k^*)$, in the direction of mean velocity is:

$$(z - \overline{z})^2 = \int_0^\infty F(k^*)\, dK^* \qquad 1.7$$

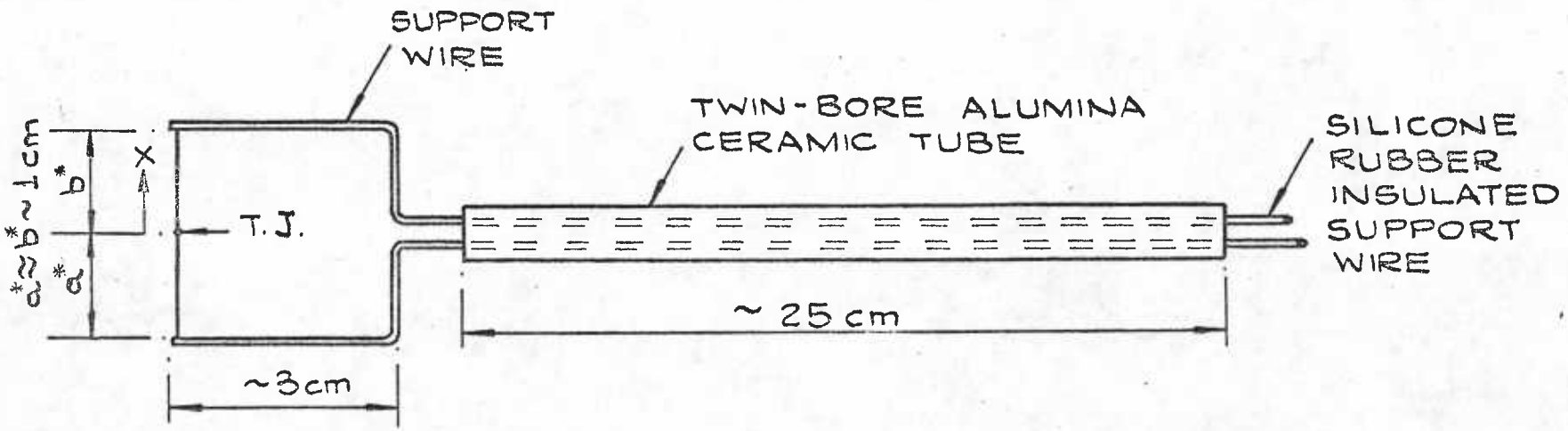
where $k^* = n^*/(2\pi.u)$

and u is the mean velocity.

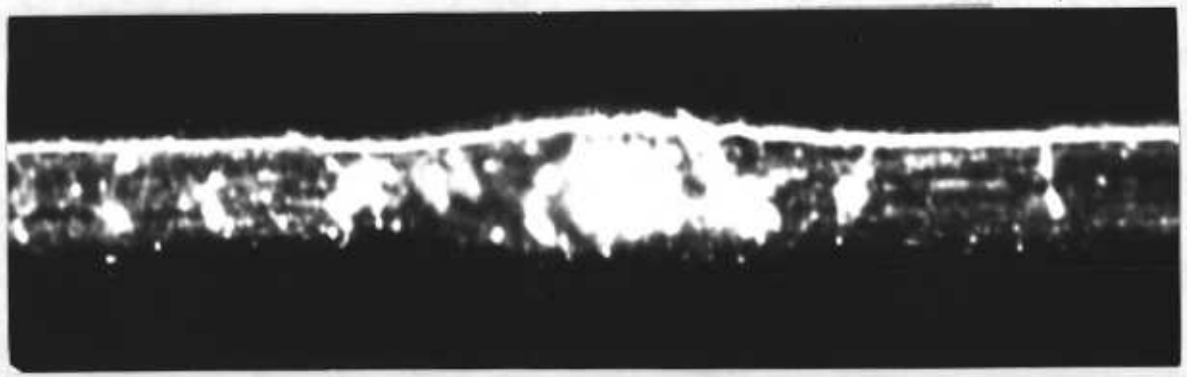
FIGURES IN CHAPTER 2

Figure	Title	Page
Fig. 2.2.1	(a) Schematic of assembled thermocouple. (b) Photomicrograph of junction of a typical 40 μm diameter 30% Rh/Pt vs. 6% Rh/Pt thermocouple.	150
Fig. 2.2.2	Typical curves of: (1) Temperature vs. radiant energy for a thermocouple in vacuo; (2) Temperature vs. heating energy for a thermocouple in a flame; and (3) $T^4 - T_{AMB}^4$ vs. heating energy for a thermocouple in vacuo.	151
Fig. 2.2.3	Photograph of the high vacuum rig.	152
Fig. 2.4.2	Curves of the amplitude ratios of thermocouple 1st and 2nd harmonics to gas temperature harmonic.	153
Fig. 2.4.3	Picture of the equipment used for heating a thermocouple and measuring its temperature.	154
Fig. 2.4.4	Schematic of high turns ratio electronic transformer, compensator and noise filter.	155
Fig. 2.4.5	Comparison of compensated and uncompensated thermocouple signal.	156
Fig. 2.4.5	Variation of the 2nd harmonic error (in compensated thermocouple signal) with frequency.	157

FIG. 2.2.1 TOP (a) BOTTOM (b)



T.J. ≡ THERMOCOUPLE JUNCTION.
FLOW DIRECTION PERPENDICULAR TO PLANE OF FIGURE.



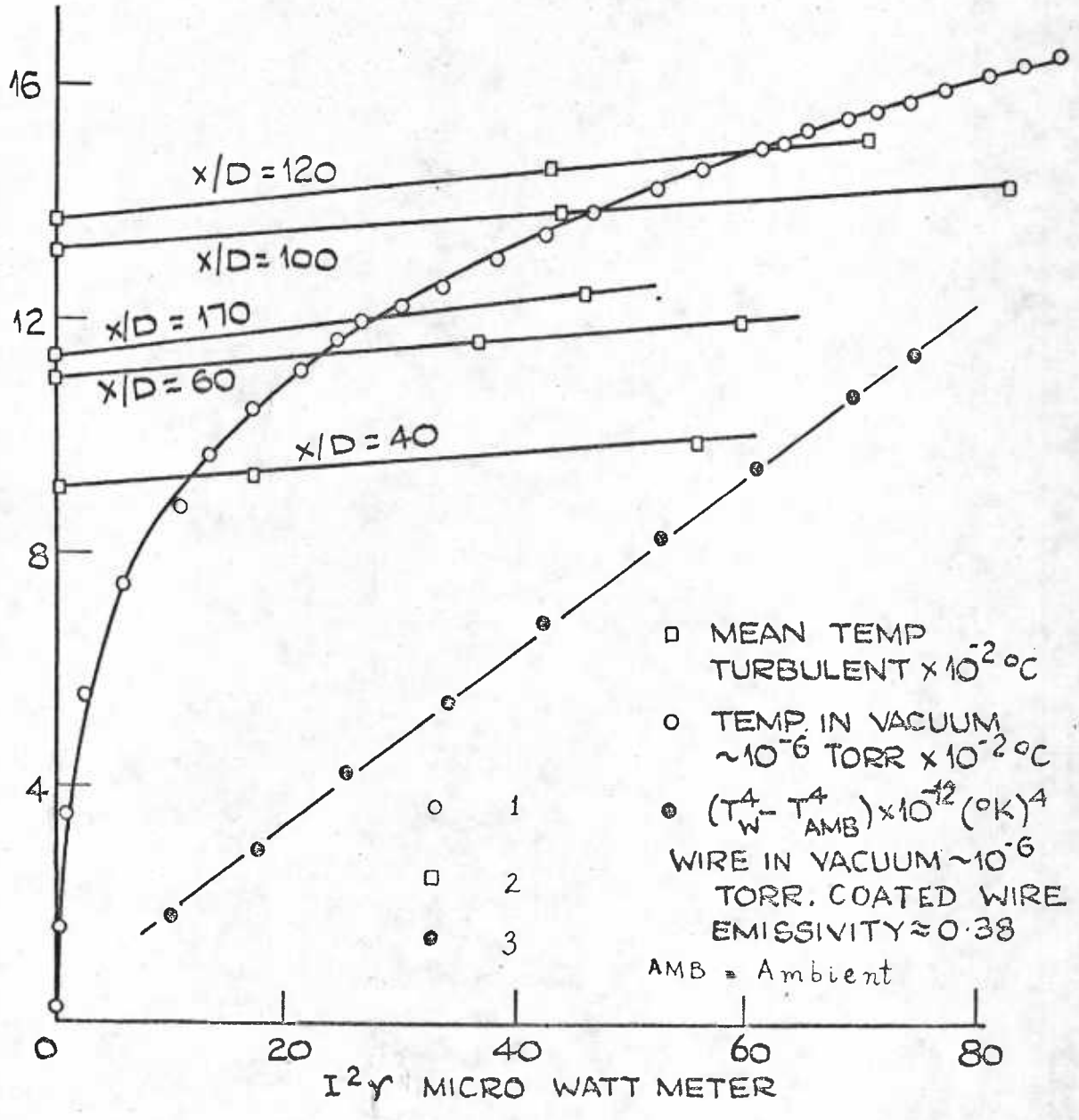

16
12
8
4
0
20
40
60
80
x/D = 120
x/D = 100
x/D = 170
x/D = 60
x/D = 40
MEAN TEMP TURBULENT x 10⁻² °C
TEMP. IN VACUUM ~10⁻⁶ TORR x 10⁻² °C
(T⁴W - T⁴AMB) x 10⁻¹² (°K)⁴
WIRE IN VACUUM ~10⁻⁶ TORR. COATED WIRE EMISSIVITY ≈ 0·38
AMB = Ambient
1
2
3
I²γ MICRO WATT METER

FIG. 2.2.2

(1) Pyrex vacuum chamber

(2) Penning Model 6 0145-08-000 Ionisation gauge

(3) Edwards Liquid-Nitrogen Vapour Trap.

(4) Edwards Vapour Diffusion Pump Model 103A

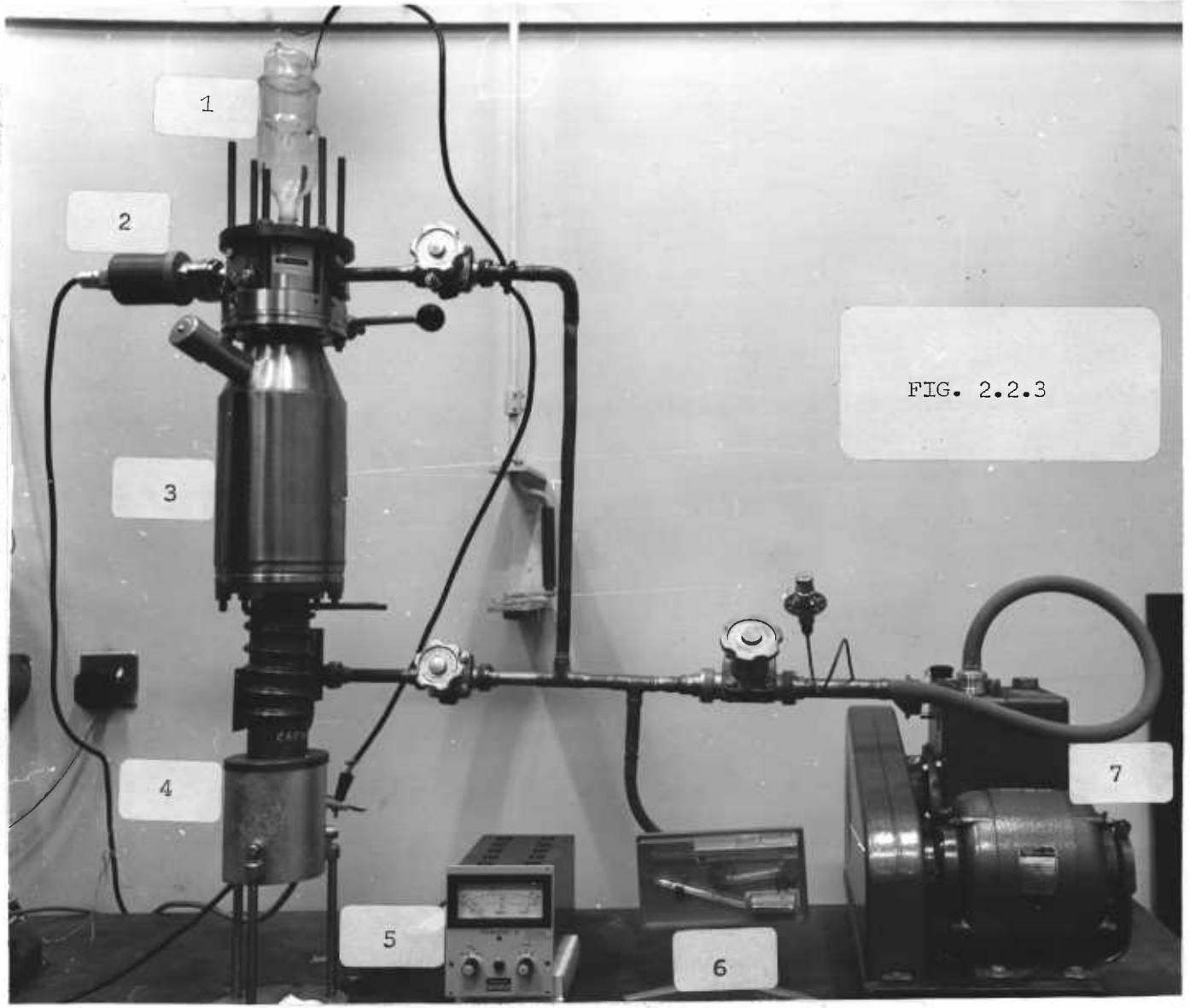


FIG. 2.2.3

(5) Penning 8 vacuum meter

(6) McLeod Vacuum Gauge

(7) Edwards ES 150 High Vacuum Pump

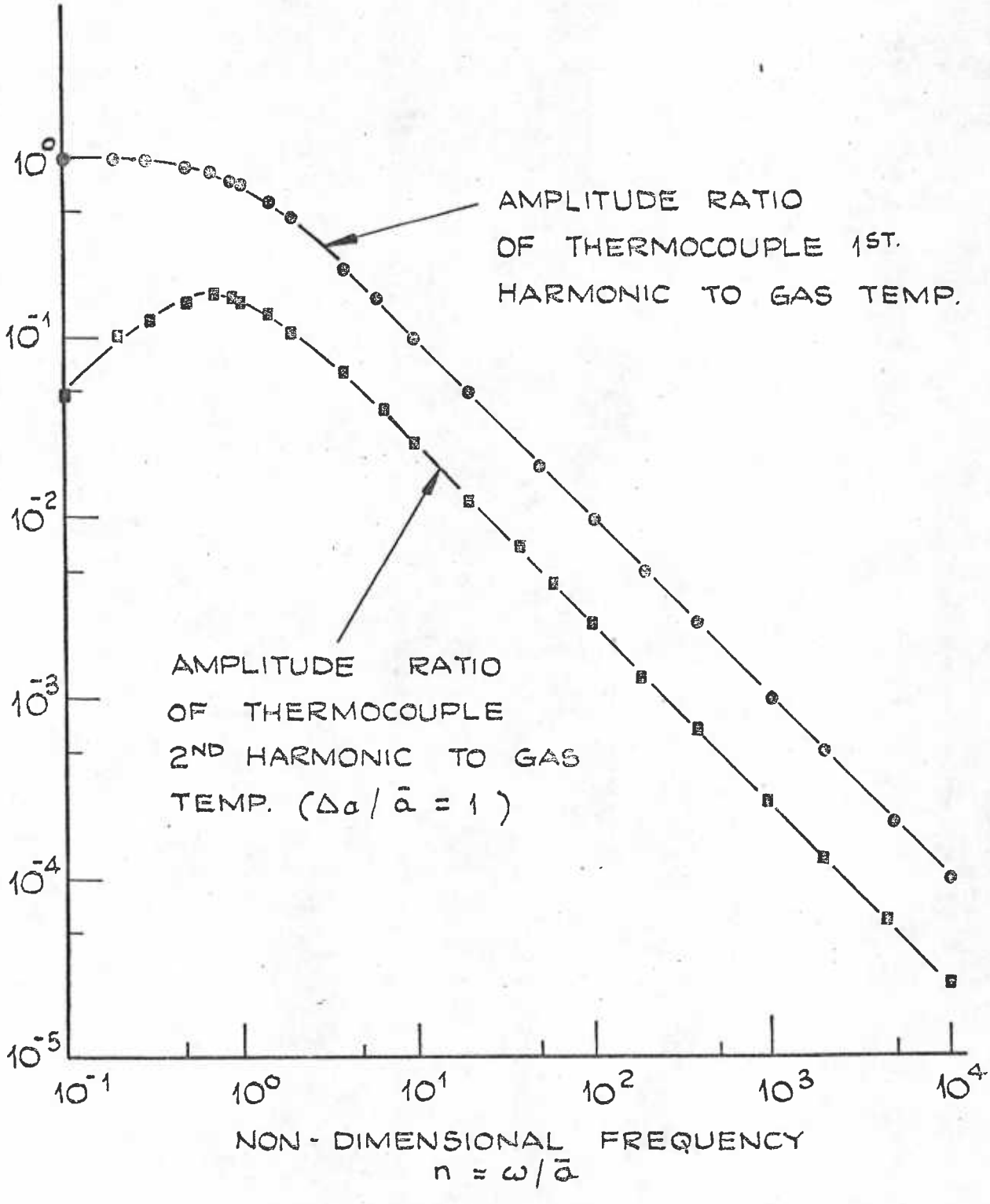

AMPLITUDE RATIO
OF THERMOCOUPLE 1ST.
HARMONIC TO GAS TEMP.
AMPLITUDE RATIO
OF THERMOCOUPLE
2ND HARMONIC TO GAS
TEMP. (Δa / ā = 1)
10^0
10^-1
10^-2
10^-3
10^-4
10^-5
10^-1
10^0
10^1
10^2
10^3
10^4
NON - DIMENSIONAL FREQUENCY
n = ω / ā

FIG. 2.4.2

1. SIGNAL GENERATOR

2. POWER AMPLIFIER (SINCLAIR Z 50)

3. AMMETER (SOLARTRON LM 1240

4. LOW-PASS, LOW-DRIFT AMPLIFYING UNIT (FOR PROBE EMF)

5. TRUE INTEGRATOR

6. THERMOCOUPLE

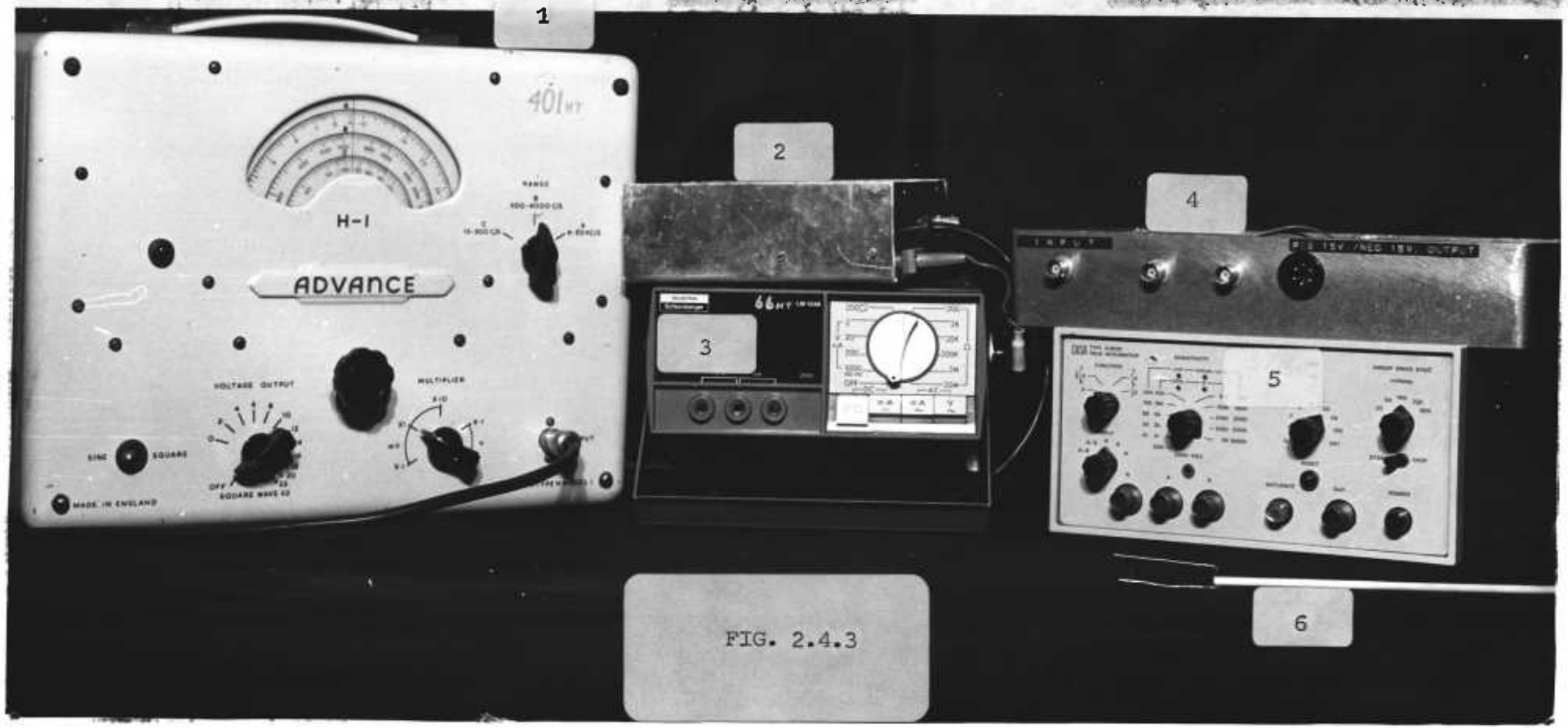
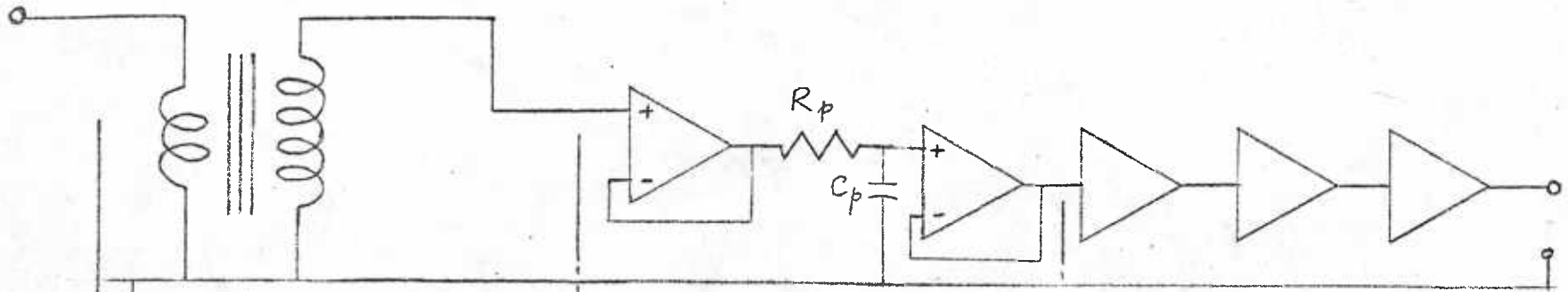


FIG. 2.4.3



330 : 1

GARDNERS ELECTRONIC TRANSFORMER.

BUFFER TO MATCH IMPEDANCES AND ELIMINATE "RINGING" OF TRANSFORMER.

THERMAL INERTIA COMPENSATOR ACTIVE FILTER. & NOISE FILTER

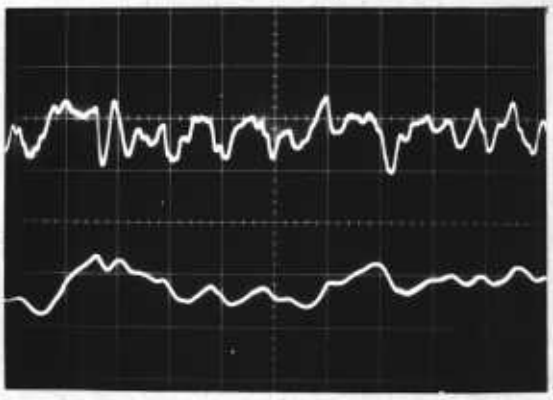
$R_p = 47\ k\Omega.$

$1/(R_p C_p) = (2\pi)(12\ kHz).$

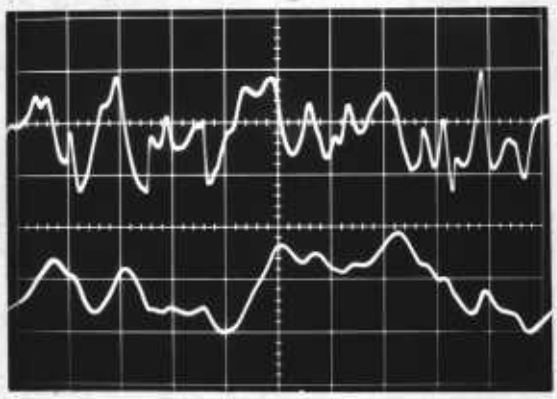
FIG. 2.4.4

Fig. 2.4.5

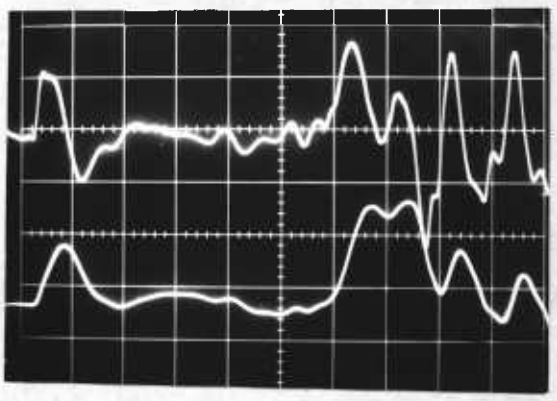
Temperature fluctuations: compensated (top trace) and uncompensated signals. Axis methane diffusion flame Re 14,500. Burner diameter 0.5 cm.



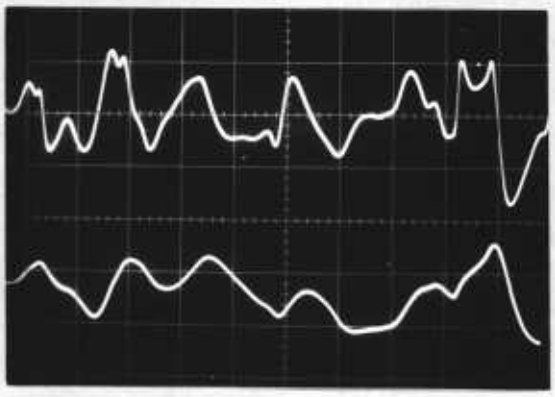
(a)



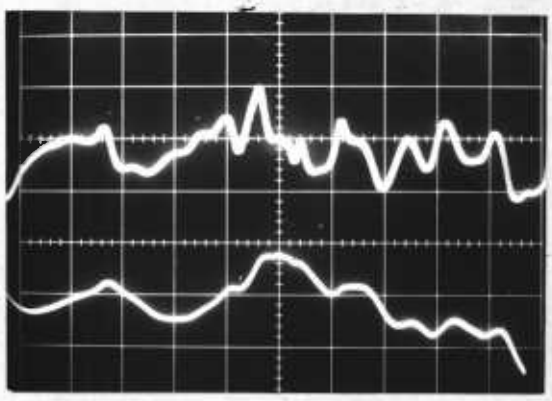
(b)



(c)



(d)

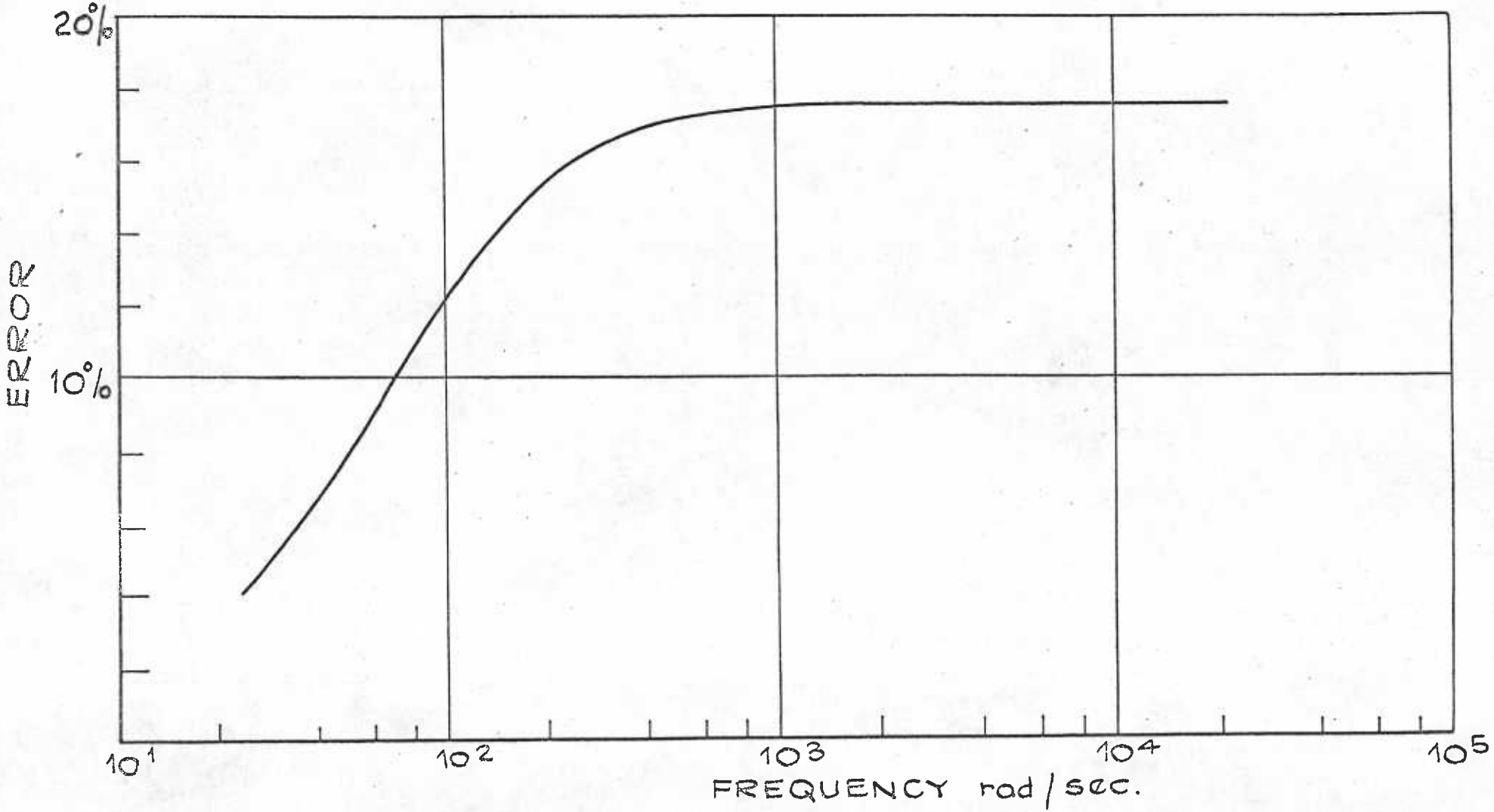


(e)

	X/D	r (mm)	Time Scale ms/div.	Amplitude Scale of Traces Top v/div.	Bottom mv/div.
(a)	40	0	5	0.5	50
(b)	60	0	5	0.5	50
(c)	80	0	10	0.5	50
(d)	120	0	10	1.0	50
(e)	140	0	10	1.0	50

Compensator DC amplification: 3.33

FIG. 2.4.6



FIGURES IN CHAPTER 3

Figure	Title	Page
Fig. 3.2.a	Principle of operation of the ionisation probe: potential diagram.	159
Fig. 3.2.b	Principle of operation of the ionisation probe: idealised current vs. voltage plot.	160
Fig. 3.2.c	Schematic of present ionisation probe.	161
Fig. 3.2.d	Photomicrograph of pointed tip of probe sensing wire.	161
Fig. 3.2.e	Sketch of composite boron nitride/brass cone.	162
Fig. 3.2.f	Picture of a bent hypodermic tube used for fabricating the water cooling jacket.	162
Fig. 3.2.g	Picture of a water cooling jacket, a composite boron nitride/brass cone and a hypodermic tube.	163
Fig. 3.3.a	Schematic of the ionisation measurement circuit.	164
Fig. 3.3.b	Comparison of probe signal before (top trace) and after squaring.	165
Fig. 3.3.c	Typical traces of comparator (top trace) and squared probe signals.	166
Fig. 3.3.d	Influence of comparator discrimination level (D.L.) on the probability of combustion and the combustion count.	167

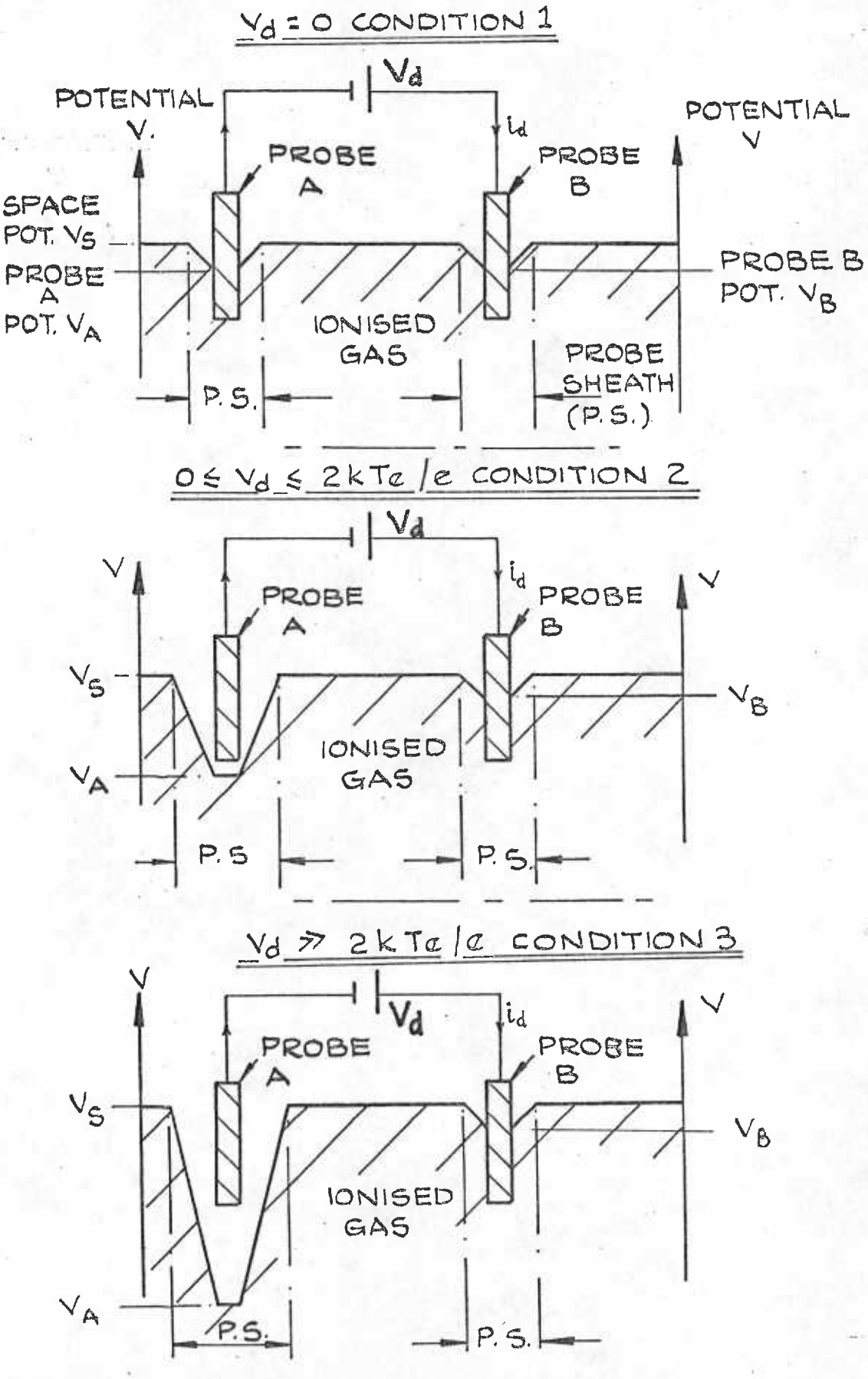

$V_d = 0$ CONDITION 1
POTENTIAL V.
V_d
i_d
POTENTIAL V
PROBE A
PROBE B
SPACE POT. V_S
PROBE A POT. V_A
PROBE B POT. V_B
IONISED GAS
PROBE SHEATH (P.S.)
P.S.
$0 \leq V_d \leq 2kT_e/e$ CONDITION 2
V
V_d
i_d
PROBE A
PROBE B
V
V_S
V_B
V_A
IONISED GAS
P.S
P.S.
$V_d \gg 2kT_e/e$ CONDITION 3
V
V_d
i_d
PROBE A
PROBE B
V
V_S
V_B
IONISED GAS
V_A
P.S.
P.S.

FIG. 3.2.a

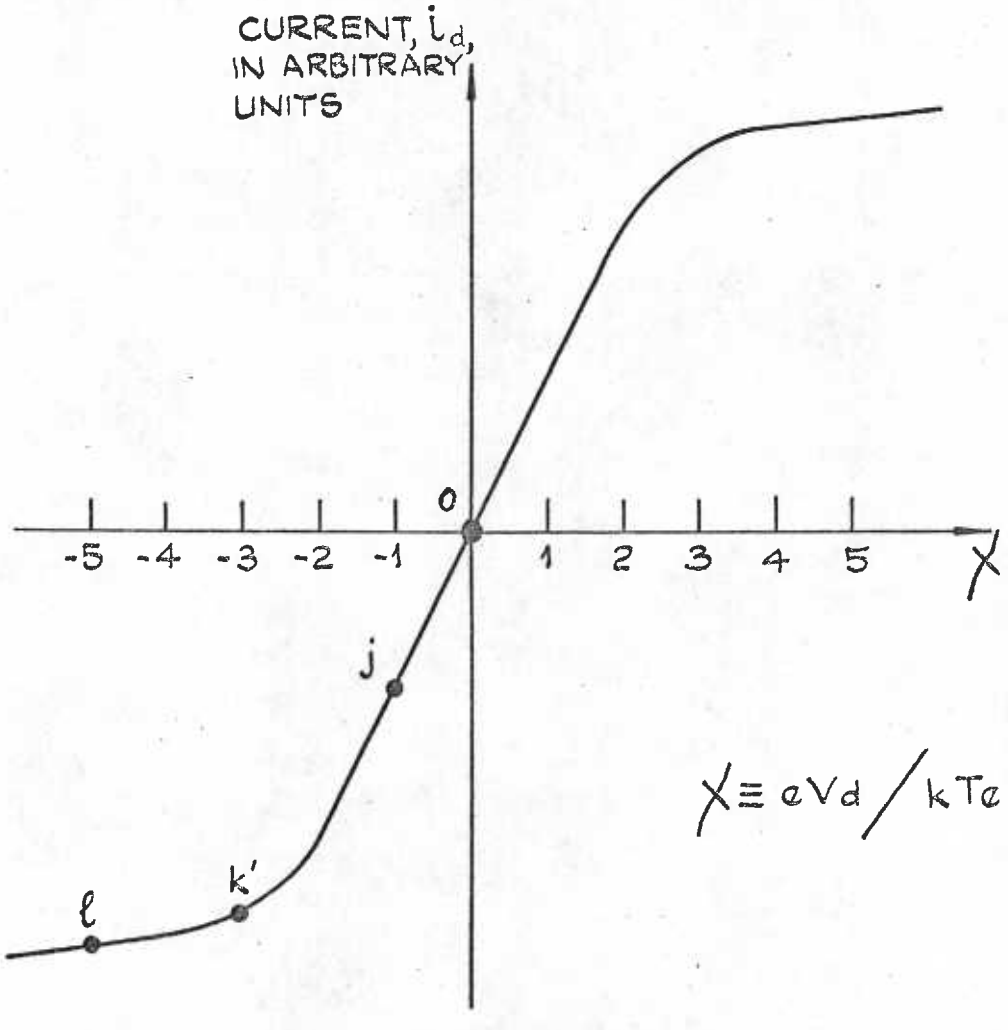
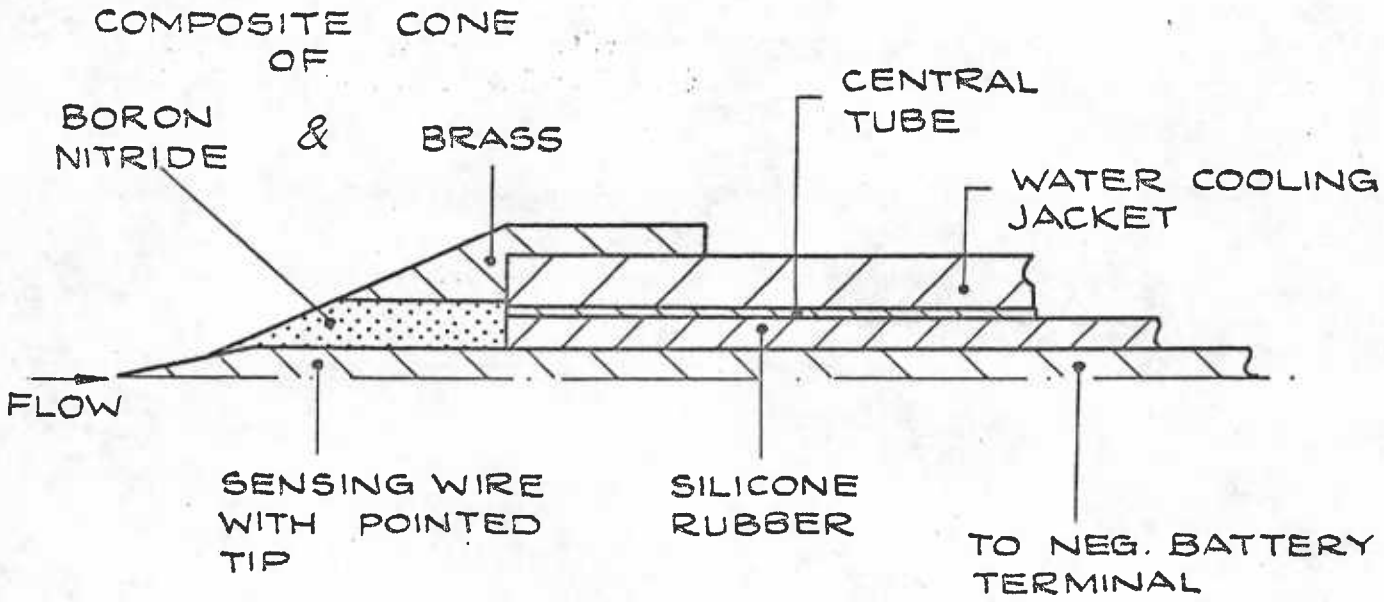
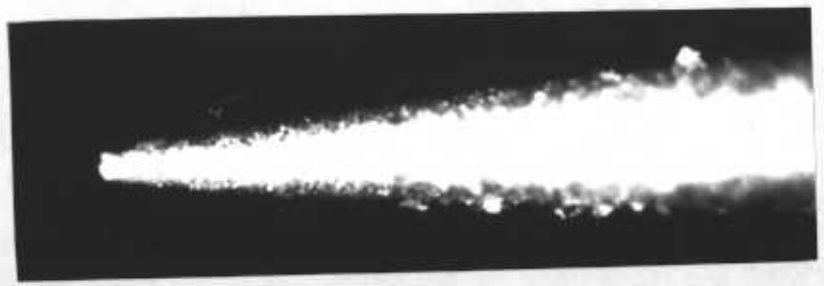

CURRENT, i_d, IN ARBITRARY UNITS
0
-5 -4 -3 -2 -1
1 2 3 4 5
X
j
k'
ℓ
$X \equiv eV_d / kT_e$

FIG. 3.2.b

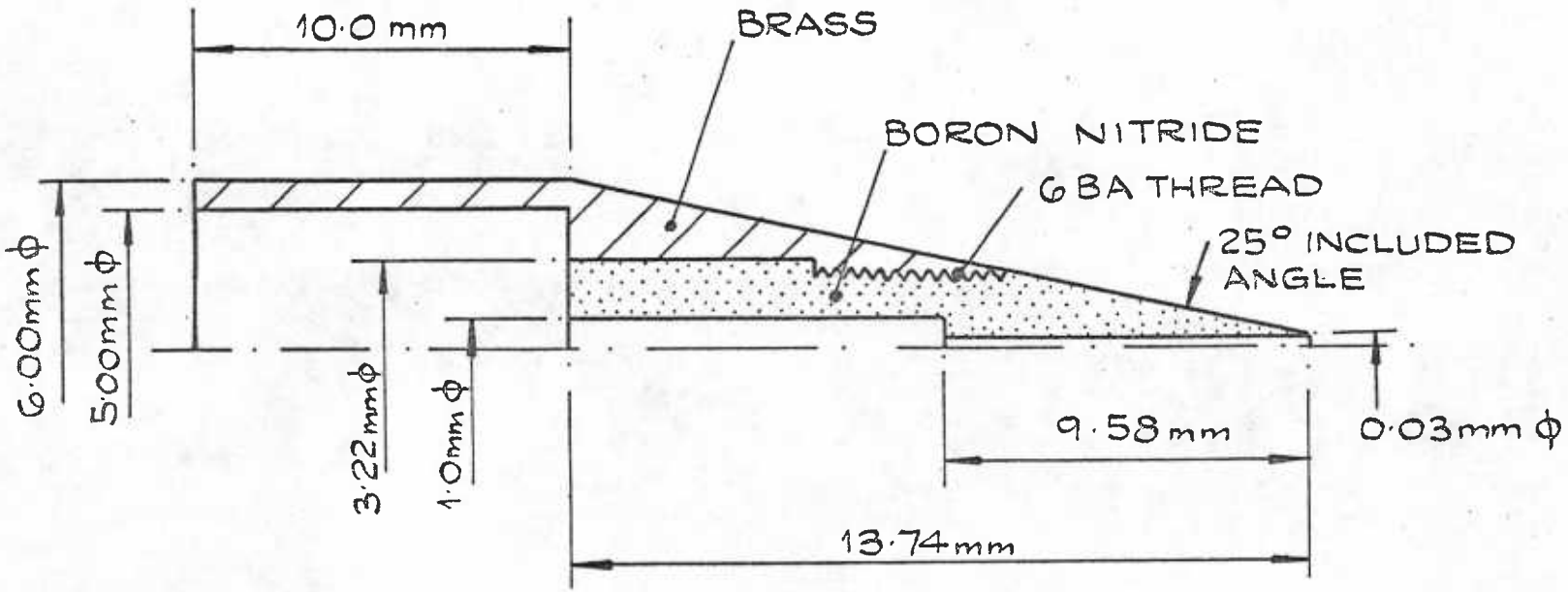
TOP FIG. 3.2c

BOTTOM FIG. 3.2d





TOP FIG. 3.2e



BOTTOM FIG. 3.2f



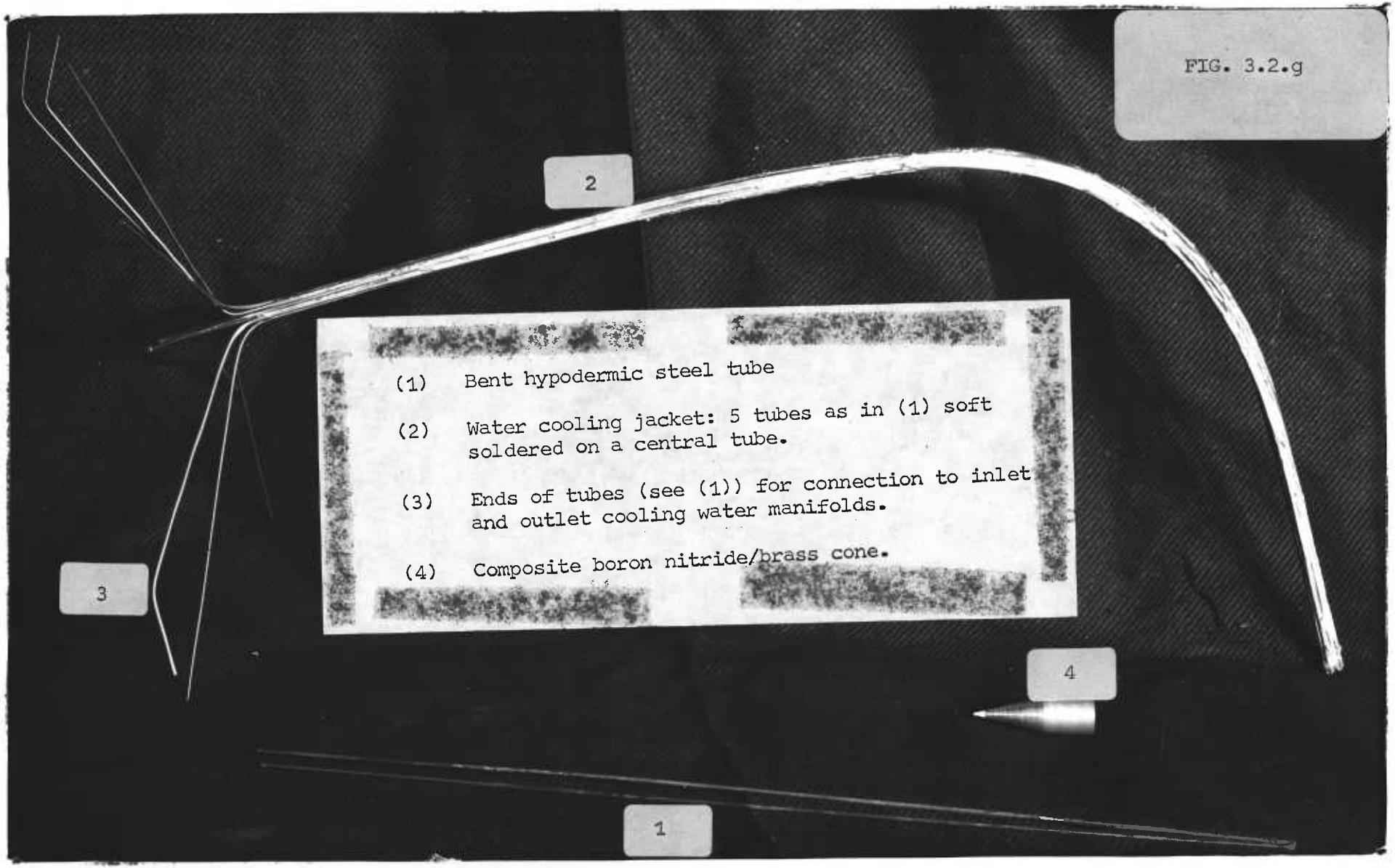


FIG. 3.2.g

(1) Bent hypodermic steel tube

(2) Water cooling jacket: 5 tubes as in (1) soft soldered on a central tube.

(3) Ends of tubes (see (1)) for connection to inlet and outlet cooling water manifolds.

(4) Composite boron nitride/brass cone.

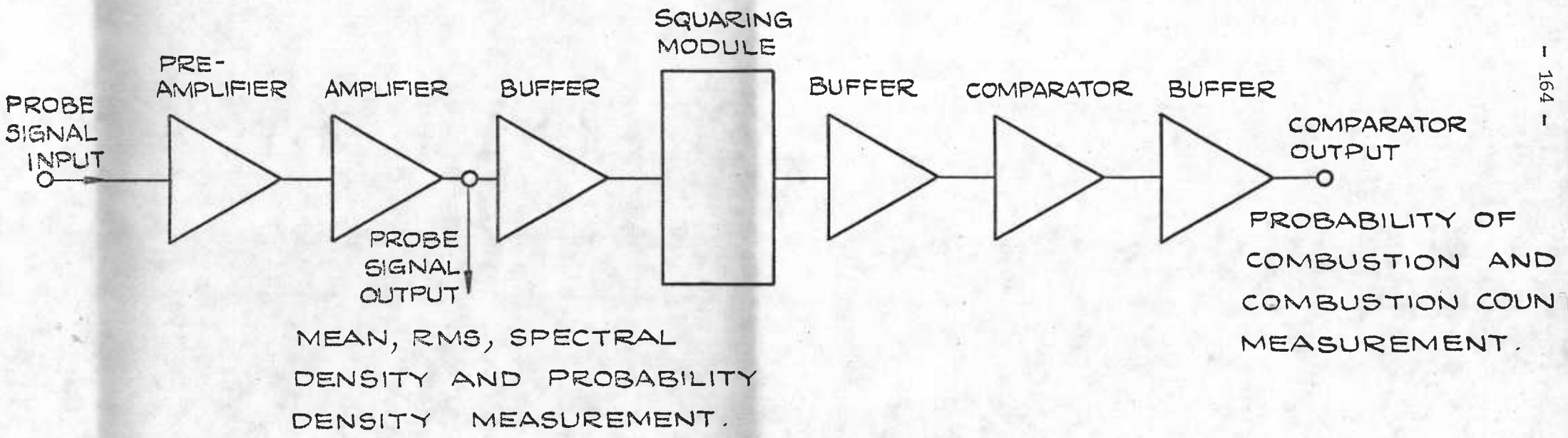
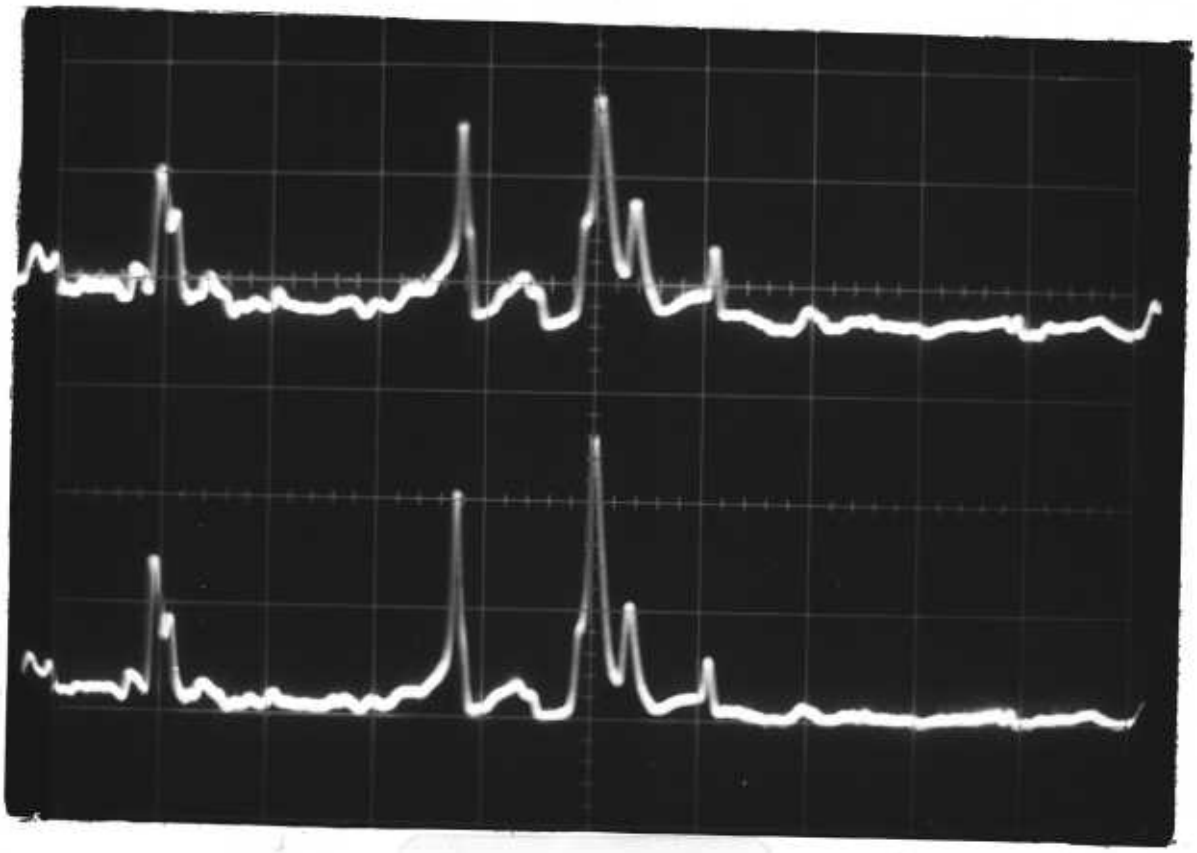

PROBE SIGNAL INPUT
PRE-AMPLIFIER
AMPLIFIER
BUFFER
SQUARING MODULE
BUFFER
COMPARATOR
BUFFER
COMPARATOR OUTPUT
PROBE SIGNAL OUTPUT
MEAN, RMS, SPECTRAL DENSITY AND PROBABILITY DENSITY MEASUREMENT.
PROBABILITY OF COMBUSTION AND COMBUSTION COUN MEASUREMENT.

FIG. 3.3.a

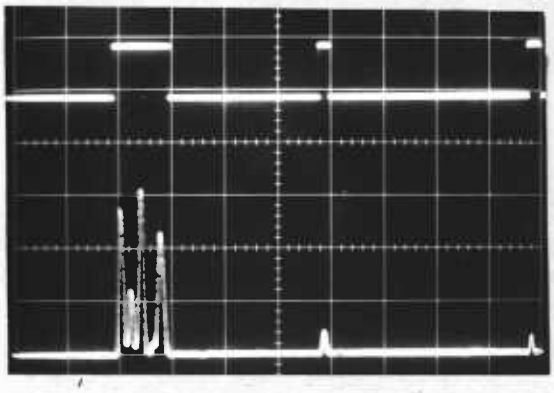


PROBE SIGNAL
BEFORE (TOP)
AND AFTER
SQUARING

FIG. 3.3.b

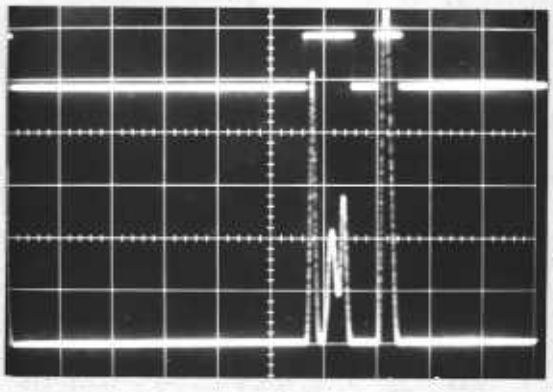
Fig. 3.3.c

Typical traces of Comparator and square of Ion current signals.



(a)

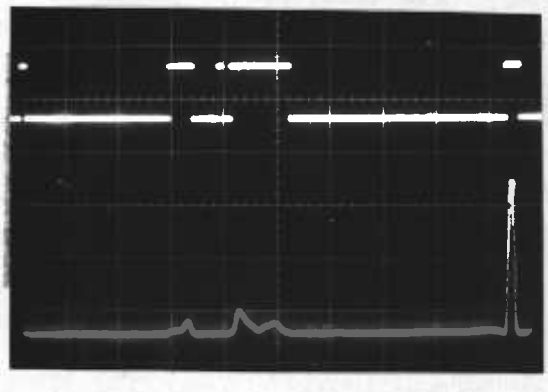
Lean Flame: $\emptyset$ = 0.91



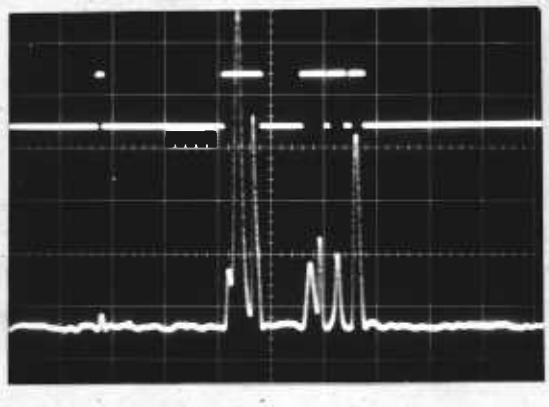
(b)

Rich Flame: $\emptyset$ = 1.16

Town Gas - Air premixed flames: Re 62,000.
Diameter of burner 2.9 cm.

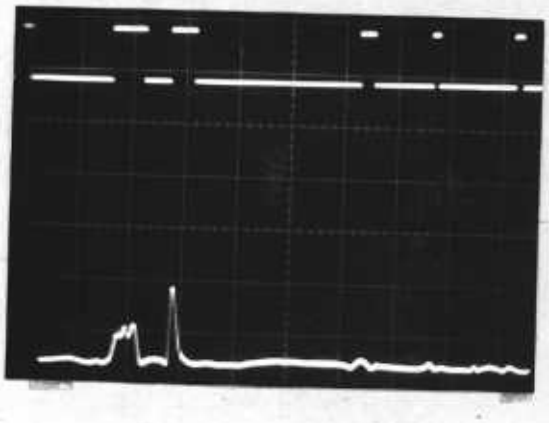


(c)



(d)

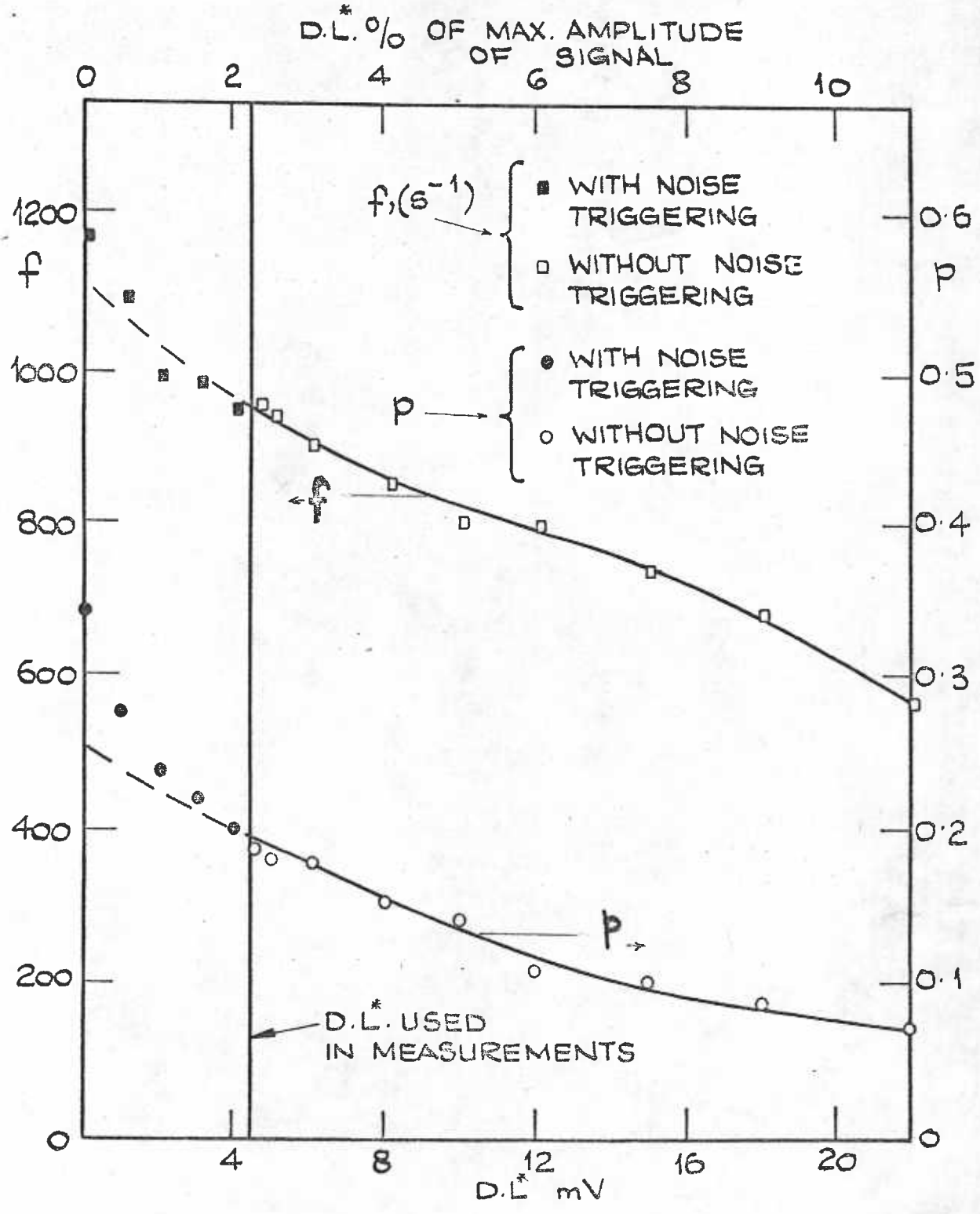
Towns Gas diffusion flame: Re 24,000.
Diameter of burner 0.5 cm.



(e)

	X/D	r (mm)	Time Scale ms/div.	Amplitude Scale of Traces Top v/div.	Bottom v/div.
(a)	2.90	0	0.5	10	0.5
(b)	2.90	0	0.5	10	0.5
(c)	40	0	1.0	10	1.0
(d)	70	15	1.0	10	1.0
(e)	80	15	1.0	10	1.0

Towns Gas diffusion flame: Re 24,000.
Diamter of burner 0.5 cm.



*D.L == Comparator Discrimination Level

FIG. 3.3.d

FIGURES IN CHAPTER 4

Figure	Title	Page
Fig. 4.2.a(i)	Details of diffusion flame burner.	169
Fig. 4.2.a(ii)	Picture of diffusion flame burner.	170
Fig. 4.2.b	Details of premixed flame burner.	171
Fig. 4.2.c	Picture of burner axis locating device (top left hand corner) and general view of apparatus during measurement in premixed flame burner (right of picture).	172
Fig. 4.3.a	Schematic of apparatus used to determine thermocouple radiation loss error and time constant.	173
Fig. 4.3.b	Schematic of burner and temperature fluctuations measurement apparatus.	174
Fig. 4.3.c	Picture of compensating active filter, gardners electronic transformer with buffer, and fluctuating temperature thermocouple.	175
Fig. 4.4a	Schematic of burner and fluctuating positive ion current measurement apparatus.	176
Fig. 4.4.b	Picture of: (1) Unit comprising pre-amplifying amplifying circuits, and squaring and comparator circuits; and (2) Ionisation probe.	177
Fig. 4.4.c	Signal traces showing relationship between squared probe signal and comparator output signal.	178

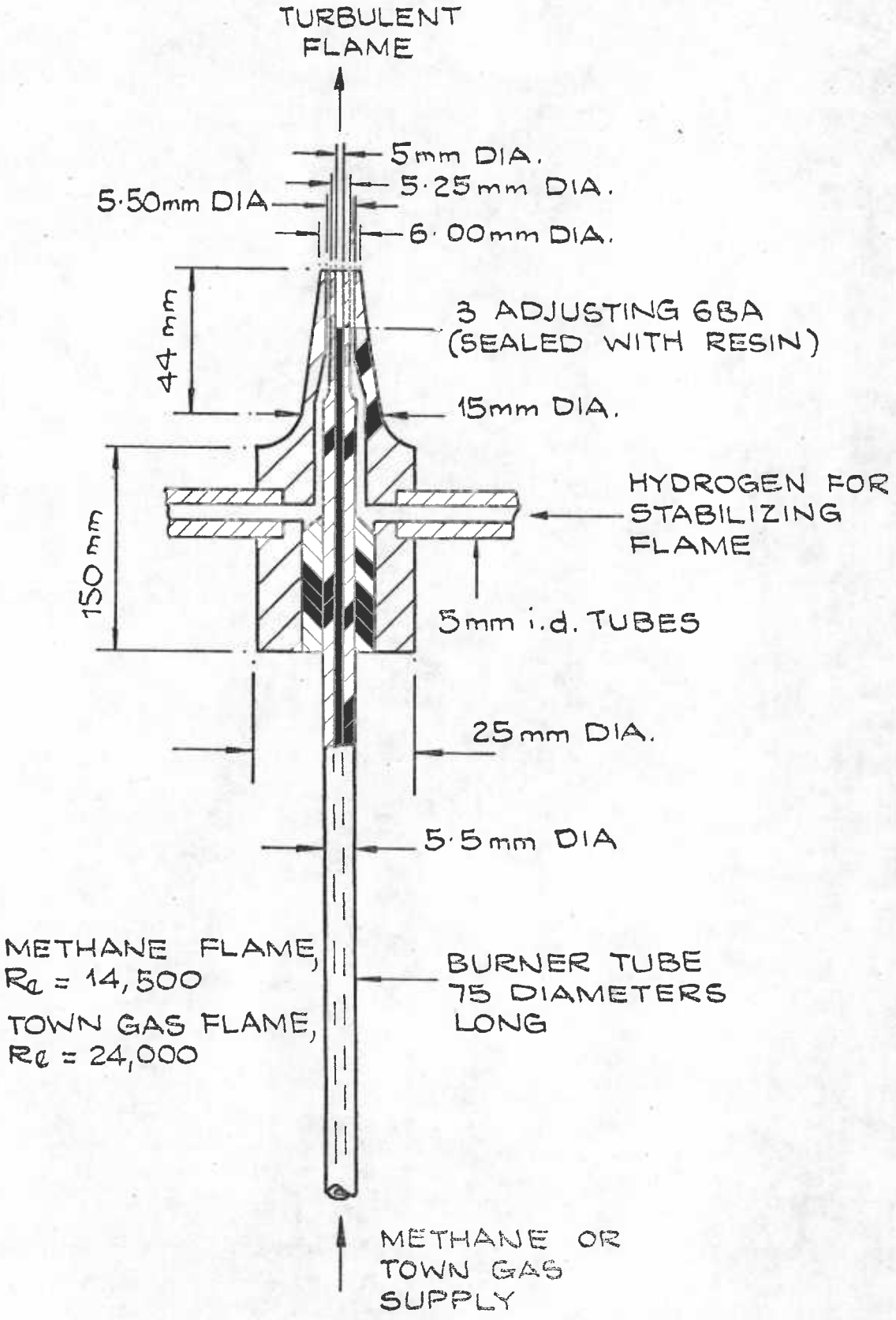

TURBULENT FLAME
5mm DIA.
5·25mm DIA.
5·50mm DIA
6·00mm DIA.
44 mm
3 ADJUSTING 6BA (SEALED WITH RESIN)
15mm DIA.
150 mm
HYDROGEN FOR STABILIZING FLAME
5mm i.d. TUBES
25mm DIA.
5·5mm DIA
METHANE FLAME, Re = 14,500
TOWN GAS FLAME, Re = 24,000
BURNER TUBE 75 DIAMETERS LONG
METHANE OR TOWN GAS SUPPLY

FIG. 4.2.a (i)

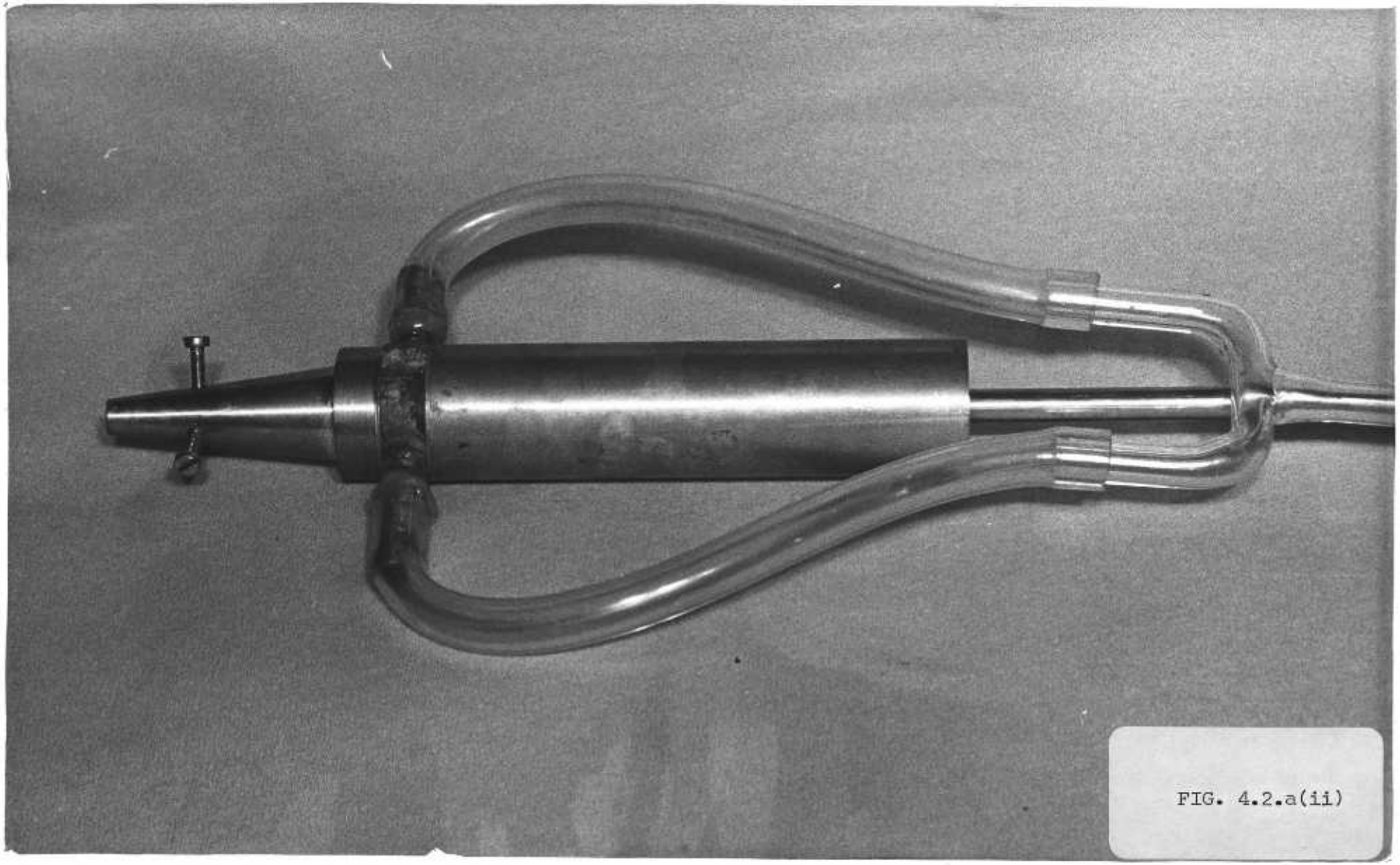


FIG. 4.2.a(ii)

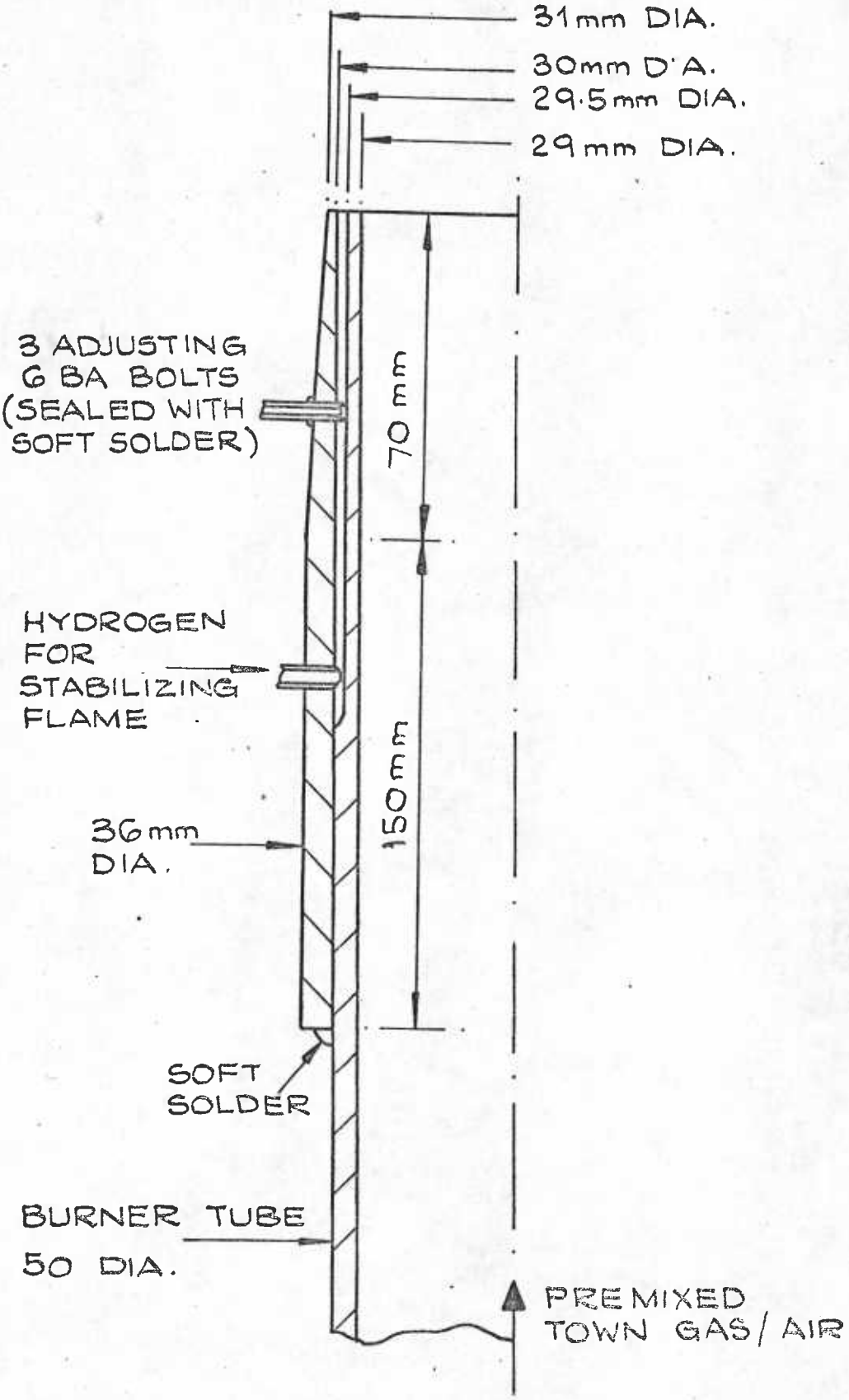
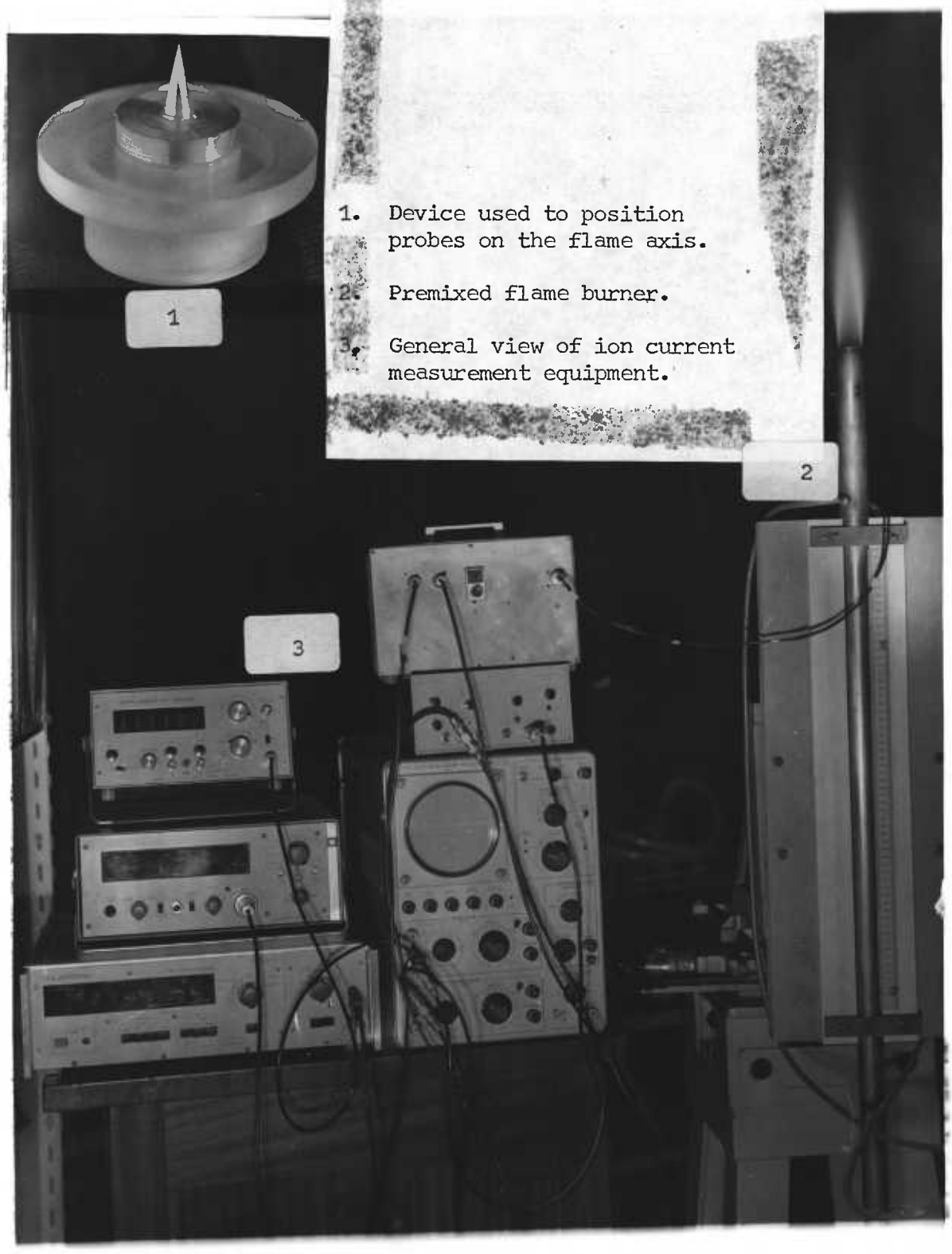

31mm DIA.
30mm DIA.
29.5mm DIA.
29mm DIA.
3 ADJUSTING
6 BA BOLTS
(SEALED WITH
SOFT SOLDER)
70 mm
HYDROGEN
FOR
STABILIZING
FLAME
150mm
36mm
DIA.
SOFT
SOLDER
BURNER TUBE
50 DIA.
PREMIXED
TOWN GAS/AIR

FIG. 4.2.b

FIG. 4.2.c



1. Device used to position probes on the flame axis.
2. Premixed flame burner.
3. General view of ion current measurement equipment.

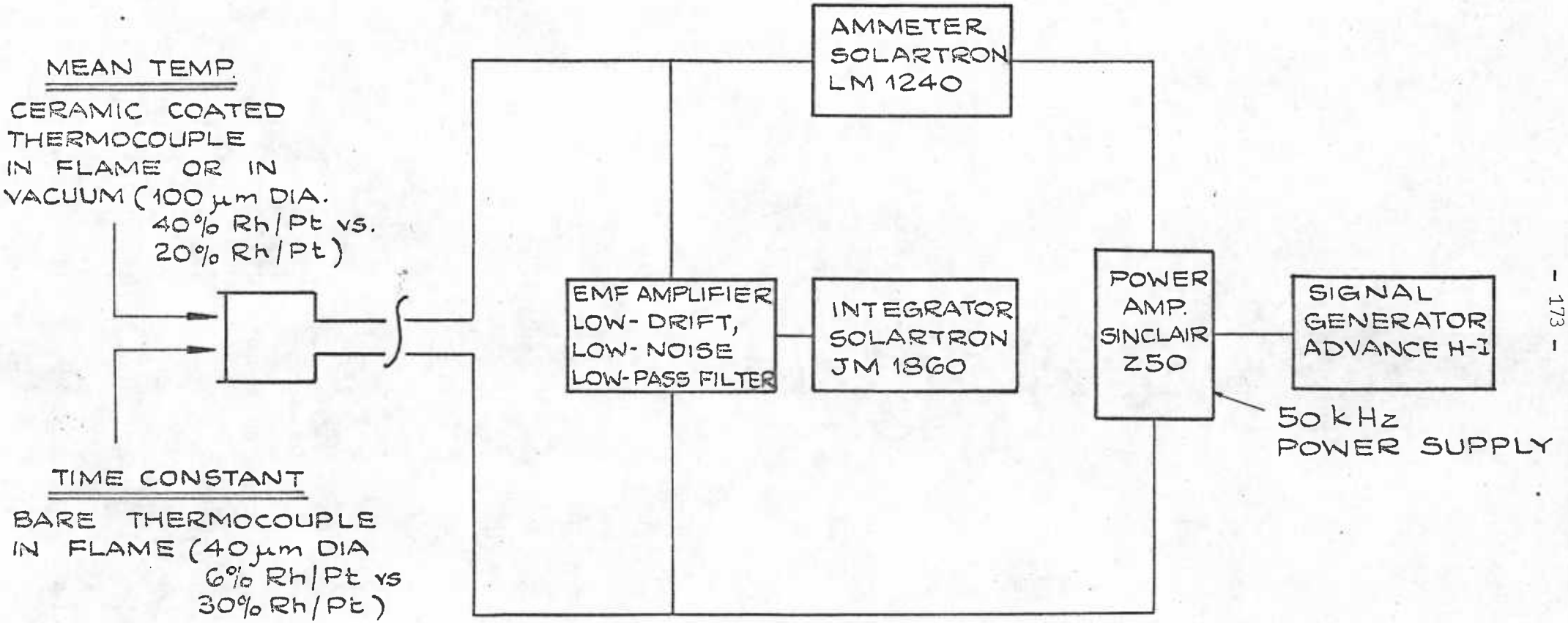

MEAN TEMP.
CERAMIC COATED THERMOCOUPLE IN FLAME OR IN VACUUM (100 μm DIA. 40% Rh/Pt vs. 20% Rh/Pt)
TIME CONSTANT
BARE THERMOCOUPLE IN FLAME (40 μm DIA 6% Rh/Pt vs 30% Rh/Pt)
AMMETER SOLARTRON LM 1240
EMF AMPLIFIER LOW-DRIFT, LOW-NOISE LOW-PASS FILTER
INTEGRATOR SOLARTRON JM 1860
POWER AMP. SINCLAIR Z50
SIGNAL GENERATOR ADVANCE H-I
50 kHz POWER SUPPLY

FIG. 4.3.a

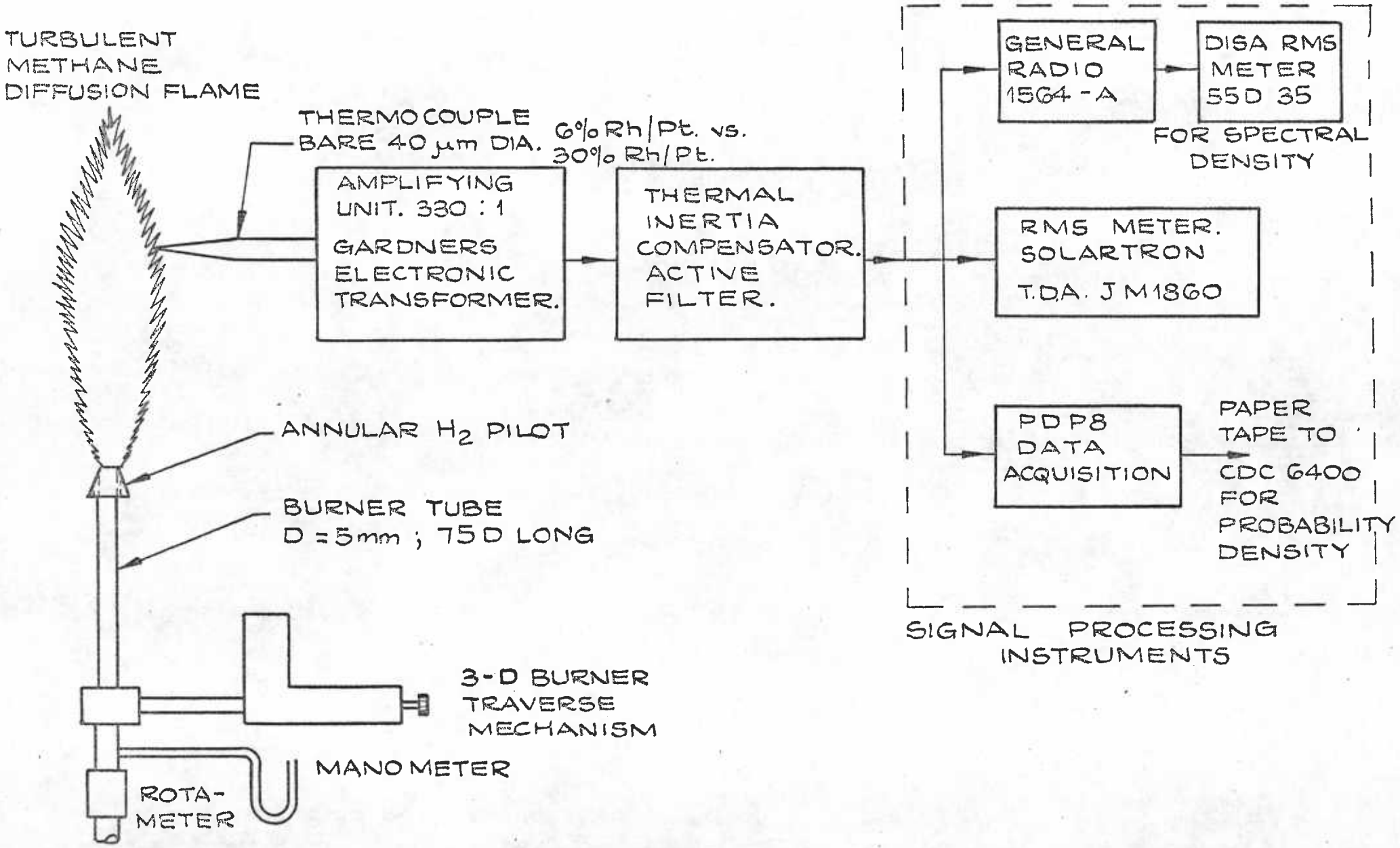

TURBULENT METHANE DIFFUSION FLAME
THERMO COUPLE BARE 40 μm DIA. 6% Rh/Pt. vs. 30% Rh/Pt.
AMPLIFYING UNIT. 330 : 1
GARDNERS ELECTRONIC TRANSFORMER.
THERMAL INERTIA COMPENSATOR. ACTIVE FILTER.
GENERAL RADIO 1564 - A
DISA RMS METER 55D 35
FOR SPECTRAL DENSITY
RMS METER. SOLARTRON T.D.A. J M1860
PDP8 DATA ACQUISITION
PAPER TAPE TO CDC 6400 FOR PROBABILITY DENSITY
SIGNAL PROCESSING INSTRUMENTS
ANNULAR H_2 PILOT
BURNER TUBE D = 5mm ; 75D LONG
3-D BURNER TRAVERSE MECHANISM
MANOMETER
ROTA-METER

FIG. 4.3.b



FIG. 4.3.c

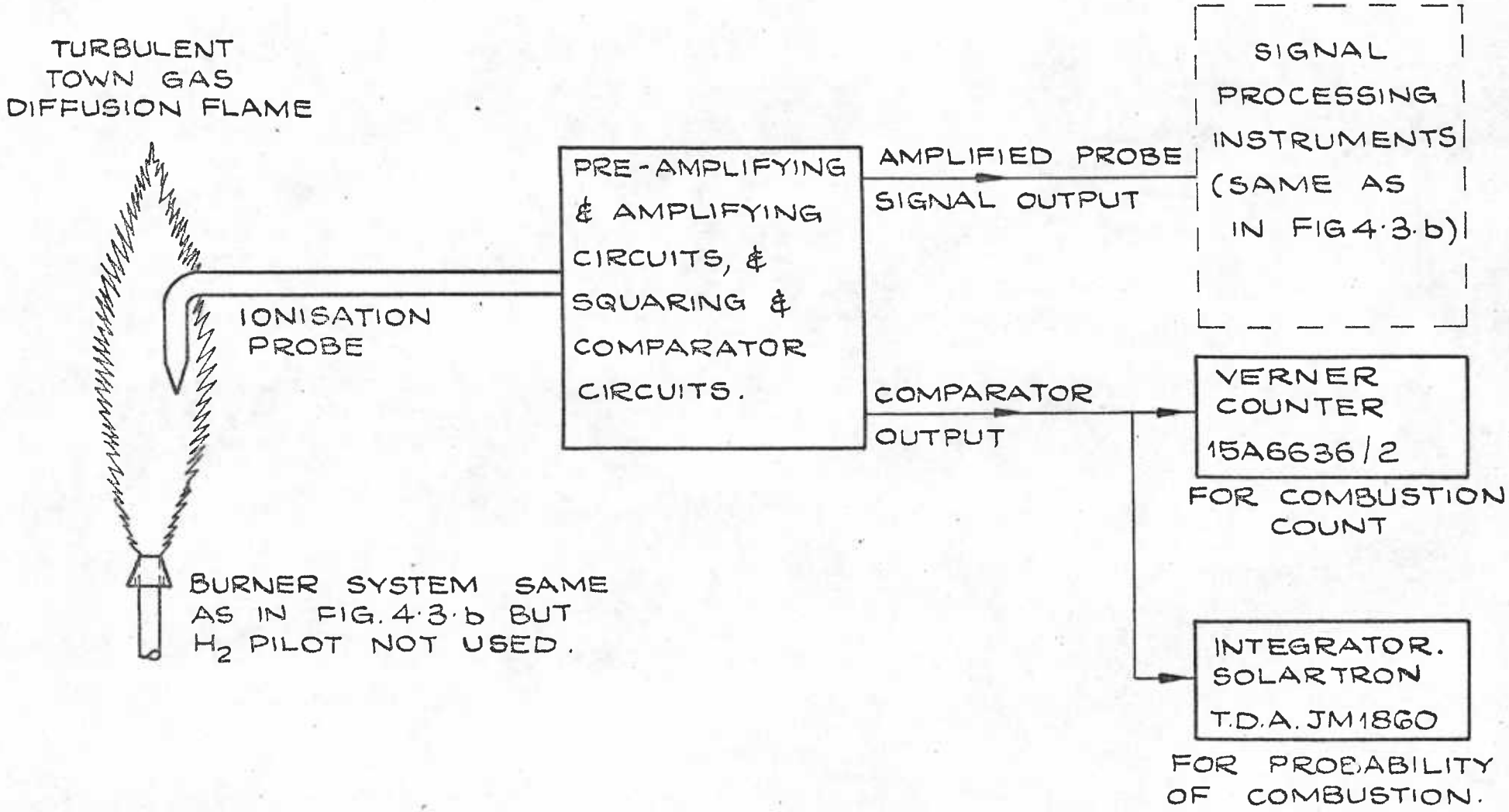

TURBULENT
TOWN GAS
DIFFUSION FLAME
IONISATION
PROBE
PRE-AMPLIFYING
& AMPLIFYING
CIRCUITS, &
SQUARING &
COMPARATOR
CIRCUITS.
AMPLIFIED PROBE
SIGNAL OUTPUT
SIGNAL
PROCESSING
INSTRUMENTS
(SAME AS
IN FIG 4·3·b)
COMPARATOR
OUTPUT
VERNER
COUNTER
15A6636/2
FOR COMBUSTION
COUNT
INTEGRATOR.
SOLARTRON
T.D.A. JM1860
FOR PROBABILITY
OF COMBUSTION.
BURNER SYSTEM SAME
AS IN FIG. 4·3·b BUT
H_2 PILOT NOT USED.

FIG. 4.4.a

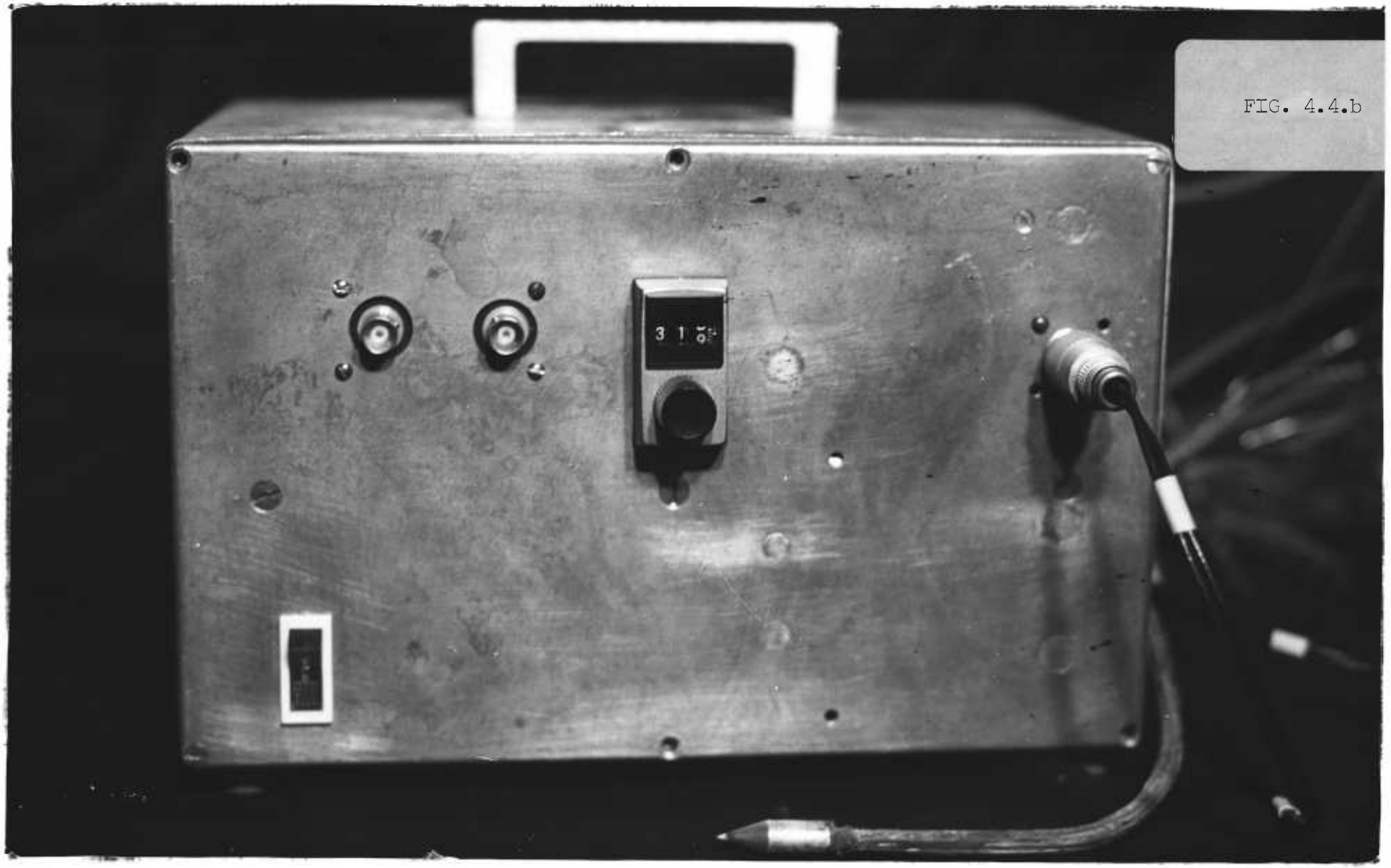


FIG. 4.4.b

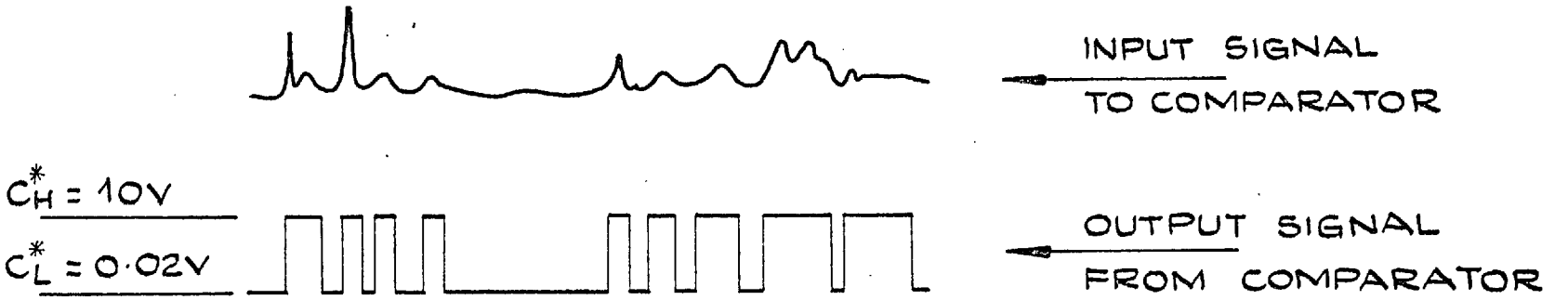

INPUT SIGNAL
TO COMPARATOR
$C_H^* = 10V$
$C_L^* = 0{\cdot}02V$
OUTPUT SIGNAL
FROM COMPARATOR

FIG. 4.4.c

FIGURES, COMPOSITIONS AND PROPERTIES OF FUELS IN CHAPTER 5.

A. METHANE DIFFUSION FLAME, REYNOLDS NO. 14,500, BURNER DIAMETER 5 mm.

Figure	Title	Page
Fig. 5.2.a	Radial profiles of rms T', mean T and probe time constant at 40 burner diameters from burner exit.	188
Fig. 5.2.b	Radial profiles of rms T', Mean T and probe time constant at 80 burner diameters from burner exit.	189
Fig. 5.2.c	Radial profiles of rms T', mean T and probe time constant at 120 burner diameters from burner exit.	190
Fig. 5.2.d	Axial distribution of rms T', mean T and probe time constant.	191
Fig. 5.2.e	Radial variation of the probability density function of T' at 40 burner diameters from burner exit.	192
Fig. 5.2.f	Axial variation of the probability density function of T'.	193
Fig. 5.2.g	The spectral density of T' in Fourier space, along axis, at 20, 40, 60, 80, 100 and 110 burner diameters from burner exit.	194
Fig. 5.2.h	The spectral density of T' in wave-number space at locations along axis as in Fig. 5.2.g.	195
Fig. 5.2.i	Comparison of the present temperature spectral density with the temperature data of Kunugi and Jinno (1959), the total emission data of Guenther and Simon (1969), and the OH-emission data of Kuhnert and Guenther (1973).	196

COMPOSITION OF METHANE GAS SUPPLIED FROM MOGDEN SEWAGE WORKS OF GREATER LONDON COUNCIL

Maximum and minimum concentrations of four constituents over a four year period.

Constituent	Maximum (%)	Minimum (%)
Methane	98.9	97.7
Carbon Dioxide	2.2	0.9
Oxygen	0.3	0.1
Nitrogen	1.6	0.4

B. TOWN GAS DIFFUSION FLAME, REYNOLDS NUMBER 24,000, BURNER DIAMETER 5 mm.

Fig.	Title	Page
Fig. 5.3.a	Radial profile of mean T, corrected for radiation error, at 10 burner diameters from burner exit.	197
Fig. 5.3.b	Radial profile of mean T, corrected for radiation error, at 40 burner diameters from burner exit.	198
Fig. 5.3.c	Radial profile of mean T, corrected for radiation error, at 90 burner diameters from burner exit.	199
Fig. 5.3.d	Radial profile of mean T, corrected for radiation error, at 120 burner diameters from burner exit.	200
Fig. 5.3.e	Radial profile of mean T, corrected for radiation error, at 150 burner diameters from burner exit.	201
Fig. 5.3.f	Graphs in Figs. 5.3 a to e plotted with normalized radius.	202
Fig. 5.3.g	Axial distribution of mean T: Curve 1 - Corrected for radiation error; non-catalytic coat on probe. Curve 2 - No correction for radiation error; non-catalytic coat on probe. Curve 3 - No correction for radiation error; bare probe. Curve 4 - As in curve 3 but after 12 hours continuous insertion of probe in the flame.	203
Fig. 5.3.h	Radial profiles at 10 burner diameters downstream of burner exit of probability of combustion p, combustion count, f, normalized mean of positive ion current, m, and normalized rms of positive ion current, ρ.	204
Fig. 5.3.i	Radial profiles at 'edge' of flame at 10 burner diameters downstream of burner exit of probability of combustion, p , and combustion count, f.	205
Fig. 5.3.j	Radial profiles at 20 burner diameters downstream of burner exit of probability of combustion, p , combustion count f, normalized mean of positive ion current, m, and normalized rms of positive ion current, ρ.	206

Figure	Title	Page
Fig. 5.3.k	Radial profiles at 'edge' of flame at 20 burner diameters downstream of burner exit of probability of combustion, p, and combustion count, f.	207
Fig. 5.3.l	Radial profiles at 35 burner diameters downstream of burner exit of probability of combustion, p, combustion count, f, normalized mean of positive ion current, m, and normalized rms of positive ion current, ρ.	208
Fig. 5.3.m	Radial profiles at 79.06, 90, 100.1 and 112.9 burner diameters downstream of burner exit of probability of combustion, p .	209
Fig. 5.3.n	Radial profiles at 79.06, 90, 100.1 and 112.9 burner diameters downstream of burner exit. of combustion count, f.	210
Fig. 5.3.o	Radial variation of the probability density function of positive ion current at 75 burner diameters downstream of burner exit.	211
Fig. 5.3.p	Axial variation of the probability density function of positive ion current.	212
Fig. 5.3.q	Comparison of the present spectral density of positive ion current with the total emission data of Guenther and Simon (1969).	213

TOWN GAS DIFFUSION FLAMES, FIGS. 5.3.a to q

FUEL PROPERTIES AND COMPOSITIONS

Town gas at Imperial College may vary significantly from day to day. Two extremes of approx. 50% to 70% H_2.

Properties:	50% H_2	70% H_2
Viscosity (Kg/ms)	1.273×10^{-5}	1.276×10^{-5}
Density (Kg/m^3)	0.633	0.584
Cp (J/Kg ^{o}C)	0.2196	0.2403
K (J/ms/^{o}C)	6.76	8.39

TABLE OF TOWN GAS COMPOSITIONS AND PERTINENT FIGURES

Figure	H_2	CH_4	CO_2	N_2	CO	O_2	C_2H_6 (ethane)	C_3H_8 (propane)	C_4H_{10} (butane)	Specific Gravity
Fig. 5.3.a	66.7	4.9	16.8	0.6	3.9	0.1	0.13	1.6	3.7	0.53
Fig. 5.3.b	66.5	5.0	16.8	0.6	3.9	0.1	0.14	1.62	3.8	0.53
Fig. 5.3.c	66.2	4.8	16.9	0.5	4.0	0.09	0.15	1.64	3.9	0.53
Fig. 5.3.d	64.9	5.1	16.8	0.5	3.8	0.09	0.16	1.66	4	0.53
Fig. 5.3.e	66.2	4.8	17.0	0.4	4.1	0.08	0.13	1.58	3.72	0.53
Fig. 5.3.g (Curve 1)	66.6	4.3	17.0	0.5	4.0	0.09	0.13	1.6	3.7	0.53
Fig. 5.3.h to k	as for Fig. 5.3.a									
Fig. 5.3.l	as for Fig. 5.3.b									
Fig. 5.3.m to p	as for Fig. 5.3.d									
Fig. 5.3.q	as for Fig. 5.3.g									

C. TOWN GAS/AIR PREMIXED FLAMES, REYNOLDS NO. 62,000, BURNER DIAMETER 29 mm

Figure	Title	Page
Fig. 5.4.a	Radial profile of mean T, corrected for radiation error, at 0.517 burner diameter downstream of burner exit. (Lean flame, equivalence ratio 0.91)	214
Fig. 5.4.b	Radial profile of mean T, corrected for radiation error, at 3.03 burner diameters downstream of burner exit. (Lean flame, equivalence ratio 0.91)	214
Fig. 5.4.c	Radial profile of mean T, corrected for radiation error, at 4.41 burner diameters downstream of burner exit. (Lean flame, equivalence ratio 0.91)	215
Fig. 5.4.d	Radial profile of mean T, corrected for radiation error, at 6.48 burner diameters downstream of burner exit (Lean flame, equivalence ratio 0.91)	215
Fig. 5.4.e	Axial distribution of mean T, corrected for Radiation error, (Lean flame, equivalence ratio 0.91)	216
Fig. 5.4.f	Radial profile of mean T, corrected for radiation error, at 0.517 burner diameter downstream of burner exit. (Rich flame, equivalence ratio 1.16)	217
Fig. 5.4.g	Radial profile of mean T, corrected for radiation error, at 3.03 burner diameters downstream of burner exit (Rich flame, equivalence ratio 1.16)	217
Fig. 5.4.h	Radial profile of mean T, corrected for radiation error, at 4.41 burner diameters downstream of burner exit (Rich flame, equivalence ratio 1.16)	218
Fig. 5.4.i	Radial profile of mean T, corrected for radiation error, at 6.48 burner diameters downstream of burner exit (Rich flame, equivalence ratio 1.16)	218
Fig. 5.4.j	Radial profile of mean T, corrected for radiation error, at 8.48 burner diameters downstream of burner exit (Rich flame, equivalence ratio 1.16)	219
Fig. 5.4.k	Axial distribution of mean T, corrected for radiation error (Rich flame equivalence ratio 1.16)	219

Figure	Title	Page
Fig. 5.4.l	Radial profiles at 3.03 burner diameters downstream of burner exit of probability of combustion, p, combustion count, f, normalised mean positive ion current, m, normalised rms positive ion current, ρ, and normalised mean T. (Lean flame, equivalence ratio 0.91).	220
Fig. 5.4.m	Radial profiles at 4.41 burner diameters downstream of burner exit of probability of combustion, p, combustion count, f, normalised mean positive ion current, m, normalised rms positive ion current, ρ, and normalised mean T. (Lean flame, equivalence ratio 0.91).	221
Fig. 5.4.n	Axial distributions of probability of combustion, p, combustion count, f, normalised mean positive ion current, m, normalised rms positive ion current, ρ, and normalised mean T. (Lean flame, equivalence ratio 0.91)	222
Fig. 5.4.o	Radial profiles at 3.03 burner diameters downstream of burner exit of probability of combustion, p, combustion count, f, normalised mean positive ion current, m, normalised rms positive ion current, ρ, and normalised mean T. (Rich flame, equivalence ration 1.16)	223
Fig. 5.4.p	Axial distributions of probability of combustion, p, combustion count, f, normalised mean positive ion current, m, normalised rms positive ion current, ρ, and normalised mean T. (Rich flame, equivalence ratio 1.16)	224
Fig. 5.4.q	Axial variation of the probability density function of positive ion current. (Lean flame, equivalence ratio 0.91).	225
Fig. 5.4.r	Axial variation of the probability density function of positive ion current. (Rich flame, equivalence ratio 1.16).	226
Fig. 5.4.s	Radial variation of the probability density function of positive ion current at 4.82 burner diameters downstream of burner exit. (Rich flame, equivalence ratio 1.16)	227
Fig. 5.4.t	The spectral density of positive ion current at 4.38 burner diameters downstream of burner exit in rich flame (equivalence ratio 1.16) and in lean flame (equivalence ratio 0.91)	228

TOWN GAS/AIR PREMIXED FLAMES

FIGS. 5.4.a to t. FUEL PROPERTIES AND COMPOSITIONS.

PROPERTIES: As for Figs. 5.3.a to q above.

TABLE OF TOWN GAS COMPOSITIONS AND PERTINENT FIGURES

Figure	H_2	CH_4	CO_2	N_2	CO	O_2	C_2H_6	C_3H_8	C_4H_{10}
Figs. 5.4a to e	49.98	24.4	16.8	1.1	3.27	0.3	0.6	0.1	1.3
Figs. 5.4f to k	49.7	26.0	12.0	4.2	2.3	1.0	0.4	0.2	1.4
Figs. 5.4l to t	49.6	26.8	11.5	6.2	2.3	1.6	0.5	0.1	1.4

FIGURES 5.5 a and b ; FIGURES 5.6 a to d

Figure	Title	Page
Fig. 5.5.a	Envisaged structure of reaction zone of free jet diffusion flame (thickness into plane of diagram of order two integral scales)	229
Fig. 5.5.b	Envisaged structure of reaction zone of free jet premixed flame (thickness into plane of diagram of order two Taylor micro scales)	230
Fig. 5.6.a	Methane diffusion flame, Reynolds number 14,500	231
Fig. 5.6.b	Town gas diffusion flame, Reynolds number 24,000	231
Fig. 5.6.c	Lean premixed town gas/air flame, equivalence ratio 0.91, Reynolds number 62,000	232
Fig. 5.6.d	Rich premixed town gas/air flame, equivalence ratio 1.16, Reynolds number 62,000	232

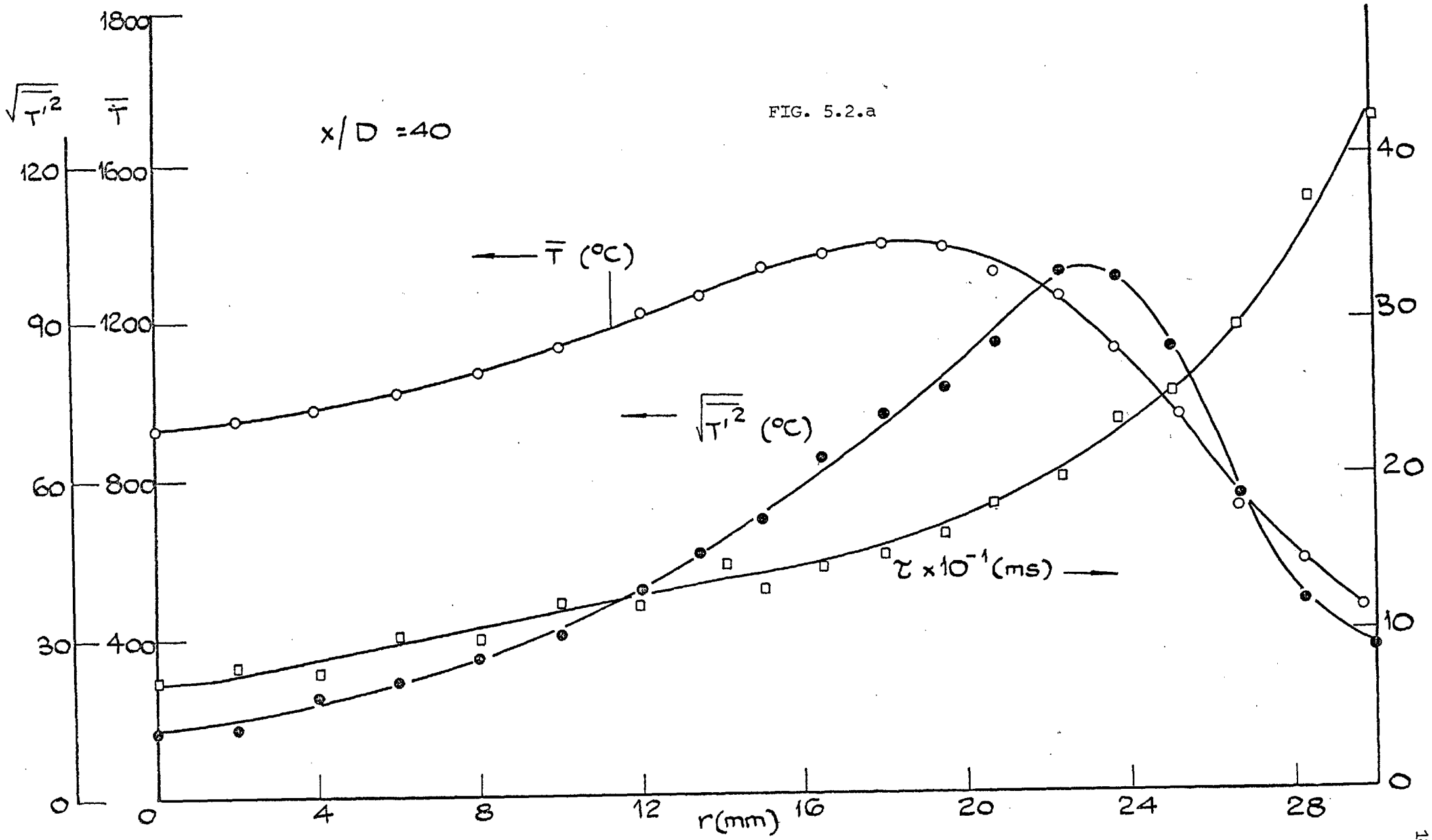

$\sqrt{\overline{T'^2}}$
$\overline{T}$
x/D =40
1800
1600
1200
800
400
120
90
60
30
0
$\overline{T}$ (°C)
$\sqrt{\overline{T'^2}}$ (°C)
$\tau \times 10^{-1}$ (ms)
40
30
20
10
0
0
4
8
12
16
20
24
28
r(mm)

FIG. 5.2.a

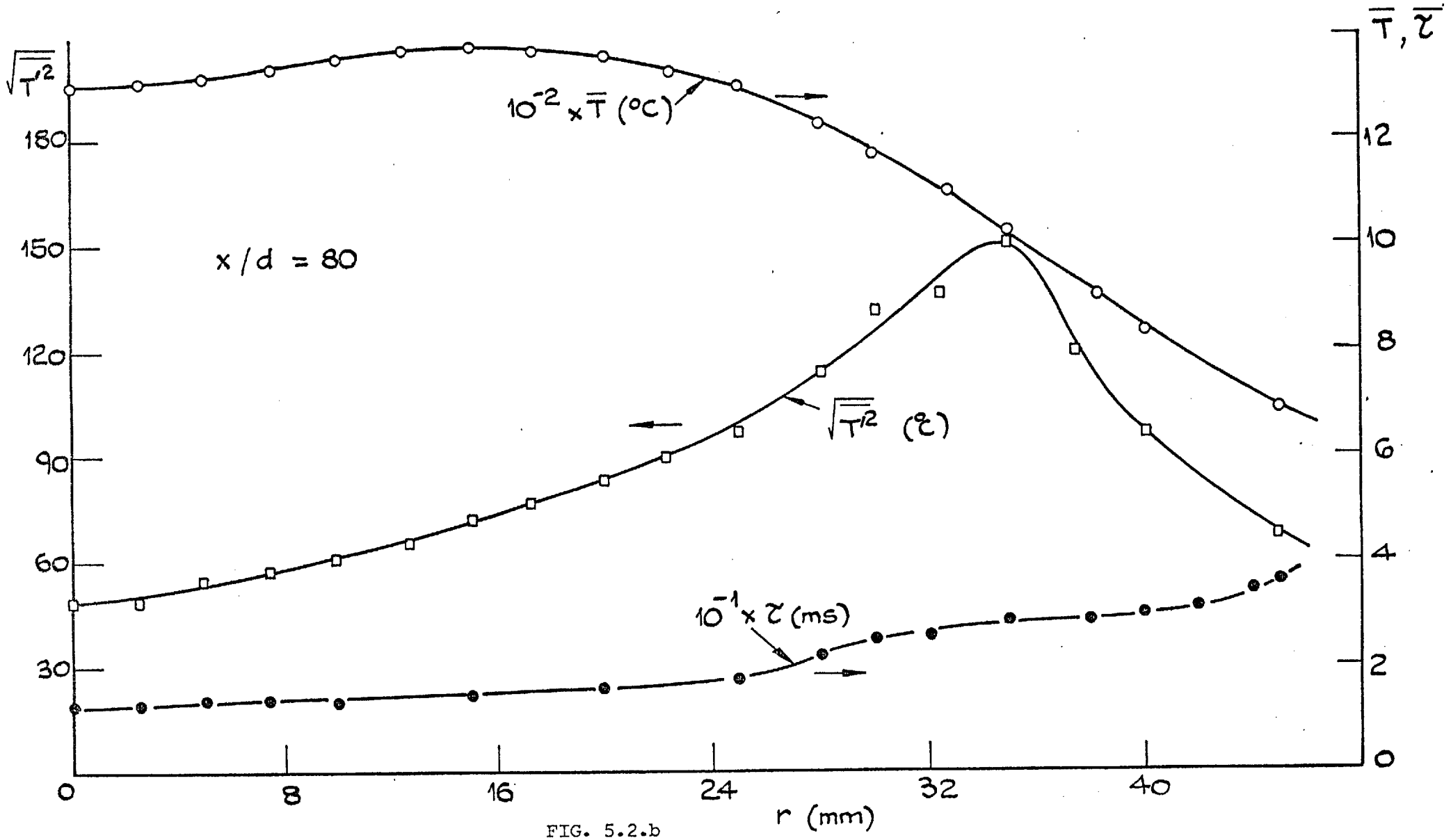

$\sqrt{\overline{T'^2}}$
$\overline{T}, \overline{\tau}$
$10^{-2} \times \overline{T}$ (°C)
180
150
120
90
60
30
12
10
8
6
4
2
0
x / d = 80
$\sqrt{\overline{T'^2}}$ (°C)
$10^{-1} \times \tau$ (ms)
0
8
16
24
32
40
r (mm)

FIG. 5.2.b

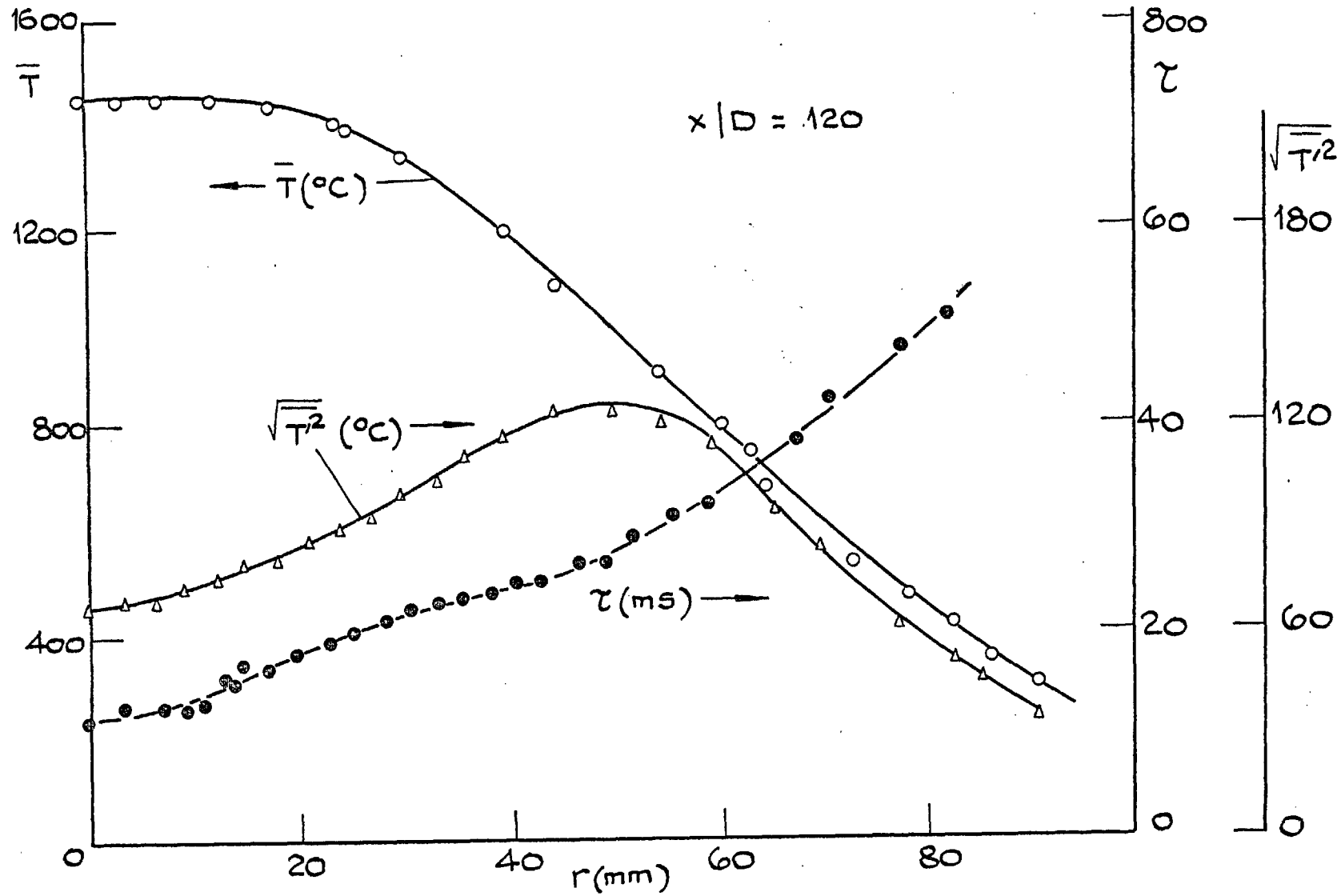

1600
$\overline{T}$
1200
800
400
0
20
40
r(mm)
60
80
x/D = 120
$\overline{T}$(°C)
$\sqrt{\overline{T'^2}}$ (°C)
τ(ms)
800
τ
60
40
20
0
$\sqrt{\overline{T'^2}}$
180
120
60
0

FIG. 5.2.c

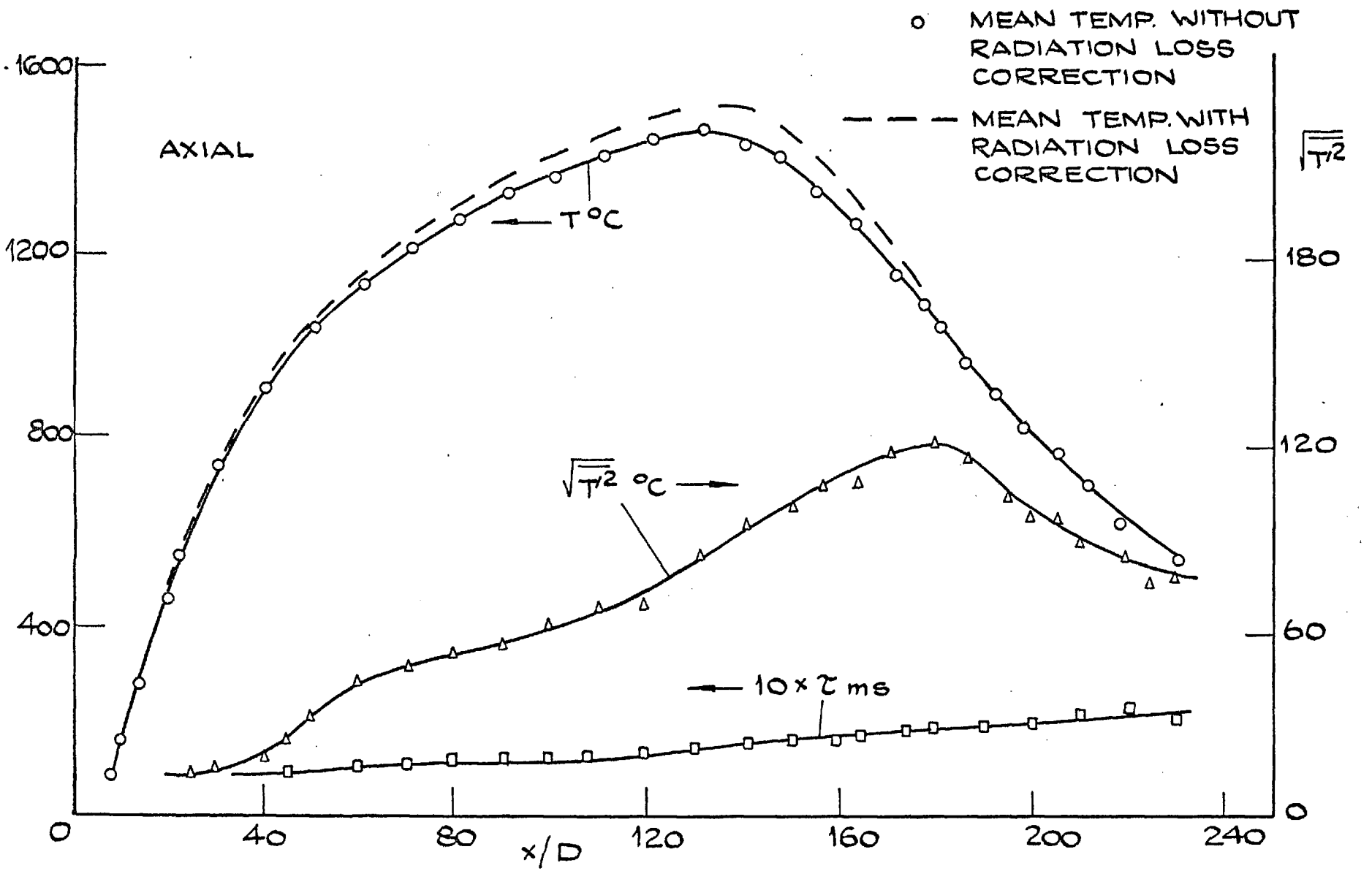

o MEAN TEMP. WITHOUT RADIATION LOSS CORRECTION
MEAN TEMP. WITH RADIATION LOSS CORRECTION
AXIAL
T °C
√T'2 °C
10 × τ ms
√T'2
1600
1200
800
400
0
180
120
60
0
40
80
120
160
200
240
x/D

FIG. 5.2.d

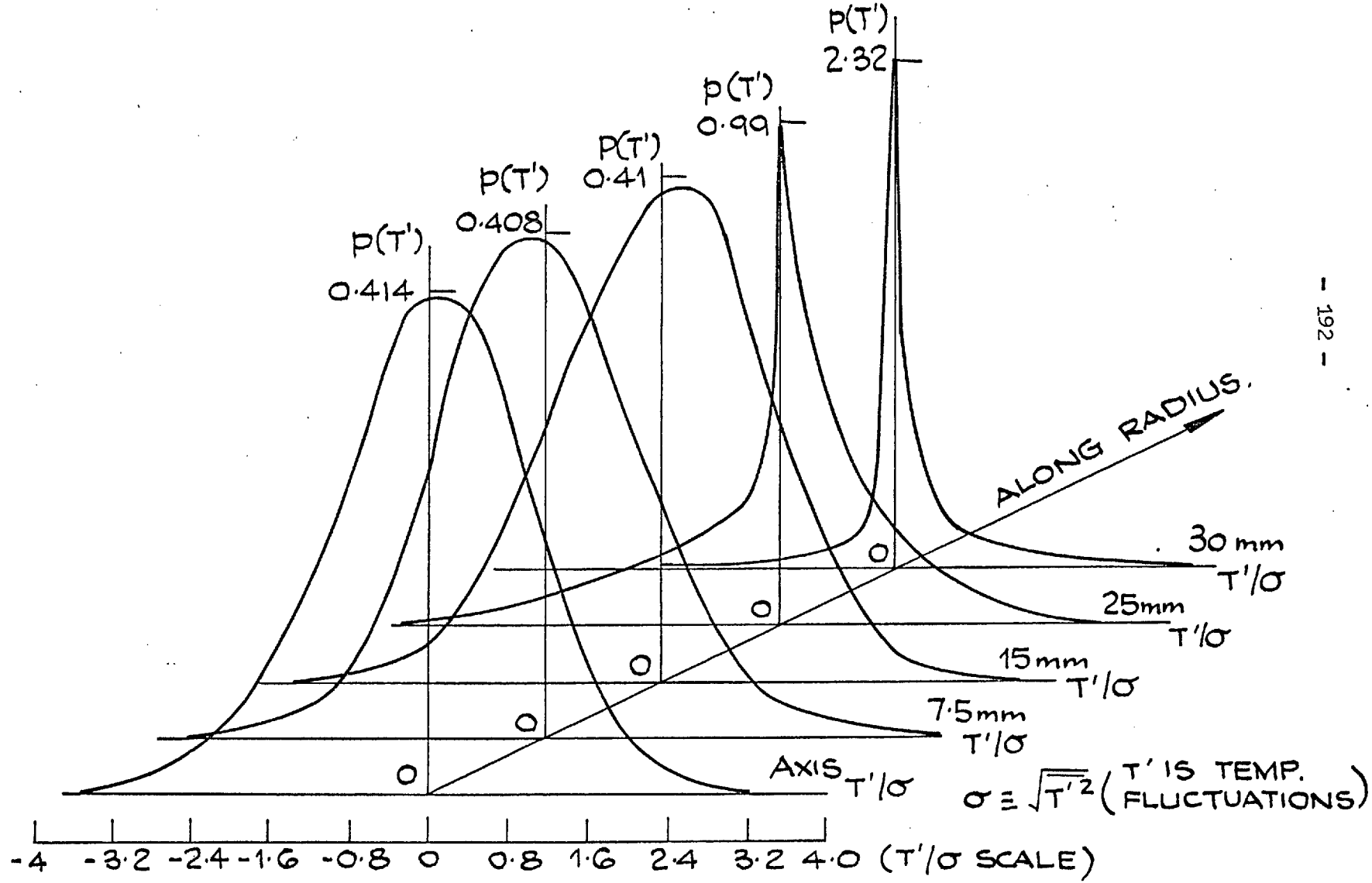

P(T')
2·32
P(T')
0·99
P(T')
0·41
P(T')
0·408
P(T')
0·414
ALONG RADIUS.
30 mm
T'/σ
25mm
T'/σ
15mm
T'/σ
7·5mm
T'/σ
AXIS T'/σ
σ ≡ √T'² (T' IS TEMP. FLUCTUATIONS)
-4 -3·2 -2·4 -1·6 -0·8 0 0·8 1·6 2·4 3·2 4·0 (T'/σ SCALE)

FIG. 5.2.e

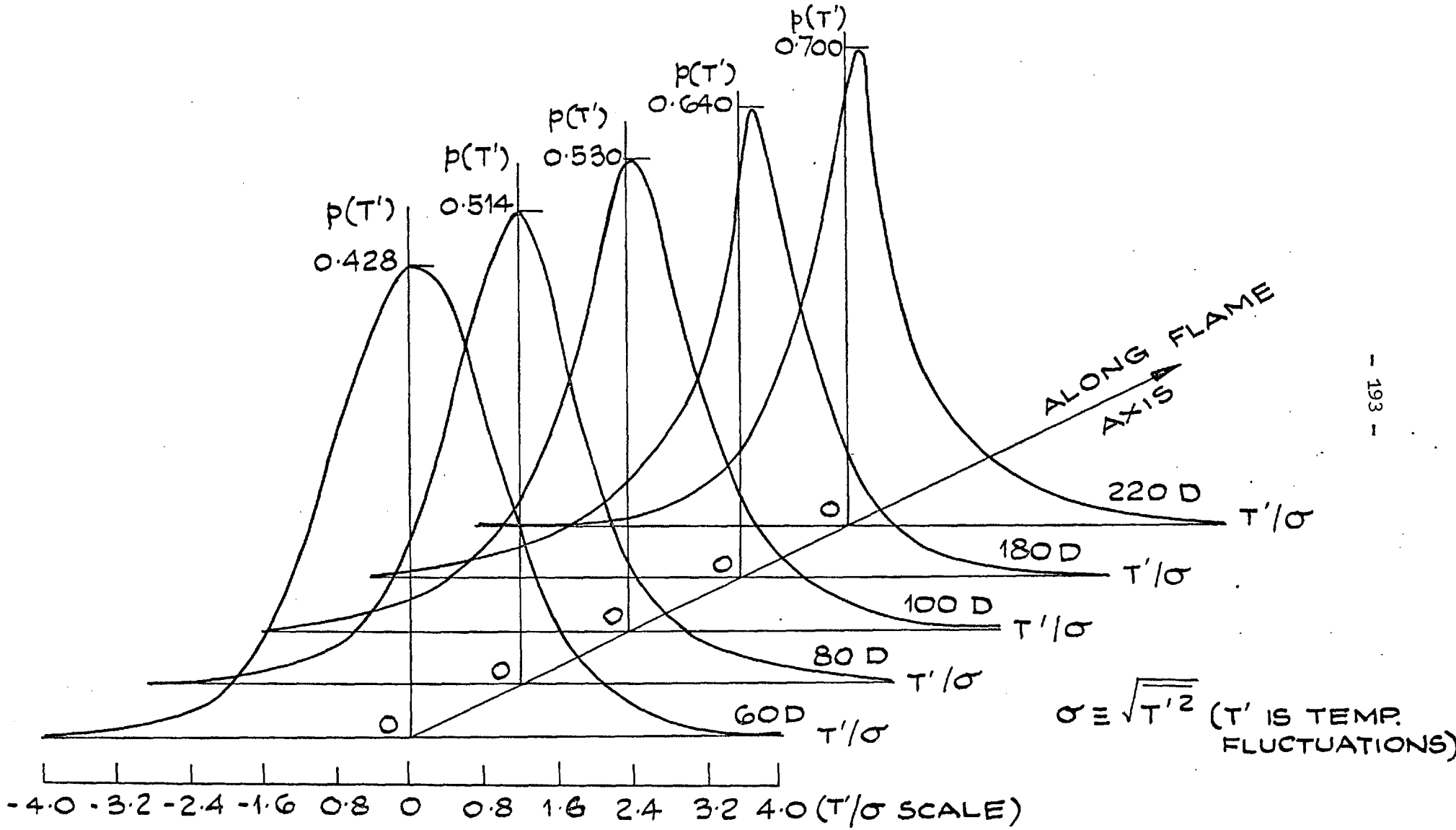

p(T')
0·700
p(T')
0·640
p(T')
0·530
p(T')
0·514
p(T')
0·428
ALONG FLAME AXIS
220 D
180 D
100 D
80 D
60D
T'/σ
0
σ ≡ √T'²
(T' IS TEMP. FLUCTUATIONS)
-4·0 -3·2 -2·4 -1·6 0·8 0 0·8 1·6 2·4 3·2 4·0 (T'/σ SCALE)

FIG. 5.2.f

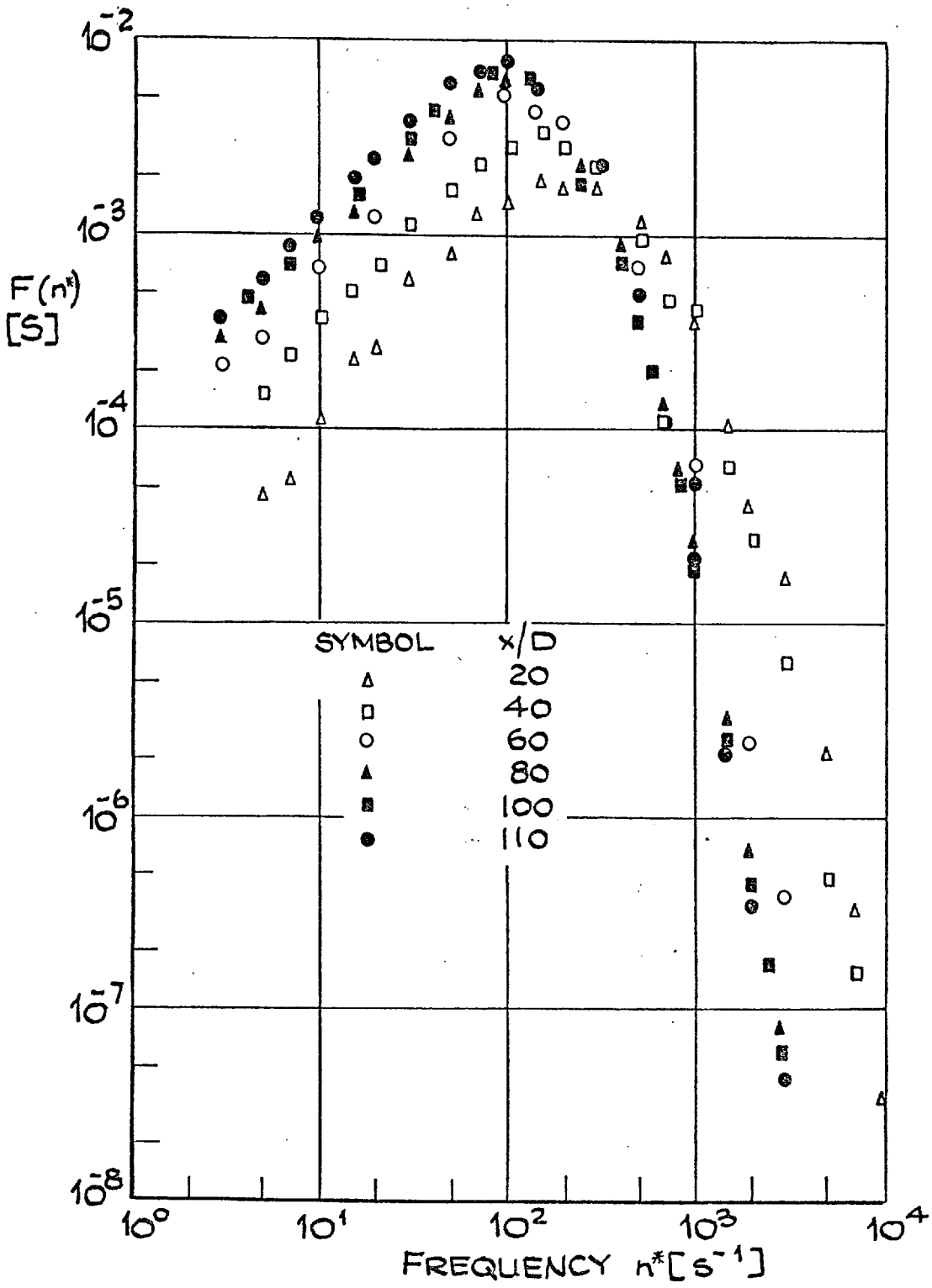

10^{-2}
10^{-3}
10^{-4}
10^{-5}
10^{-6}
10^{-7}
10^{-8}
F(n*)
[S]
SYMBOL x/D
20
40
60
80
100
110
10^{0}
10^{1}
10^{2}
10^{3}
10^{4}
FREQUENCY n*[s^{-1}]

FIG. 5.2.g

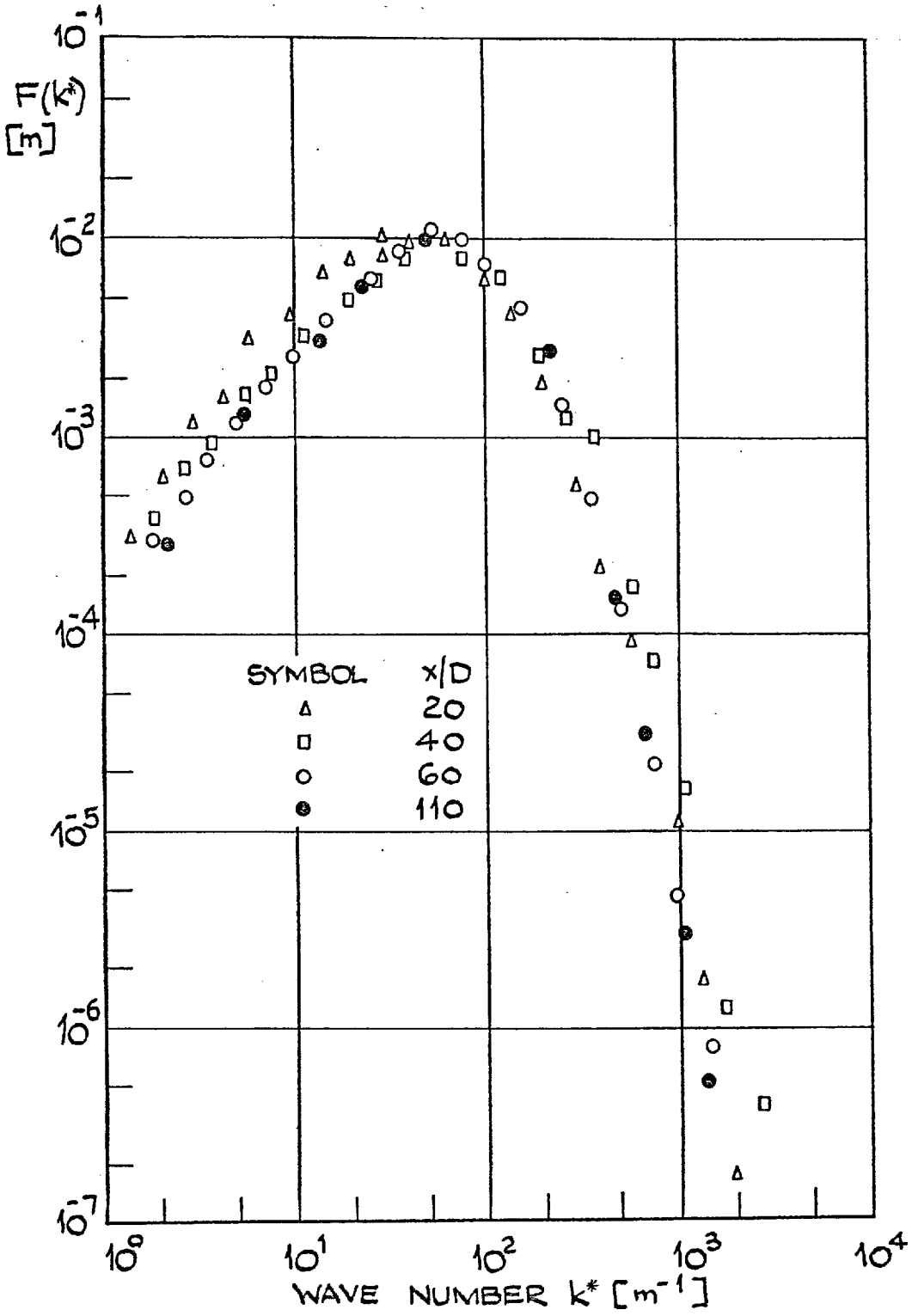

F(k*)
[m]
10^{-1}
10^{-2}
10^{-3}
10^{-4}
10^{-5}
10^{-6}
10^{-7}
SYMBOL x/D
20
40
60
110
10^{0}
10^{1}
10^{2}
10^{3}
10^{4}
WAVE NUMBER k* [m^{-1}]

FIG. 5.2.h

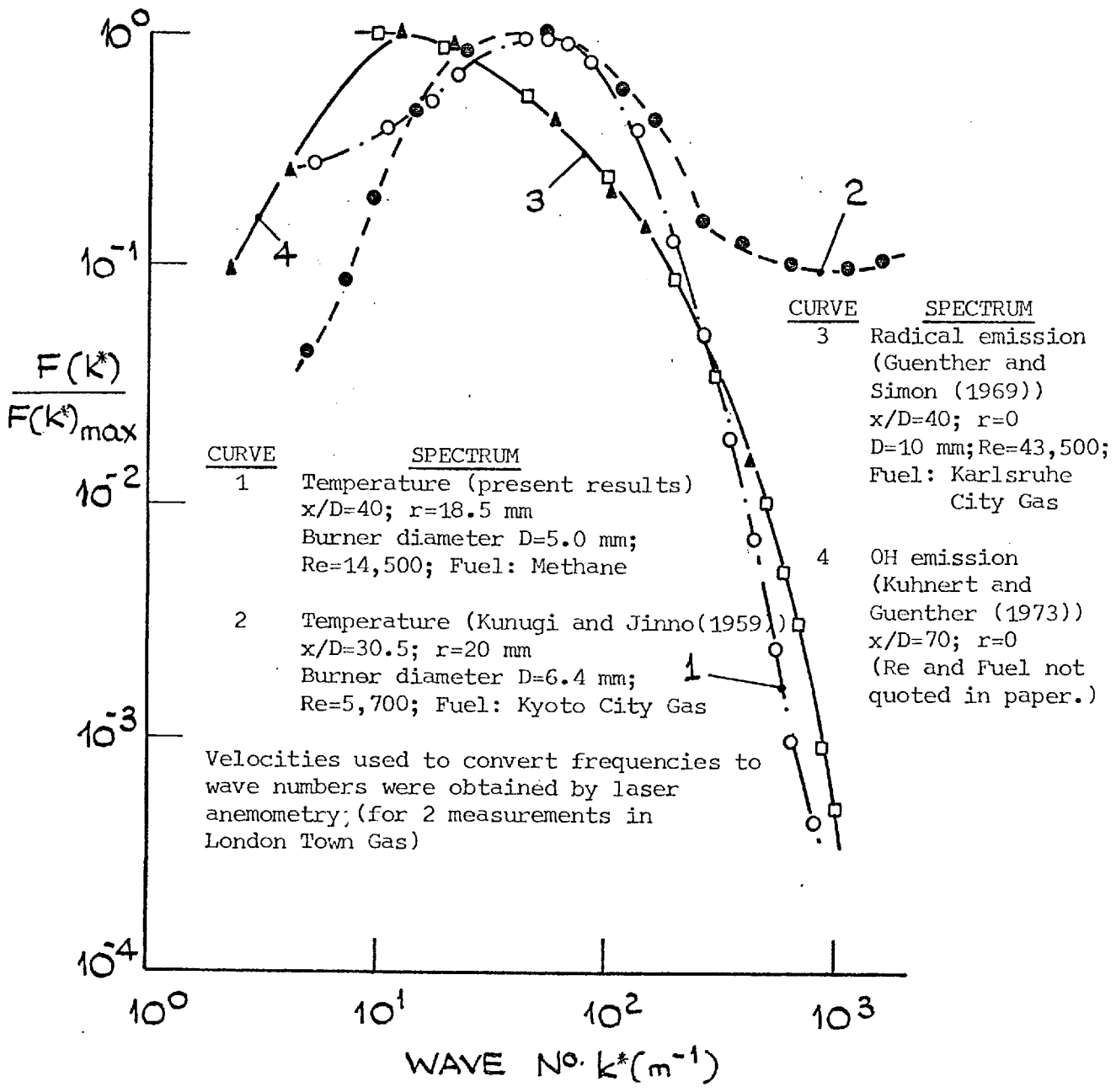

10^0
10^{-1}
10^{-2}
10^{-3}
10^{-4}
$\frac{F(k^*)}{F(k^*)_{max}}$
10^0
10^1
10^2
10^3
WAVE No. $k^*(m^{-1})$
1
2
3
4
5
6
CURVE SPECTRUM
1 Temperature (present results) x/D=40; r=18.5 mm Burner diameter D=5.0 mm; Re=14,500; Fuel: Methane
2 Temperature (Kunugi and Jinno(1959)) x/D=30.5; r=20 mm Burner diameter D=6.4 mm; Re=5,700; Fuel: Kyoto City Gas
Velocities used to convert frequencies to wave numbers were obtained by laser anemometry; (for 2 measurements in London Town Gas)
CURVE SPECTRUM
3 Radical emission (Guenther and Simon (1969)) x/D=40; r=0 D=10 mm; Re=43,500; Fuel: Karlsruhe City Gas
4 OH emission (Kuhnert and Guenther (1973)) x/D=70; r=0 (Re and Fuel not quoted in paper.)

FIG. 5.2.i

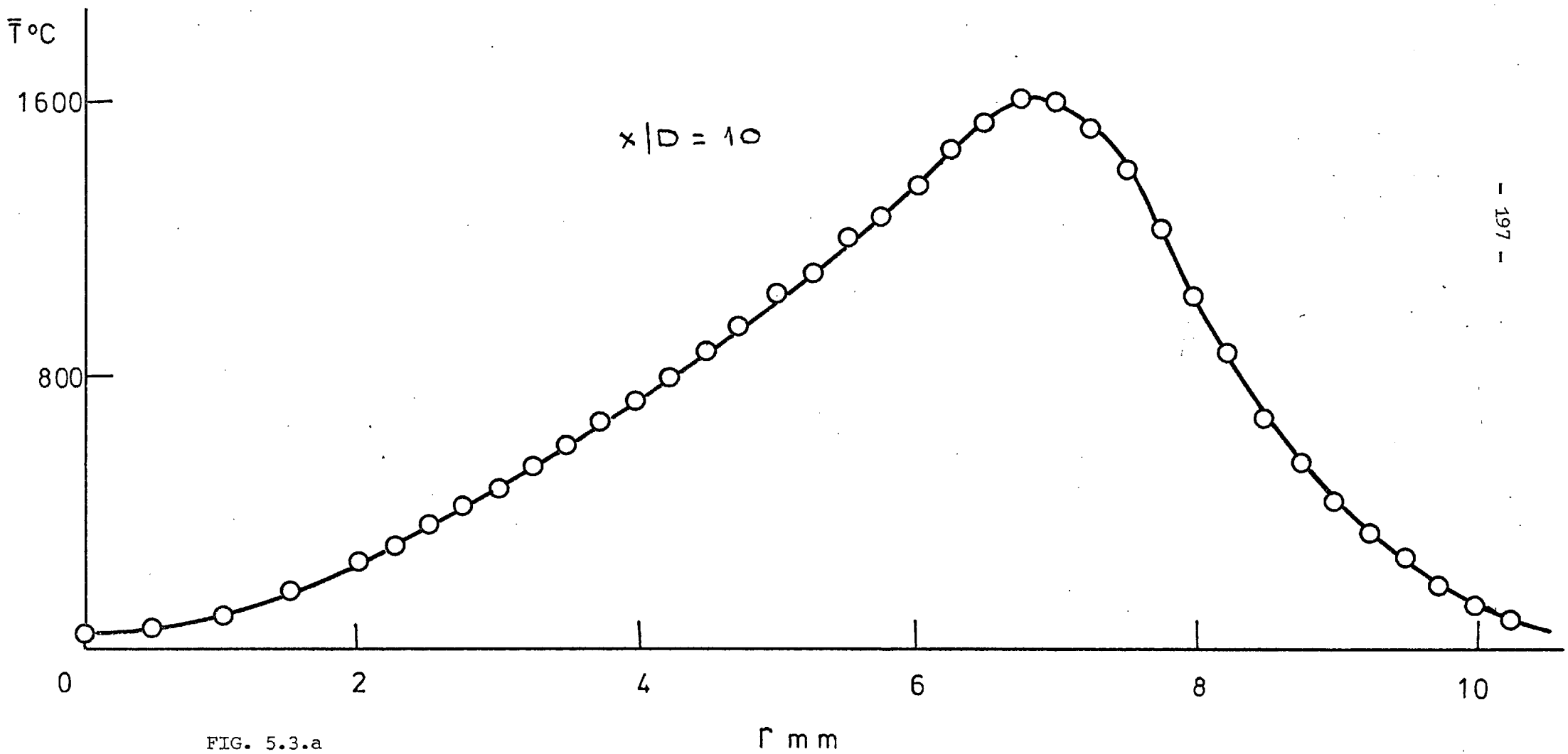


FIG. 5.3.a

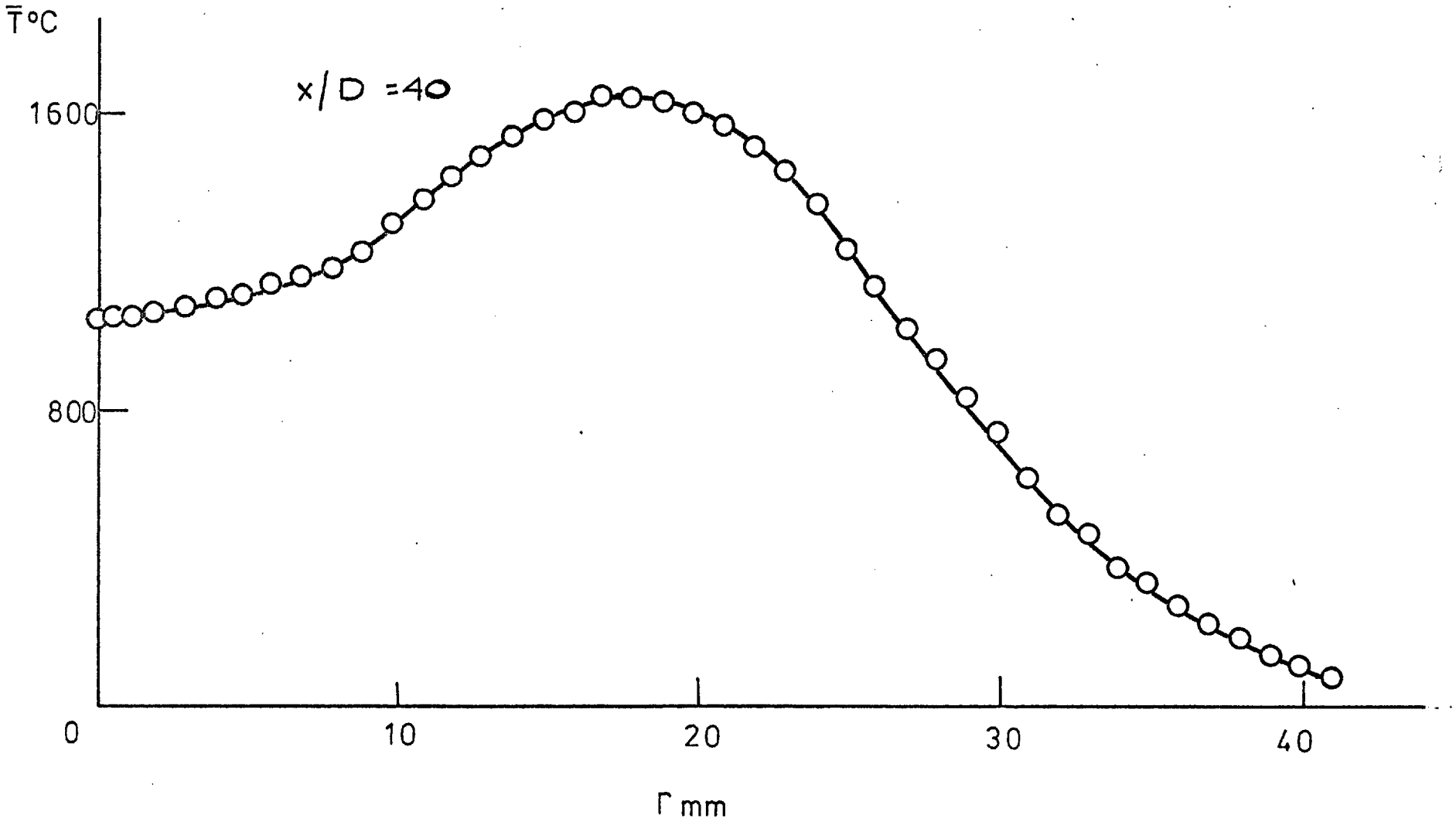


FIG. 5.3.b

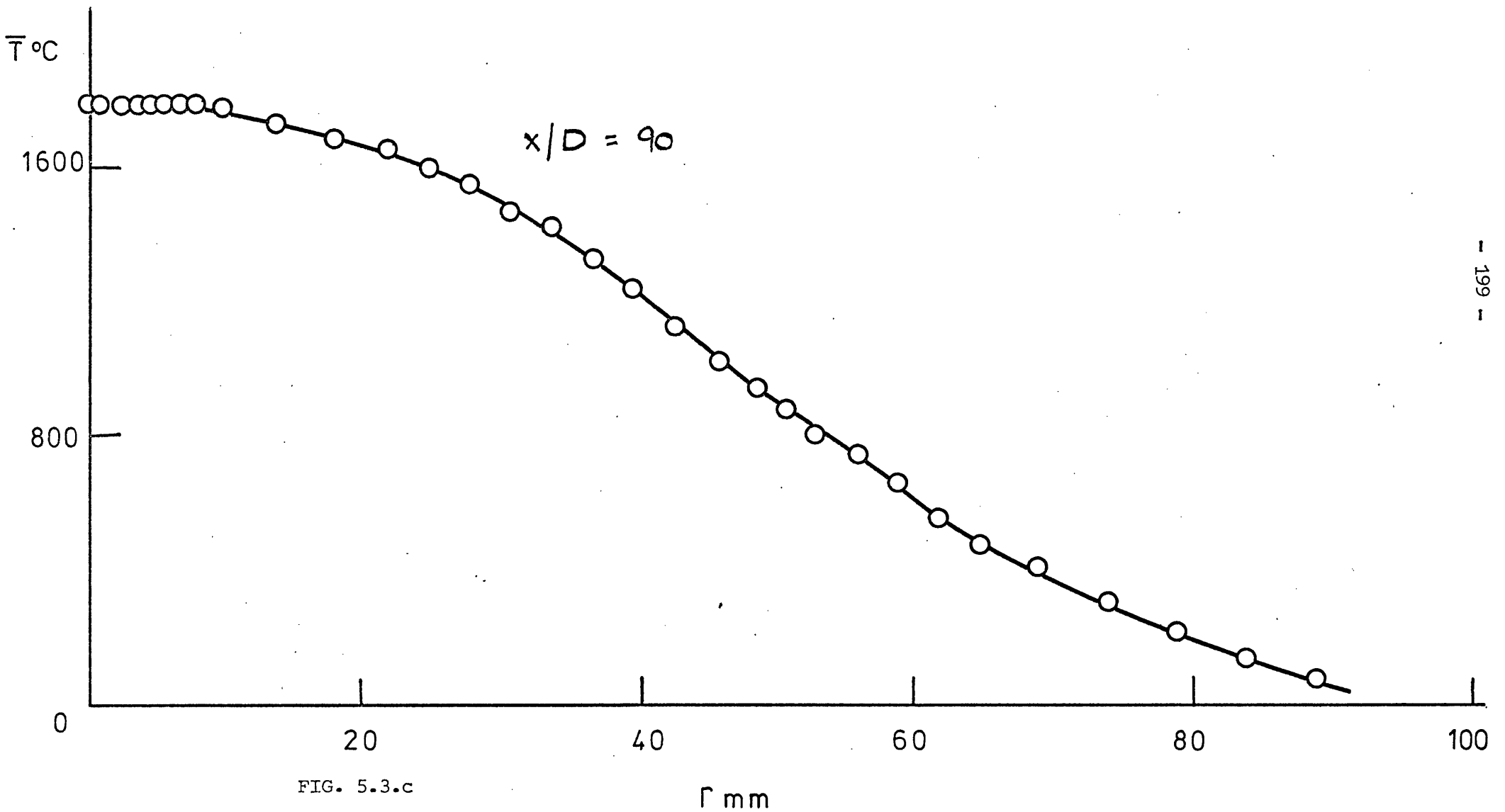


FIG. 5.3.c

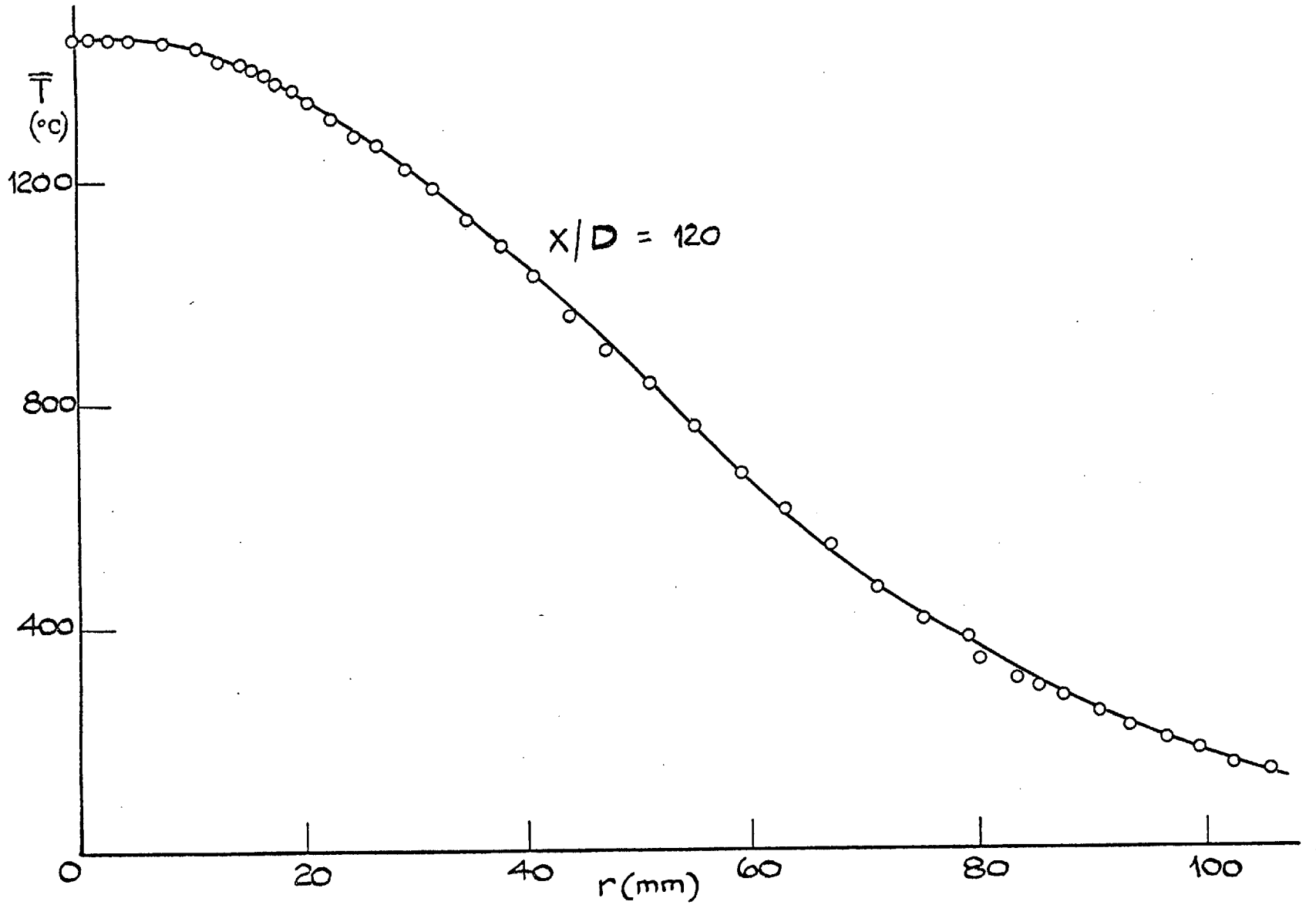


FIG. 5.3.d

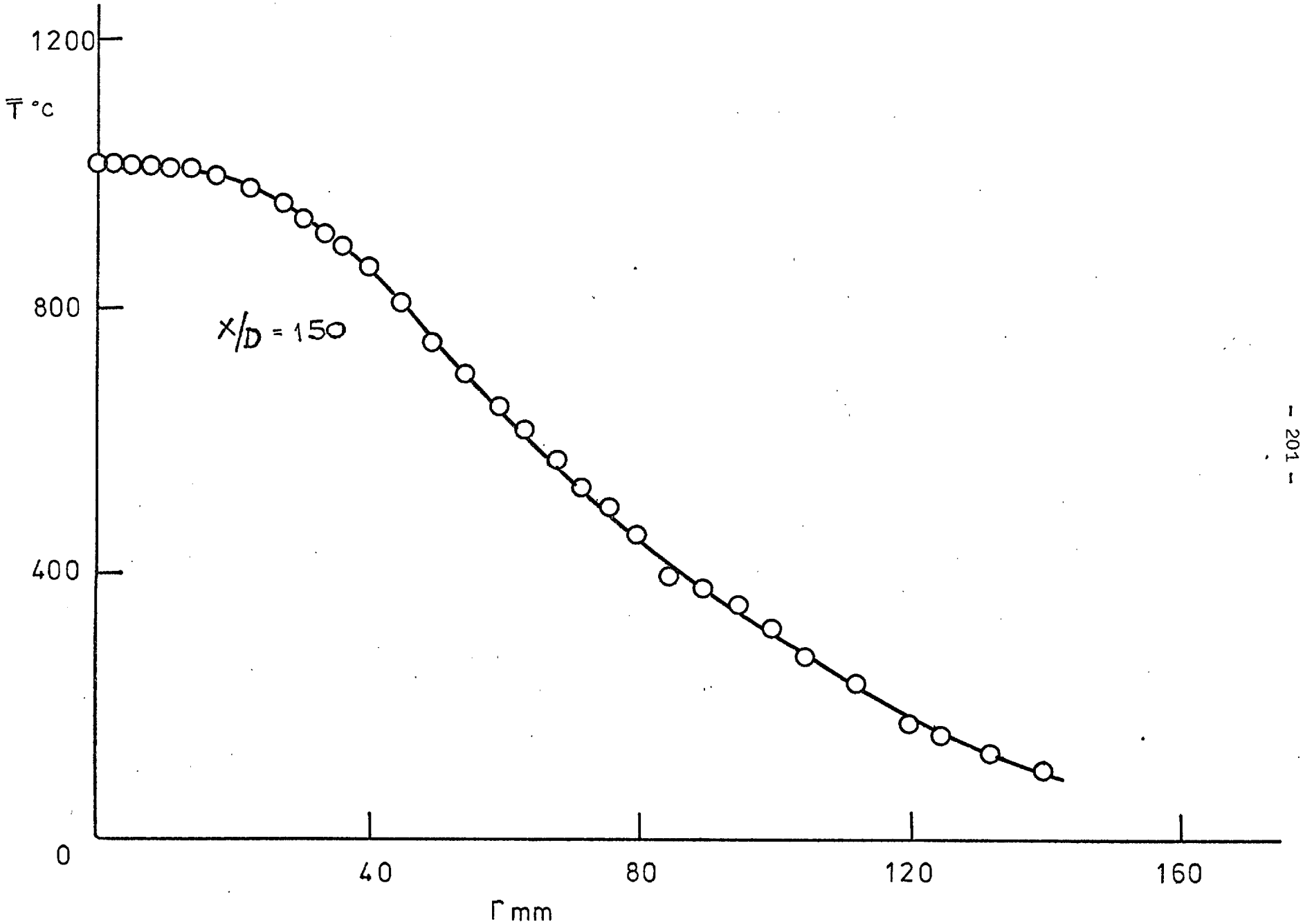


FIG. 5.3.e

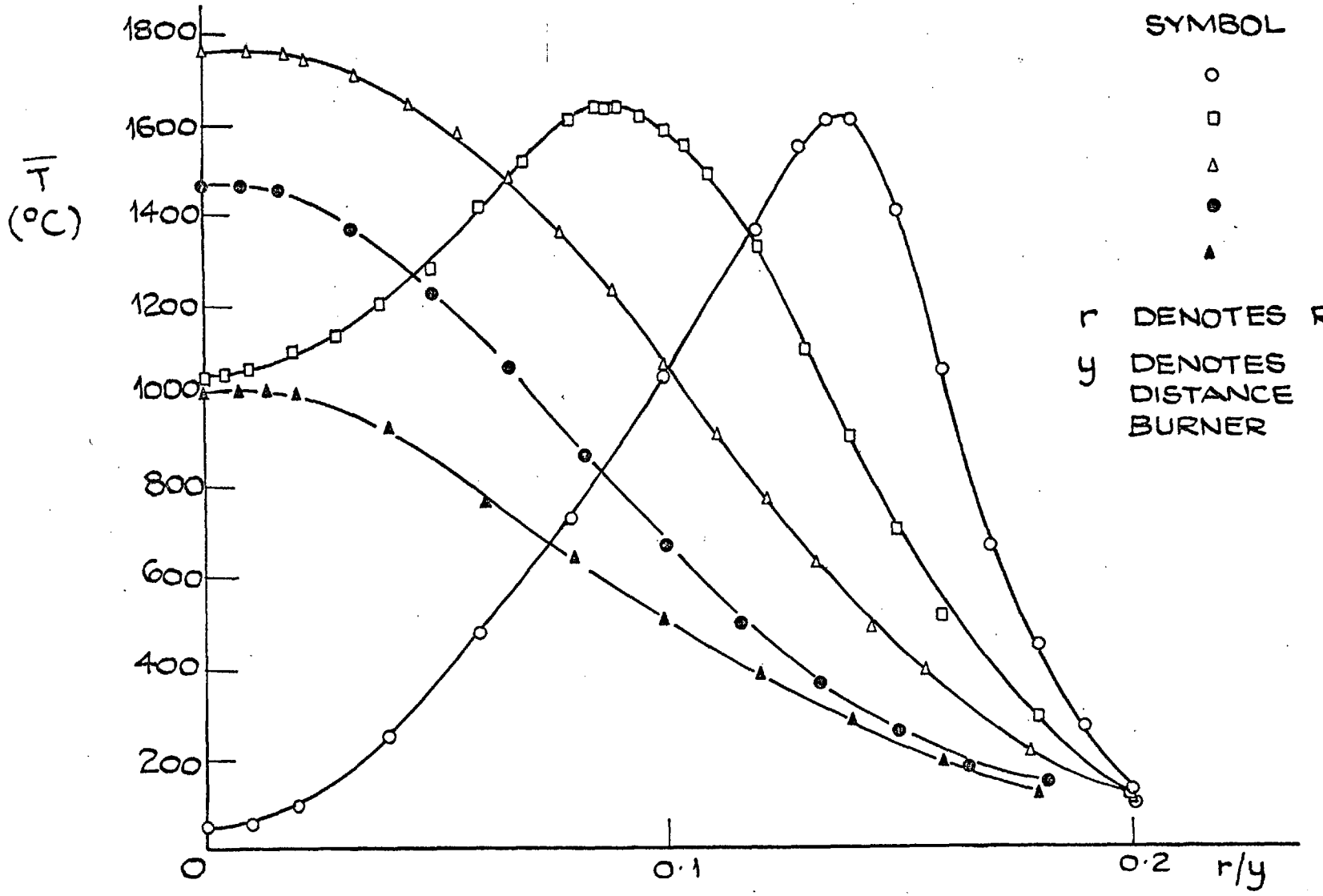

1800
1600
1400
1200
1000
800
600
400
200
0
0·1
0·2
r/y
$\overline{T}$ (°C)
SYMBOL x/D
10
40
90
120
150
r DENOTES RADIUS
y DENOTES AXIAL DISTANCE FROM BURNER

FIG. 5.3.f

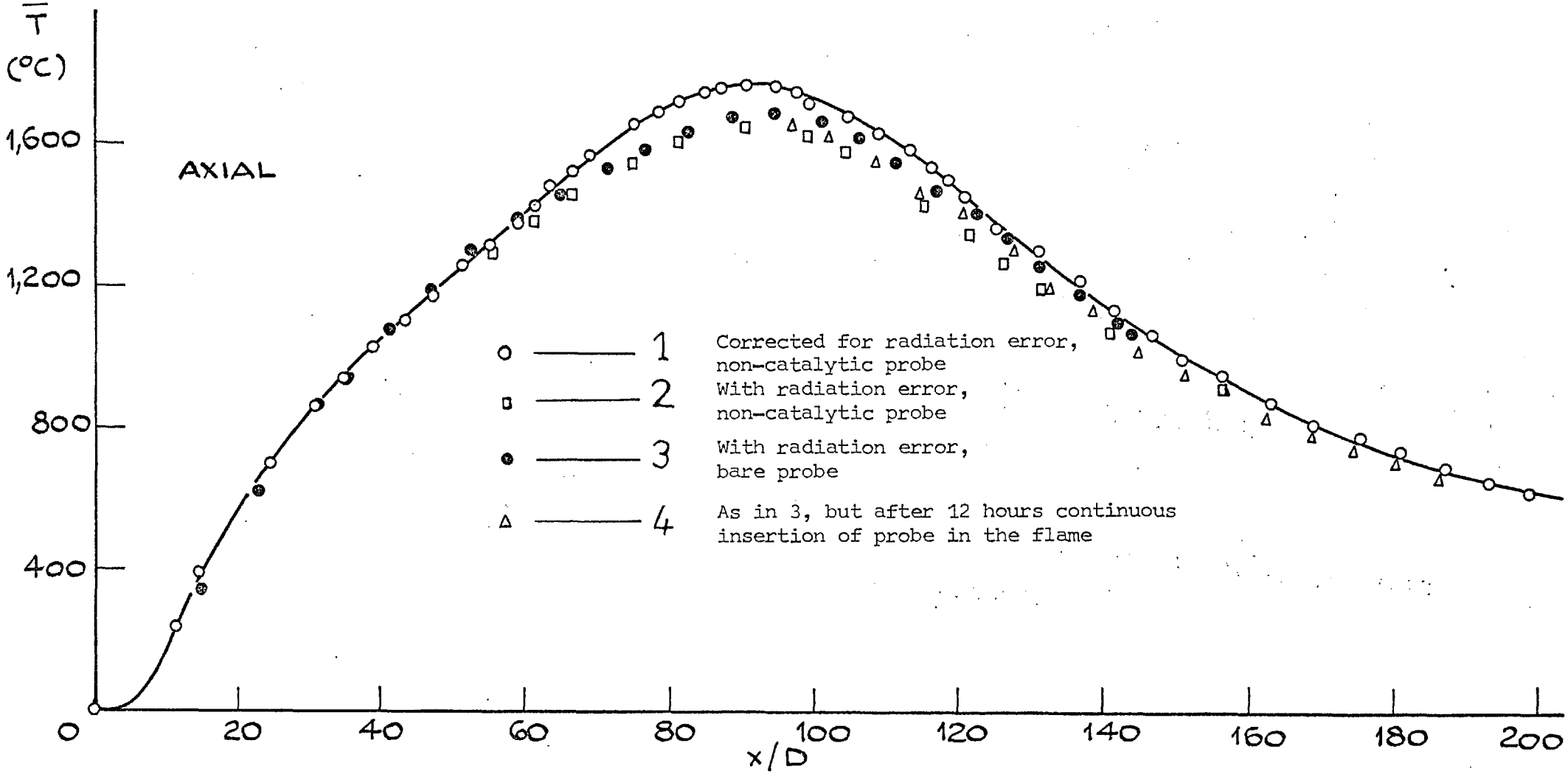
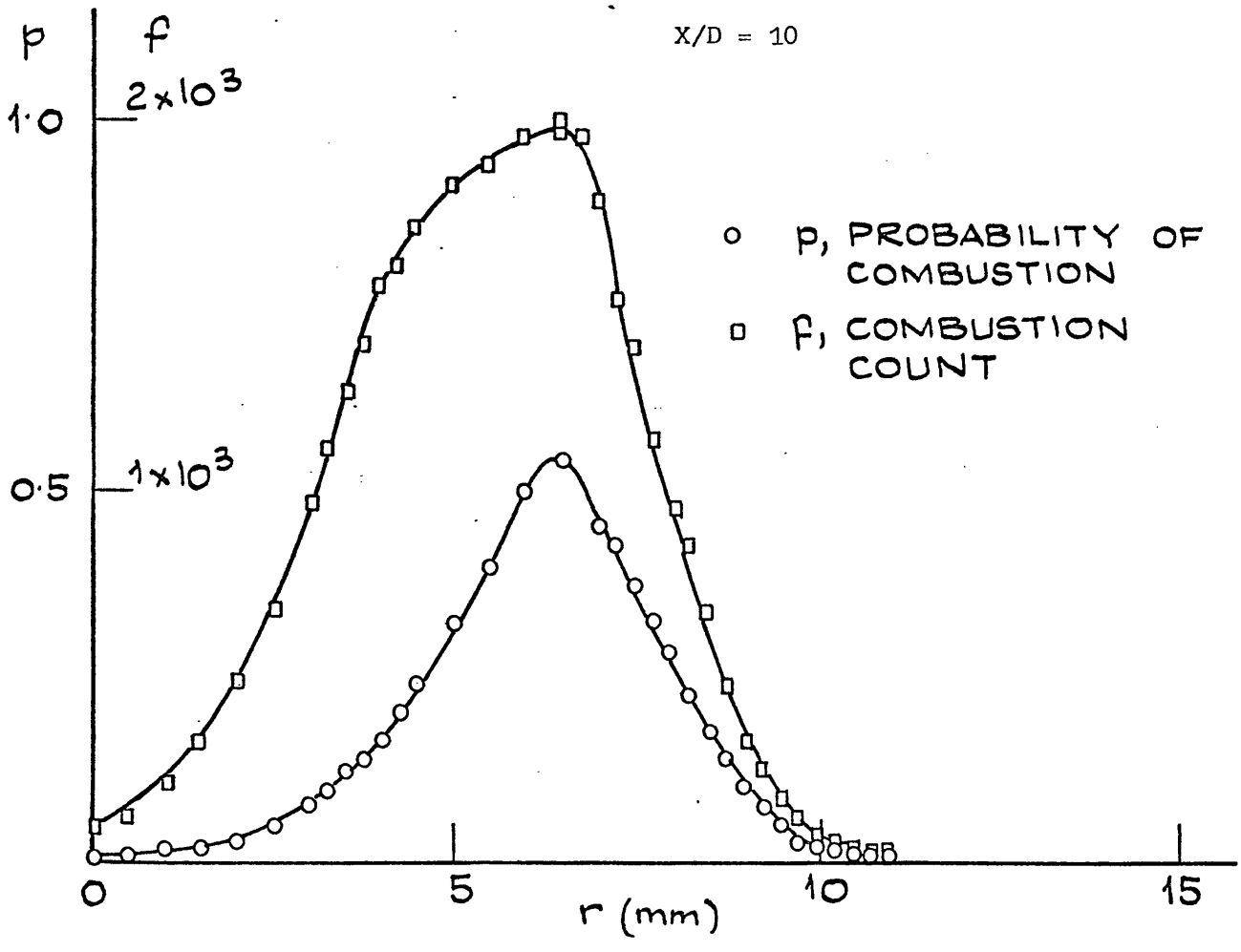

$\overline{T}$
(°C)
1,600
1,200
800
400
0
AXIAL
1
2
3
4
Corrected for radiation error, non-catalytic probe
With radiation error, non-catalytic probe
With radiation error, bare probe
As in 3, but after 12 hours continuous insertion of probe in the flame
20
40
60
80
100
120
140
160
180
200
x/D

FIG. 5.3.g


p
f
X/D = 10
1·0
2x10³
0·5
1x10³
o p, PROBABILITY OF COMBUSTION
□ f, COMBUSTION COUNT
0
5
10
15
r (mm)

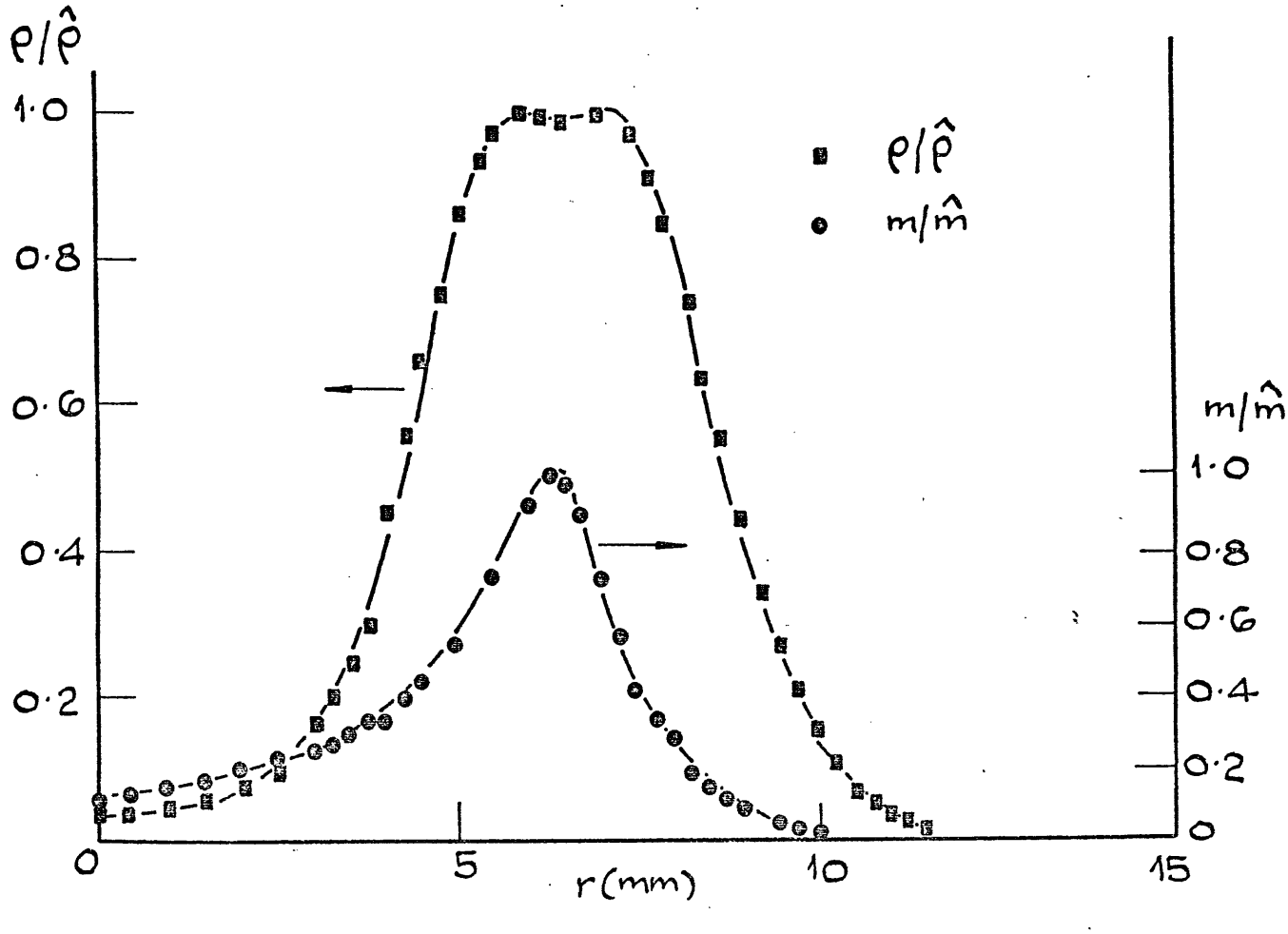
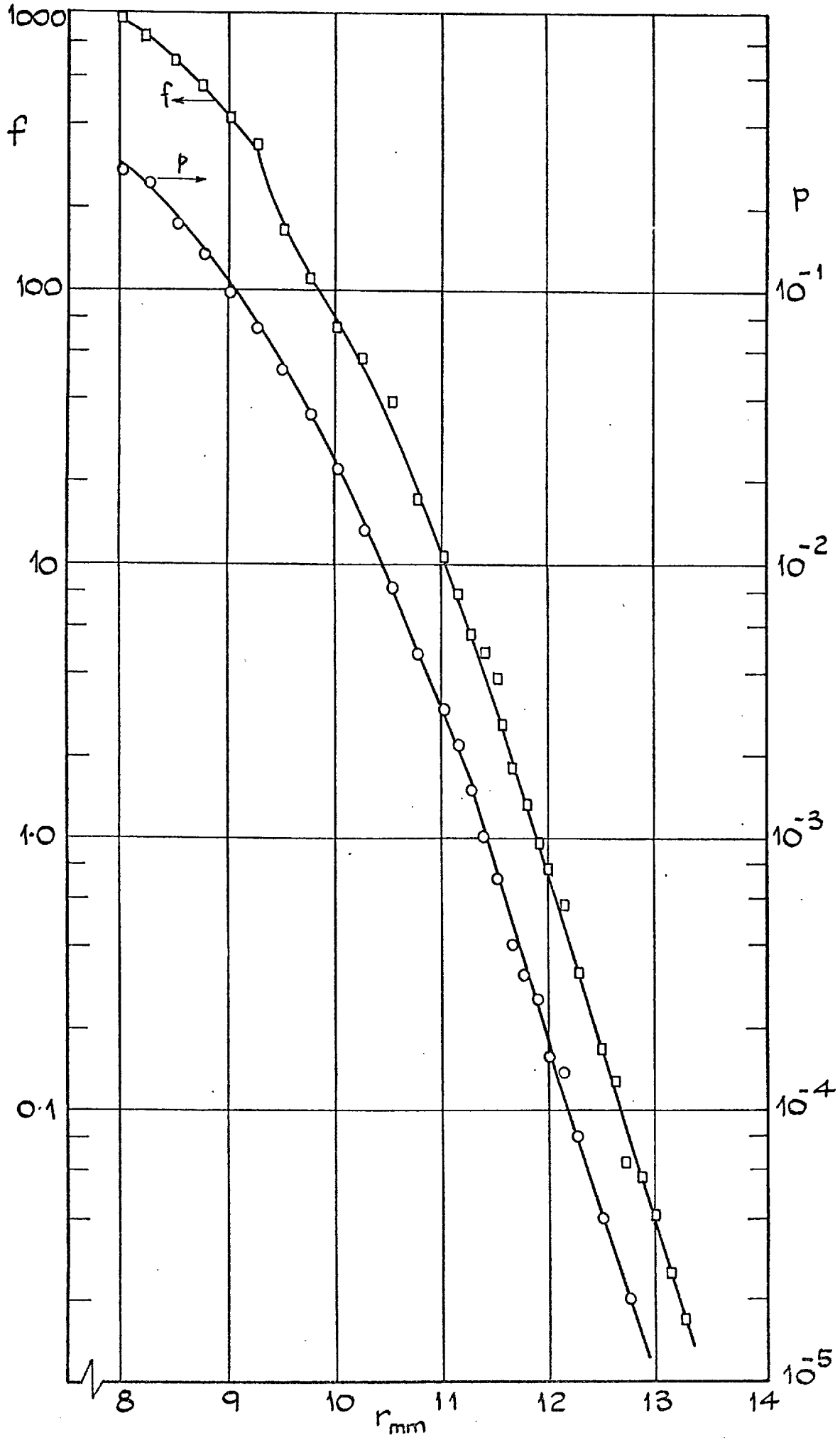
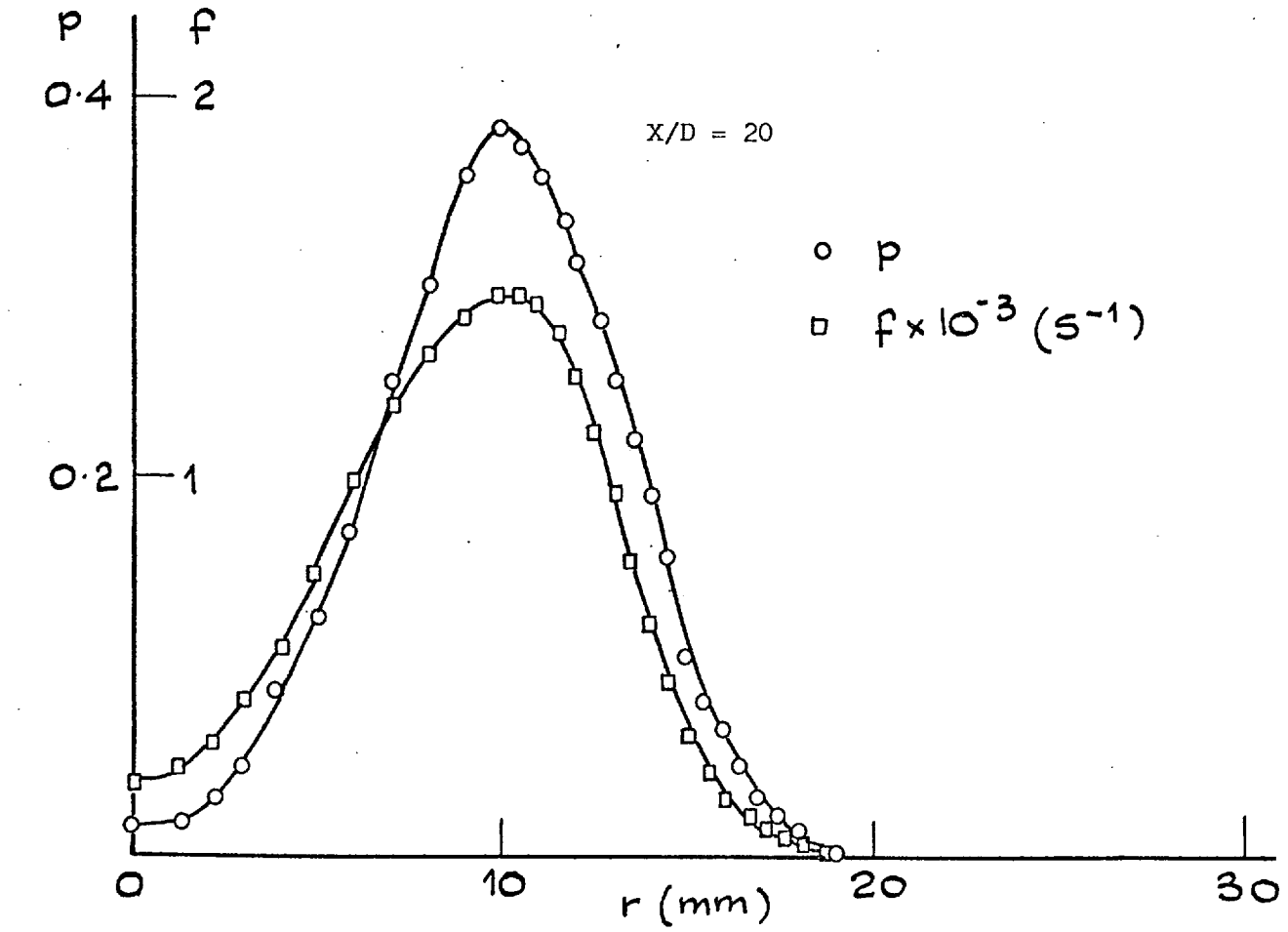

ρ/ρ̂
1·0
0·8
0·6
0·4
0·2
ρ/ρ̂
m/m̂
m/m̂
1·0
0·8
0·6
0·4
0·2
0
0
5
10
15
r(mm)

FIG. 5.3.h



X/D = 10 "EDGE OF FLAME"

FIG. 5.3.i


p
f
0·4
2
X/D = 20
o p
□ f x 10⁻³ (s⁻¹)
0·2
1
0
10
20
30
r (mm)

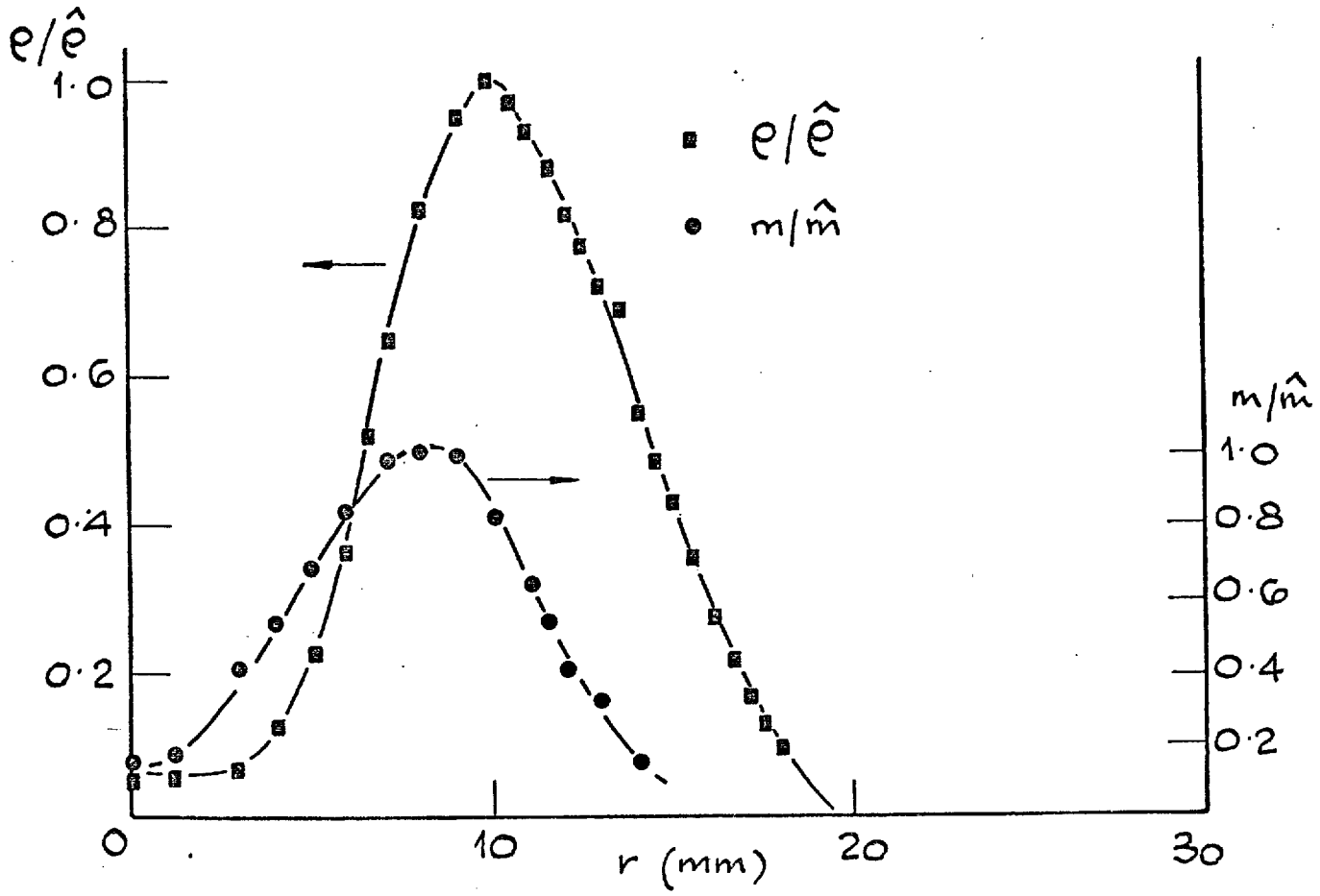

ρ/ρ̂
1·0
0·8
0·6
0·4
0·2
ρ/ρ̂
m/m̂
m/m̂
1·0
0·8
0·6
0·4
0·2
0
10
20
30
r (mm)

FIG. 5.3.j

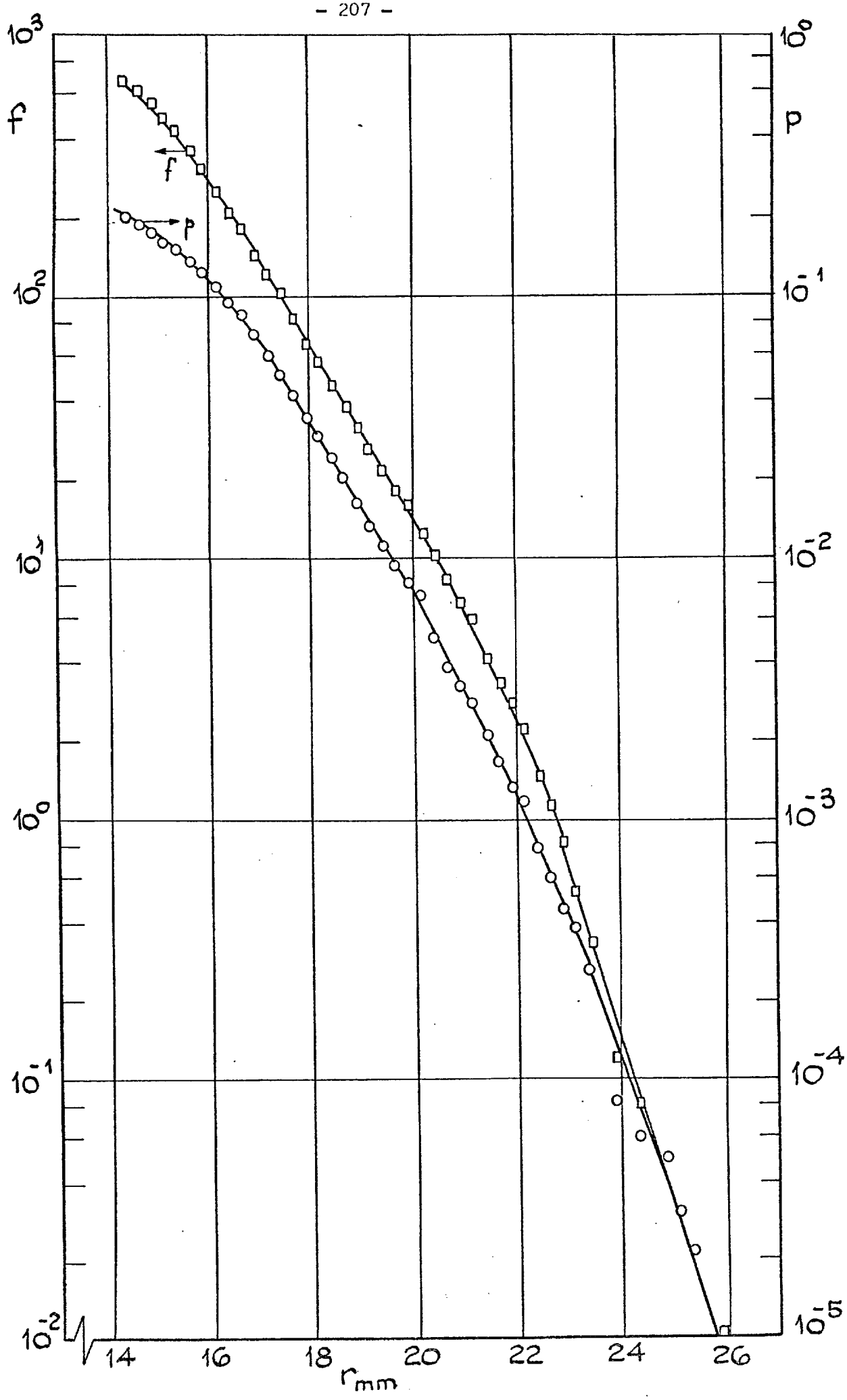
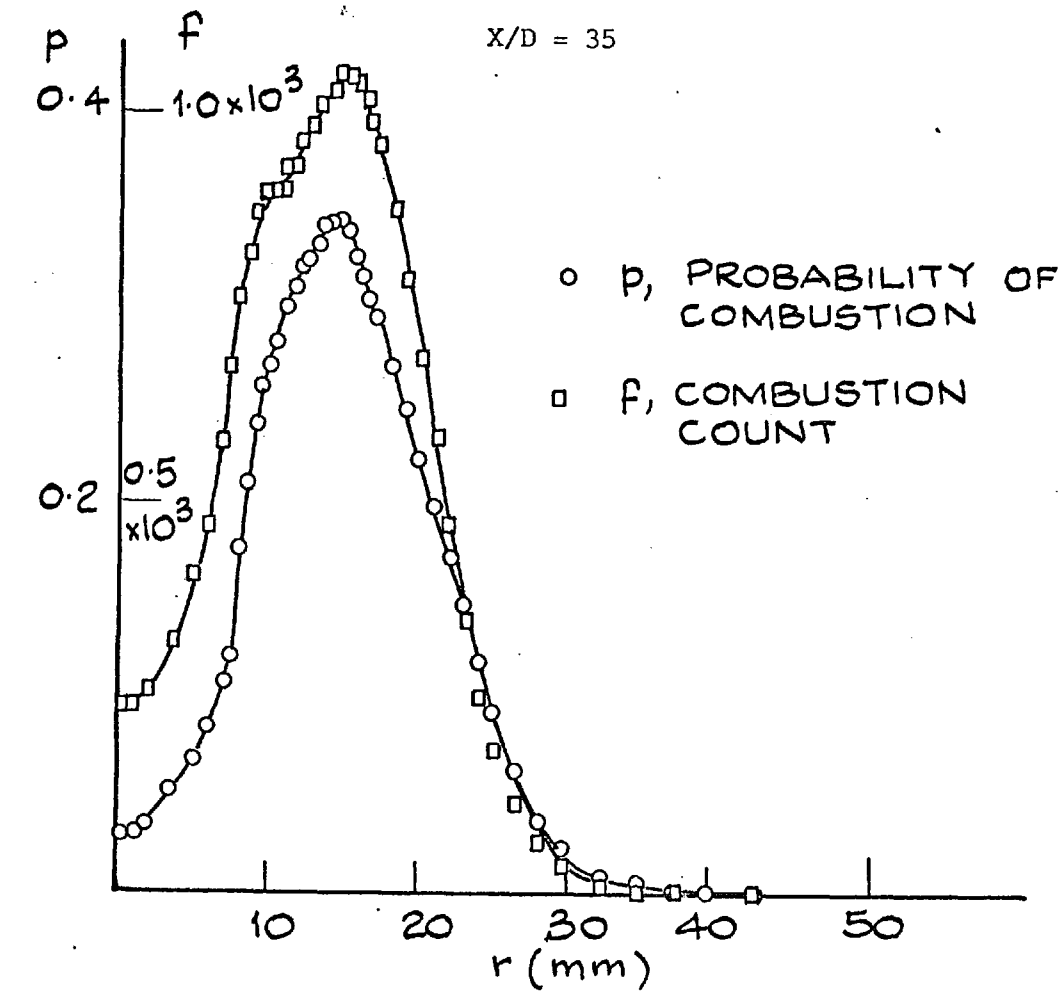


FIG. 5.3.k X/D = 20 EDGE OF FLAME


p
f
X/D = 35
0·4
1·0×10³
0·2
0·5
×10³
o p, PROBABILITY OF COMBUSTION
□ f, COMBUSTION COUNT
10
20
30
40
50
r (mm)

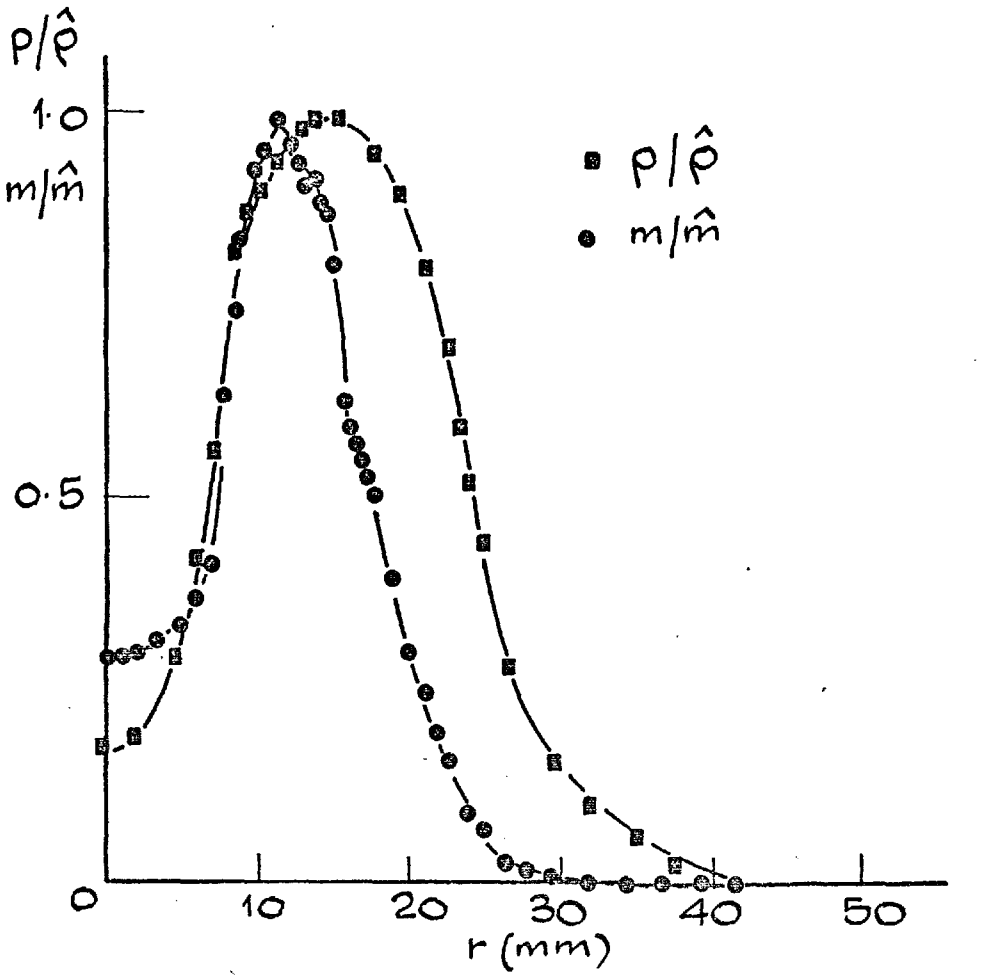

p/p̂
1·0
m/m̂
0·5
0
■ p/p̂
● m/m̂
10
20
30
40
50
r (mm)

FIG. 5.3.*l*

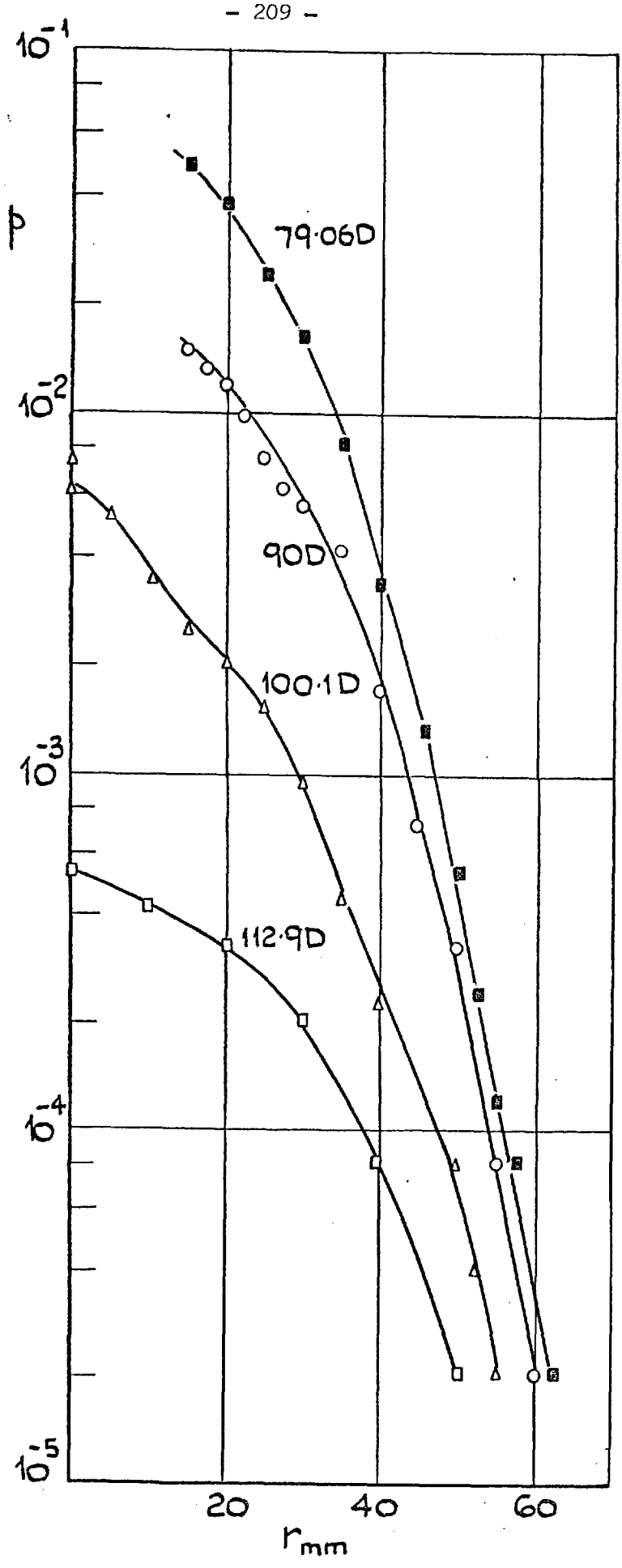


FIG. 5.3.m

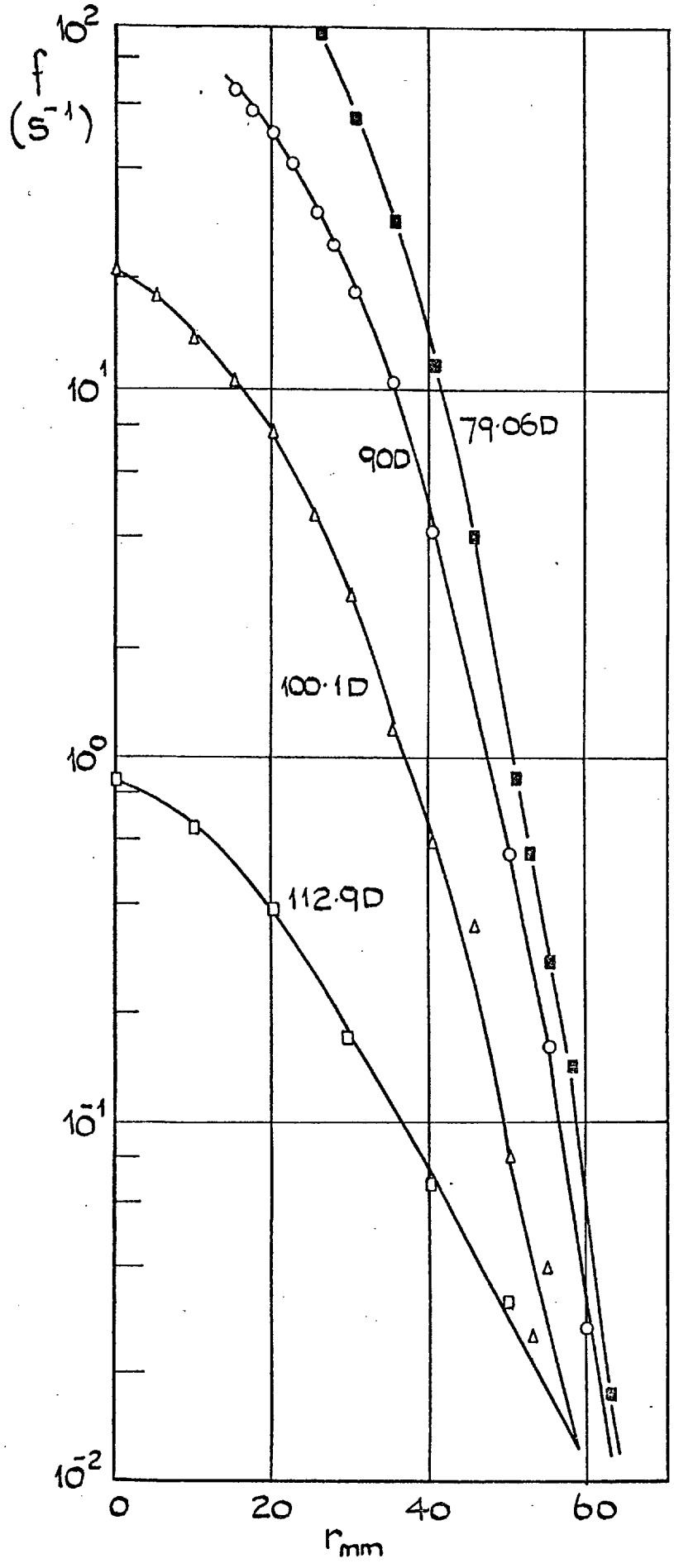


FIG. 5.3.n

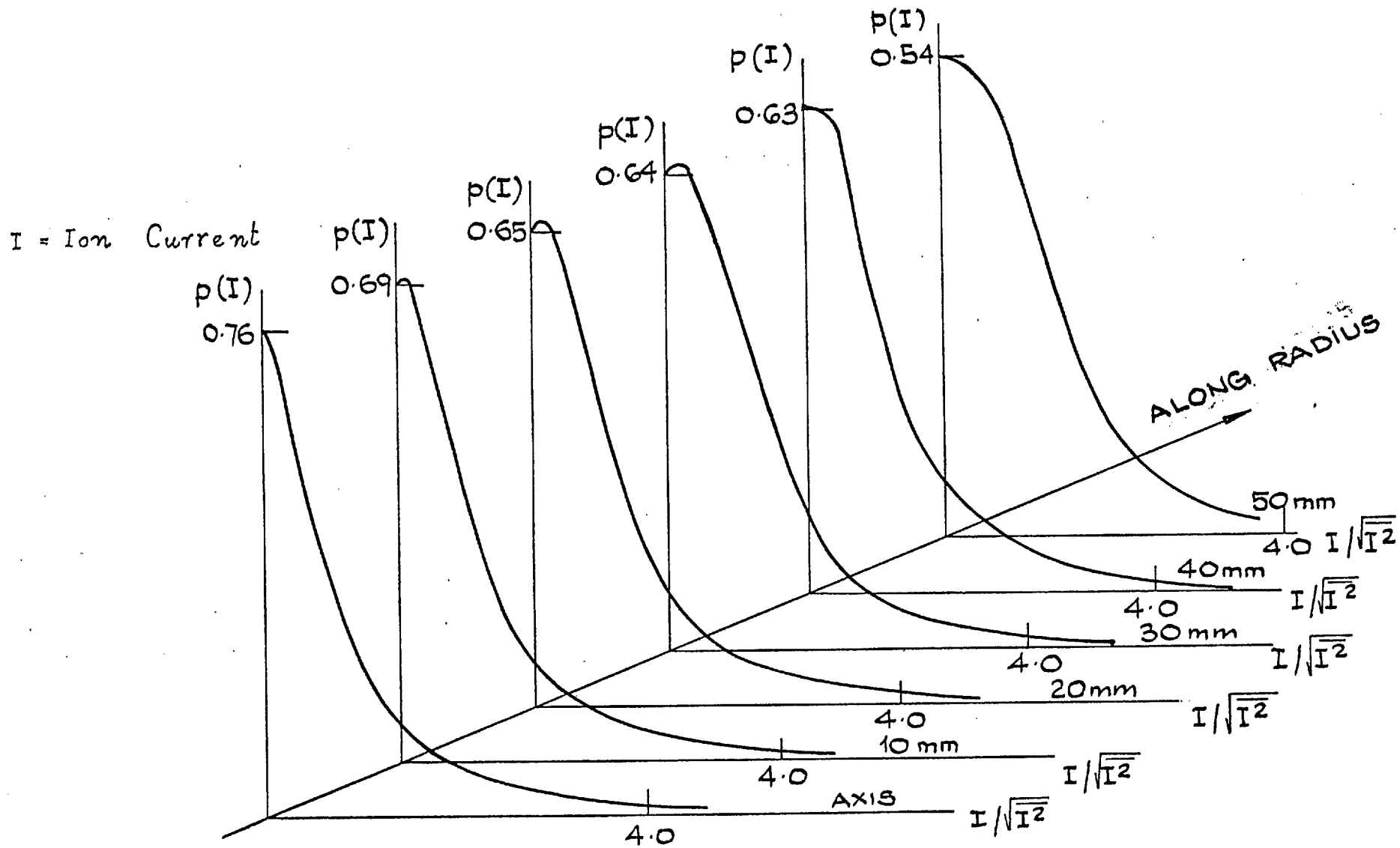

I = Ion Current
p(I)
0·76
p(I)
0·69
p(I)
0·65
p(I)
0·64
p(I)
0·63
p(I)
0·54
ALONG RADIUS
50 mm
40 mm
30 mm
20 mm
10 mm
AXIS
4·0
I/√I²

FIG. 5.3.o

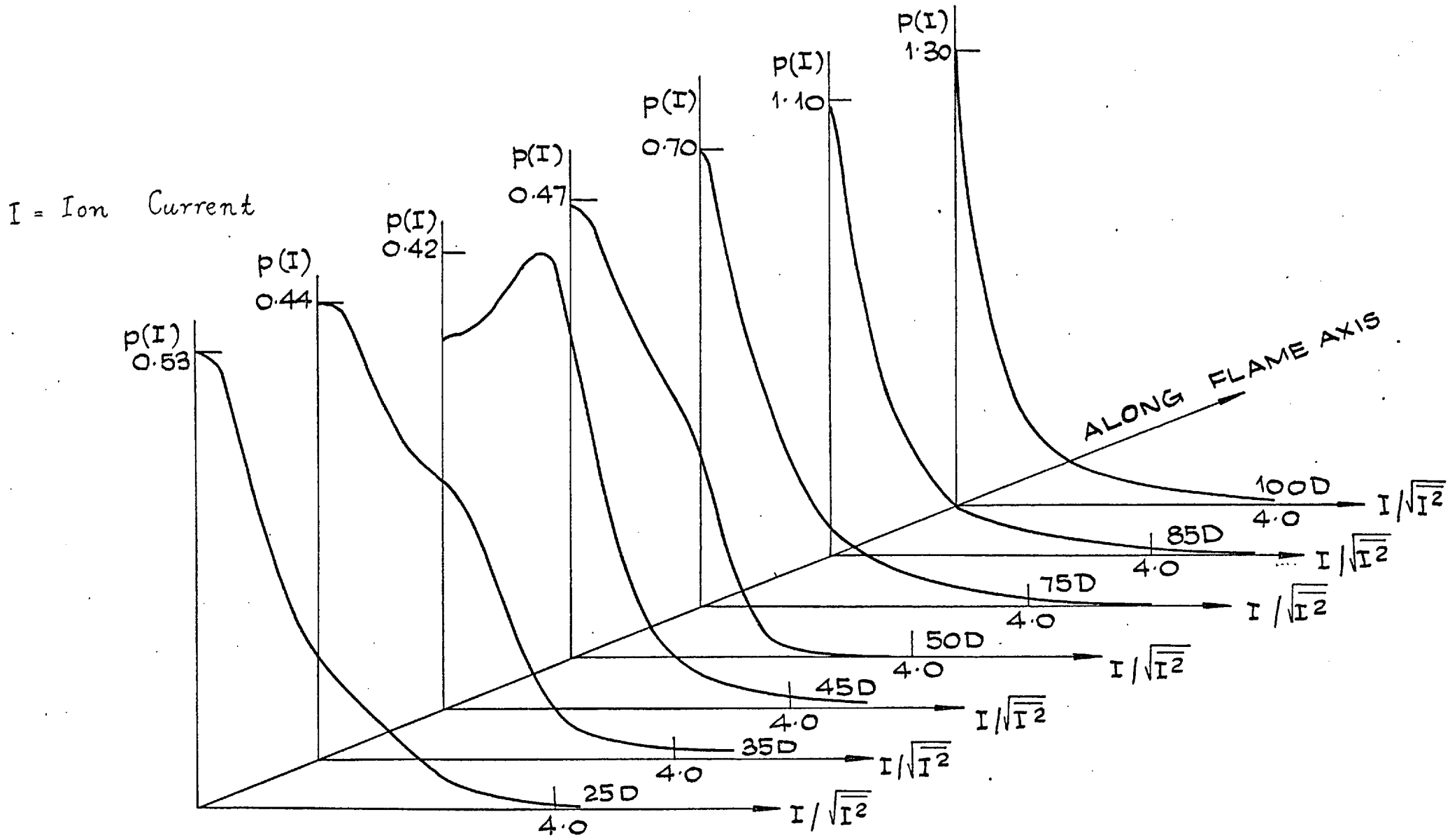

I = Ion Current
p(I)
0·53
p(I)
0·44
p(I)
0·42
p(I)
0·47
p(I)
0·70
p(I)
1·10
p(I)
1·30
ALONG FLAME AXIS
100D
85D
75D
50D
45D
35D
25D
4·0
I/√I²

FIG. 5.3.p

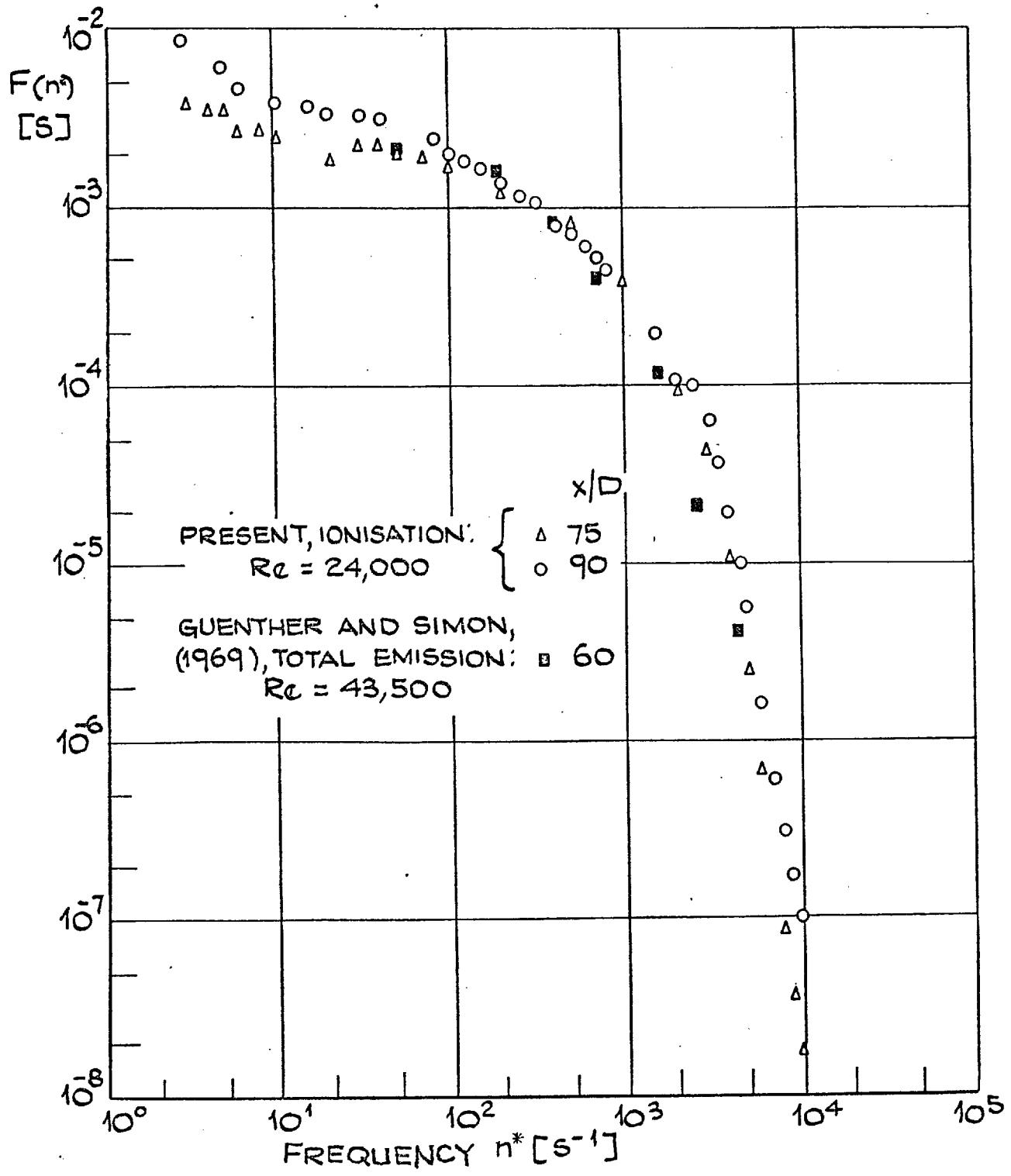

F(n*) [S]
10^-2
10^-3
10^-4
10^-5
10^-6
10^-7
10^-8
PRESENT, IONISATION: Re = 24,000
x/D
75
90
GUENTHER AND SIMON, (1969), TOTAL EMISSION: Re = 43,500
60
10^0
10^1
10^2
10^3
10^4
10^5
FREQUENCY n* [s^-1]

FIG. 5.3.q

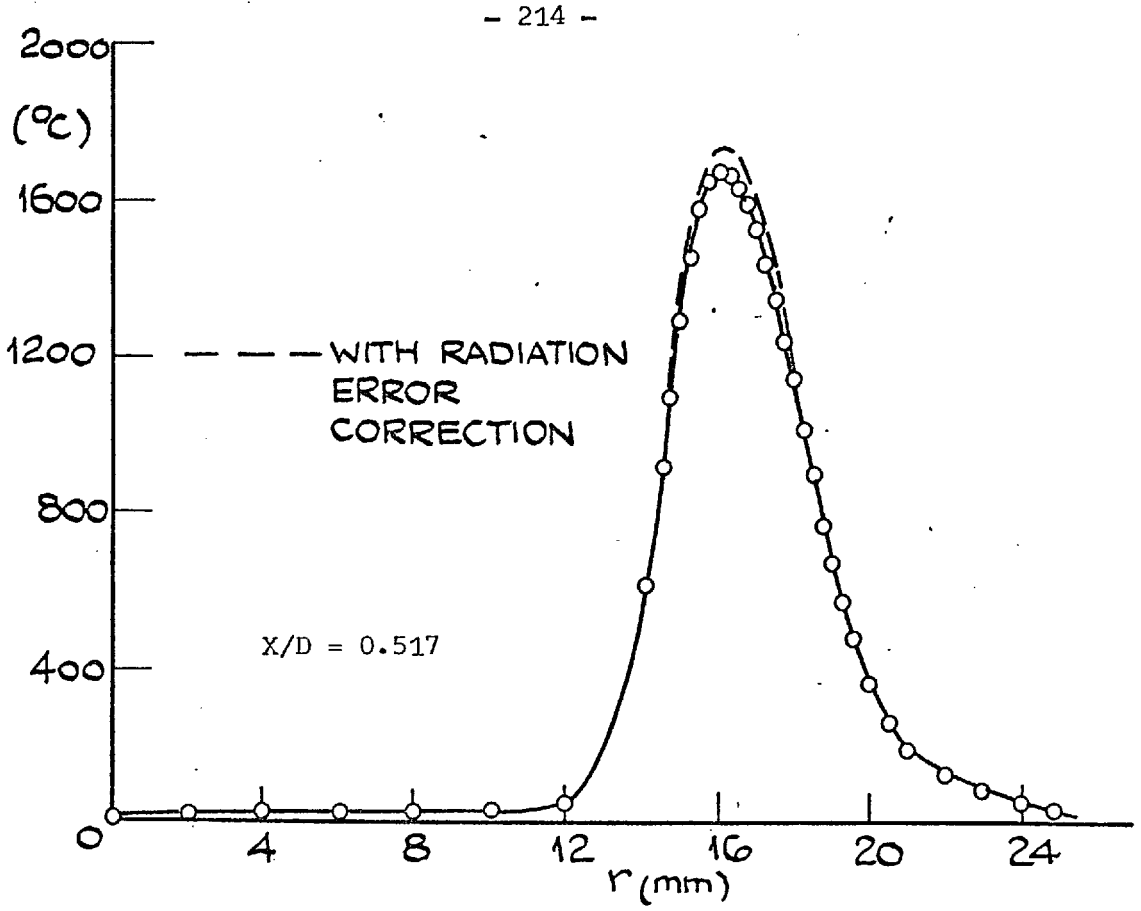


FIG. 5.4.a

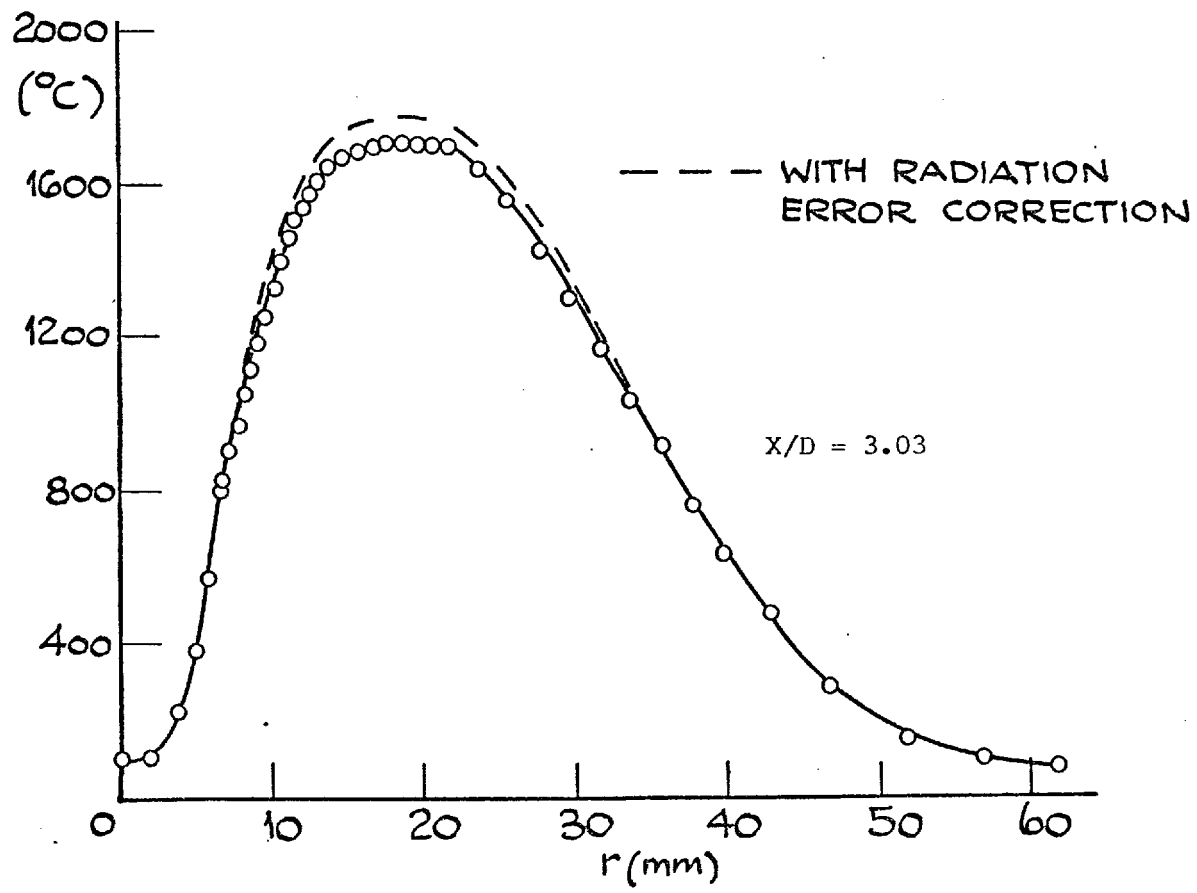


FIG. 5.4.b

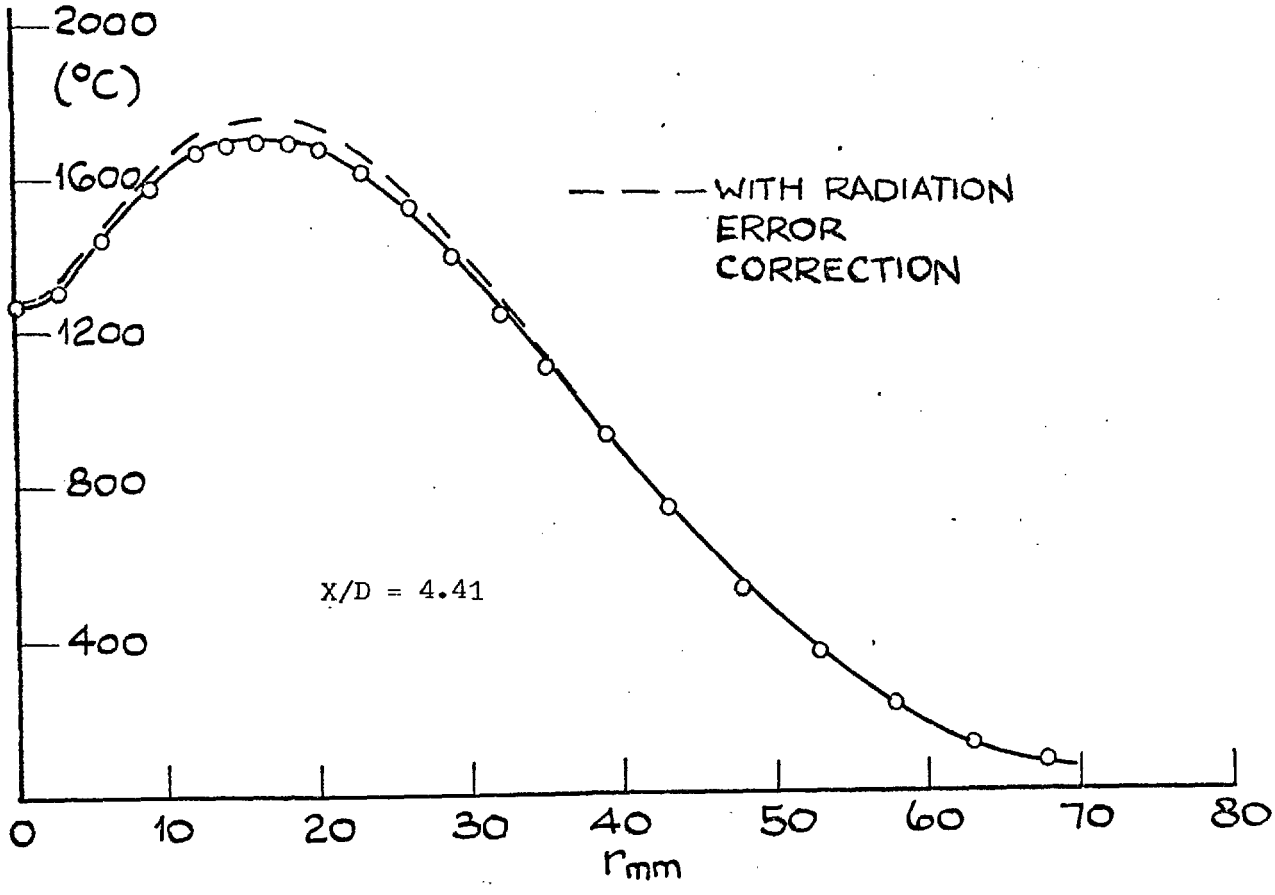


FIG. 5.4.c

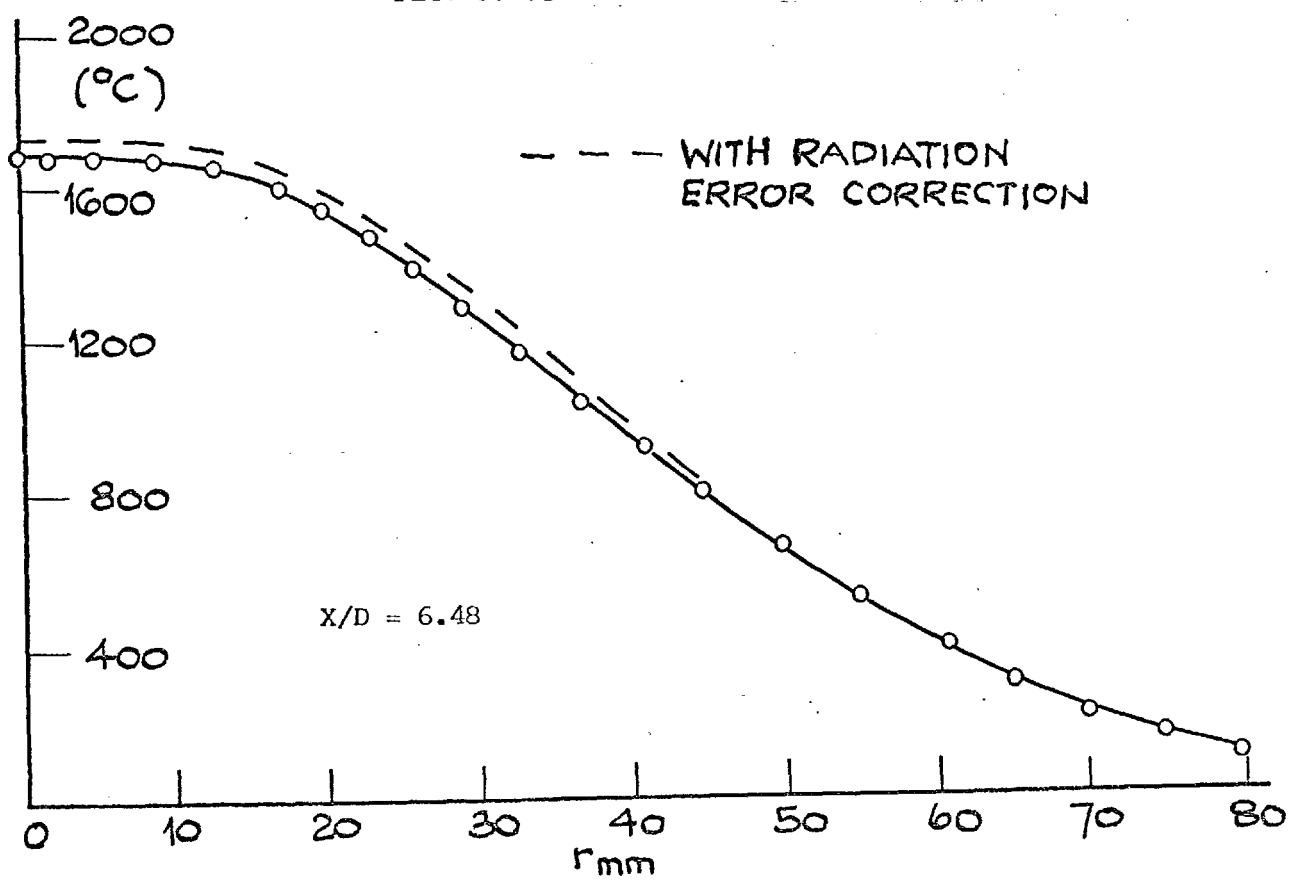


FIG. 5.4.d

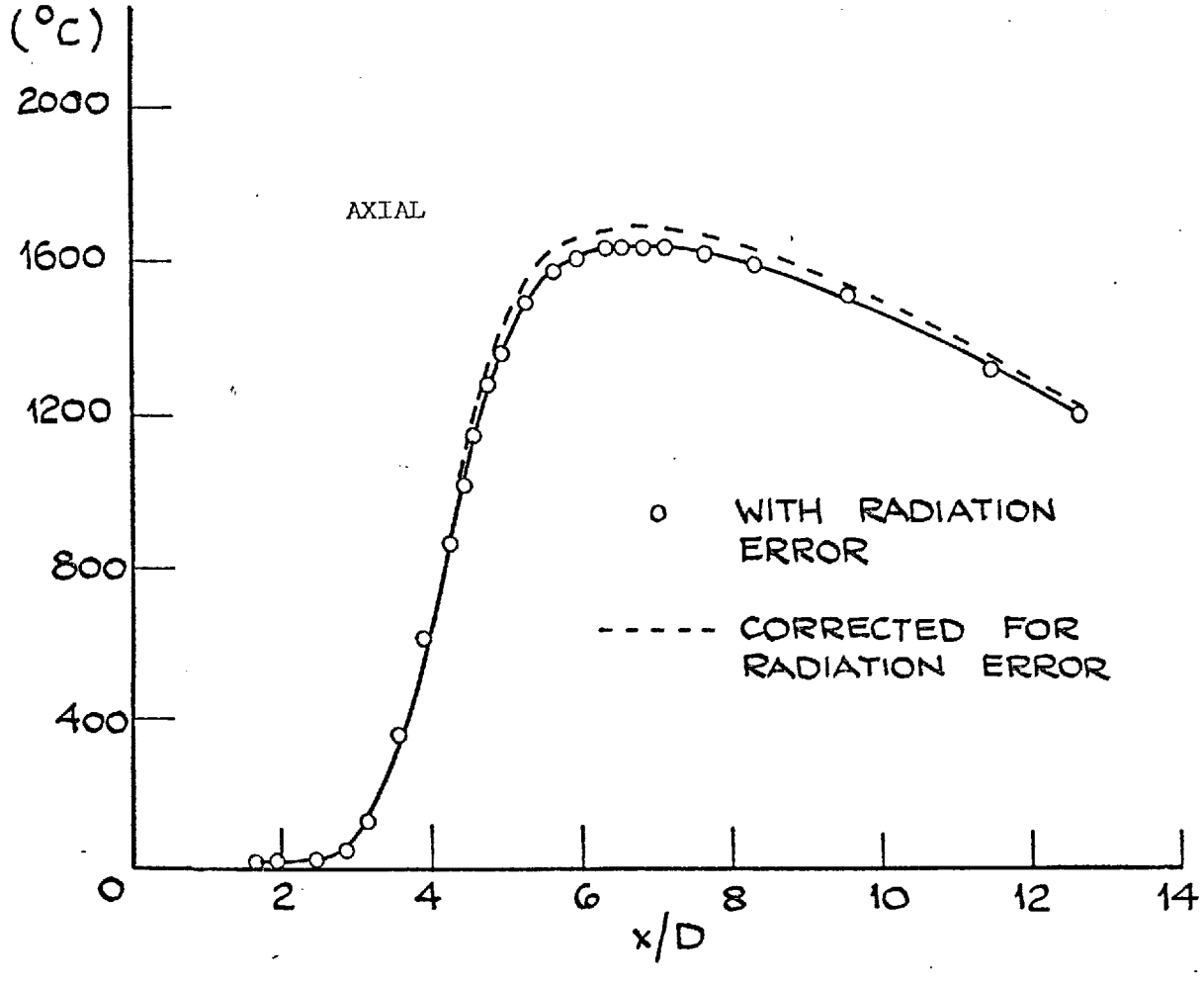

(°C)
2000
1600
1200
800
400
0
AXIAL
o WITH RADIATION ERROR
----- CORRECTED FOR RADIATION ERROR
2
4
6
8
10
12
14
x/D

FIG. 5.4.e

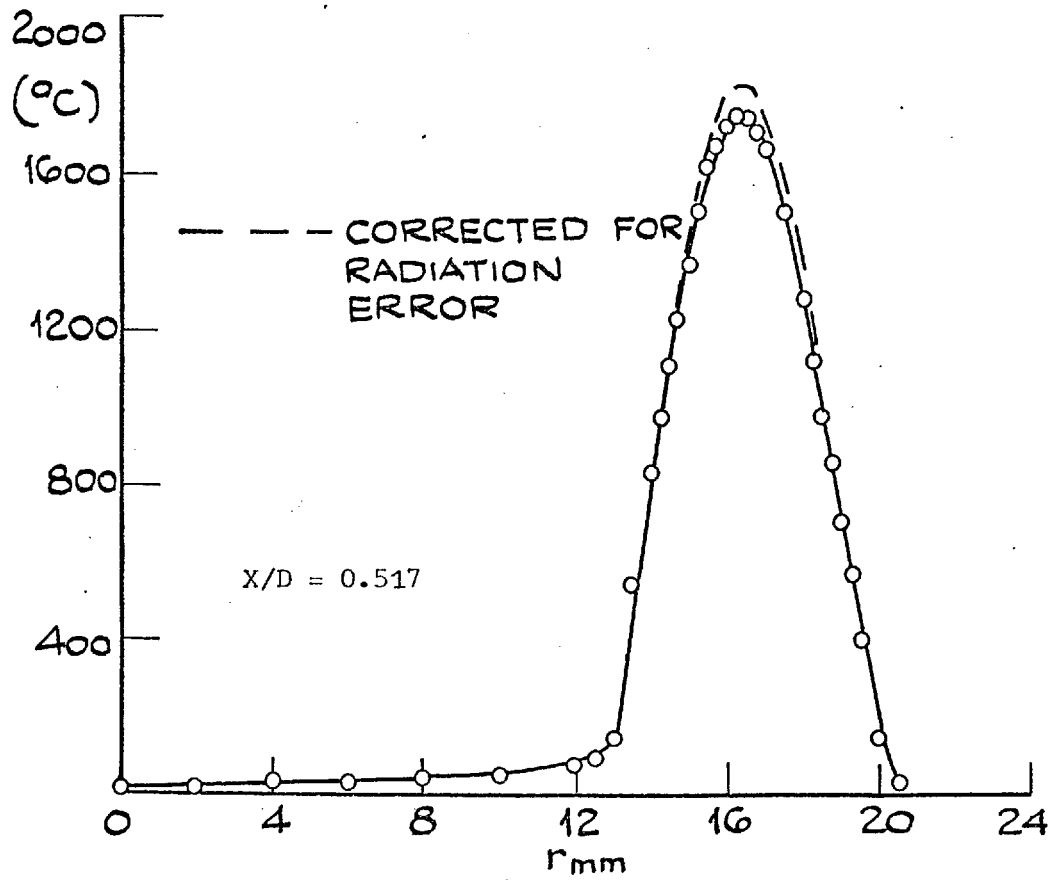


FIG. 5.4.f

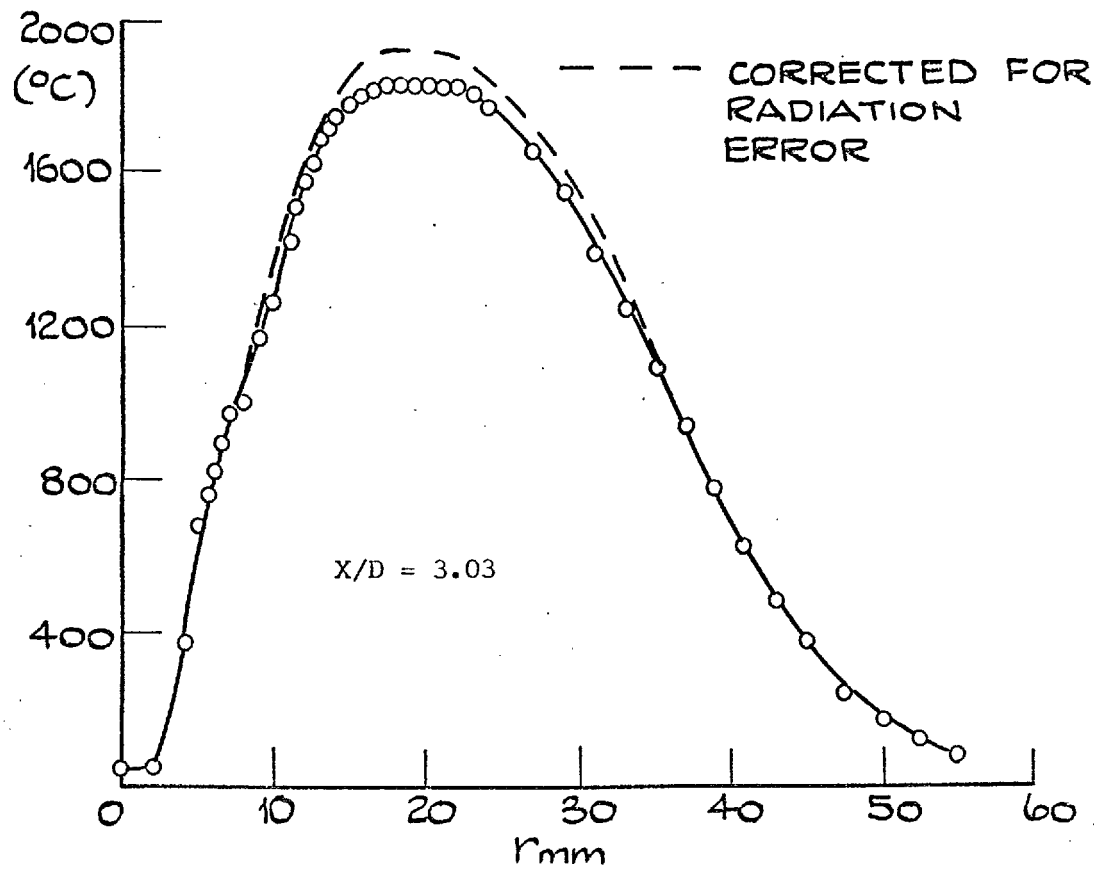


FIG. 5.4.g

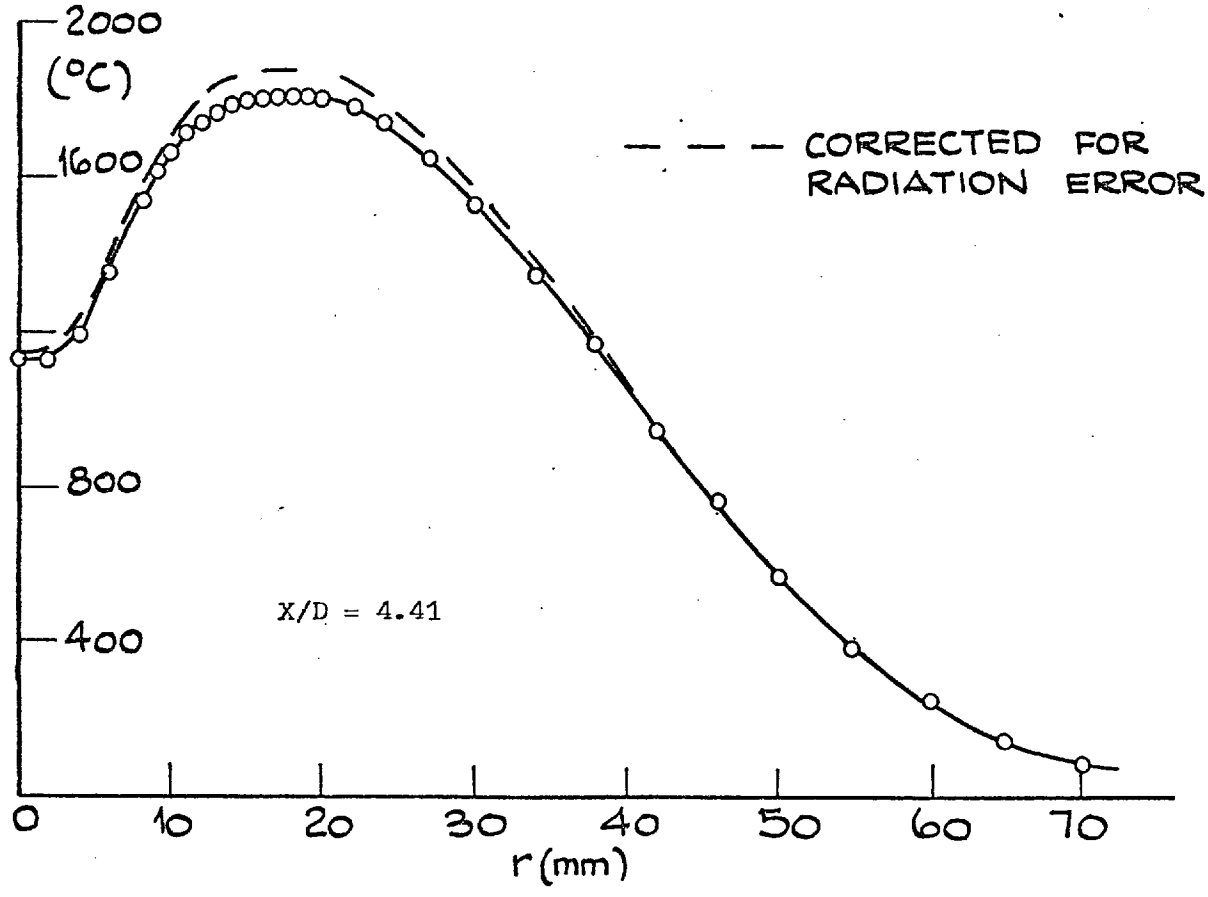


FIG. 5.4.h

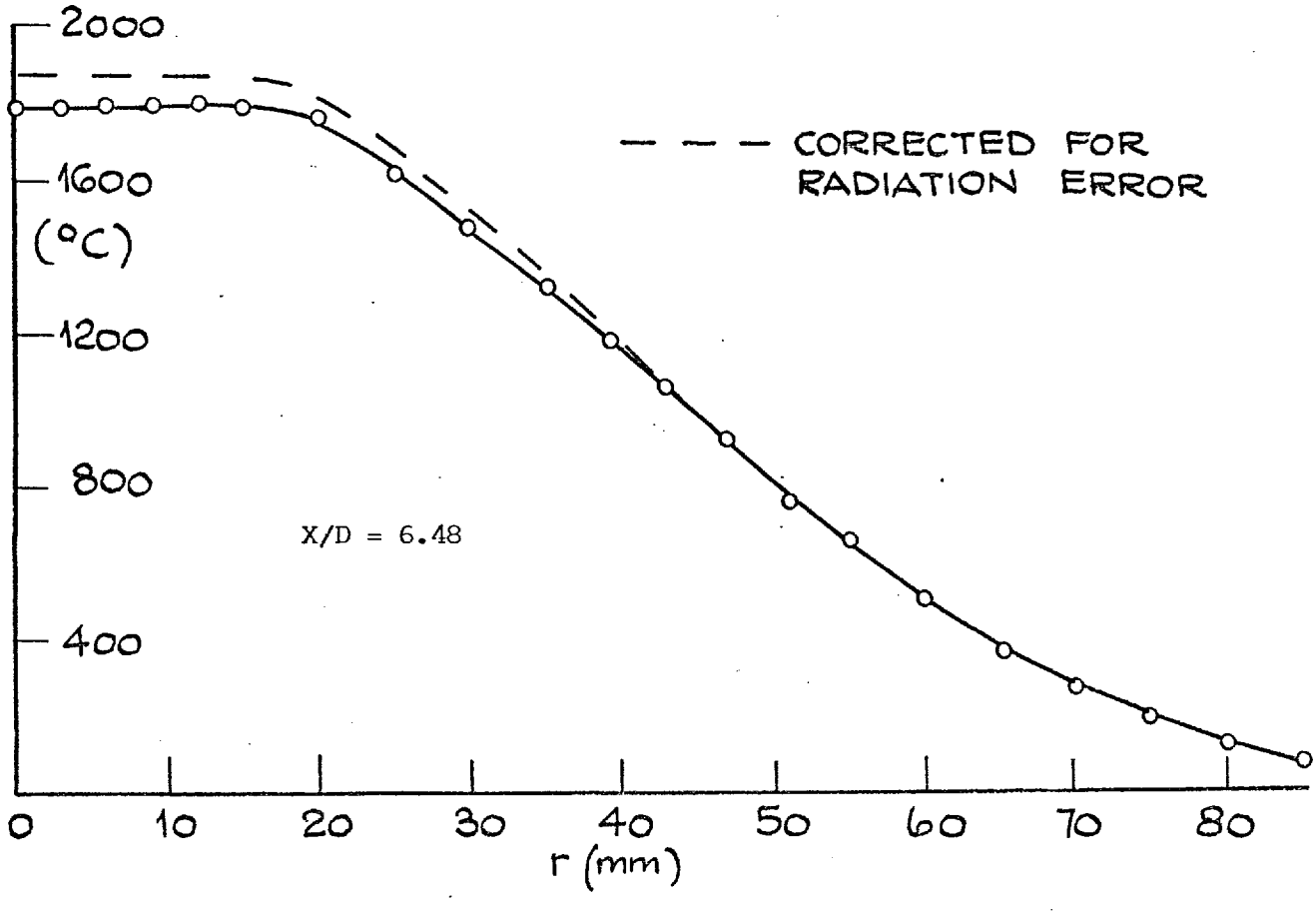


FIG. 5.4.i

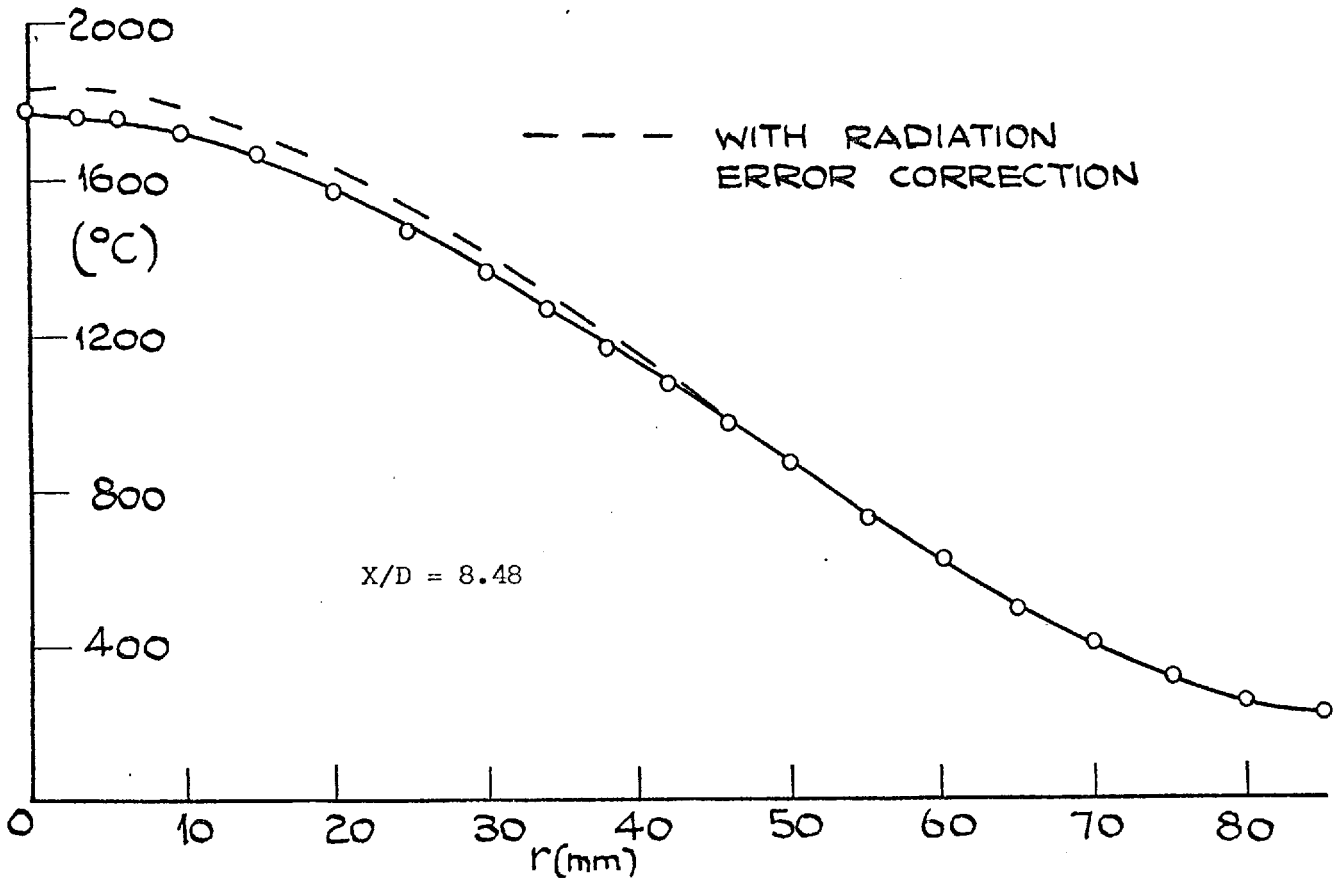


FIG. 5.4.j

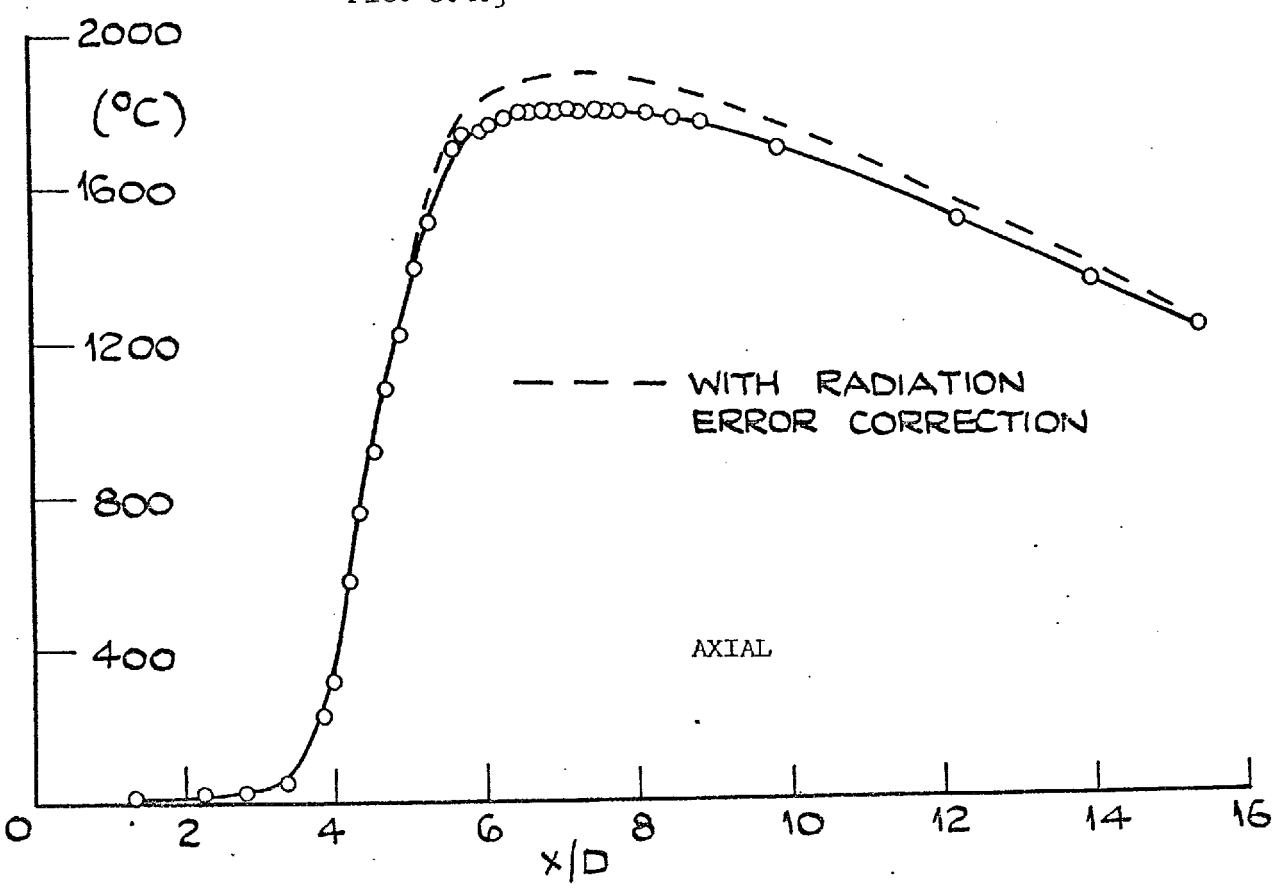
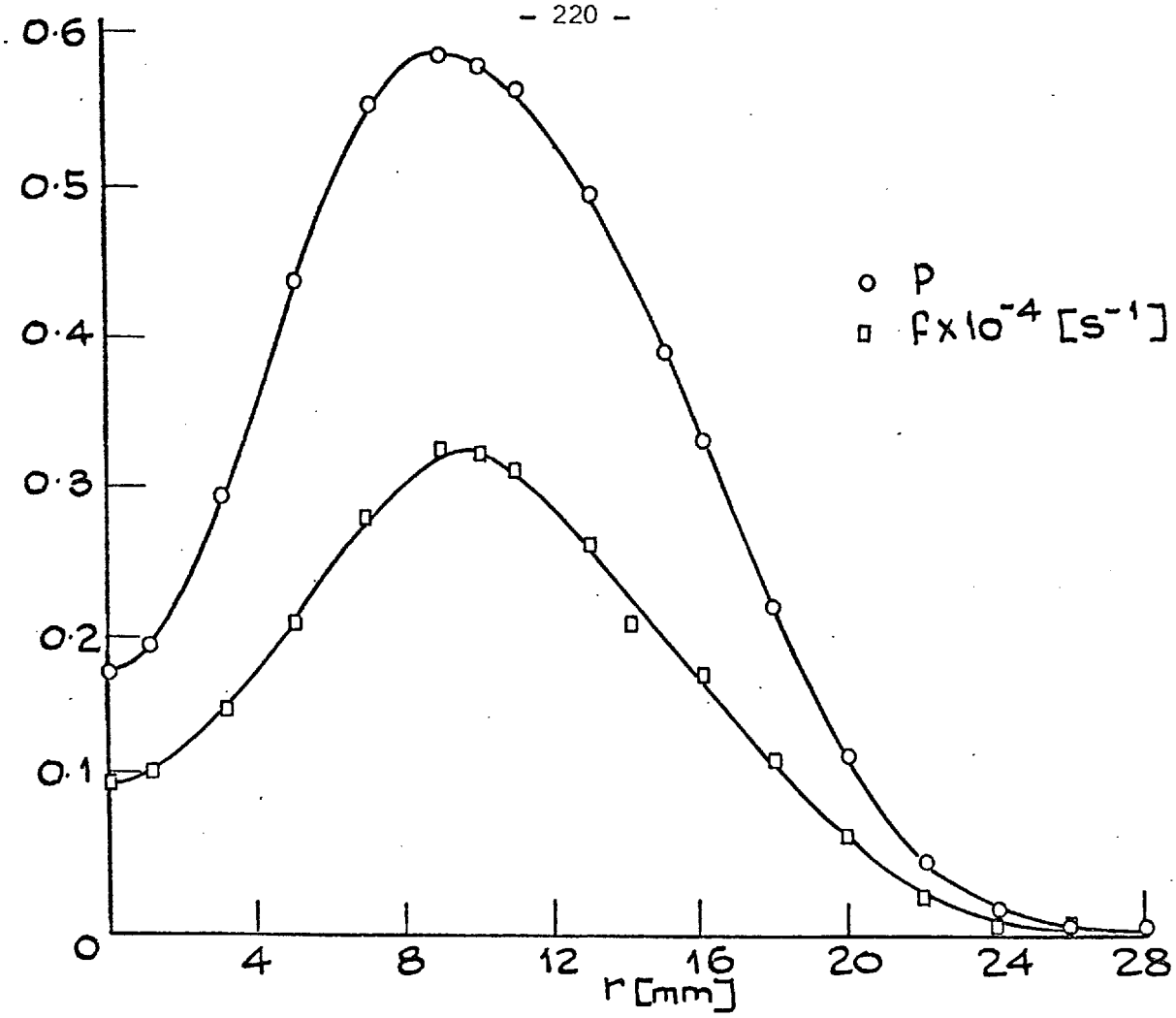


FIG. 5.4.k



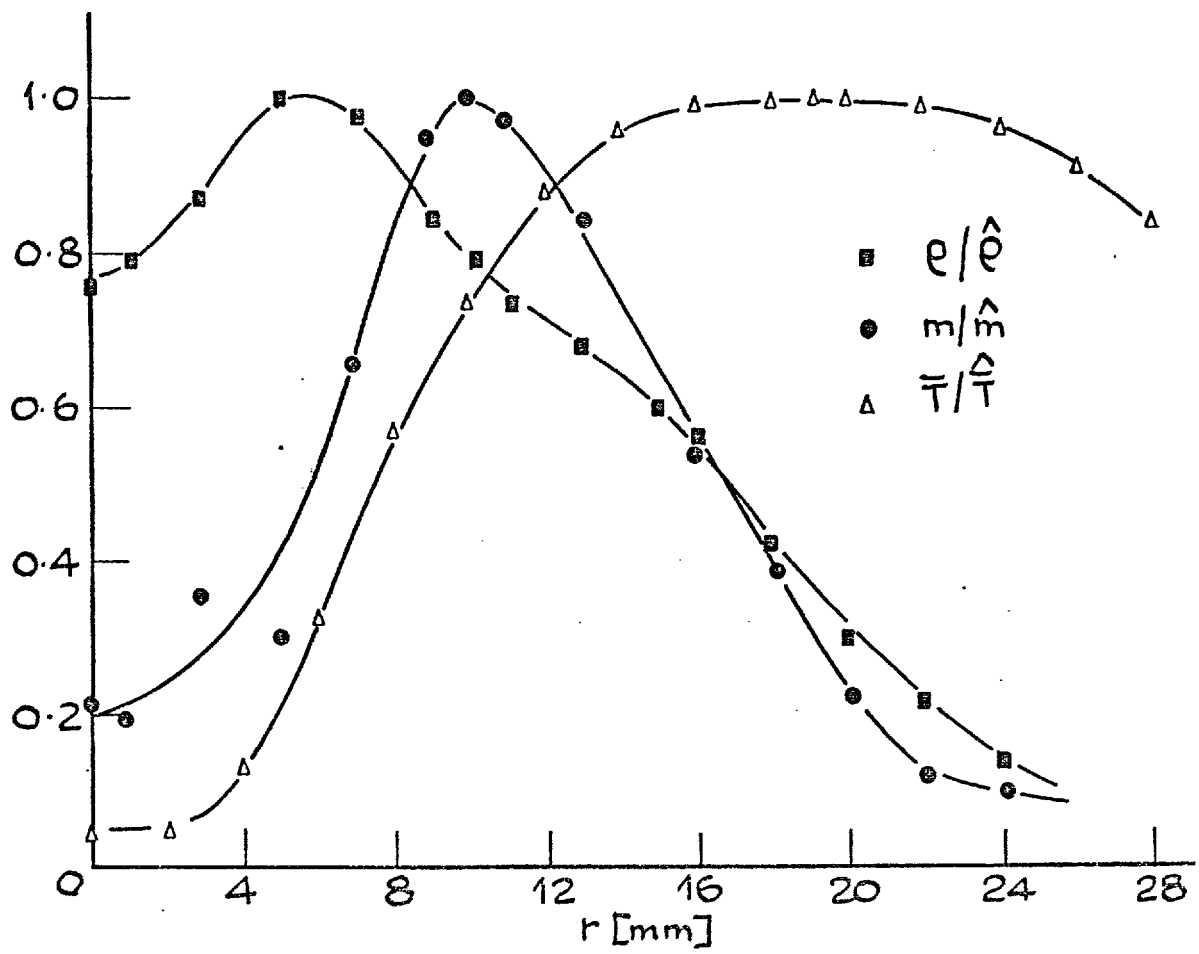
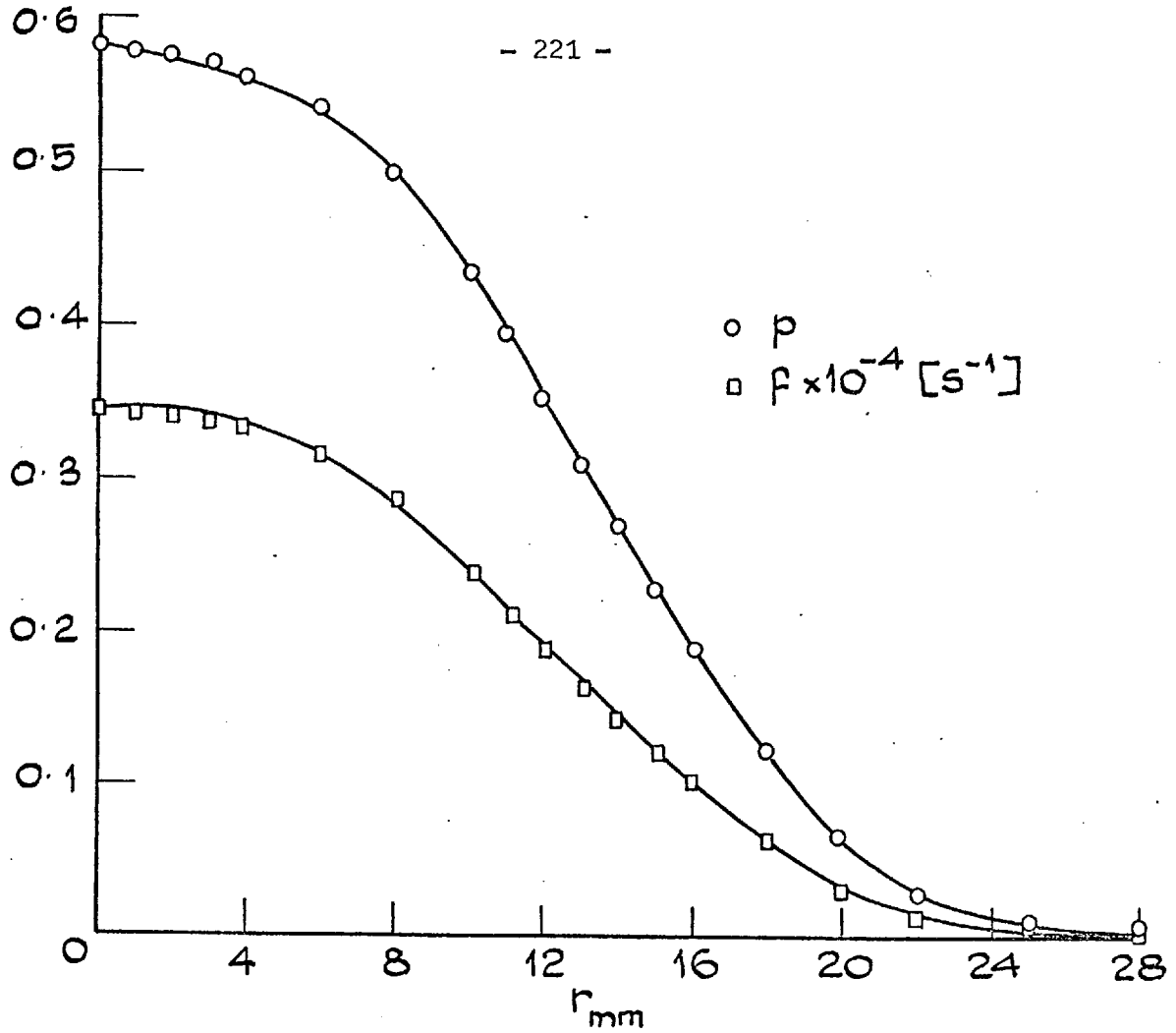


FIG. 5.4.ℓ X/D = 3.03



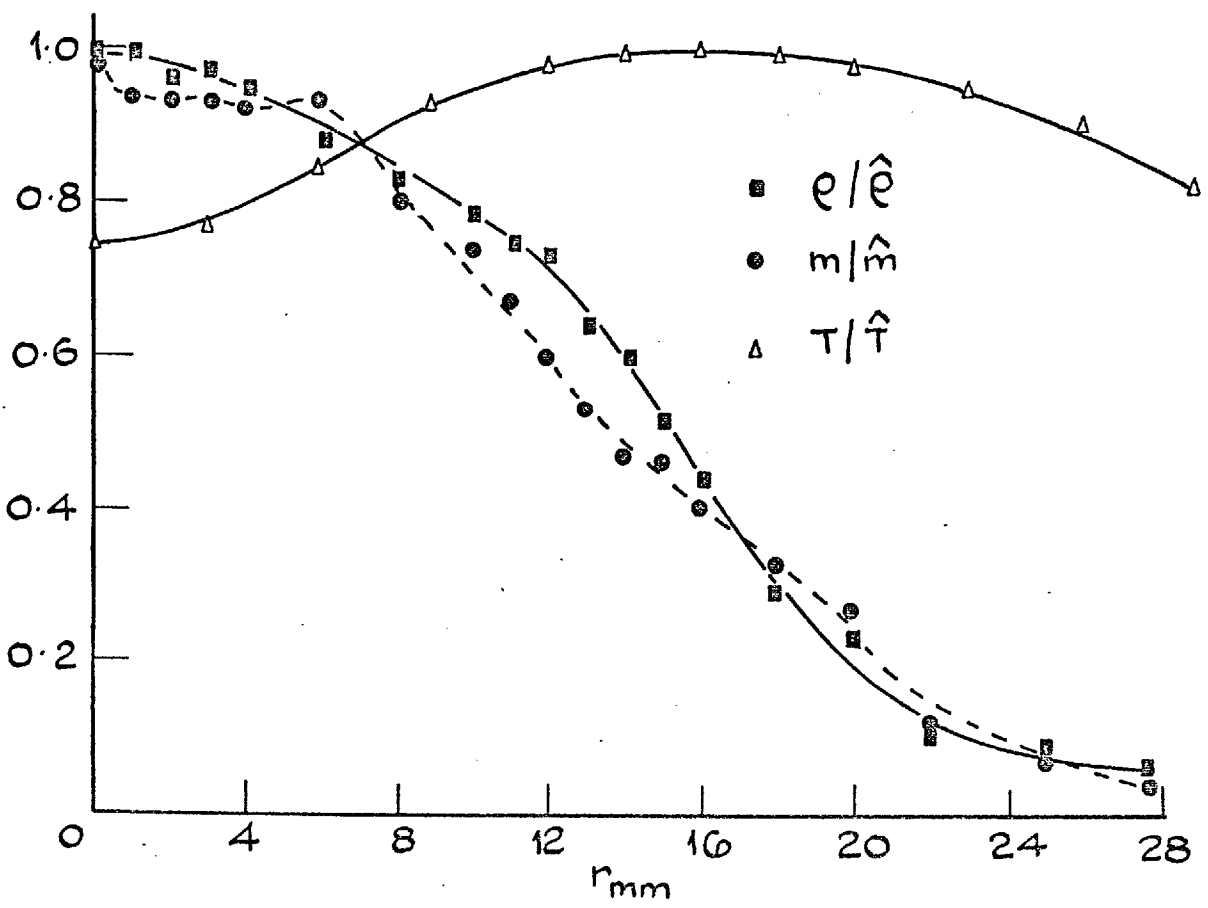
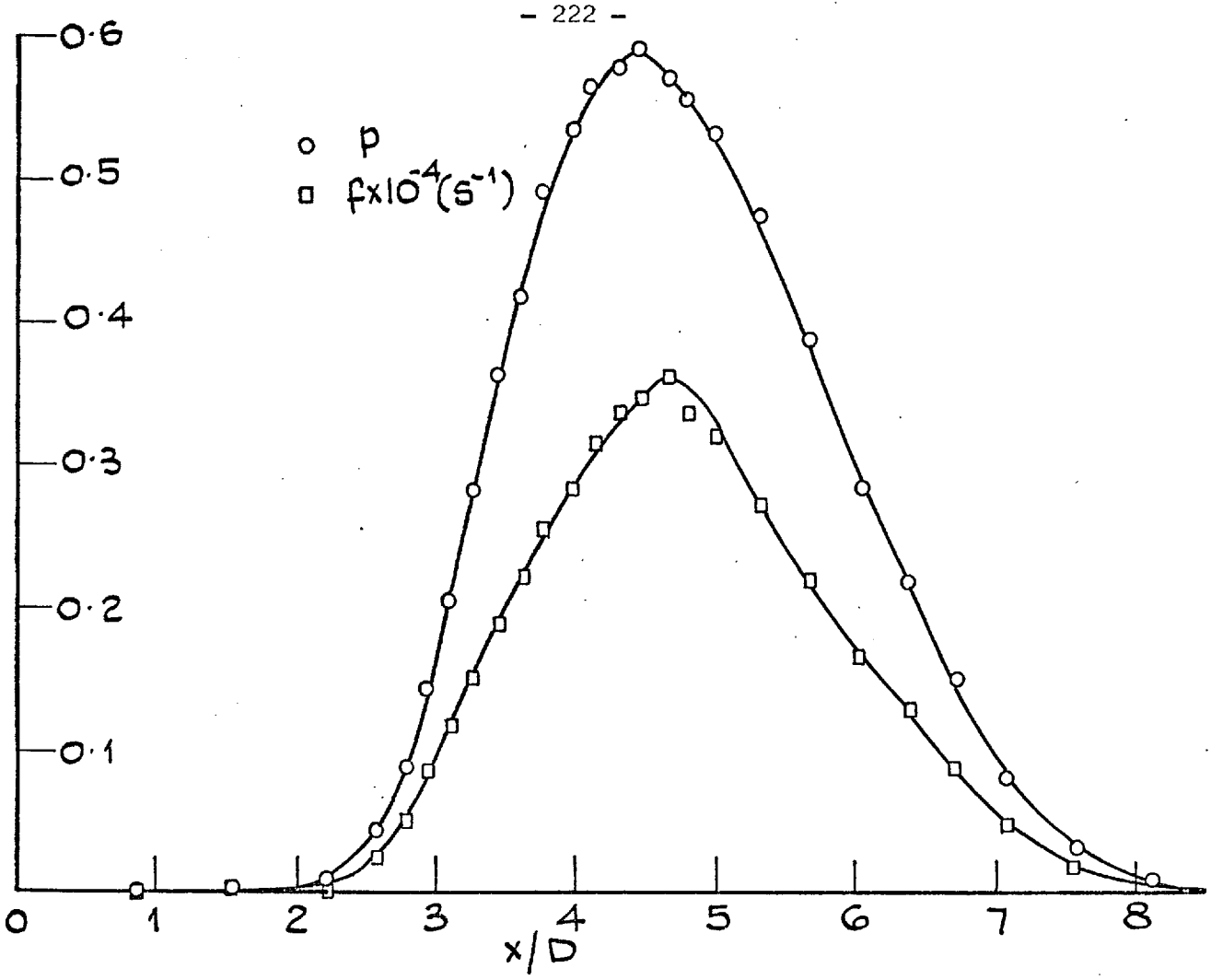


FIG. 5.4.m X/D = 4.41



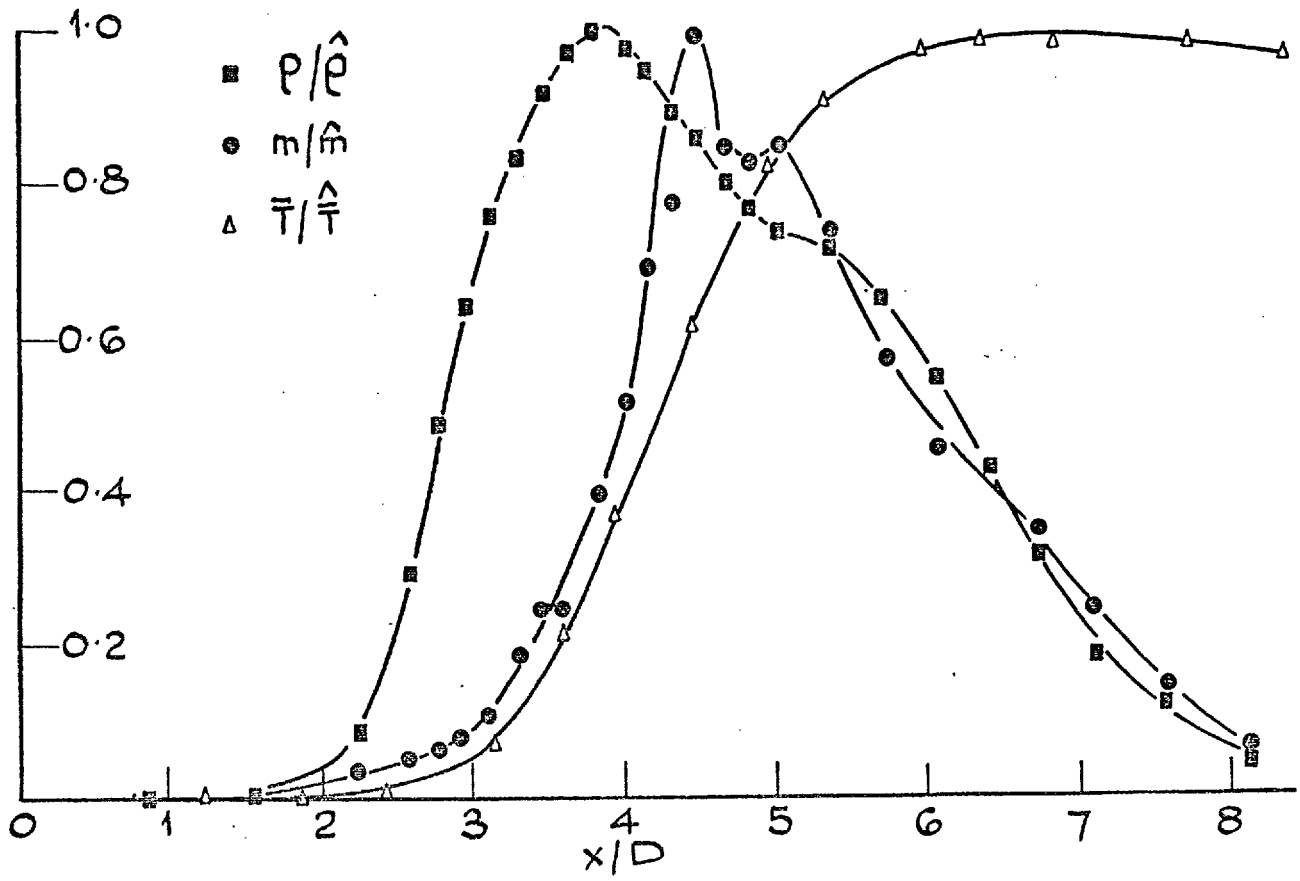
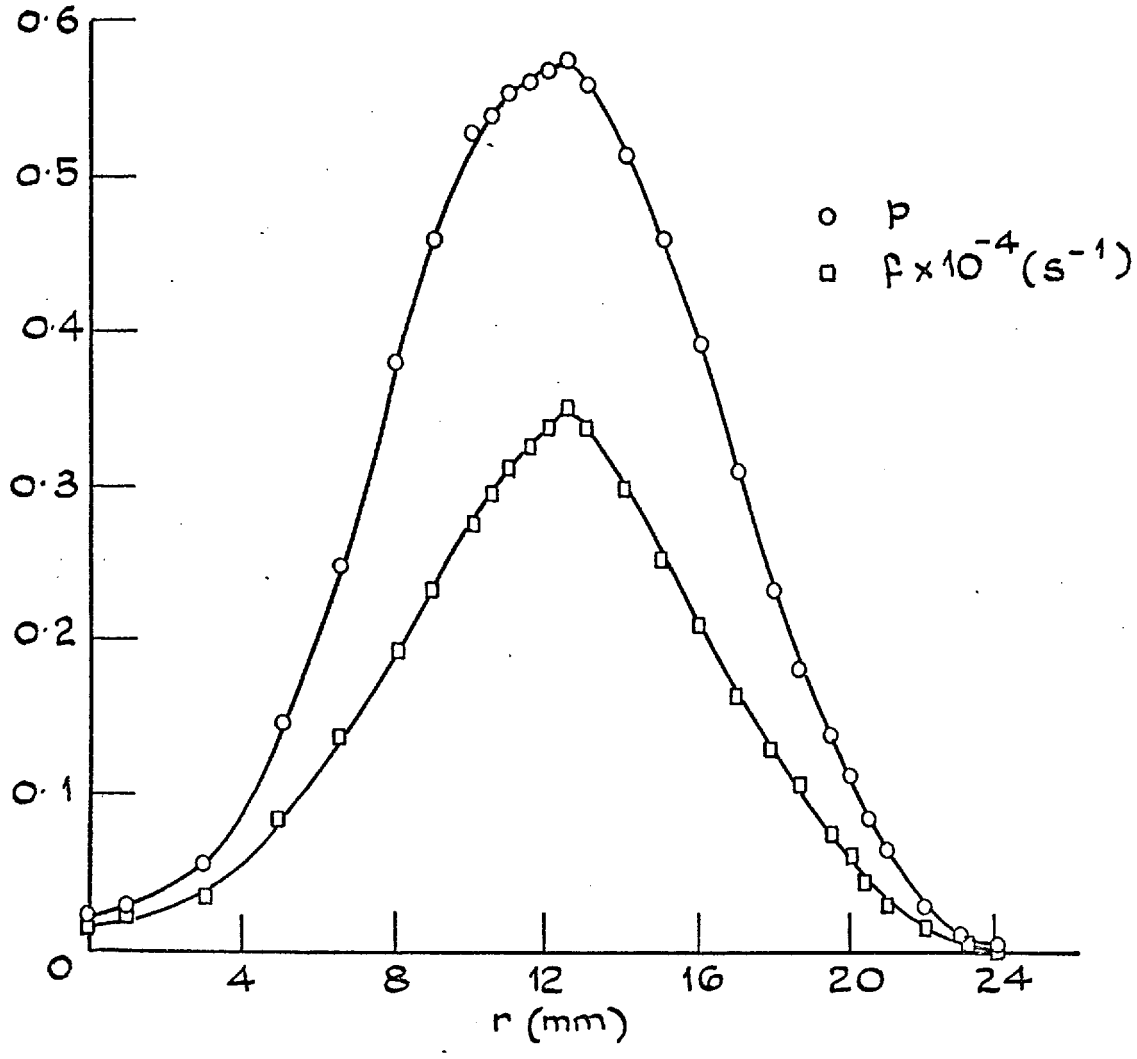


FIG. 5.4.n AXIAL



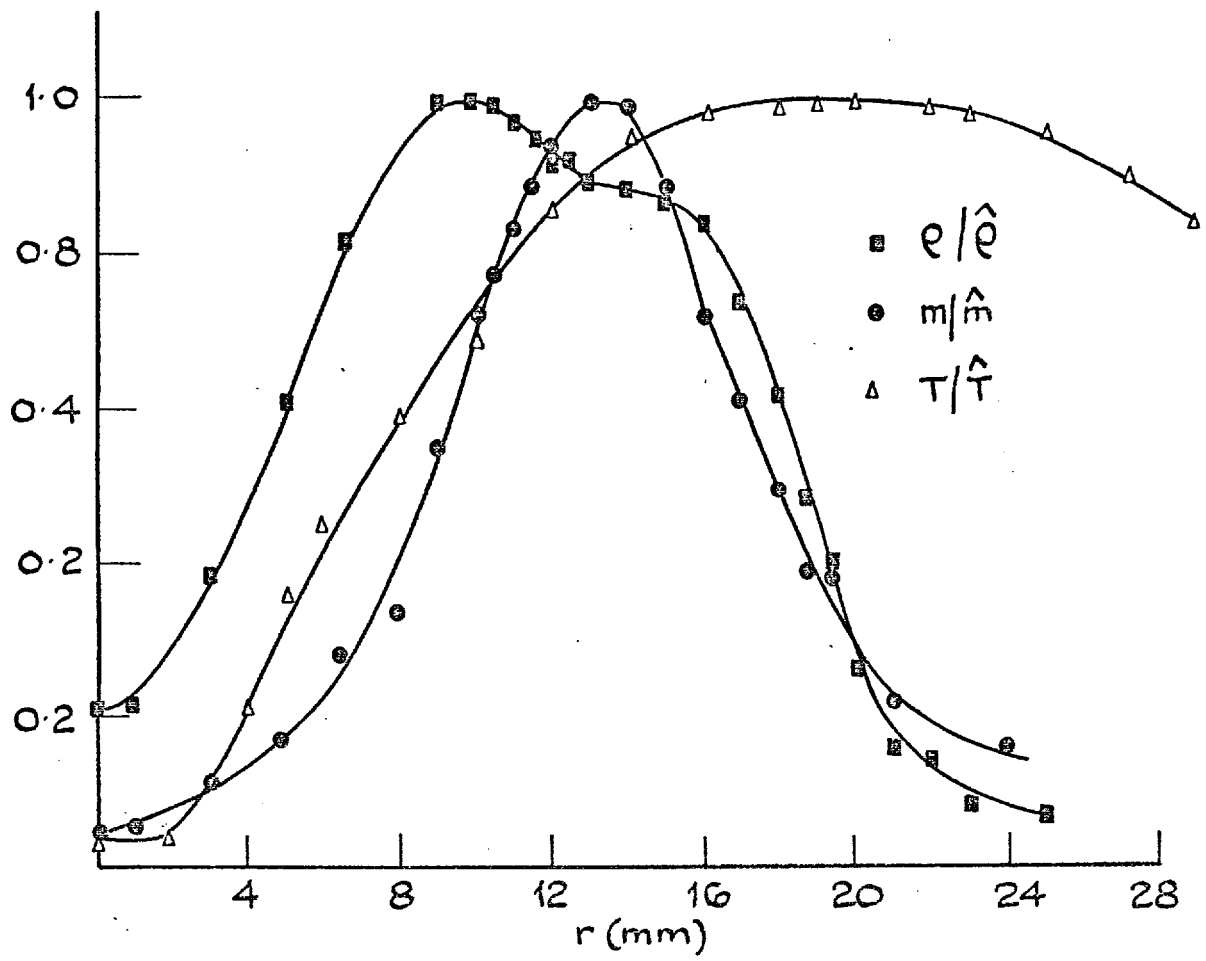


FIG. 5.4.o X/D = 3.03

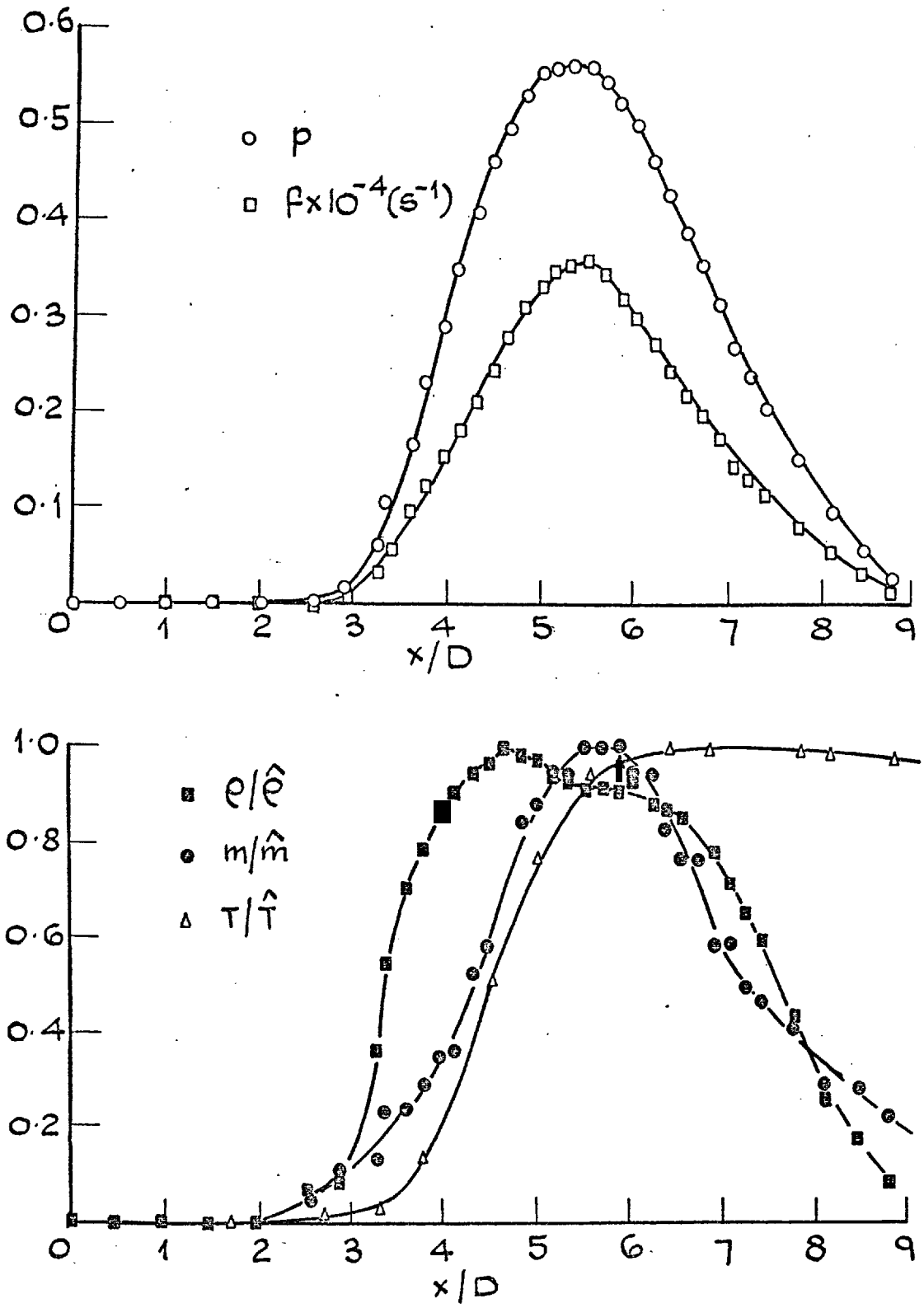


FIG. 5.4.p AXIAL

I = Ion Current

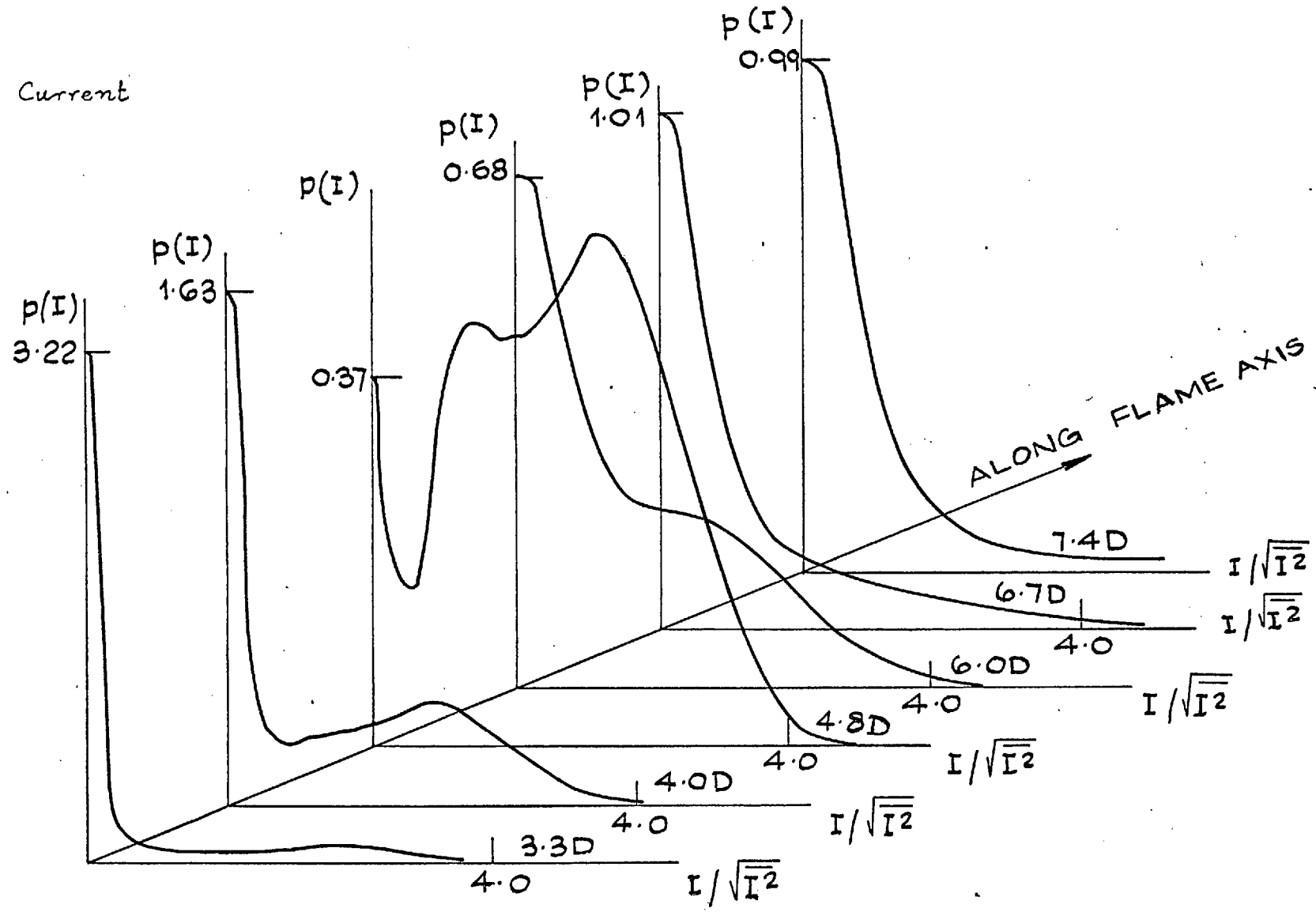


FIG. 5.4.q

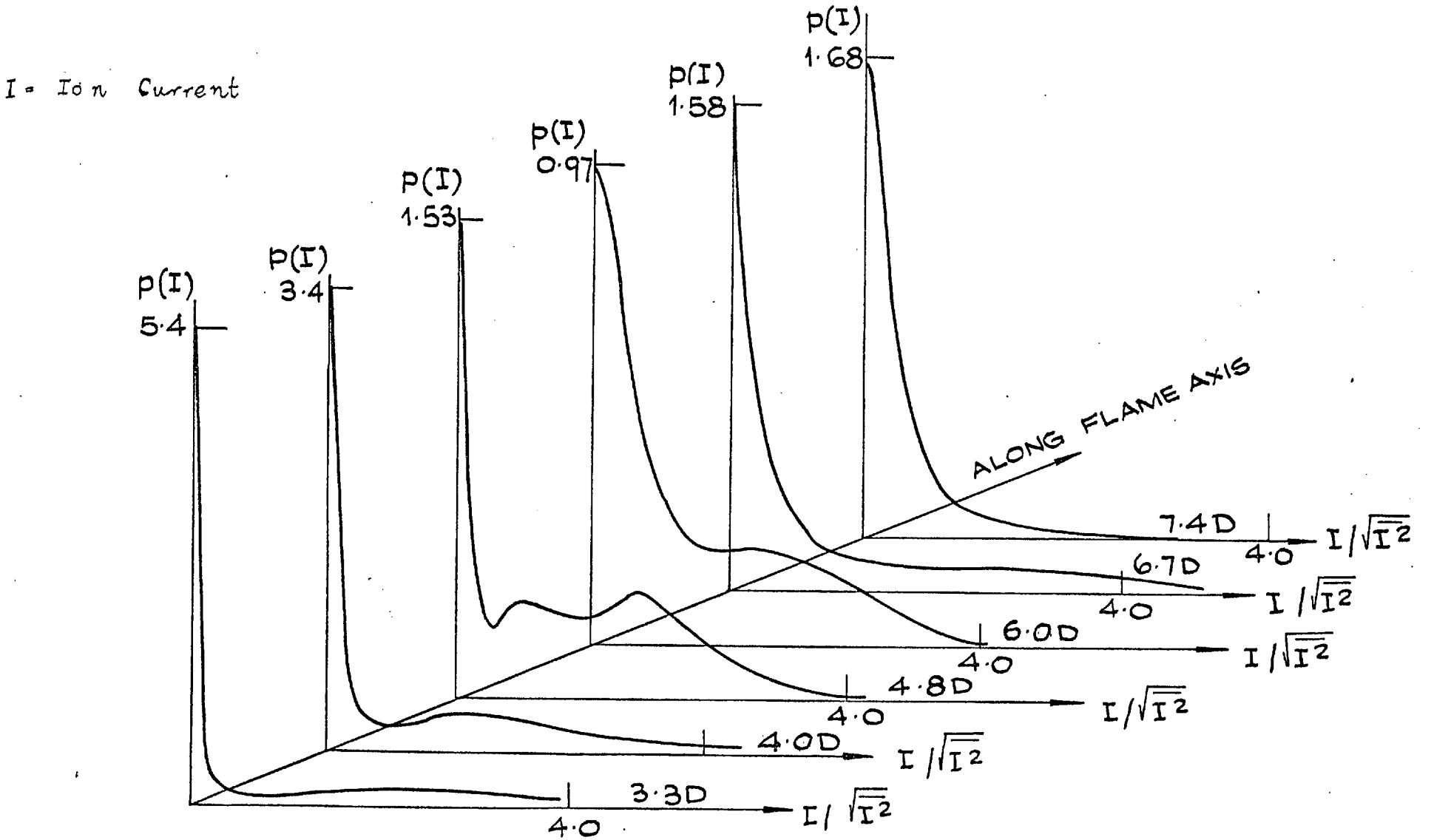

I = Ion Current
P(I)
1·68
P(I)
1·58
P(I)
0·97
P(I)
1·53
P(I)
3·4
P(I)
5·4
ALONG FLAME AXIS
7·4D
4·0
I/√I²
6·7D
4·0
I/√I²
6·0D
4·0
I/√I²
4·8D
4·0
I/√I²
4·0D
I/√I²
3·3D
4·0
I/√I²

FIG. 5.4.r

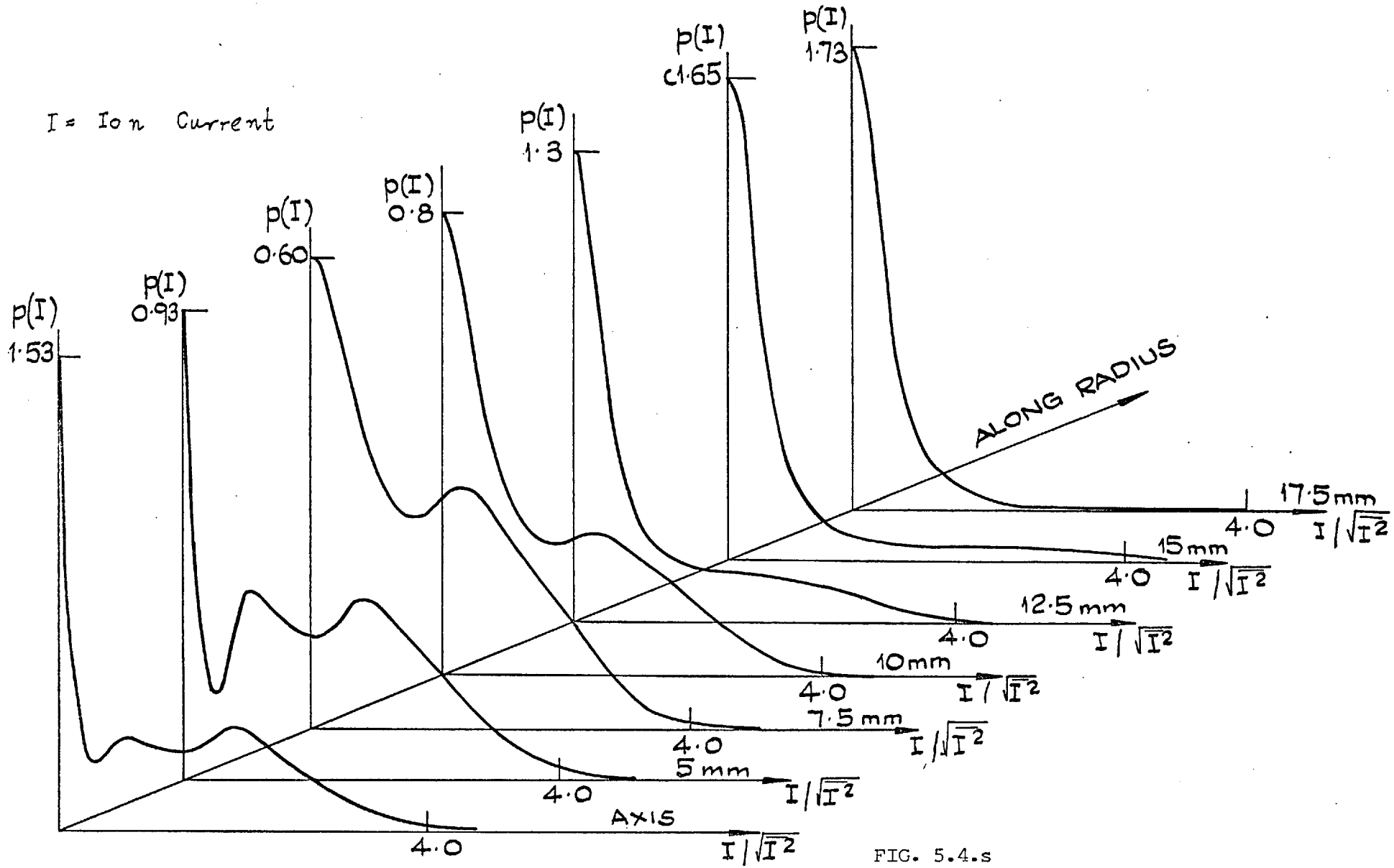

I = Ion Current
p(I)
1·53
p(I)
0·93
p(I)
0·60
p(I)
0·8
p(I)
1·3
p(I)
1·65
p(I)
1·73
ALONG RADIUS
17·5mm
15mm
12·5mm
10mm
7·5mm
5mm
AXIS
4·0
I/√I²

FIG. 5.4.s

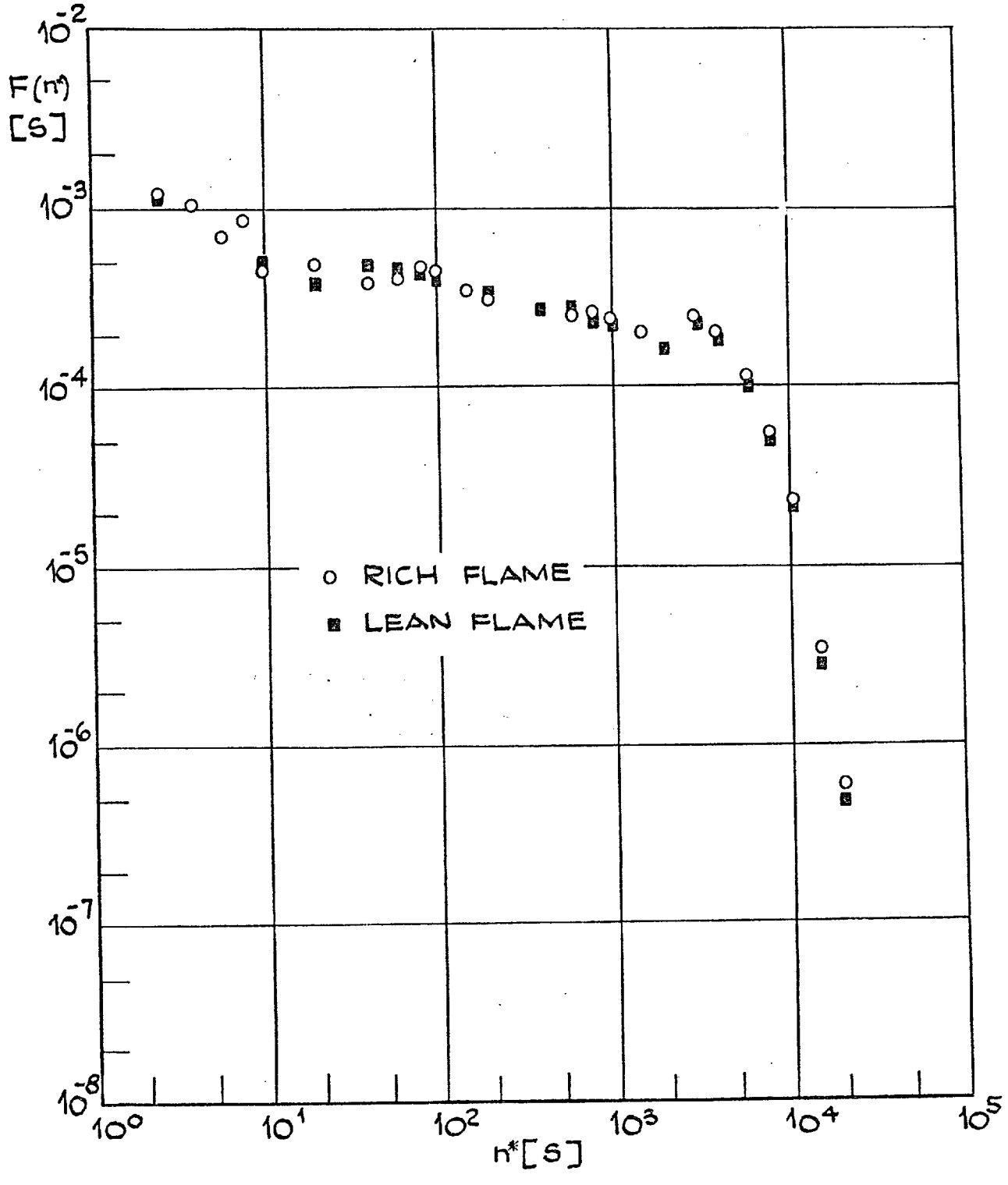

10^{-2}
F(n*)
[s]
10^{-3}
10^{-4}
10^{-5}
10^{-6}
10^{-7}
10^{-8}
o RICH FLAME
■ LEAN FLAME
10^{0}
10^{1}
10^{2}
10^{3}
10^{4}
10^{5}
n*[s]

FIG. 5.4.t

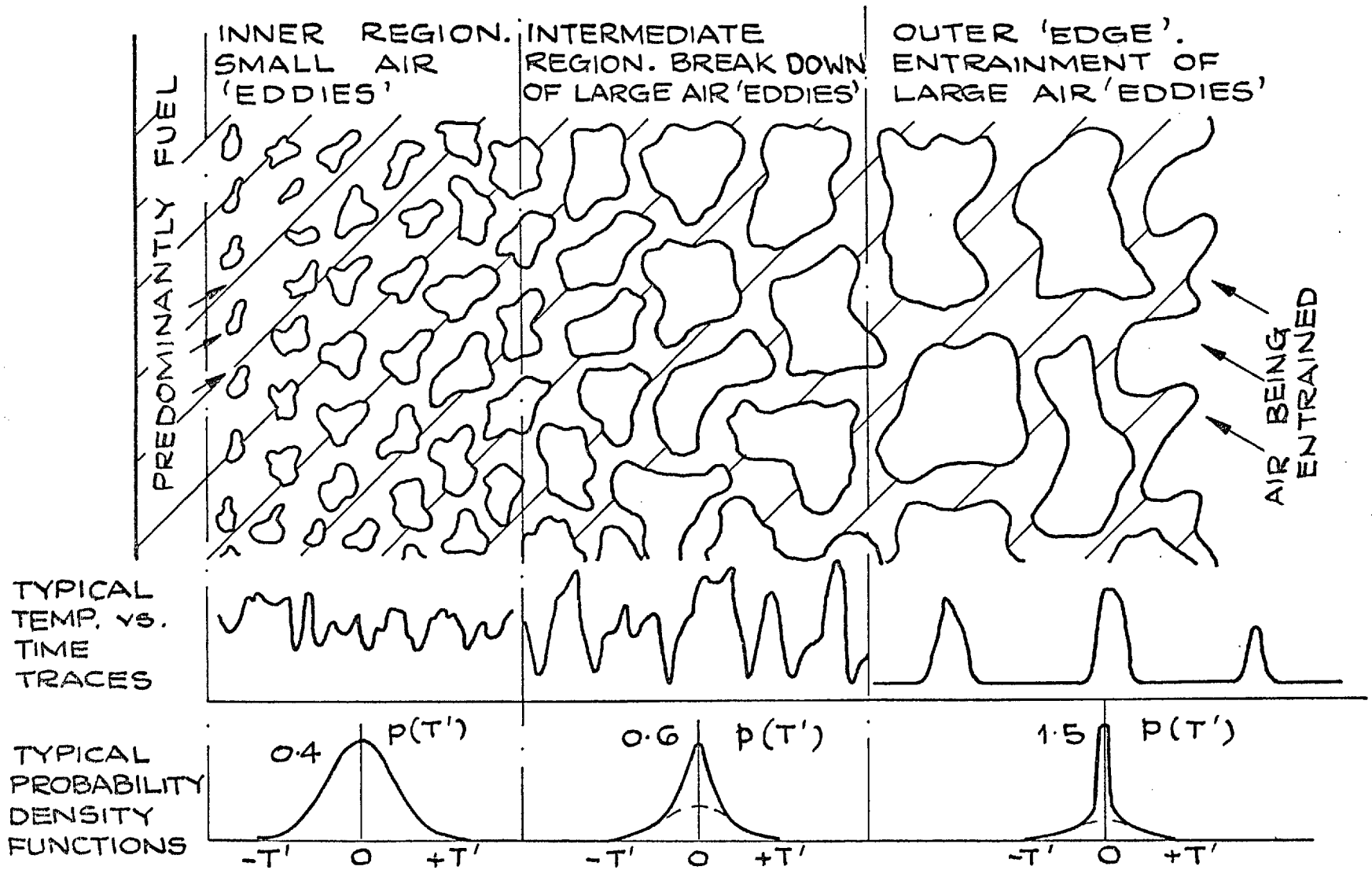


Fig. 5.5.a Envisaged structure of free jet diffusion flame (thickness into plane of diagram is ~2 x integral scale of turbulence).

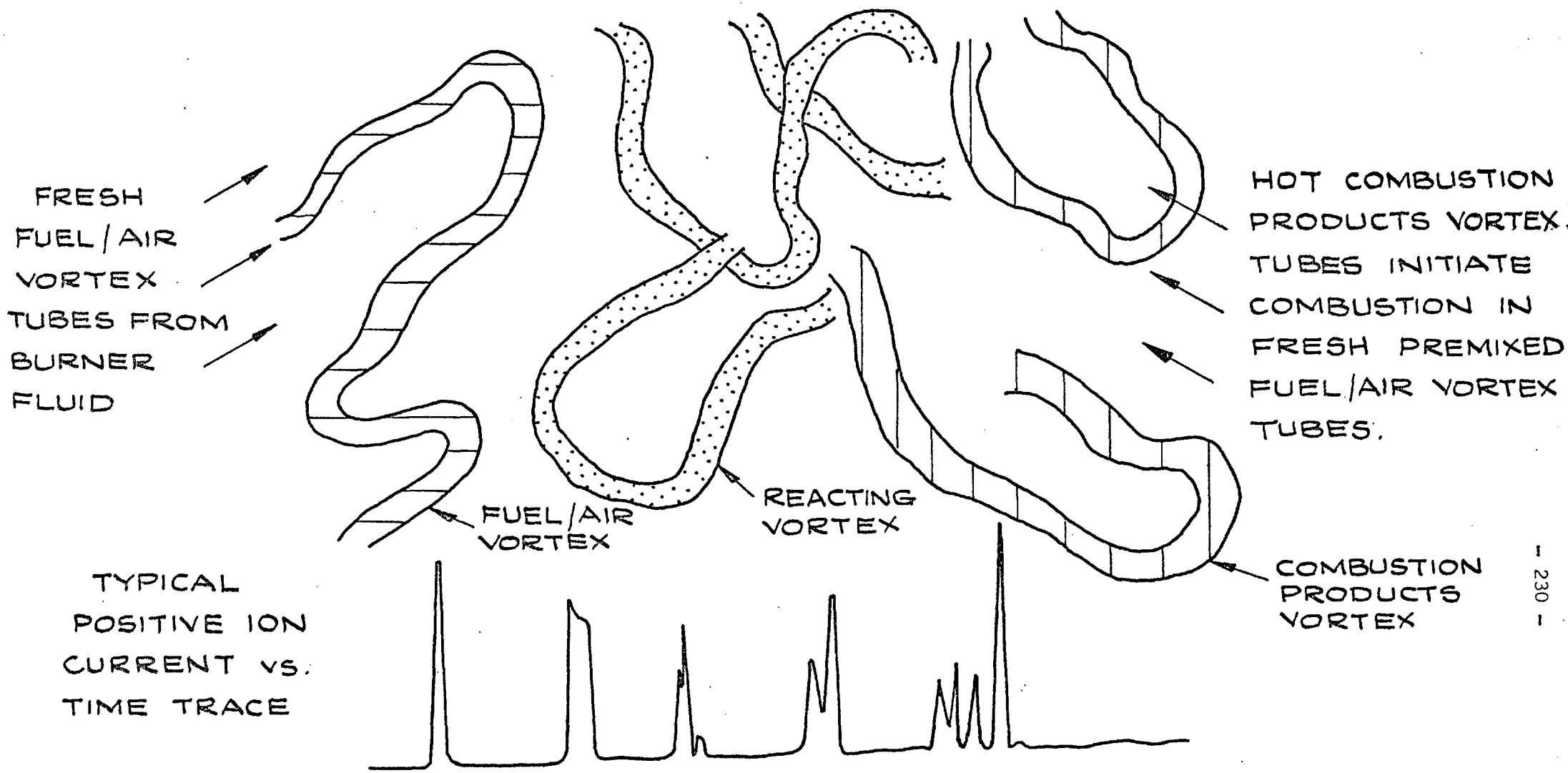
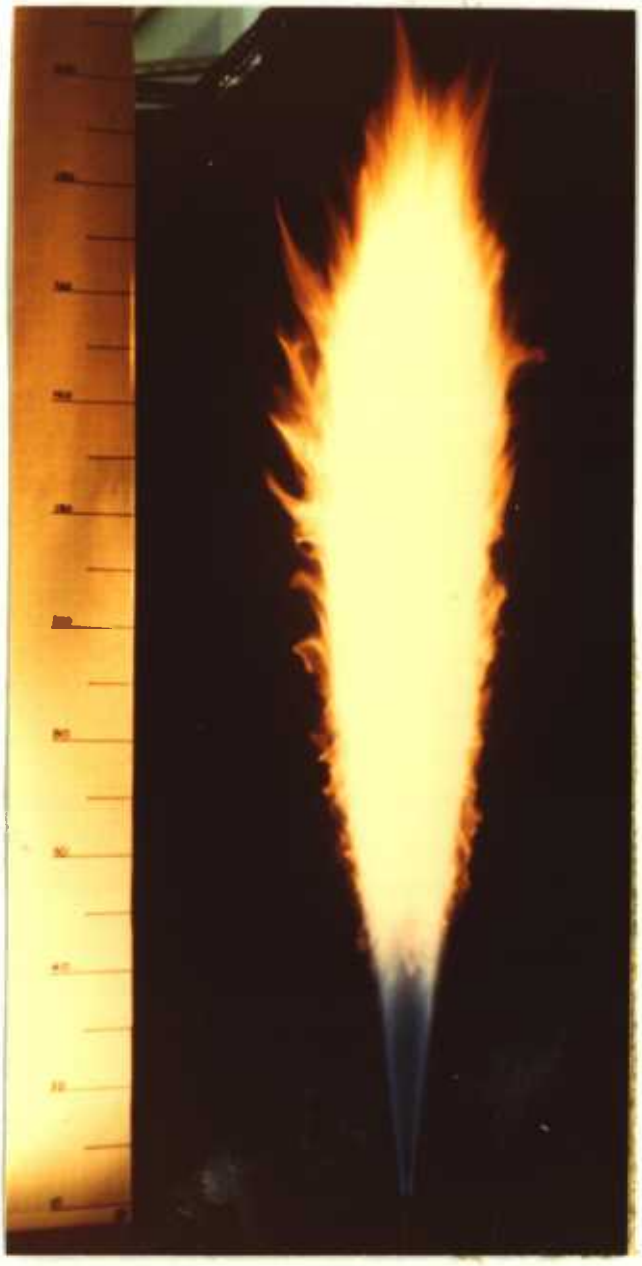


Fig. 5.5.b Envisaged structure of free jet premixed flame (thickness into plane of diagram is ~ 2 x Taylor micro scale).





SCALE : X/D , EACH DIVISION = 10 FOR BOTH PHOTOGRAPHS

FIG. 5.6.a

FIG. 5.6.b



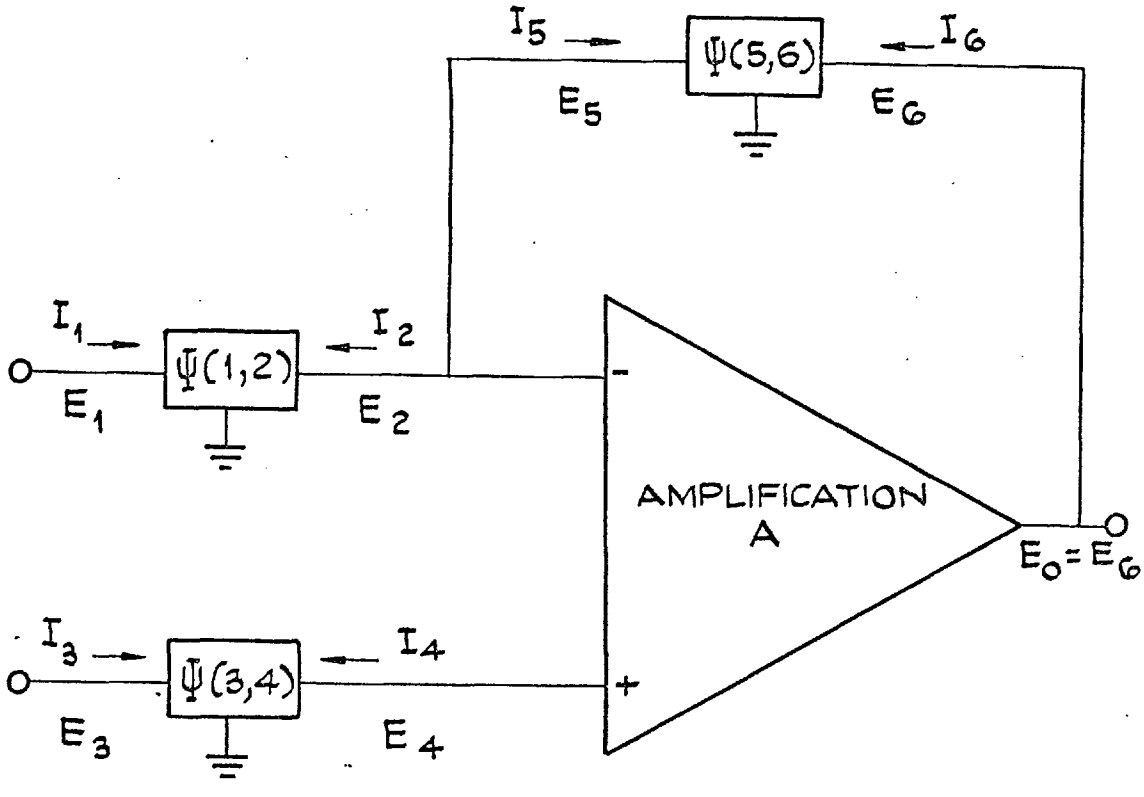
FIG. 5.6.c



FIG. 5.6.d

FIGURES IN APPENDIX A

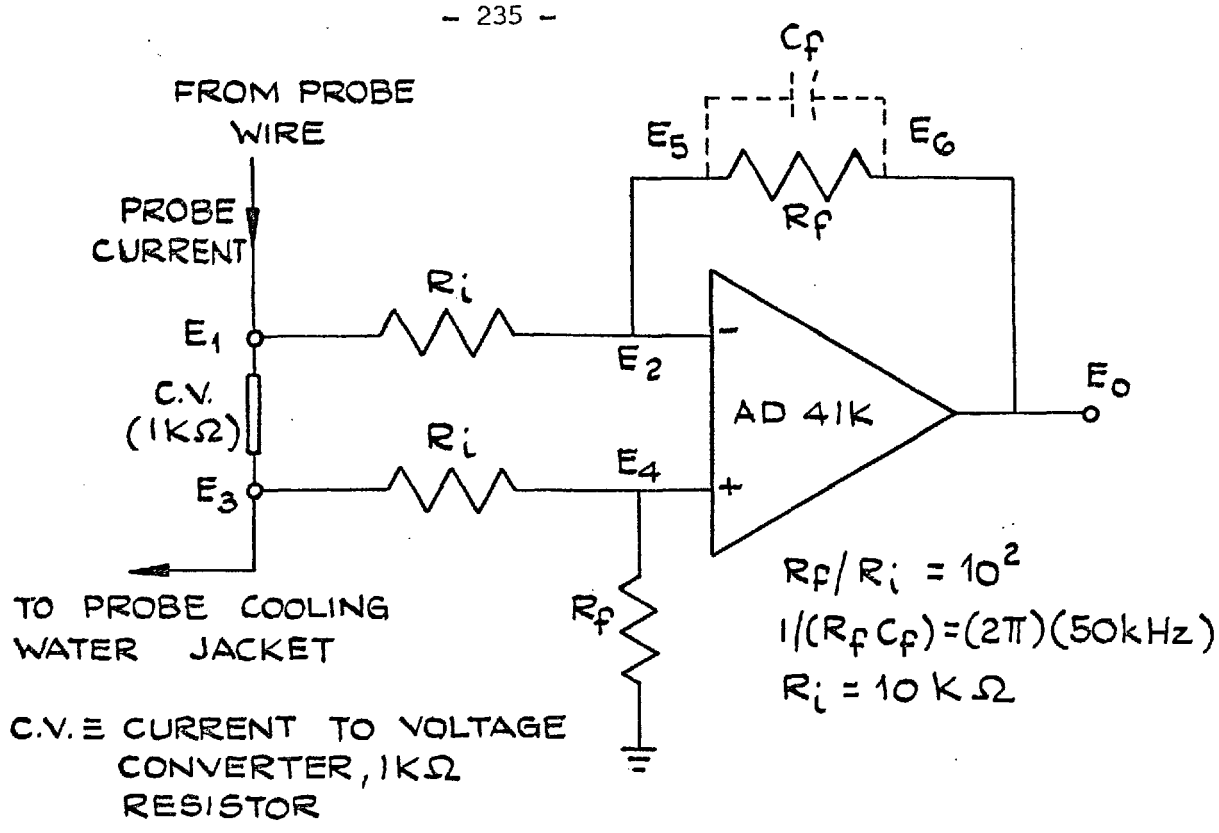
Figure	Title	Page
Fig. A.1	Notation for an op-amp with negative feed-back and two-port components.	234
Fig. A.2	Circuit diagram for ionisation probe pre-amplifier.	235
Fig. A.3	Circuit diagram for ionisation probe second stage amplifier.	235
Fig. A.4	Frequency response curves of ionisation probe pre-amplifier and second stage amplifier.	236
Fig. A.5	Circuit diagram for thermal inertia simulation unit.	237
Fig. A.6	Circuit diagram for thermal inertia compensator.	237
Fig. A.7	Frequency response curves of: 1. Thermal inertia simulation unit 2. Thermal inertia compensator 3. Combination of simulation unit and compensator 4. Electronic transformer (with impedance matching buffers).	238
Fig. A.8	Circuit diagram of noise filter.	239
Fig. A.9	Frequency response curve of noise filter.	240
Fig. A.10	Circuit diagram of amplifying low-noise, low-drift, low-pass filter used for time constant determination and radiation error correction.	241
Fig. A.11	Frequency response curve of amplifying low-noise, low-drift, low-pass filter.	242

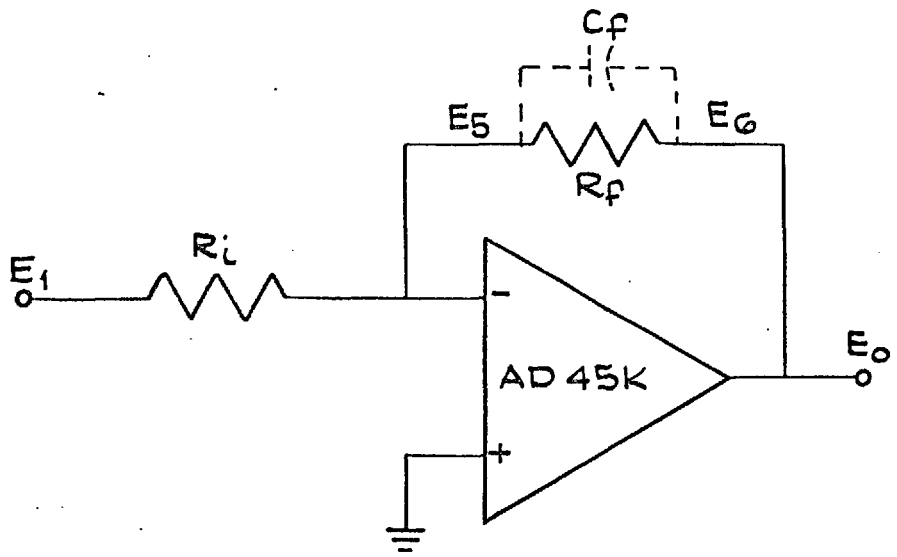


IN GENERAL : $y_{mn} = I_m / E_n \Big|_{E_m = 0}$

$y_{mm} = I_m / E_m \Big|_{E_n = 0}$

FIG. A.1





TOP FIG. A.2

BOTTOM FIG. A.3

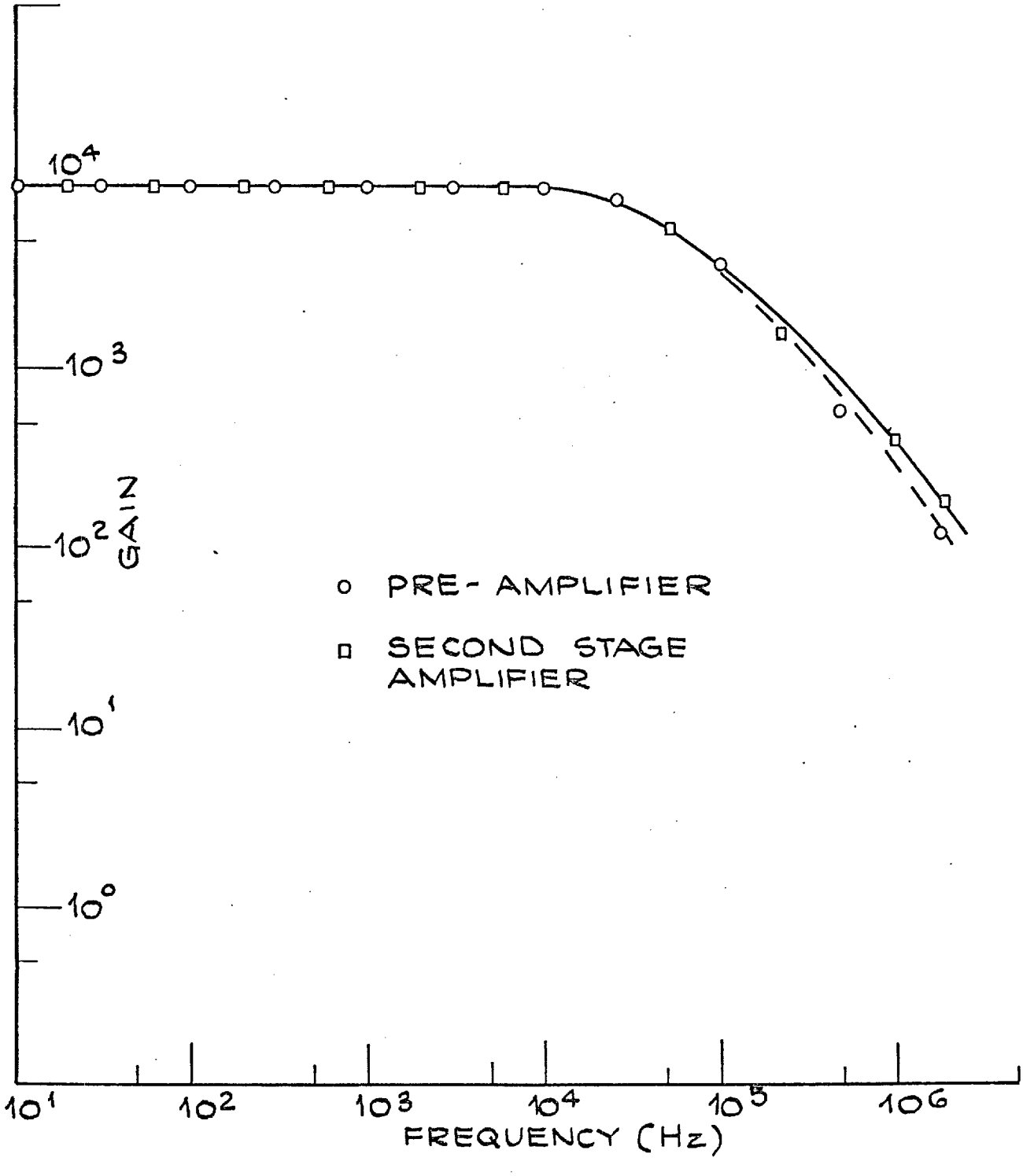
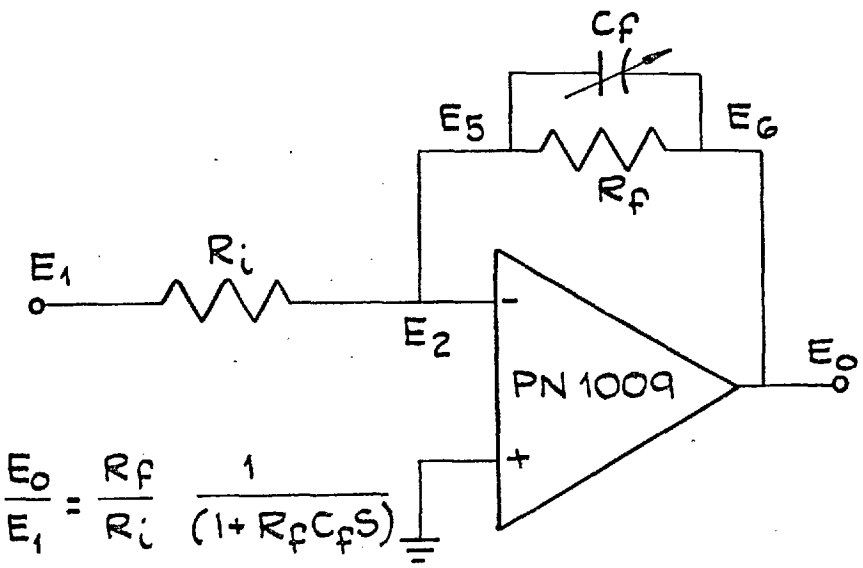

10^4
10^3
10^2
GAIN
10^1
10^0
o PRE-AMPLIFIER
□ SECOND STAGE AMPLIFIER
10^1
10^2
10^3
10^4
10^5
10^6
FREQUENCY (Hz)

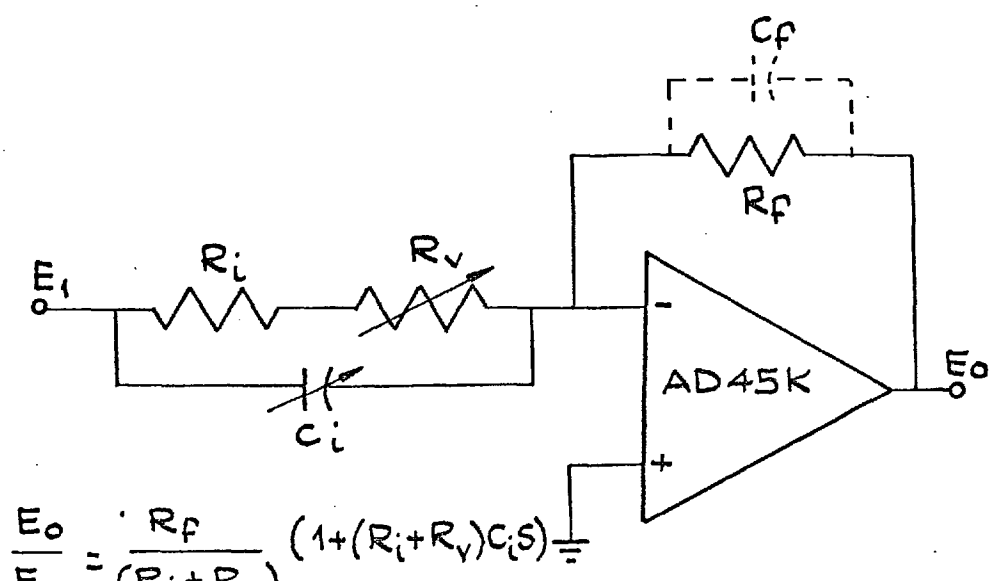
FIG. A.4



$$\frac{E_o}{E_1} = \frac{R_f}{R_i}\,\frac{1}{(1+R_fC_fS)} = \frac{1}{1+\tau S}$$

$$\left[\begin{array}{l} R_i = R_f = 1\,M\Omega \\ C_f = 0{\cdot}1\,\mu F,\ 0{\cdot}15\,\mu F,\ 0{\cdot}2\,\mu F,\ {\cdot}03\,\mu F \end{array}\right]$$

FIG. A.5



$$\frac{E_o}{E_1} = \frac{R_f}{(R_i+R_v)}\,(1+(R_i+R_v)C_iS) = \eta\,(1+\tau S)$$

$$\left[\begin{array}{l} R_p = R_i/10 = 100\,K\Omega \\ 0 \le R_v \le 100\,K\Omega \\ 1/R_pC_f = (2\pi)(15kHz) \end{array}\right]$$

FIG. A.6

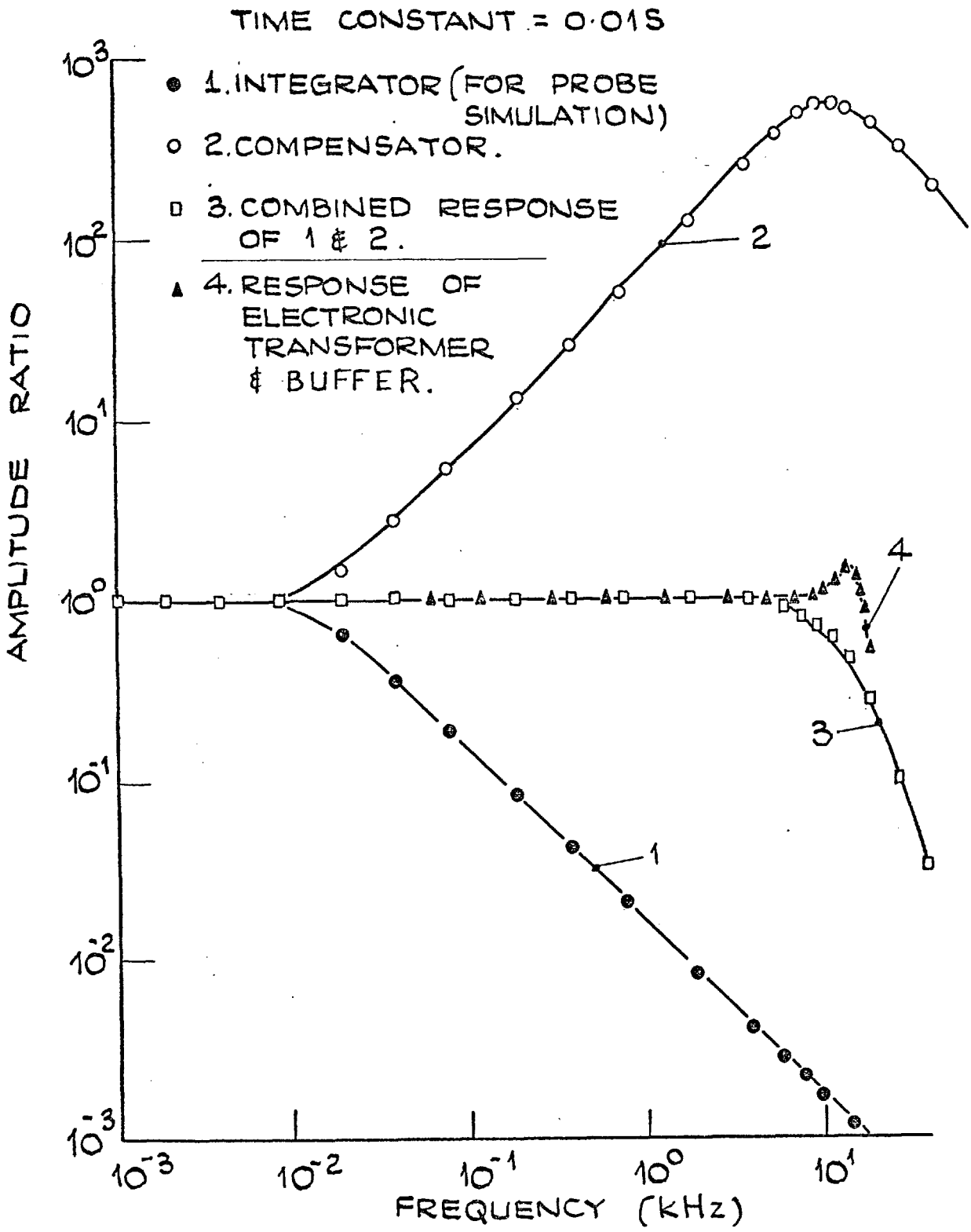

TIME CONSTANT = 0·01S
1. INTEGRATOR (FOR PROBE SIMULATION)
2. COMPENSATOR.
3. COMBINED RESPONSE OF 1 & 2.
4. RESPONSE OF ELECTRONIC TRANSFORMER & BUFFER.
AMPLITUDE RATIO
FREQUENCY (kHz)
10^{3}
10^{2}
10^{1}
10^{0}
10^{-1}
10^{-2}
10^{-3}
10^{-3}
10^{-2}
10^{-1}
10^{0}
10^{1}
1
2
3
4

FIG. A.7

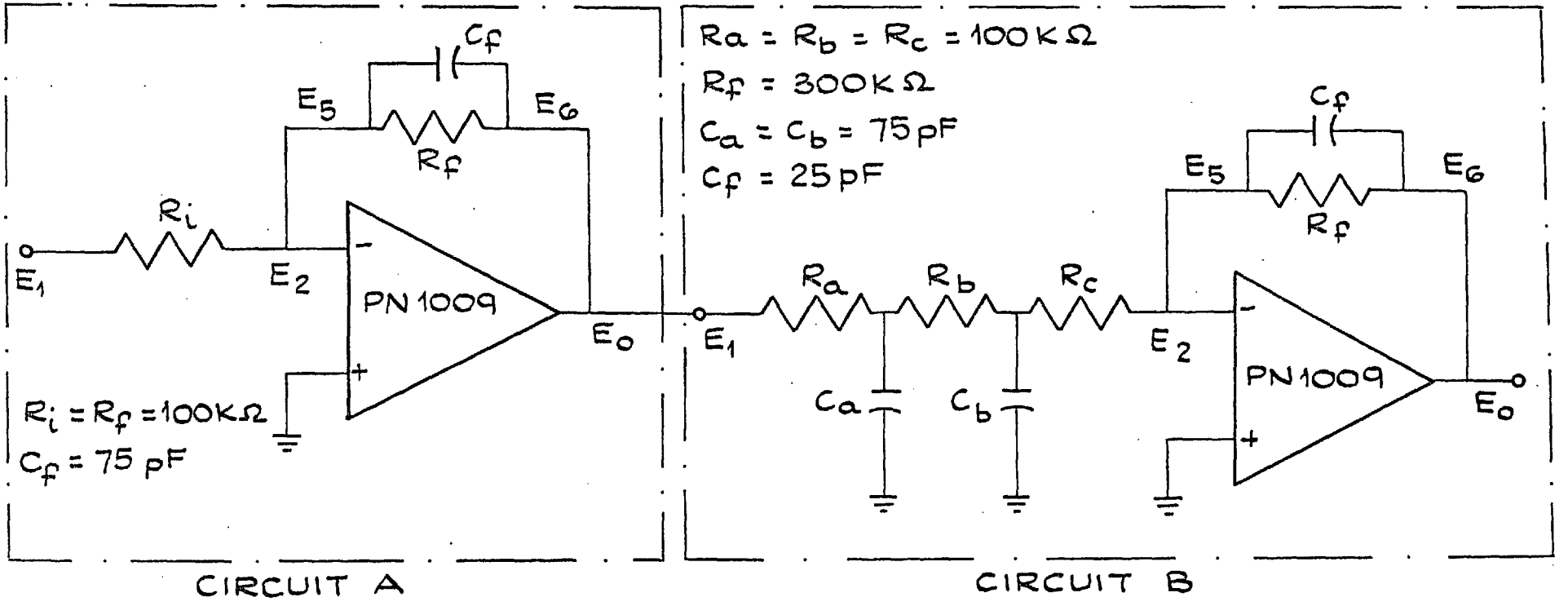

C_f
E_5
E_6
R_f
R_i
E_1
E_2
PN 1009
E_o
$R_i = R_f = 100K\Omega$
$C_f = 75$ pF
CIRCUIT A
$R_a = R_b = R_c = 100K\Omega$
$R_f = 300K\Omega$
$C_a = C_b = 75$ pF
$C_f = 25$ pF
R_a
R_b
R_c
C_a
C_b
CIRCUIT B

FIG. A.8

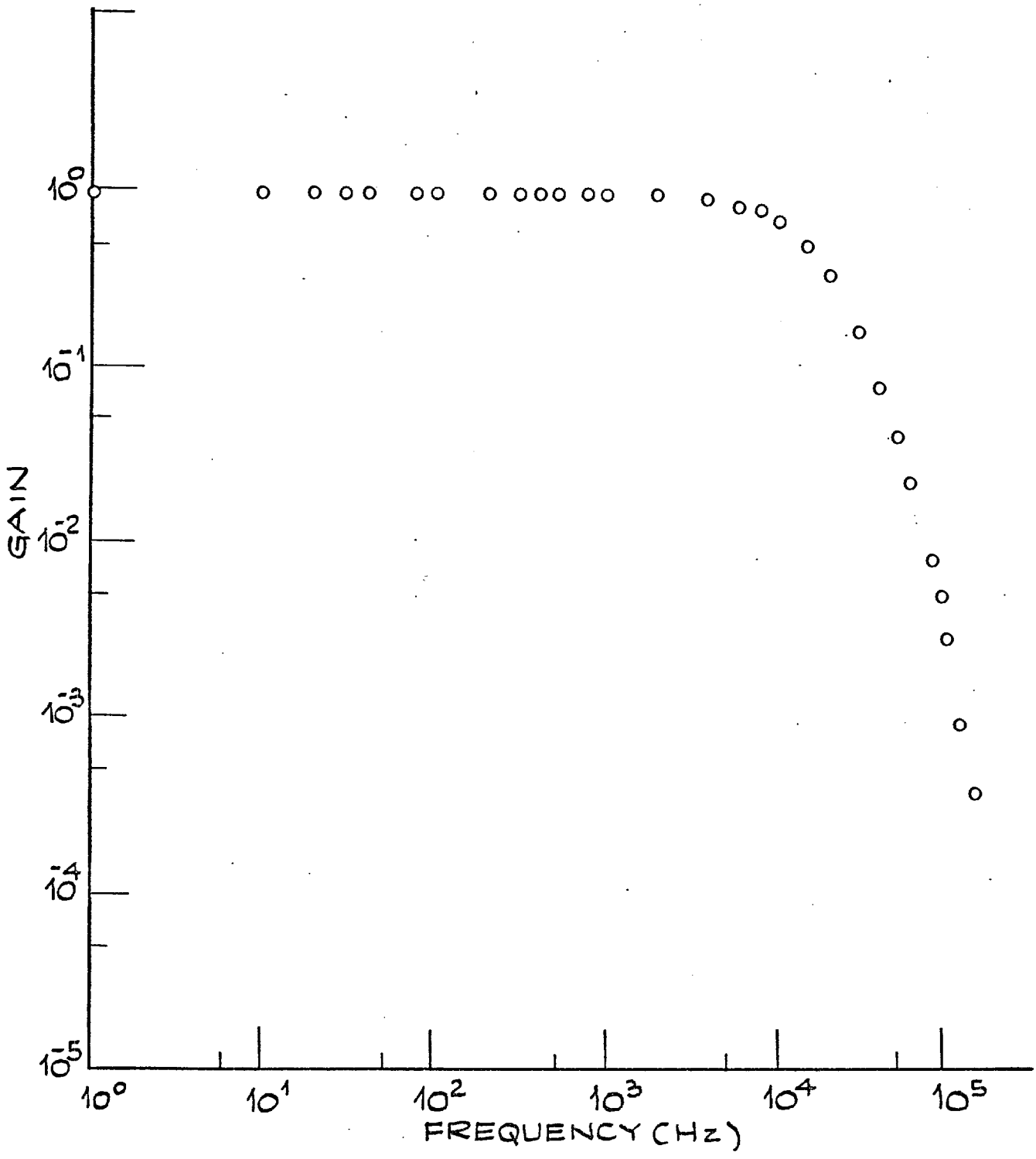
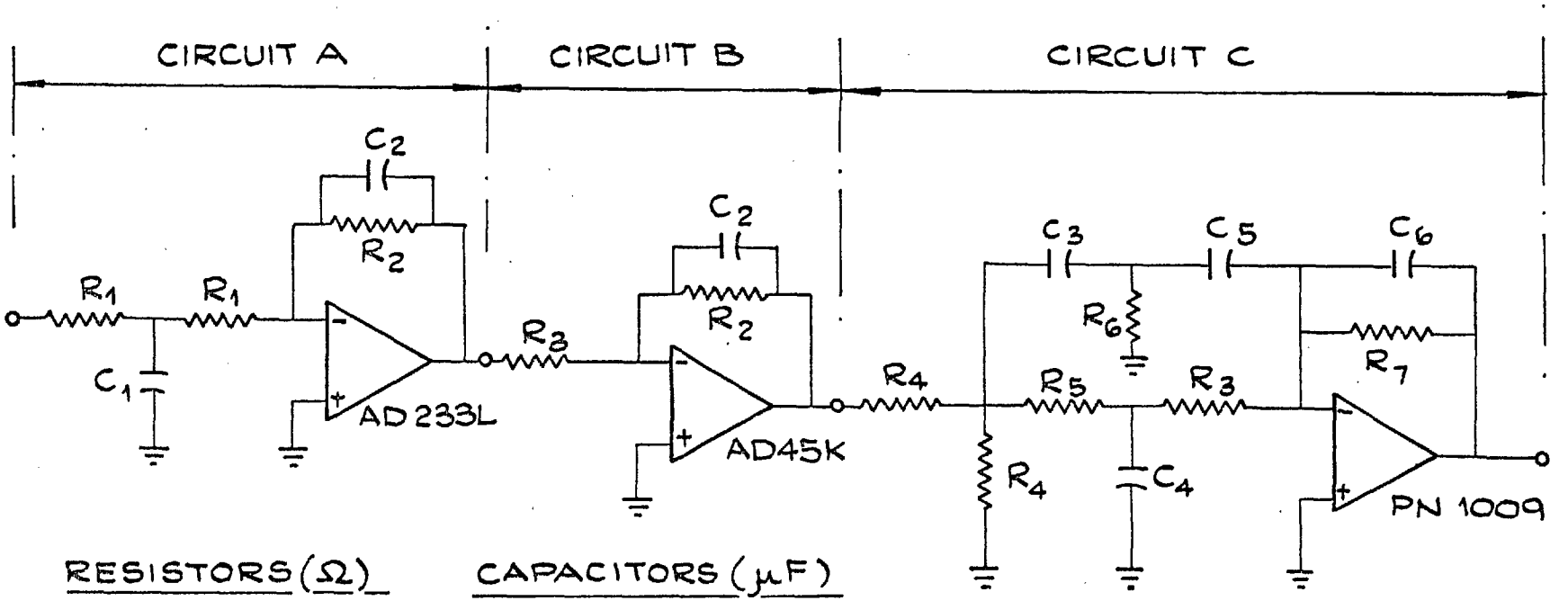

GAIN
10^{0}
10^{-1}
10^{-2}
10^{-3}
10^{-4}
10^{-5}
10^{0}
10^{1}
10^{2}
10^{3}
10^{4}
10^{5}
FREQUENCY (Hz)

FIG. A.9



RESISTORS (Ω)	
R_1	5 K
R_2	1 M
R_3	100 K
R_4	62 K
R_5	33K
R_6	24K
R_7	330K

CAPACITORS (μF)	
C_1	0·068
C_2	0·00033
C_3	0·1
C_4	0·133
C_5	0·033
C_6	0·001

FIG. A.10

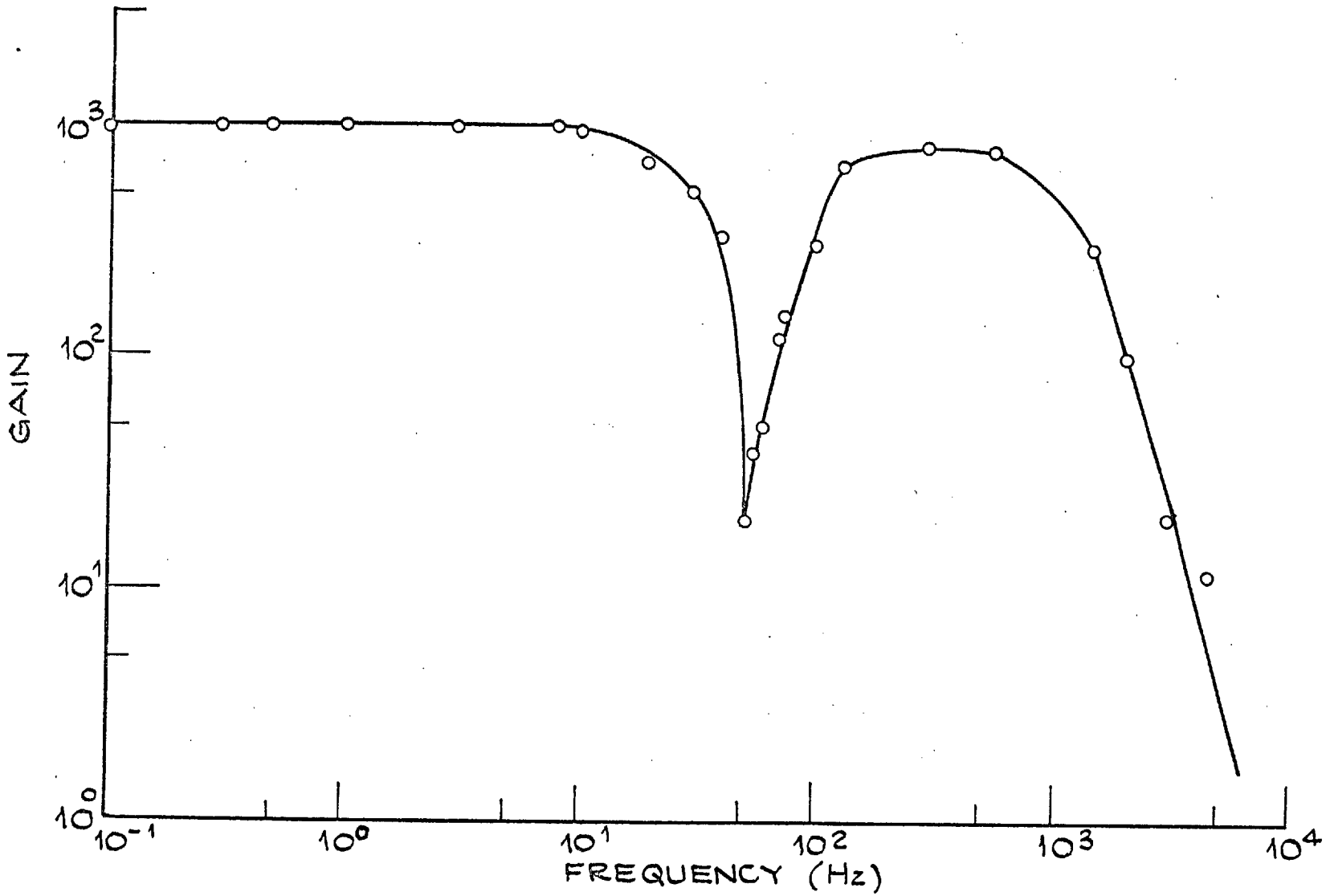
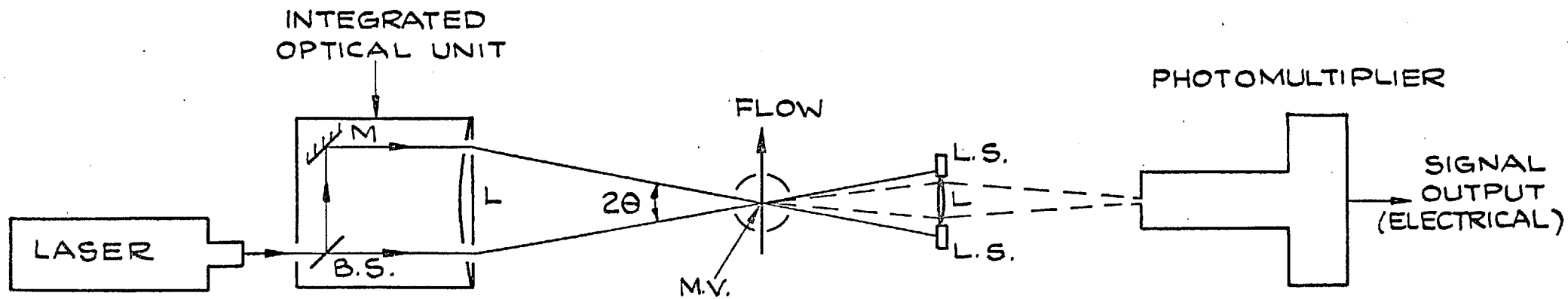


FIG. A.11

FIGURES IN APPENDIX B

Figure	Title	Page
Fig. B.1	Schematic of Laser Doppler Anemometer in fringe mode.	244
Fig. B.2	Schematic of formation of fringe pattern.	245
Fig. B.3	Geometric relationship between light-scattering particle velocity, signal frequency and anemometer properties.	246
Fig. B.4	Radial velocity profiles at 40 and 80 burner diameters downstream of burner exit in methane diffusion flame, Reynolds number, 14,500.	247
Fig. B.5	Axial velocity distribution in methane diffusion flame, Reynolds number, 14,500	248



M = MIRROR

B.S = BEAM SPLITTER

L = LENS

M.V.=MEASUREMENT VOLUME
WITH FRINGE PATTERN

FIG. B.1

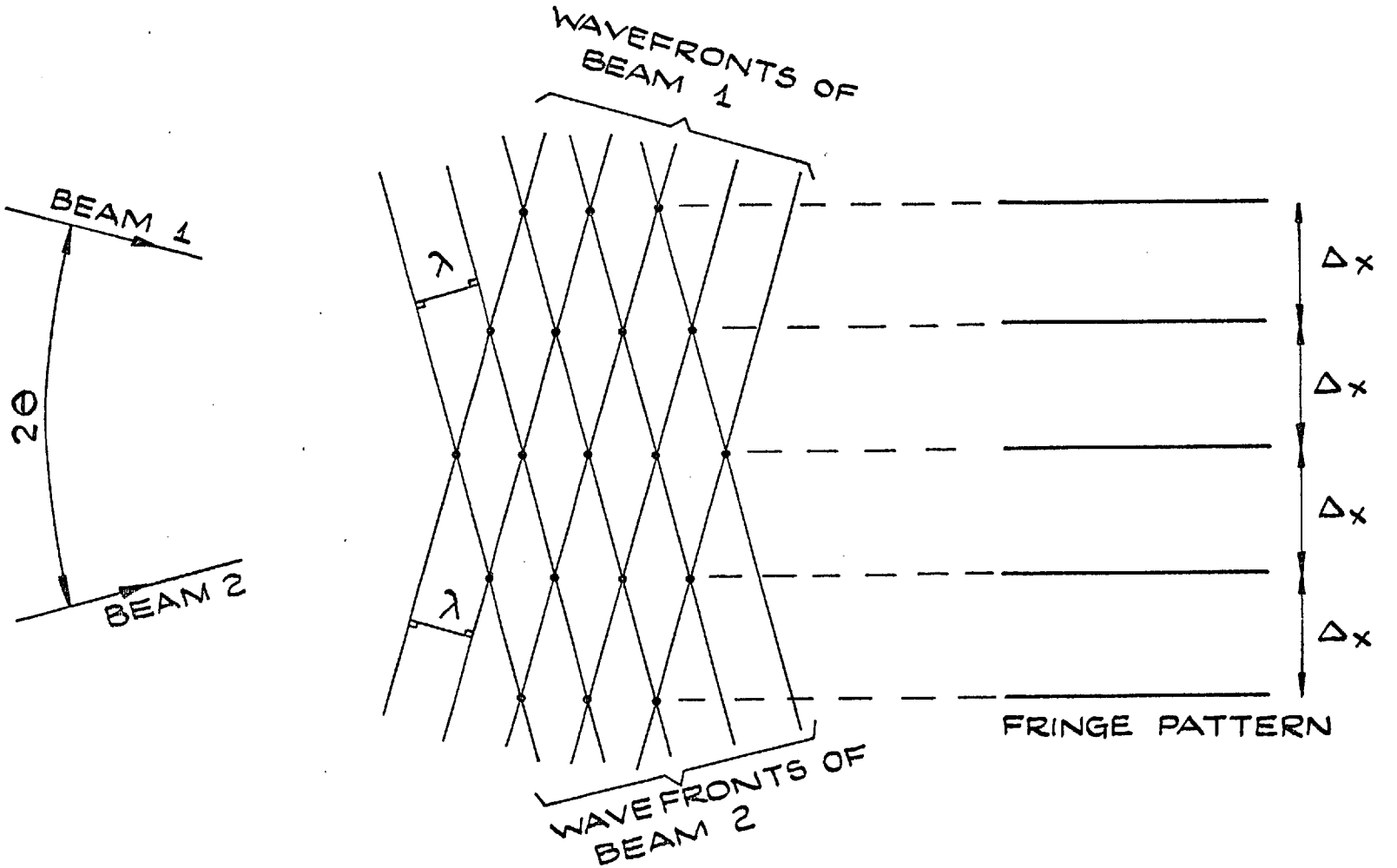

WAVEFRONTS OF
BEAM 1
BEAM 1
2θ
BEAM 2
λ
λ
Δx
Δx
Δx
Δx
FRINGE PATTERN
WAVEFRONTS OF
BEAM 2

FIG. B.2

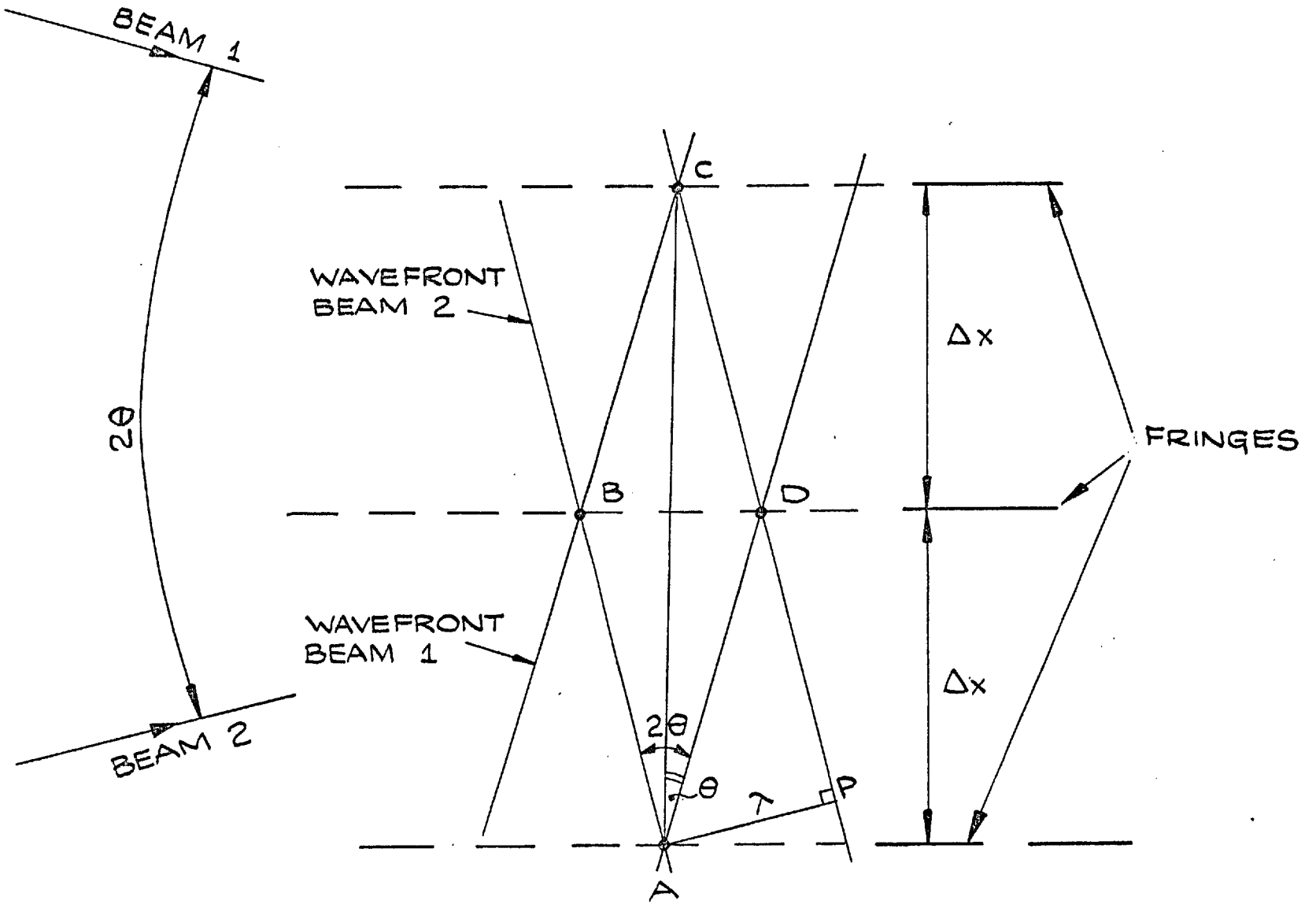

BEAM 1
2θ
BEAM 2
WAVEFRONT
BEAM 2
WAVEFRONT
BEAM 1
C
B
D
A
2θ
θ
λ
P
Δx
Δx
FRINGES

FIG. B.3

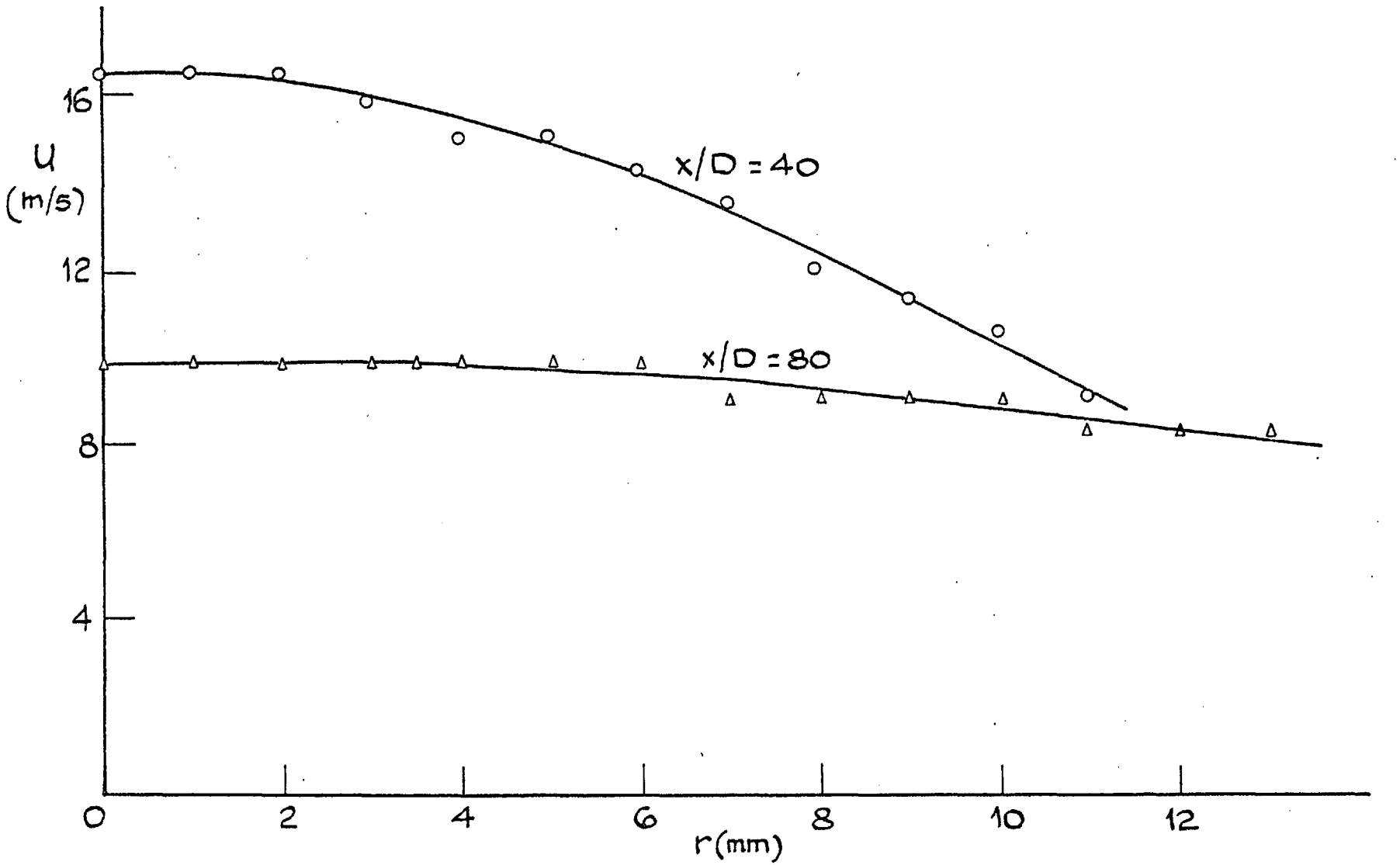


FIG. B.4

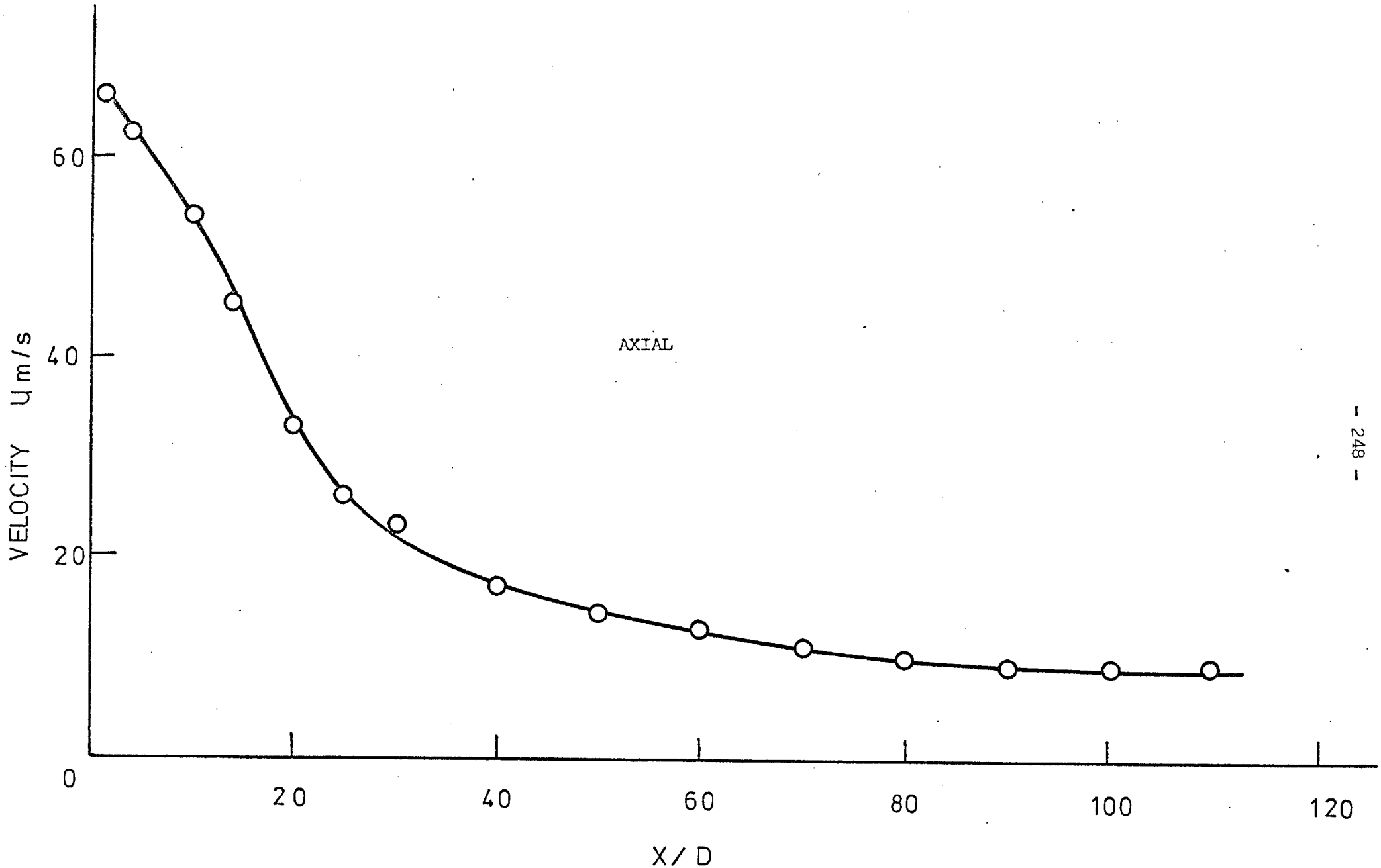


FIG. B.5